MCEER

EARTHQUAKE ENGINEERING TO EXTREME EVENTS

ISSN 1520-295X

Experimental Seismic Performance Evaluation of Isolation/Restraint Systems for Mechanical Equipment

Part 1: Heavy Equipment Study

by

Saeed Fathali and André Filiatrault

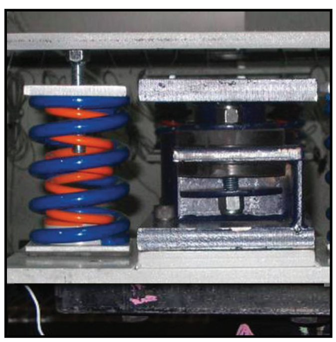

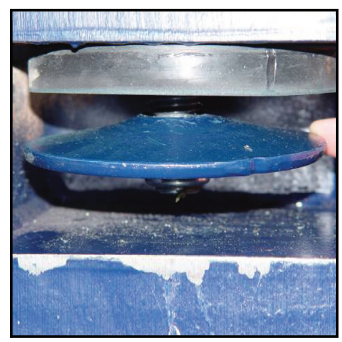

Technical Report MCEER-07-0007

June 6, 2007

This research was conducted at the University at Buffalo, State University of New York and was supported primarily by the Earthquake Engineering Research Centers Program of the National Science Foundation under award number EEC 9701471 and the American Society of Heating, Refrigerating and Air Conditioning Engineers project number 1323-RP.

MCEER
EARTHQUAKE ENGINEERING TO EXTREME EVENTS

Experimental Seismic Performance Evaluation of Isolation/Restraint Systems for Mechanical Equipment
Part I: Heavy Equipment Study

by

Saeed Fathali[1] and Andre Filiatrault[2]

Publication Date: June 6, 2007
Submittal Date: April 6, 2007

Technical Report MCEER-07-0007

Task Number 9.2.1

NSF Master Contract Number EEC 9701471
and
ASHRAE Project Number 1323-RP-Static/Dynamic
Equipment Testing and Certification

1 Graduate Student, Department of Civil, Structural and Environmental Engineering, University at Buffalo, State University of New York
2 Professor, Department of Civil, Structural and Environmental Engineering, University at Buffalo, State University of New York

MCEER
University at Buffalo, The State University of New York
Red Jacket Quadrangle, Buffalo, NY 14261
Phone: (716) 645-3391; Fax (716) 645-3399
E-mail: *mceer@buffalo.edu*; WWW Site: *http://mceer.buffalo.edu*

Preface

The Multidisciplinary Center for Earthquake Engineering Research (MCEER) is a national center of excellence in advanced technology applications that is dedicated to the reduction of earthquake losses nationwide. Headquartered at the University at Buffalo, State University of New York, the Center was originally established by the National Science Foundation in 1986, as the National Center for Earthquake Engineering Research (NCEER).

Comprising a consortium of researchers from numerous disciplines and institutions throughout the United States, the Center's mission is to reduce earthquake losses through research and the application of advanced technologies that improve engineering, pre-earthquake planning and post-earthquake recovery strategies. Toward this end, the Center coordinates a nationwide program of multidisciplinary team research, education and outreach activities.

MCEER's research is conducted under the sponsorship of two major federal agencies: the National Science Foundation (NSF) and the Federal Highway Administration (FHWA), and the State of New York. Significant support is derived from the Federal Emergency Management Agency (FEMA), other state governments, academic institutions, foreign governments and private industry.

MCEER's NSF-sponsored research objectives are twofold: to increase resilience by developing seismic evaluation and rehabilitation strategies for the post-disaster facilities and systems (hospitals, electrical and water lifelines, and bridges and highways) that society expects to be operational following an earthquake; and to further enhance resilience by developing improved emergency management capabilities to ensure an effective response and recovery following the earthquake (see the figure below).

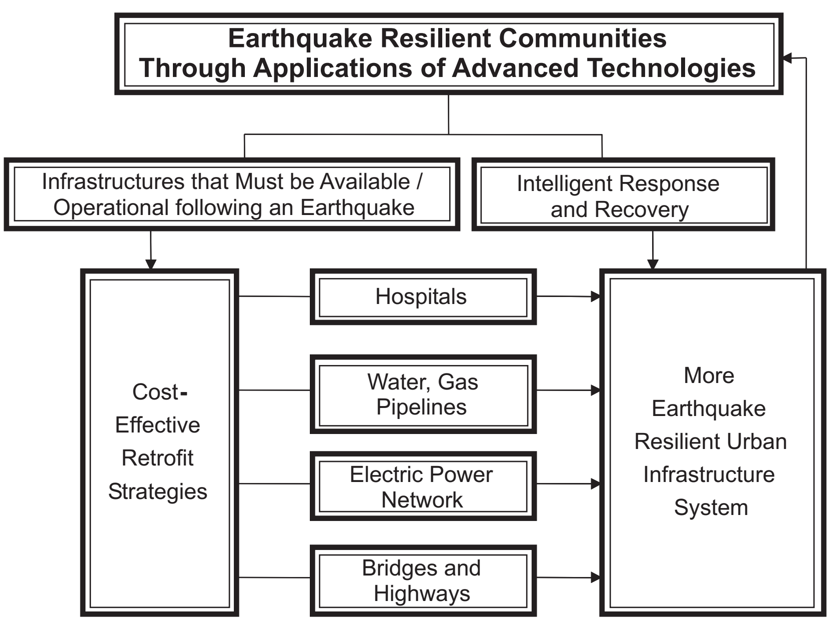

A cross-program activity focuses on the establishment of an effective experimental and analytical network to facilitate the exchange of information between researchers located in various institutions across the country. These are complemented by, and integrated with, other MCEER activities in education, outreach, technology transfer, and industry partnerships.

This report describes experimental research aimed at evaluating the seismic performance of an isolation/restraint system, typical of the systems designed by the American Society of Heating, Refrigerating and Air Conditioning Engineers (ASHRAE) members, supporting heavy mechanical equipment. The ASHRAE-type isolation/restraint system consisted of coil springs and rubber snubbers constraining the displacement in the horizontal and vertical direction. The heavy HVAC-type mechanical equipment used as test specimen was a centrifugal liquid chiller. System-identification and seismic shake table tests were conducted on the test specimen mounted on four of the isolation/restraint systems. The test plan included variation of design parameters of the restraint component of the systems, such as gap size, rubber pad thickness and hardness, and static capacity. The tri-axial acceleration response at the center of mass and corners of the chiller, displacement response of the chiller, and the dynamic forces induced into the isolation/restraint systems were recorded in each test. The experimental results were analyzed to determine the response amplification due to the engagement of the restraint components, to investigate the sensitivity of the seismic performance of the isolation/restraint systems to the variations of their restraint component design parameters, and to compare the static design capacity of the restraint components to their dynamic (actual) capacity. A companion report describing light mechanical equipment is under preparation.

ABSTRACT

This report describes an experimental research aimed at evaluating the seismic performance of an isolation/restraint system, typical of the systems designed by the ASHRAE members, supporting heavy mechanical equipment. The ASHRAE-type isolation/restraint system consisted of coil springs and rubber snubbers constraining the displacement in the horizontal and vertical direction. The heavy HVAC-type mechanical equipment used as test specimen was a centrifugal liquid chiller. System-identification and seismic shake table tests were conducted on the test specimen mounted on four of the isolation/restraint systems. The test plan included variation of design parameters of the restraint component of the systems namely the gap size, rubber pad thickness and hardness, and the static capacity. The tri-axial acceleration response at the center of mass and corners of the chiller, displacement response of the chiller, and the dynamic forces induced into the isolation/restraint systems were recorded in each test. The experimental results were analyzed to determine the response amplification due to the engagement of the restraint components, to investigate the sensitivity of the seismic performance of the isolation/restraint systems to the variations of their restraint component design parameters, and to compare the static design capacity of the restraint components to their dynamic (actual) capacity.

ACKNOWLEDGEMENTS

This project was supported by the American Society of Heating, Refrigerating, and Air-Conditioning Engineers (ASHRAE) and by the Earthquake Engineering Research Centers Program of the National Science Foundation (NSF) under Award Number EEC-9701471 to the Multidisciplinary Center for Earthquake Engineering Research (MCEER).

Any opinions, findings, conclusions, and recommendations presented in this reports are those of the authors and do not necessarily reflect the views of the sponsors.

The authors gratefully acknowledge members of the ASHRAE technical oversight committee for their guidance during the course of the project, Mason Industries for providing the snubber systems tested, Kinetics Noise Control for providing the isolation system tested, York International for providing the centrifugal chiller unit tested and the technical staff of the Structural Engineering and Earthquake Simulation Laboratory (SEESL) of the Department of Civil, Structural, and Environmental Engineering at University at Buffalo, the State University of New York, for their support in the execution of the seismic tests described in this report.

TABLE OF CONTENTS

TABLE OF CONTENTS (CONT'D)

LIST OF ILLUSTRATIONS

LIST OF ILLUSTRATIONS (cont'd)

LIST OF ILLUSTRATIONS (cont'd)

LIST OF TABLES

LIST OF TABLES (cont'd)

SECTION 1

INTRODUCTION

Achieving a target seismic performance for a building requires the harmonization of the performance levels between structural and nonstructural components. Recent studies have shown that even if the structural components of a building achieve an immediate occupancy performance level after a seismic event, failure of nonstructural components of the building such as mechanical and electrical equipment can lower the performance level of the entire building and result in significant financial loss (Gould et al., 2003; Kircher, 2003; Filiatrault et al., 2001). The 2003 edition of the International Building Code (ICC, 2003) defines minimum seismic loads against which equipment installed in buildings should be capable of resisting. The IBC 2003 requires certification for the capability of the equipment to resist the defined seismic loads. Several methods of certification including dynamic testing, analysis, and historical data are allowed. However, the cost of dynamic testing, difficulty of accurate dynamic analysis, and lack of historical data on the seismic performance of nonstructural components make such certification problematic.

Heating, Ventilation, and Air-Conditioning (HVAC) equipment is an important category of nonstructural components in buildings, which needs to meet the IBC 2003 certification requirements. Some HVAC-type equipment items are conventionally suspended from or mounted on a building floor by rigid interfacing links. However, in many cases the HVAC-type equipment is mounted on, or hung from isolation devices. The isolation devices, interfacing the equipment and the building, are used to control the transmission of noise, shock, and vibration produced by the equipment into the building structure or into other equipment installed in the building. Furthermore, the same devices isolate the equipment from vibration generated by other equipment items installed in the building. In strong seismic events, massive rigid equipment suspended by or mounted on flexible vibration isolation devices may experience displacement significantly larger than the isolator capacity. Whilst the isolators should continuously play the important role of supporting the equipment, large displacements may result in the undesirable isolator failure.

Application of rubber or neoprene snubber elements in conjunction with vibration isolation devices has been proposed and implemented successfully to control the displacement response of HVAC-type equipment suspended by or mounted on vibration isolation devices. The snubber elements and isolation devices can be placed around or connected to different locations of the equipment separately. More efficiently, the snubber elements and isolation devices can be unified into one isolation/restraint system (for brevity in this report, I/R is used as the acronym of isolation/restraint). Presence of such impact-type displacement control devices may introduce large seismic acceleration into the supported equipment and large dynamic forces into the I/R systems. Consequently, studying the seismic performance of HVAC-type nonstructural components mounted on I/R systems requires the consideration of the seismic performance of I/R systems.

The experimental research presented in this report focused on the seismic performance evaluation of an I/R system typical of systems designed by the members of the American Society of Heating, Refrigerating, and Air-Conditioning Engineers (ASHRAE). The heavy (HVAC-type) mechanical equipment used as test specimen in this study was a liquid centrifugal chiller weighing 11997 kg (26450 lb). The chiller was mounted on four I/R systems located at its four corners. Determination of the amplified seismic forces and accelerations experienced by the mounted equipment and the relationship between the static capacities and the actual dynamic capacities of the I/R system and the test specimen were investigated. The relationship between the static and actual dynamic capacities of I/R systems is an expedient tool for evaluation of the dynamic system capacity from individual component static testing results. The sensitivity of the seismic performance of the I/R systems to the change in their component properties and configuration was experimentally examined by repeating the shake table tests of the chiller mounted on the systems with different properties and configurations.

SECTION 2

TEST SPECIMEN

2.1 General Description of Test Specimen

The heavy mechanical equipment used as test specimen in this study was a centrifugal liquid chiller provided by York International Corporation. Centrifugal chillers are HVAC-type equipment, and are utilized for cooling of large buildings with centralized air conditioning system. They are heat-exchange equipment and use air, refrigerant, water, and evaporation (for transferring heat) to produce air conditioning. The cold liquid generated in the centrifugal chiller is circulated through a cooling coil of an air-handling unit (AHU) to cool the air supplied to a building. Figure 2-1 shows the test specimen placed on one of the two six-degree-of freedom earthquake simulators of the Structural Engineering and Earthquake Simulation Laboratory (SEESL) of the Department of the Civil, Structural, and Environmental engineering at University at Buffalo, the State University of New York.

Figure 2-1 Test Specimen: Centrifugal Liquid Chiller

2.2 Test Equipment Components

A brief description of the seven major components of the test specimen and their close up photographs are presented in table 2-1. Figure 2-2 indicates the location of the seven major components on the chiller assembly.

Table 2-1 Major Components of Centrifugal Liquid Chiller

Component	Function	Close-up View
Evaporator	Absorbs heat from building environment.	
Condenser	Removes the heat absorbed by the evaporator.	
Opti-View Control Center (OCC)	Electrically detects basic system information namely pressure, temperature, electrical systems, etc.	
Variable Speed Drive (VSD)	Controls the speed of the motor.	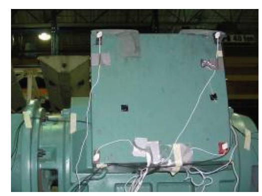
Compressor	Raises the refrigerant pressure and pump it into the condenser and through the air conditioning system.	
Motor	Drives the compressor.	
Oil Pump (OS)	Provides oil for lubrication.	

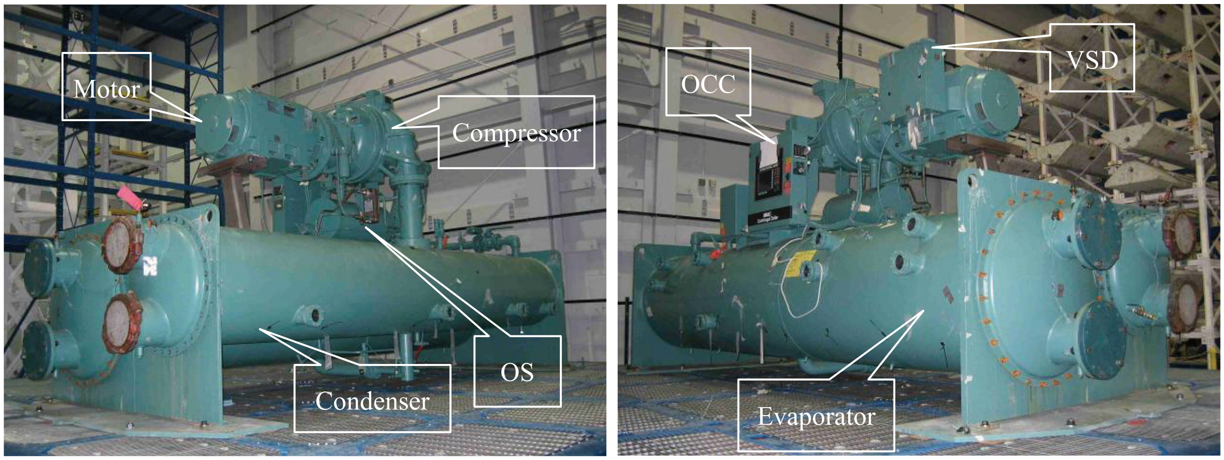

Figure 2-2 Test Specimen Overall Views

2.3 Test Specimen Dimensions and Mass

The test specimen overall dimensions were 4.88 meters by 2.11 meters (192 inches by 83 inches) in plan, and 2.87 m (113 in) in height. The chiller dimensions are presented in figure 2-3. The chiller could be tested in two different extreme conditions: dry condition (without any water) and wet condition (full of water and refrigerant). Expecting the chiller filled with water would experience larger dynamic responses, only the wet condition of the chiller was considered in this study. According to the data provided by York International Corporation and the data from the measurement in the laboratory, the chiller filled with water weighed 11997 kg (26450 lbs). More than 98% of the mass of the chiller was provided by the evaporator, condenser, compressor, motor, oil pump, suction pipe, and the water and refrigerant inside the condenser and evaporator. Table 2-2 lists the chiller components mass. Table 2-3 presents the coordinates of the center of mass of the chiller with respect to the coordinate system defined in figure 2-4(a). As shown in figure 2-4(b), the transverse, longitudinal, and vertical directions are associated with y, x, and z axes, respectively. Table 2-4 lists the eccentricities between the center of mass of the chiller and the geometric center of four corners of the chiller in the transverse, longitudinal, and vertical directions.

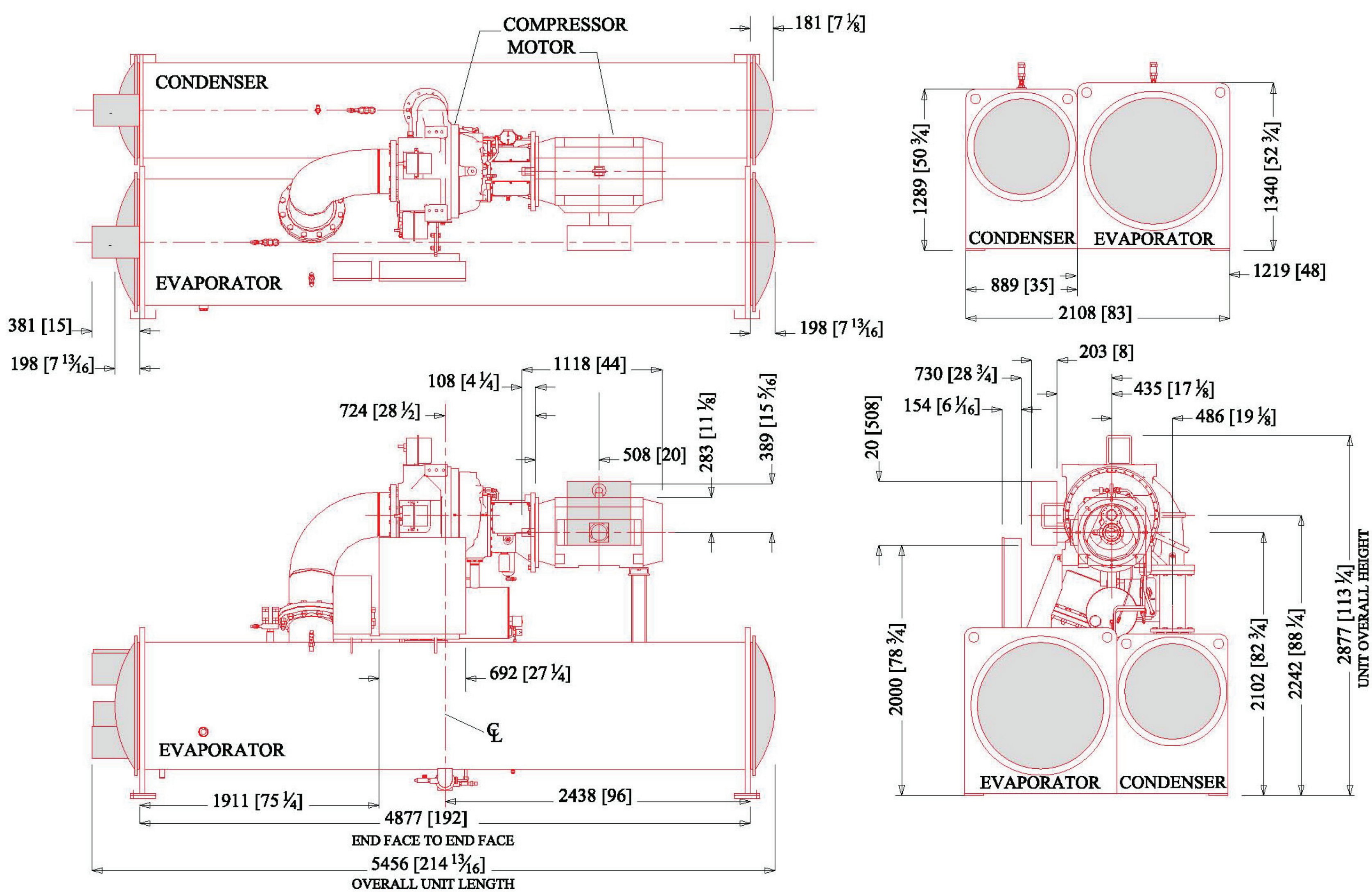

Figure 2-3 Test Specimen (Centrifugal Chiller) Dimensions (units : mm[in])

Table 2-2 Chiller Components Mass

Component	Mass	
	kg	lb
Evaporator	3589	7912
Condenser	2822	6222
Compressor	1323	2917
Motor	989	2180
Oil Pump	195	430
Suction Pipe	204	449
Others	219	482
Water and Refrigerant	2657	5858
Total	11997	26450

Table 2-3 Coordinates of Center of Mass of Chiller

x		y		z	
cm	in	cm	in	cm	in
235.4	92.7	102.1	40.2	96.9	38.2

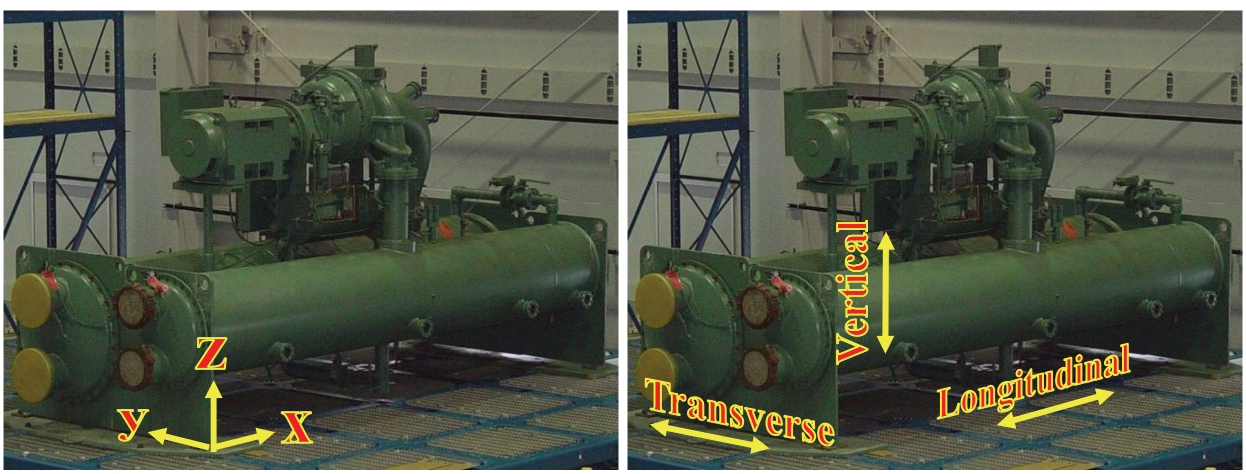

(a) Reference Coordinate System (b) Reference Directions

Figure 2-4 Reference Coordinate System and Directions for Center of Mass of Chiller

Table 2-4 Eccentricities between Center of Mass of Chiller and Geometric Center of Four Corners of Chiller

Transverse		Longitudinal		Vertical	
cm	in	cm	in	cm	in
3.3	1.3	8.4	3.3	96.9	38.2

SECTION 3

ISOLATION/RESTRAINT SYSTEMS

3.1 General Description of Isolation/Restraint Systems

Coil springs have been vastly used for vibration control of many types of mechanical equipment such as HVAC-type machinery (ASHRAE, 2003). Spring-type isolation devices control the transmission of noise, shock, and vibration produced by mechanical equipment into the building structure or other equipment items installed in the building. Figure 3-1 illustrates two common types of the isolation devices used for mounted and suspended equipment.

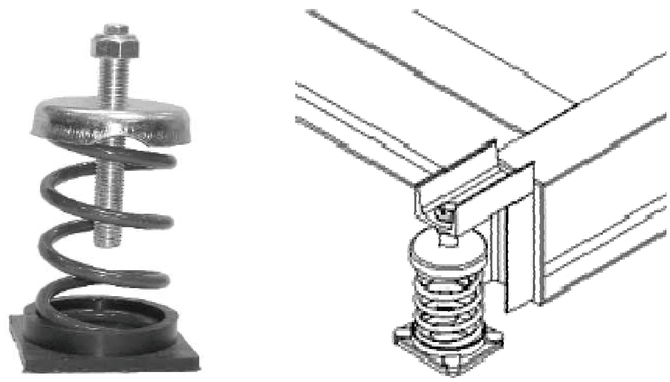

(a) Spring-Type Isolation Device for Floor Mounted Equipment

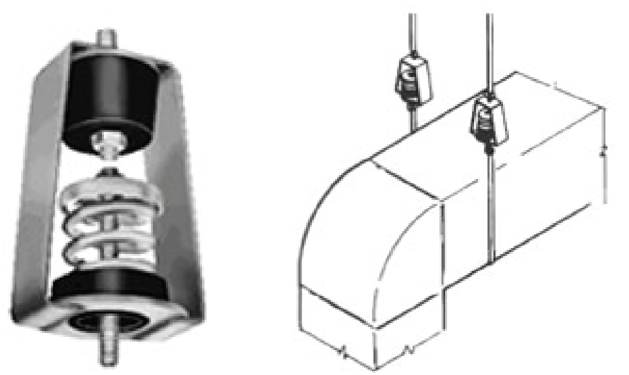

(b) Spring-Type Isolation Device for Suspended Equipment

Figure 3-1 Spring-Type Vibration Isolation Devices
(Kinetics Noise Control, 2006, MASON Industries Inc., 2006)

While spring-type isolators are quite capable of mitigating the operation-induced vibration, their performance in severe seismic events is seriously questioned. During an earthquake, due to the lateral flexibility of the springs, massive equipment supported by isolators may experience displacements much larger than the isolator capacity. Displacements larger than the isolator capacity result in the failure of the isolator. When the isolators supporting the equipment fail, the equipment falls on the building floor, and its dynamic response is not controlled anymore. This type of failure may cause significant damage to the equipment itself, to the other equipment items installed in the building, and even to the building structure.

The displacement response of an isolated equipment item can be limited by using snubber elements. Snubbers are designed and implemented in different shapes and properties. When the moving equipment hits the snubber, impact occurs and the equipment bounces back to move within the accepted range of displacement. The impact intensity can be reduced by implementing snubbers made of flexible materials such as neoprene or natural rubber. Figure 3-2 presents one simple snubber utilized to restrain the displacement of an equipment item supported by spring isolators.

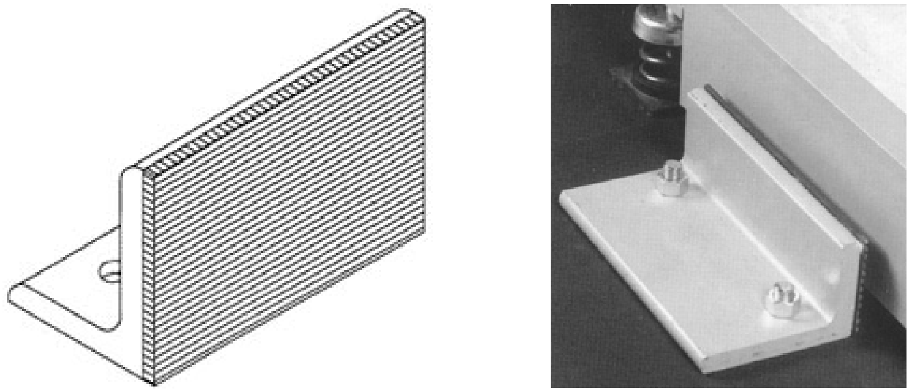

Figure 3-2 Displacement Restraint Device: Neoprene Pad Snubber (Kinetics Noise Control, 2006)

Compared to the systems with snubber elements and isolation springs installed around the equipment separately (figure 3-2), systems with devices capable of simultaneous vibration isolation and displacement restraining (spring and snubber integrated into a common device) are more efficient, more stable, and easier to install. The ASHRAE-type I/R system used for supporting the test specimen in this study is an example of such systems. In this system, spring elements provide vibration isolation for the supported equipment in three orthogonal directions and the supported equipment can move within a range of spatial displacement defined and limited by the restraining elements.

3.2 Isolation/Restraint System Configuration

The ASHRAE-type I/R system considered in this experimental study consists of two major components that are oriented orthogonally with respect to each other: an isolation component and a restraint component. The isolation component consists of two coil springs embedded between two parallel rectangular steel plates. The bottom steel plate interfaces the I/R system and the building floor and the top plate interfaces the supported equipment and the I/R system. Enough clearance is provided between the two coil springs to allow the installation of the restraint component of the I/R system in a perpendicular direction relative to the axis connecting the centers of the two coil springs. As shown in figure 3-3(a), coaxial coil springs with different vertical stiffness values are used to provide the required vertical stiffness. A leveling bolt passes through the center of the coil springs. At the end of the leveling bolt, a nut is welded that provides the proper contact area with the top plate. Once the equipment is mounted on the I/R systems, by losing or fastening the rods through the square washers (load plate) on top of the springs, the distance between the top and bottom plates is adjusted according to the height required for proper operation of the restraining component. If there is no seismic consideration, the isolation components of the I/R systems, assembled as shown in figure 3-3(b), provide sufficient control for noise and vibrations encountered by the equipment during operation.

The restraint component of the I/R system consists of two major sub-assemblies that limits the displacement in the horizontal and vertical directions. Figures 3-4(a) and 3-4(b) show details of these two sub-assemblies. The top part of the restraint component, shown in figure 3-4(a), consists of two threaded rods (and two nut and two steel washers for each rod) and a piece of steel pipe welded to a rectangular steel plate. A steel bushing may circumscribe the steel pipe to adjust the displacement limit.

(a) Coaxial Coil Springs in Isolation Component of I/R System

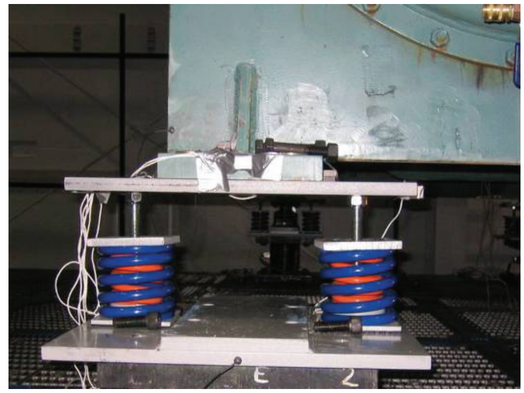

(b) Test Equipment Supported by Isolation Component of I/R System

Figure 3-3 Isolation Component of ASHRAE-Type Isolation/Restraint System

The bottom part of the restraint component, shown in figure 3-4(b), consists of two rigid steel bearings and a piece of steel pipe welded to a rectangular steel plate, two rubber grommets, and one tubular rubber pad. The tubular rubber pad, shown in figure 3-4 (c), is placed inside the steel pipe. Figure 3-4(d) shows the grommets, which are fitted into the holes of the steel bearings. Once the restraint component of the system is fully assembled, as shown in figure 3-4(e), the top and bottom parts can move relative to each other. The relative horizontal motion of the top and bottom part of the restraint component is free until the steel pipe (or the steel bushing around it) of the top part makes contact with the tubular rubber pad. In other words, the cylindrical gap left between the steel pipe of the top part and tubular rubber pad defines the horizontal distance within which two parts of the restraint component can move freely. The relative vertical motion of the top and bottom part of the restraint component is free until any of the two nuts of the rods makes contact with the steel washers located between the nuts and the grommet. In fact, the relative distance between the two nuts of the rods welded to the top plate adjusts the vertical displacement limit.

The two components of the I/R system are tied together by bolting the top and bottom plates of the restraint component to the top and bottom plate of the isolation component. Figures 3-5 shows the assembled I/R system before and after mounting the test specimen (chiller).

3.3 Dimensions and Details of Isolation/Restraint Systems

Coil springs, as vibration isolation component of the I/R systems, are designed only based on the weight of the equipment to be supported without any seismic considerations. On the other hand, the restraint component of the I/R system is designed for the supplemental dynamic loads resulting from the impacts inside the restraint component during a seismic event. The maximum dynamic load introduced into the restraint component of the I/R system is estimated by an equivalent static load, which is equal to the mass carried by the I/R system multiplied by a design peak acceleration. The restraint component should be capable of withstanding the equivalent static load applied in all directions.

The restraint components used in this experimental study were designed for two design peak accelerations: 1.0 g and 3.0 g. Each I/R system was named according to the peak acceleration used to design its restraint component. The 1.0 g design I/R system was an I/R system whose restraint component was designed to withstand static loads equal to the weight carried by the I/R system in all directions. Similarly, the 3.0 g design I/R system was an I/R system whose restraint component was designed to withstand static loads up to three times of the weight carried by the I/R system in all directions.

Each I/R system carried almost one quarter of the weight of chiller (one quarter of 117.7 kN). Therefore, the static capacity of the 1.0 g and 3.0 g design I/R systems was 29.4 and 88.3 kN, respectively. The details and dimensions of the 1.0 g and 3.0 g design restraint component are shown in figures 3-6 and 3-7, respectively. Table 3-1 lists the bill of materials used to build the 1.0 g and 3.0 g design restraint components. Figures 3-8 and 3-9 show the dimensions and details of the assembled 1.0 g and 3.0 g design I/R systems and the top and bottom plates of their isolation component. The weight of the assembled 1.0 g and 3.0 g design I/R system was 156 kg (344 lbs) and 281 kg (620 lbs), respectively.

(a) Top Part of Restraint Component

(b) Bottom Part of Restraint Component

(c) Tubular Rubber Pad Placed in Steel Pipe Welded to Lower Part of Restraint Component

(d) Grommets Fitted in Holes of Bearings in Lower Part of Restraint Component

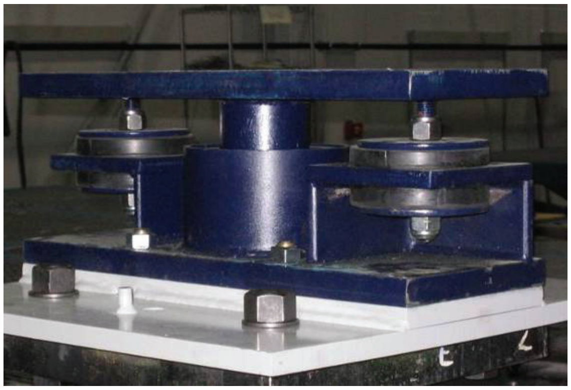

(e) Assembled Restraint Component

Figure 3-4 Restraint Component of ASHRAE-Type Isolation/Restraint System

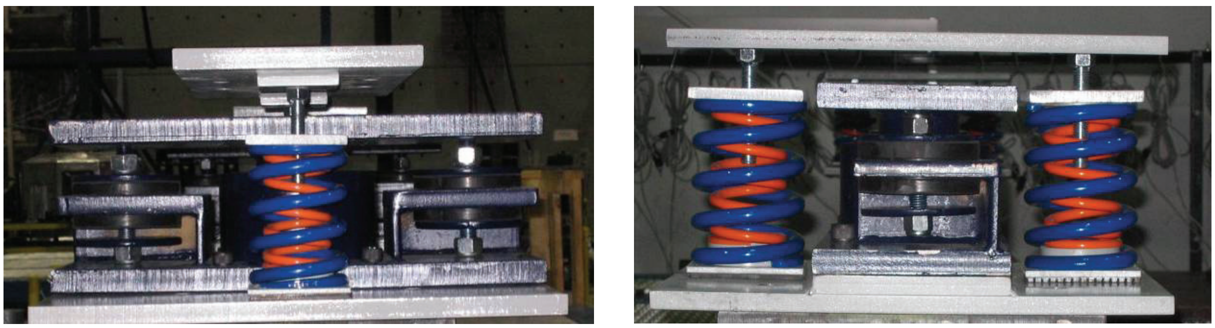

(a) Before Mounting Test Specimen

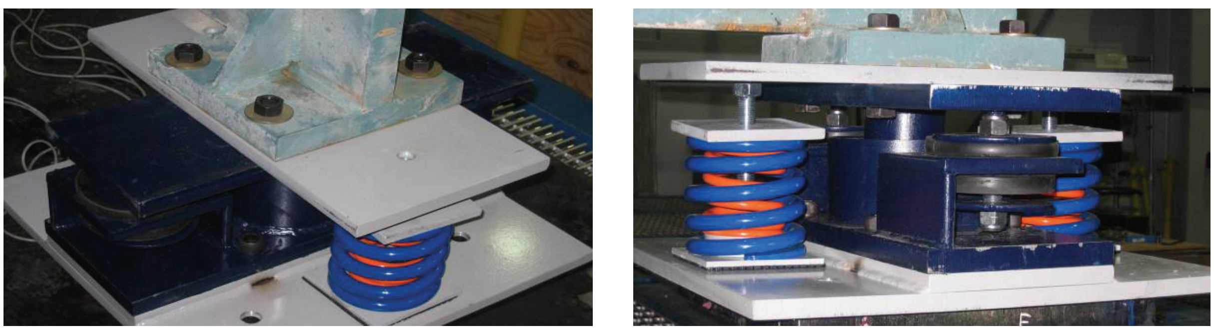

(b) After Mounting Test Specimen

Figure 3-5 Assembled ASHRAE-Type Isolation/Restraint System

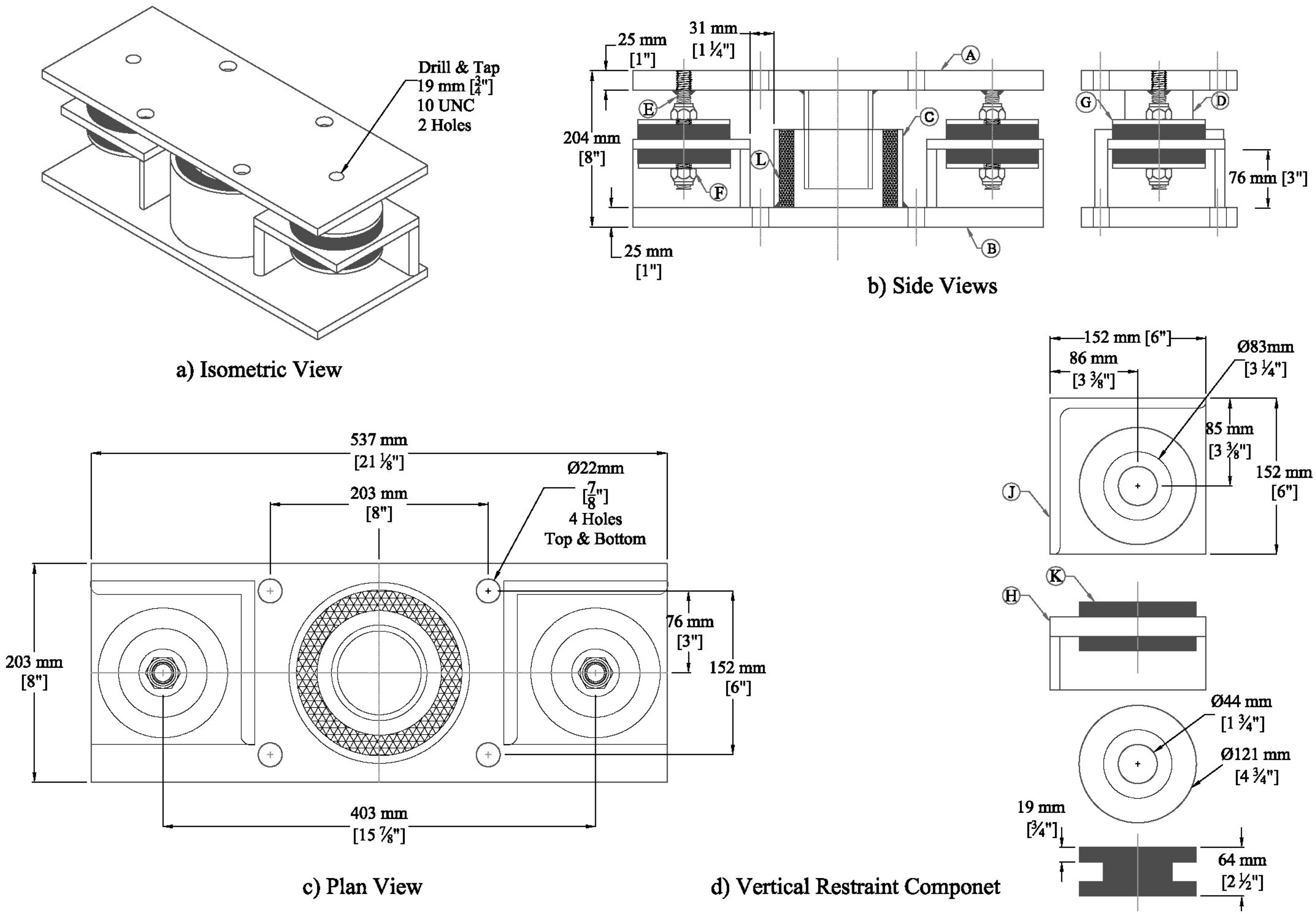

Figure 3-6 Dimensions and Details of 1.0 g Design Restraint Component (units: mm [in])

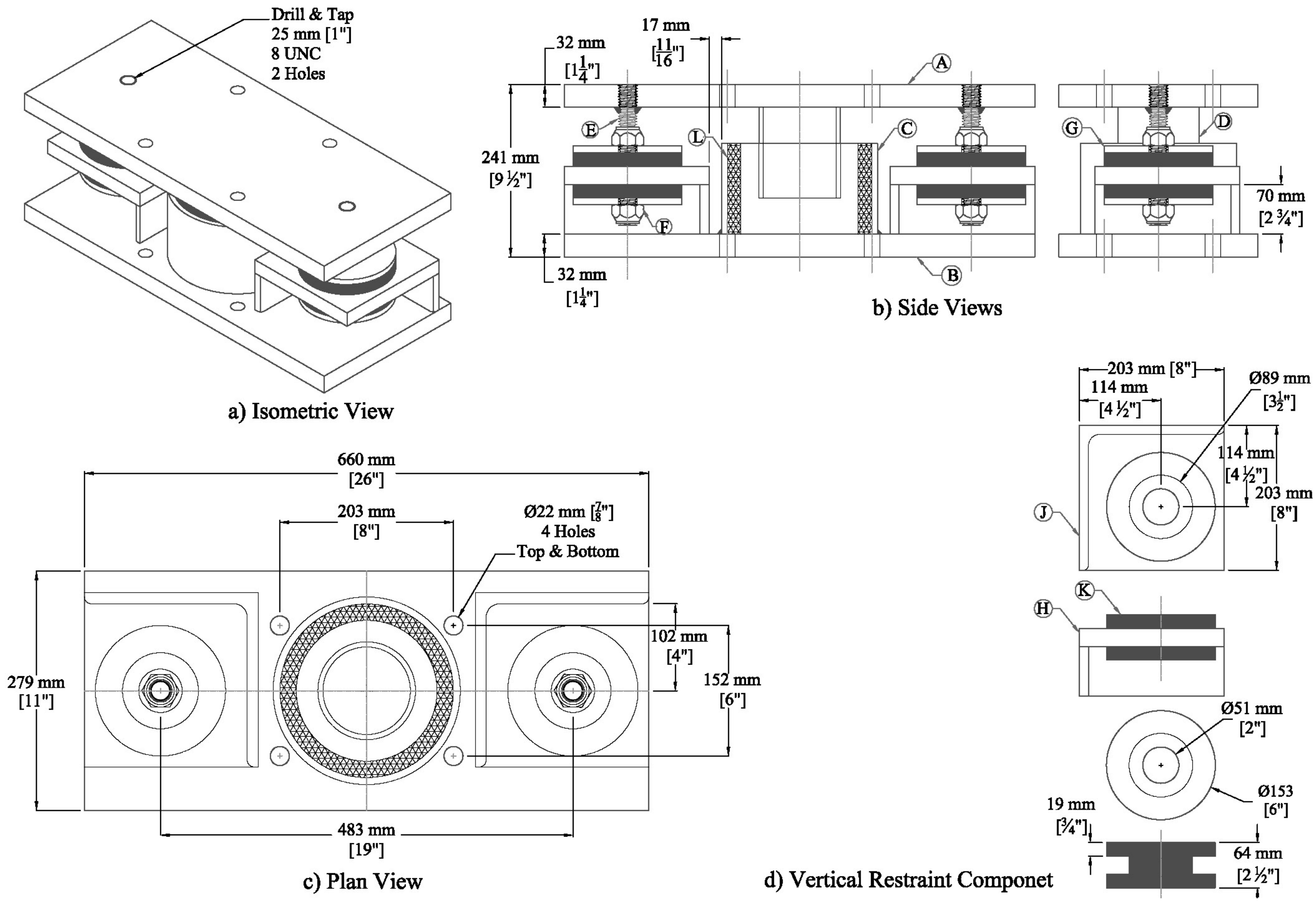

Figure 3-7 Dimensions and Details of 3.0 g Design Restraint Component (units: mm [in])

Table 3-1 Details of 1.0 g and 3.0 g Design Restraint Component (units: mm [in])

Part [2]	Quantity	Description	Size[1]	
			1.0 g Design	3.0 g Design
A	1	Top Steel Plate	25 [1] × 203 [8] × 536 [$21\frac{1}{8}$]	32 [$1\frac{1}{4}$] × 279 [11] × 660 [26]
B	1	Bottom Steel Plate	25 [1] × 203 [8] × 536 [$21\frac{1}{8}$]	32 [$1\frac{1}{4}$] × 279 [11] × 660 [26]
C	1	Bottom Steel Pipe	152 [6] Sch.40 Pipe-102 [4] Long	203 [8] Sch.40 Pipe-127 [5] Long
D	1	Top Steel Pipe	76 [3] Sch.40 Pipe-127 [5] Long	102 [4] Sch.40 Pipe-127 [5] Long
E	2	Threaded Rod	19 [$\frac{3}{4}$]-10 UNC Threaded Rod-154 [$6\frac{1}{16}$] Long	25 [1]-8 UNC Threaded Rod-197 [$7\frac{3}{4}$] Long
F	4	UNC Torque Hex. Nut	19 [$\frac{3}{4}$]-10 UNC Torque Hex. Nut	25 [1]-8 UNC Torque Hex Nut
G	4	Thick Steel Washer	O.D.: 121 [$4\frac{3}{4}$], I.D.: 21 [$\frac{13}{16}$], Th.: 6 mm [$\frac{1}{4}$]	O.D.: 152 [6], I.D.: 27 [$1\frac{1}{16}$], Th.: 9 [$\frac{3}{8}$]
H	2	Steel Plate with Hole	152 [6] × 152 [6] × 13 [$\frac{1}{2}$], Hole: 95 [$3\frac{1}{4}$]	152 [8] × 152 [8]× 13 [1], Hole: 89 [$3\frac{1}{2}$]
J	2	Steel Angle	152 [6] × 152 [6] × 13 [$\frac{1}{2}$], 76 [3] Long	152 [8] × 152 [8] × 13 [$\frac{1}{2}$], 70 [$2\frac{3}{4}$] Long
K	2	Rubber Grommet	See Figure 3-6	See Figure 3-7
L	1	Tubular Rubber Pad	Variable	Variable

1. The values in brackets show the sizes in inch unit, Sch: Schedule, UNC: Uniform Coarse Thread, Hex. Nut: Nut with six sides, O.D.: Outside Diameter, I.D.: Inside Diameter, Th.: Thickness
2. Shown in figures 3-6 and 3-7

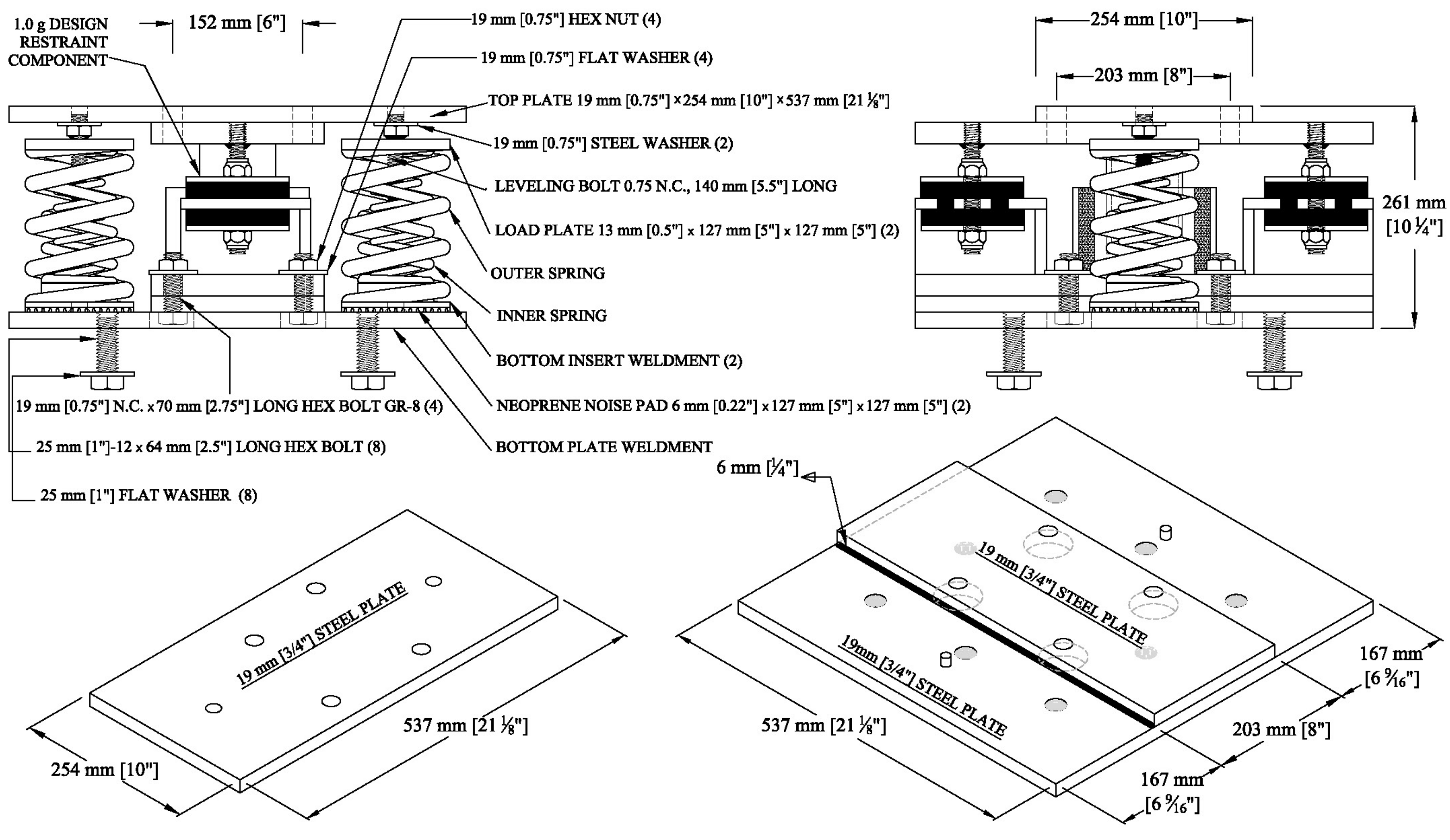

Figure 3-8 Assembly Details of 1.0 g Design ASHRAE-Type I/R System (units: mm [in])

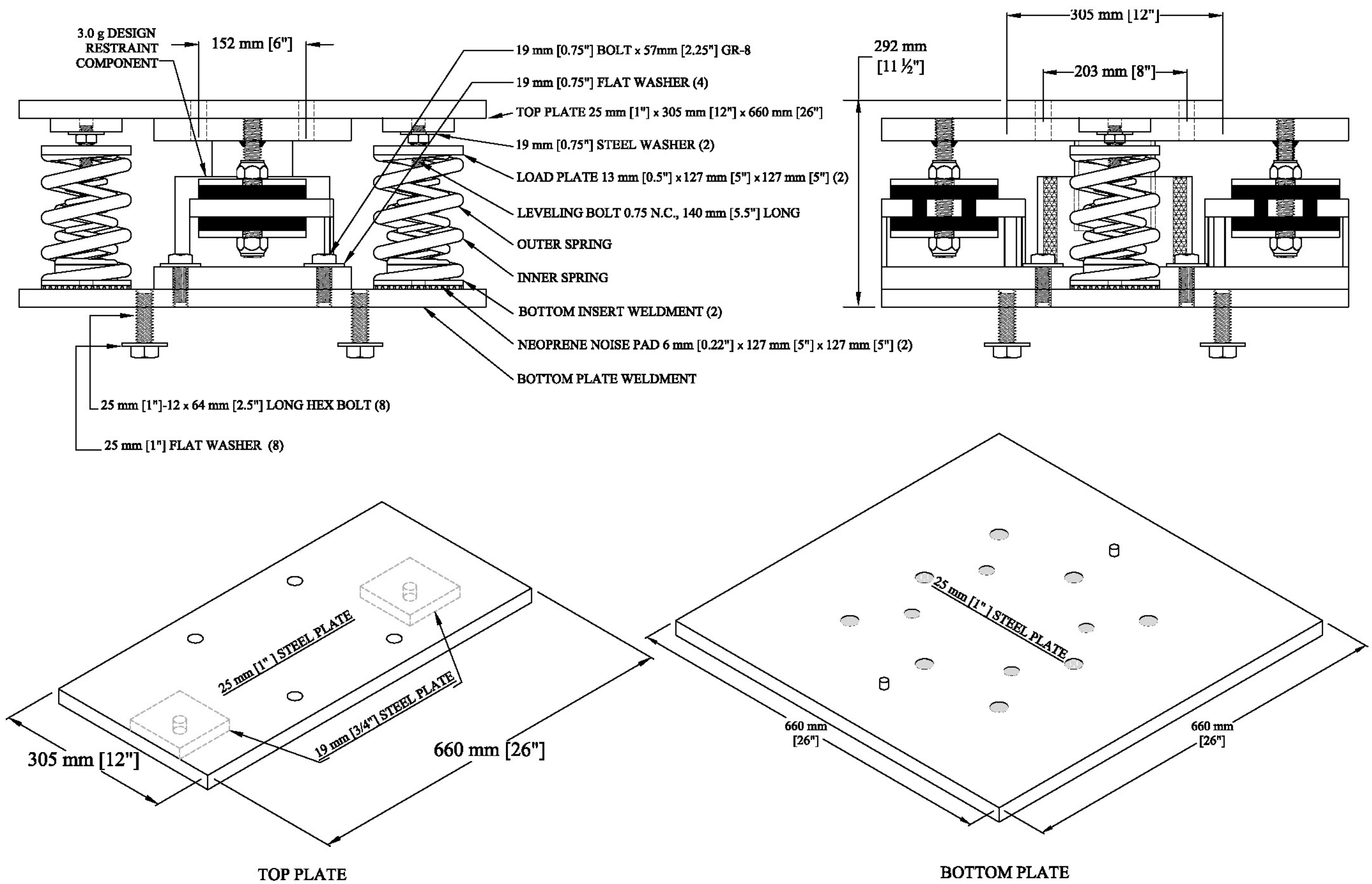

Figure 3-9 Assembly Details of 3.0 g Design ASHRAE-Type I/R System (units: mm [in])

3.4 Isolation/Restraint System Design Parameters

The horizontal and vertical stiffness of the coil springs are the only design parameters of the isolation component of the I/R system. As mentioned earlier, the isolation component of the I/R system is designed based on the weight of the supported equipment without any seismic considerations. The restraint component of the I/R system, on the other hand, is designed for the dynamic loads induced by the impacts during a seismic event. The intensity of an impact between an accelerated rigid mass and a surface is controlled by several parameters including the distance within which the accelerated rigid mass moves freely before hitting the surface and the stiffness and energy dissipation ability of the surface. Analogously, the impact intensity in the restraint component of the I/R system, which directly influences the seismic performance of the I/R system, is function of the design parameters listed below:

1) Horizontal Gap: The cylindrical space between the tubular rubber pad and the steel pipe welded to the top plate of the restraint component defines how much the supported equipment can freely move in the horizontal direction before an impact occurs. The horizontal gap can be adjusted by either the rubber pad thickness or steel bushing circumscribing the steel pipe. In this study, the following nominal horizontal gap sizes were investigated: 3 mm [0.125 in], 6 mm [0.25 in], 11 mm [0.4325 in], and 12 mm [0.5 in].

2) Vertical Gap: Subtracting the total thickness of the grommet and the two steel washers from the distance left between the two nuts of the threaded rod (welded to the top plate of the restraint component and passing through the grommet center) gives the effective vertical gap of the restraint component. In this series of experiments, the vertical gap size was always nominally equal to the horizontal gap size. However, as will be explained in Section 5.6, in practice the horizontal and vertical gaps were not necessarily equal.

3) Rubber Thickness: The thickness of the rubber pad and grommets have direct influence on the impact intensity inside the restraint component of the I/R systems. In an impact event, the rubber pad and grommets are squeezed between two rigid parts. Therefore, it is expected that the thicker rubber pad and grommet would correspond to the smaller dynamic forces introduced into the I/R systems. In this series of experiments, the nominal thickness of the rubber pad was selected as: 3 mm [0.125 in], 6 mm [0.25 in], 12 mm [0.5 in], or 18 mm [0.75 in]. The grommets for each I/R system design were the same in all experiments, as shown earlier in figures 3-6 and 3-7.

4) Rubber Hardness: The capability of rubber to dissipate the energy in an impact loading has an inverse relationship with the rubber hardness. The rubber hardness is measured by a standard durometer and is presented in Duro value. In this study, two nominal hardness values were investigated for the tubular rubber pad: 50 Duro and 60 Duro. However, the hardness of the thinnest rubber pads with thickness of 3 mm [0.125in] reached 70 Duro. All grommets used in this study had nominal hardness of 60 Duro.

3.5 Mechanical Properties of Isolation/Restraint Systems

Each I/R system unit can be considered in two different states: (1) the moving parts of the restraint component are not in contact and all the loads are carried only by the isolation component of the I/R system and (2) the moving parts of the restraint component are in contact (impact occurs). In state (1), the horizontal and vertical stiffness of the system are provided only by the coil springs, whereas in state (2), the stiffness of the grommets and tubular rubber pads significantly contribute to the total horizontal and vertical stiffness of the I/R system, respectively. Both lateral load resistant elements of the I/R system (coil springs and tubular rubber pads) have axisymmetric characteristics and provide the same stiffness in any horizontal direction. Therefore, instead of evaluating the stiffness of the I/R system in a Cartesian coordinate system (x-y-z or transverse-longitudinal-vertical), it is necessary to consider the similar horizontal stiffness in all directions (axisymmetric) with a separate vertical stiffness.

The isolation component of the I/R system consists of two sets of coil springs. Each set of coil springs of the isolation component is made up of two coaxial coil springs (inner and outer coil spring). The axial stiffness of the outer and inner coil spring is 219 kN/m (1250 lb/in) and 88 kN/m (500 lb/in), respectively. For the outer and inner coil spring fixed at both ends (two ends of the spring remain always parallel), the ratio of the lateral to vertical stiffness is estimated 1.43 and 1.12, respectively (Tauby, 2005). The ASHRAE-type I/R system installation is such that the top end of the coil springs does not have fixed condition (see the details of the end of the leveling bolts shown in figures 3-8 and 3-9). The lateral stiffness of a coil spring fixed only at one end is approximately one quarter of the lateral stiffness of the same spring fixed at both ends. The vertical and horizontal stiffness of isolation component of the I/R system provided by four coil springs operating in parallel, K_v and K_h , are estimated as:

$$K_v = 2\times219 + 2\times88 = 614 \text{ kN/m (3500 lb/in)} \qquad (3\text{-}1)$$

$$K_h = 2\times(0.25\times1.43\times219) + 2\times(0.25\times1.12\times88) = 206 \text{ kN/m (1174 lb/in)} \qquad (3\text{-}2)$$

The values calculated above are the vertical and horizontal stiffness of the ASHRAE-type I/R system when all the loads are carried only by the coil springs (when there is no contact in the restraint component). During the short time of each impact, when the moving parts of the restraint component are in contact with each other, the tubular rubber pad in the horizontal direction and the rubber grommets in the vertical direction significantly increase the stiffness of the I/R system. Based on the rubber properties and the dimensions of the contact area, the horizontal stiffness provided by tubular rubber pad and the vertical stiffness provided by grommets can be estimated for statically applied loads. It is assumed that the stiffness against dynamic loading (impact) is one and half times of the stiffness against statically applied loads. Table 3-2 lists the estimated stiffness provided by each component of the two I/R system designs. Table 3-3 summarizes the maximum stiffness of each I/R system design in the two different states: with and without occurrence of impact in the restraint component. All of the values presented in tables 3-2 and 3-3 were provided by MASON Industries, Inc.

Table 3-2 Stiffness of I/R System Components (units: kN/m [lb/in])

Direction	Isolation Component	Restraint Component			
		1.0 g Design		3.0 g Design	
		Static	Dynamic	Static	Dynamic
Horizontal	206 [1174]	5721 [32666]	8581 [49000]	7589 [43333]	11383 [65000]
Vertical	614 [3500]	5370 [30666]	8056 [46000]	7355 [42000]	11033 [63000]

Table 3-3 Maximum Stiffness of an I/R System (units: kN/m [lb/in])

Direction	1.0 g Design		3.0 g Design	
	Without Impact	With Impact	Without Impact	With Impact
Horizontal	206 [1174]	8787 [50174]	206 [1174]	11589 [66174]
Vertical	614 [3500]	8669 [49500]	613 [3500]	11646 [66500]

SECTION 4

LABORATORY EQUIPMENT

4.1 Earthquake Simulator

The six-degree-of-freedom shake table utilized in this series of experiments is located in the Structural Engineering and Earthquake Simulation Laboratory (SEESL) of the Department of Civil, Structural, and Environmental Engineering at University at Buffalo, the State University of New York. The shake table is capable of the nominal performance listed in table 4-1. The performance data is based on the continuous uniaxial sinusoidal motion of the shake table with a 20 mton rigid specimen installed on it. Performance levels are reduced with payloads larger than this nominal value. Figure 4-1 shows photographs of the shake table with and without its extension. The plan dimensions of the shake table extension, a welded steel truss with the approximate mass of 9.8 mton, are indicated in figure 4-2. More details on the shake table characteristics can be found on-line at: http://nees.buffalo.edu/Facilities/Major_Equipment/.

Table 4-1 Nominal Performance of Six-Degree-of-Freedom Shake Table

Table Size without Table Extension	3.6 m × 3.6 m [12 ft × 12 ft]		
Table Size with Extension Platform in Place	7.0 m × 7.0 m [23 ft × 23 ft]		
Maximum Specimen Mass	50 mton maximum / 20 mton nominal [110 kips maximum / 44 kips nominal]		
Maximum Specimen Mass with Table Extension Platform in Place	40 mton maximum [88 kips maximum]		
Maximum Overturning Moment	46 ton-m [333 kips-ft]		
Maximum off-Center Loading Moment	15 ton-m [108 kips-ft]		
Frequency of Operation	0.1~50 Hz nominal/100 Hz maximum		
Nominal Performance	X axis	Y axis	Z axis
Stroke	±0.15 m [±6 in]	±0.15 m [±6 in]	±0.075 m [±3 in]
Velocity	1250 mm/sec [49.2 in/sec]	1250 mm/sec [49.2 in/sec]	500 mm/sec [19.7 in/sec]
Acceleration (with 20 mton Specimen)	±1.15 g	±1.15 g	±1.15 g[1]

1. g is the acceleration due to gravity

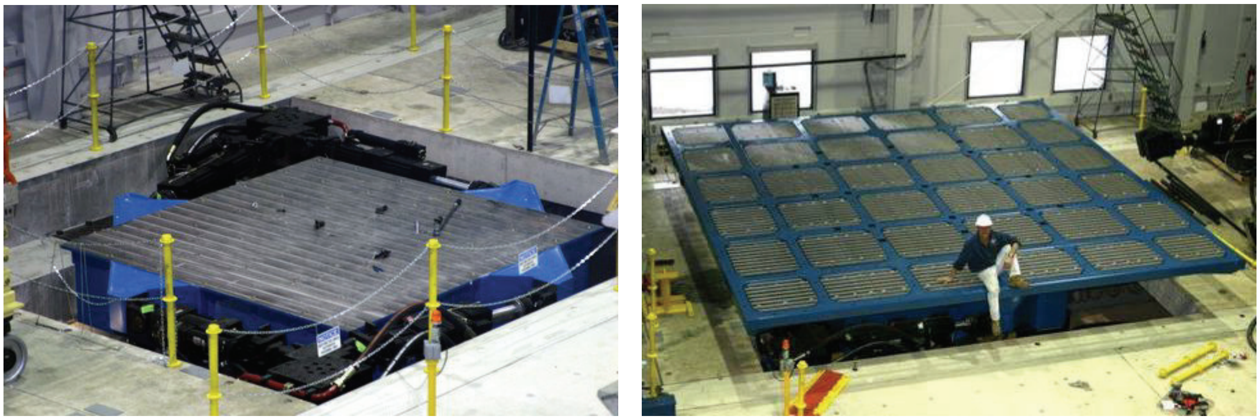

(a) Without Table Extension (b) With Table Extension

Figure 4-1 Six-Degree-of-Freedom Shake Table

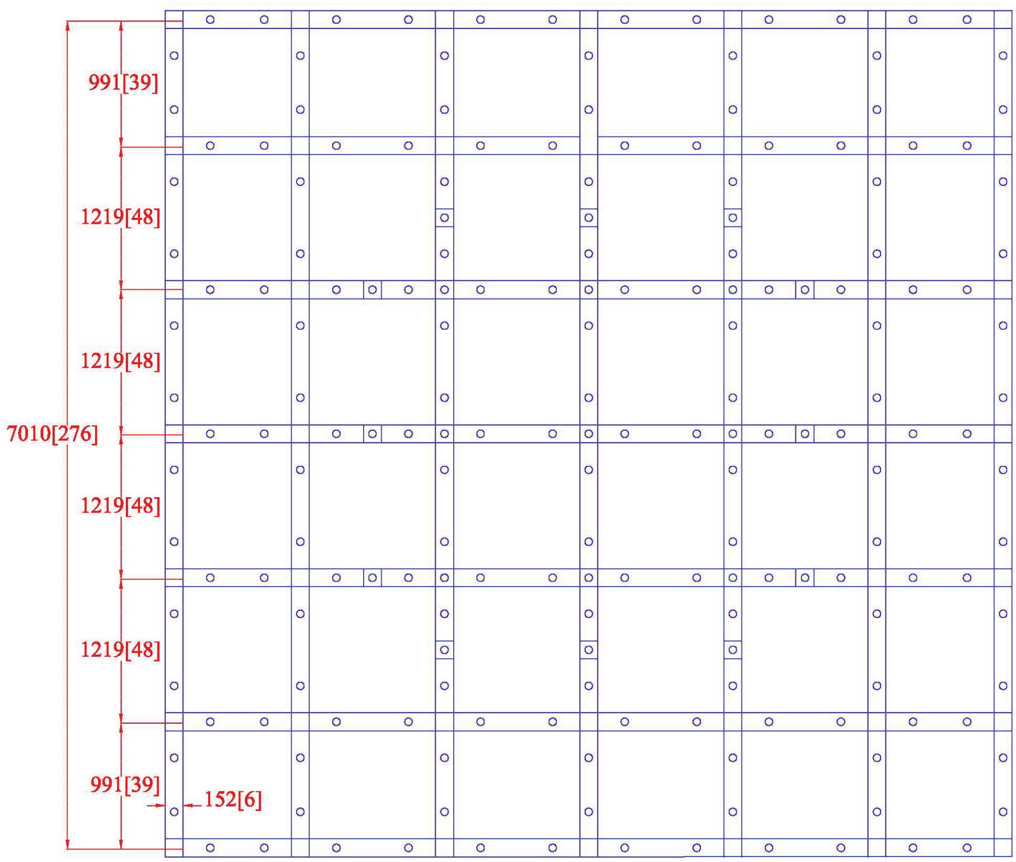

Figure 4-2 Plan Dimension of Shake Table Extension (units: mm[in])

4.2 Instrumentation

Measurements of the acceleration and displacement of the chiller, the displacement, force, and acceleration introduced to the I/R systems, and the displacement and acceleration of the shake table (table extension) were required to provide sufficient data for of the seismic performance evaluation of the I/R systems. The instrumentation used for the target measurements was a total of 4 load cells, 48 accelerometers, and 7 Light Emitting Diodes (LEDs) detected by a coordinate measurement machine (CMM).

To measure the dynamic forces (specifically the axial and shear forces) introduced into the I/R systems, one load cell was located under each I/R system in the four corners of the chiller. Each load cell could measure five different force components just below the I/R system: the normal force, the shear forces in the two horizontal orthogonal directions (transverse and longitudinal), and two in-plane moments (around the transverse and longitudinal axes). The capacity of each load cell was 1130 kN [254 kips] in pure axial force (without moment and shear force), 29kN-m [261kips-in] in pure moment (without axial and shear force), and 329 kN [74 kips] in pure shear force (without moment and axial force). Figure 4-3 shows a photograph of one of the load cells along with its capacity interaction chart. Each line in the chart indicates the shear force capacity (indicated by a number in kN unit on each line) associated with the simultaneous applications of an axial force (vertical axis) and a bending moment (horizontal axis).

One set of three accelerometers (in three orthogonal directions) was installed at each of the following three locations: the center of the shake table (to validate the shake table performance during the experiments), the center of the table extension, and the center of mass of the chiller. It will be explained in Section 6 that the chiller is assumed as a rigid body supported by flexible links. Therefore, the response measured at a reference point such as the center of mass along with the geometry-based kinematics equations are sufficient to calculate the response of any other point on the chiller.

In order to verify that the presence of the load cells interfacing the I/R systems and the shake table extension would not change the acceleration introduced to the bottom level of the I/R systems, in each of the three diagonal directions one accelerometer was installed on the bottom level of the I/R systems (a total of three accelerometers per each I/R system). To measure the acceleration responses at the corners of the chiller seven accelerometers were installed on the top level of each I/R system: two accelerometers in each of the transverse and longitudinal direction and three accelerometers in the vertical direction. Figure 4-4 shows the accelerometers installed at the center of mass of the chiller and top and bottom level of the I/R systems.

A Krypton CMM detected the three-dimensional displacement of seven different locations: 4 points on the south face of the chiller, 2 points on the I/R systems located at the south corners of the chiller, and one point on the south face of the shake table extension. Figure 4-5 shows the Krypton CMM and the LEDs attached to the chiller, to the I/R system, and to the table extension.

Figures 4-6 and 4-7, associated with tables 4-2 and 4-3, show the accelerometer and LED locations, respectively. Table 4-2 and 4-3 summarize all the instrumentation used in the shake table tests.

All accelerometers and load cells signals were sampled at 256 Hz through the LABVIEW data acquisition software. The three-dimensional displacement measurements from the Krypton CMM were recorded at 125 Hz by the software integrated with the Krypton CMM. An anti-aliasing filter with a corner frequency of 50 Hz was applied to all channels during data acquisition. Figures 4-8 and 4-9 show the accelerometer and load cell channel locations, respectively. All acquired data have been included in the CD-ROM accompanying this report.

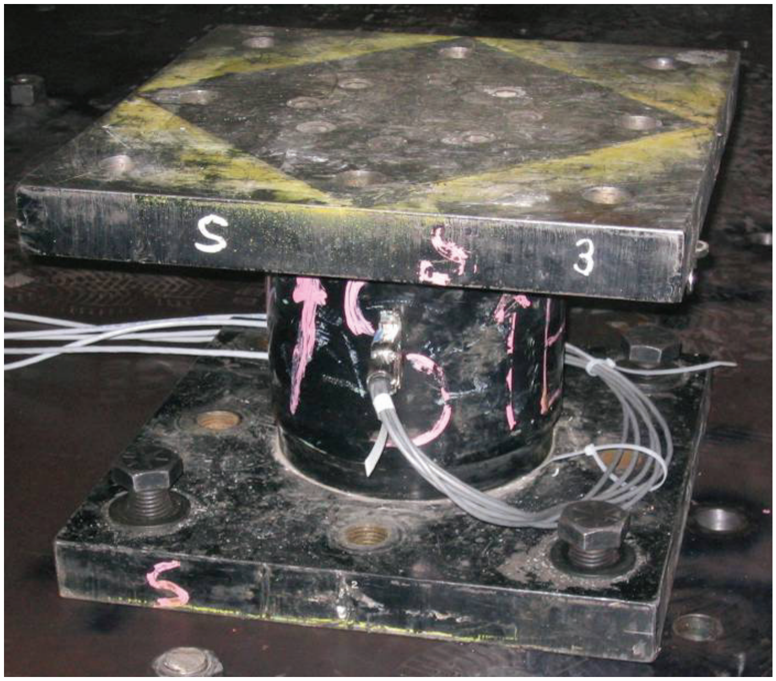

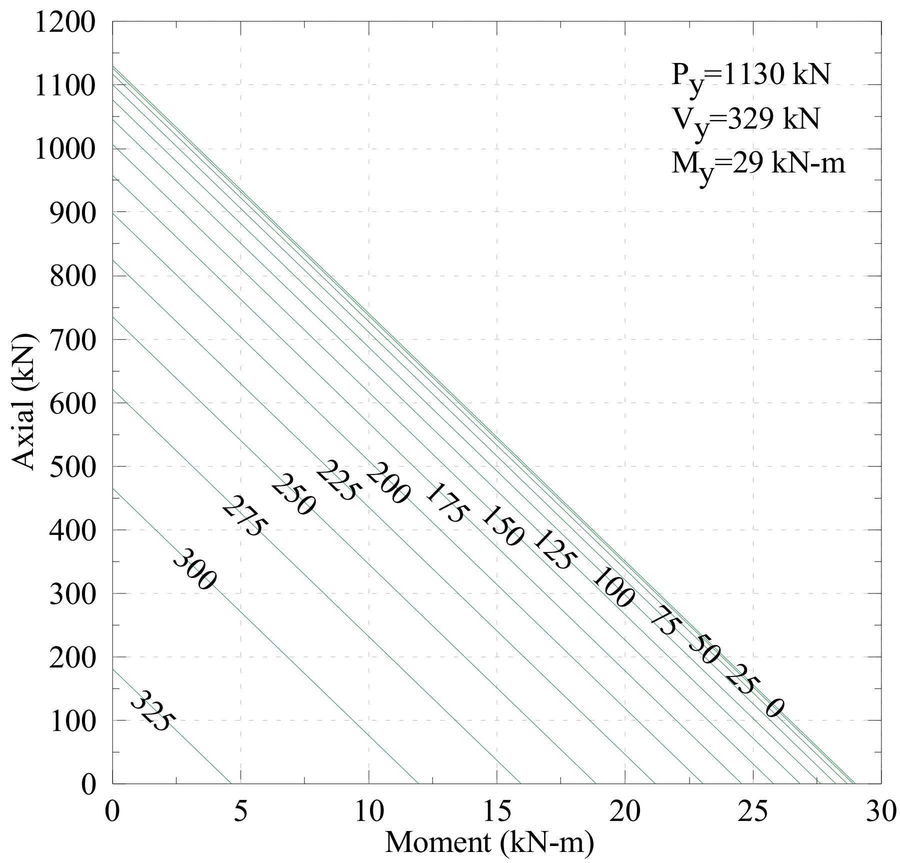

Figure 4-3 Load Cell (Top) and its Capacity Interaction Chart (Bottom)

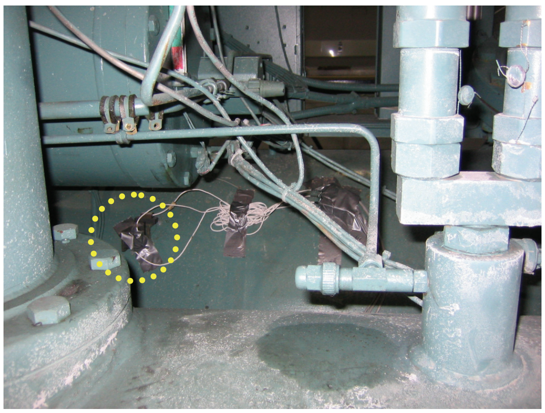

(a) Accelerometers in Three Directions Installed at Center of Mass of Chiller

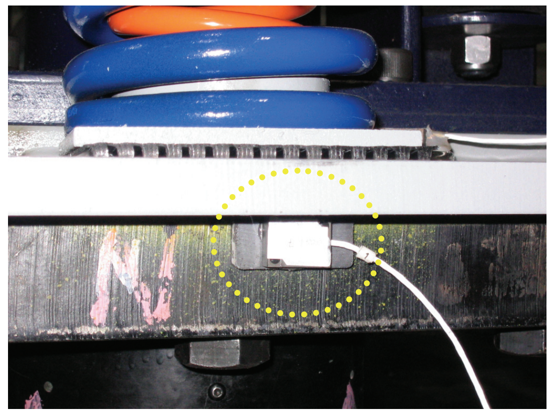

(b) Horizontal Accelerometers Installed on Top Level of Load Cells

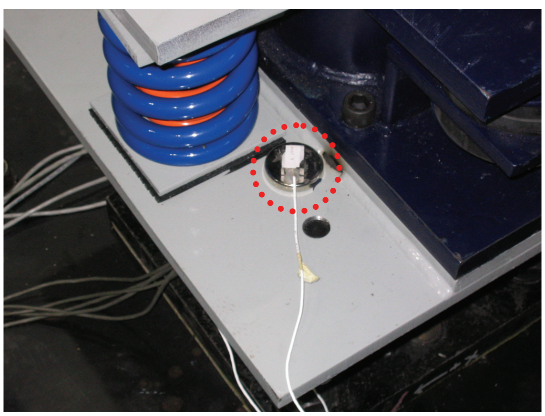

(c) Vertical Accelerometers Installed on Top Level of Load Cells

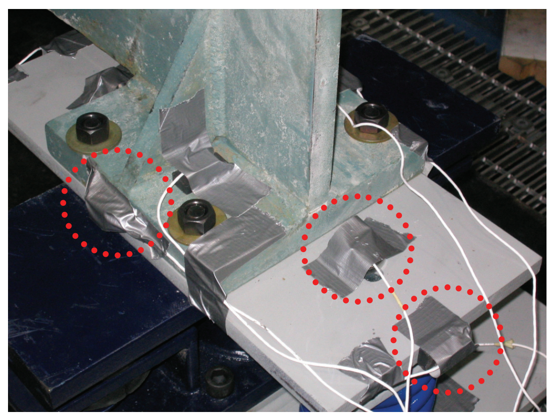

(d) Accelerometers in Three Directions Installed on Top Level of I/R Systems

Figure 4-4 Accelerometer Locations

(a) Krypton Coordinate Measurement Machine

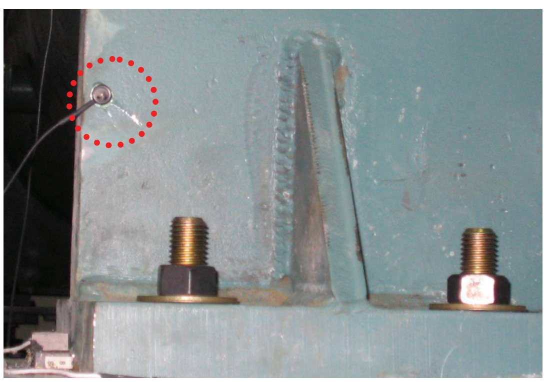
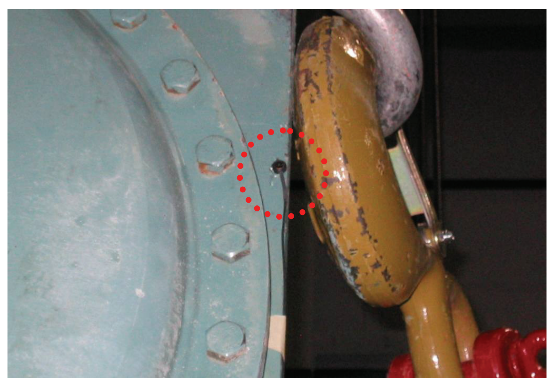

(b) LEDs Attached to South Face of Chiller

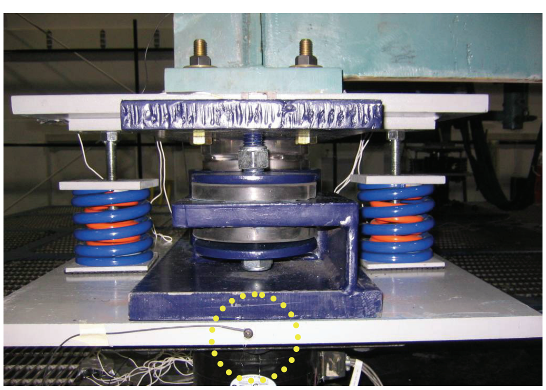

(c) LED Attached to Top Level of Load Cell

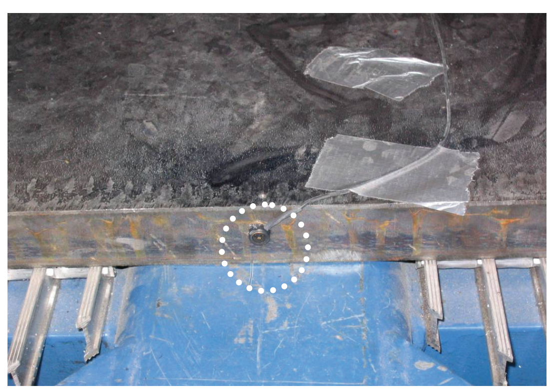

(d) LED Attached to Shake Table

Figure 4-5 Displacement Instrumentation: Coordinate Measurement Machine and LEDs

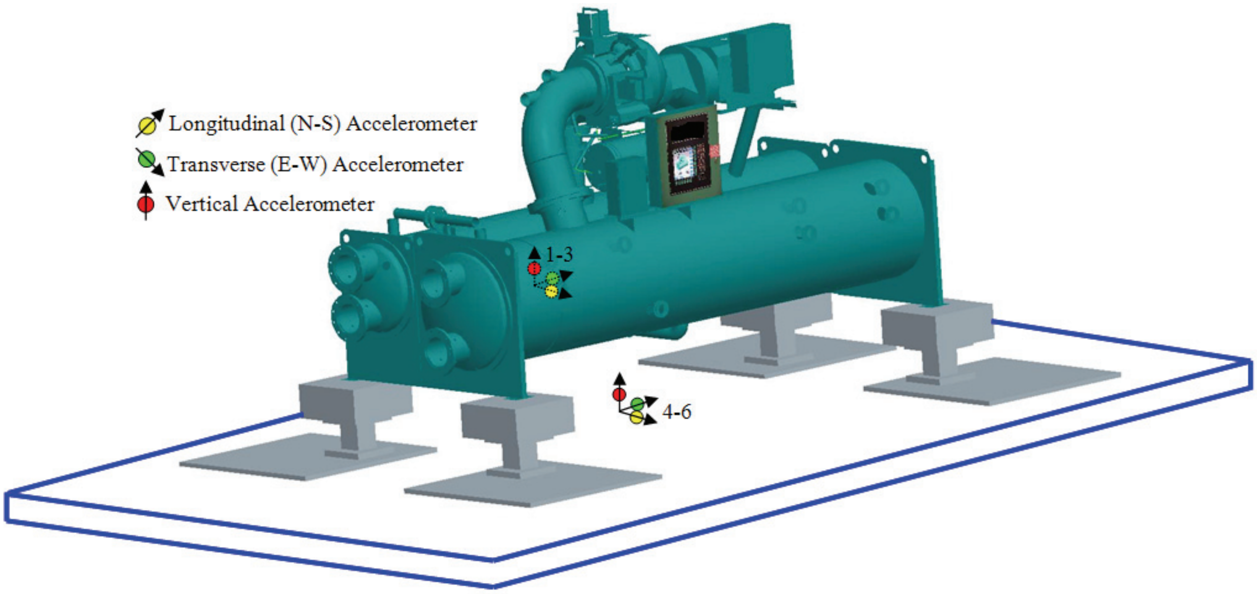

(a) Center of Mass of Chiller and Shake Table Center

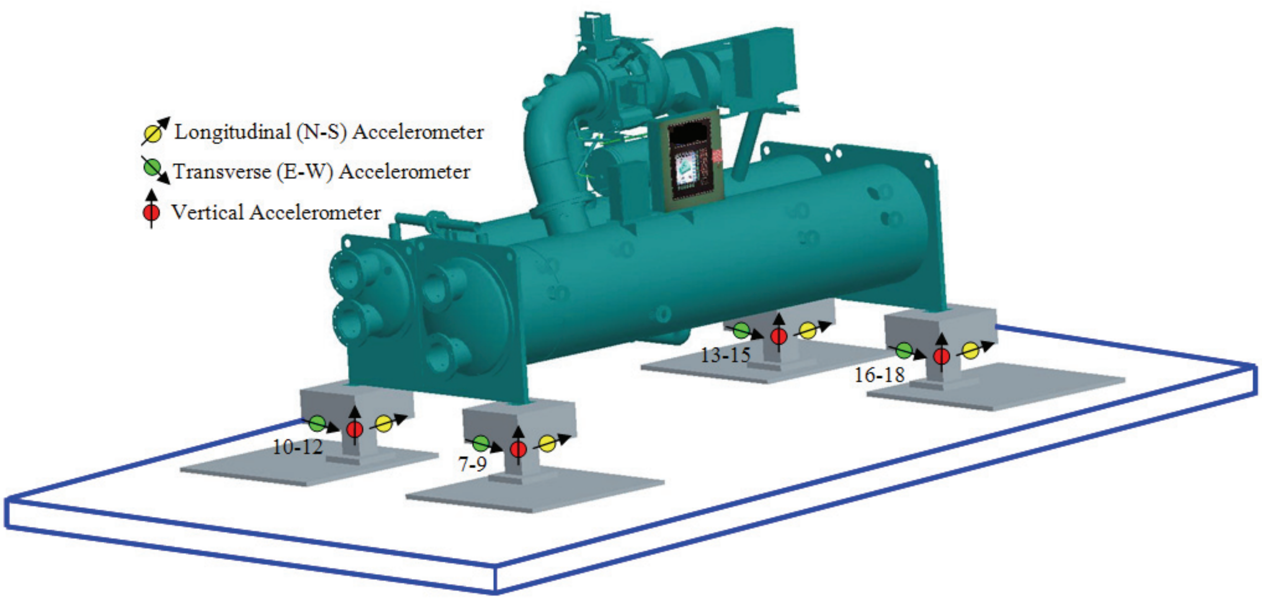

(b) Top Level of Load Cells

Figure 4-6 Accelerometer Locations

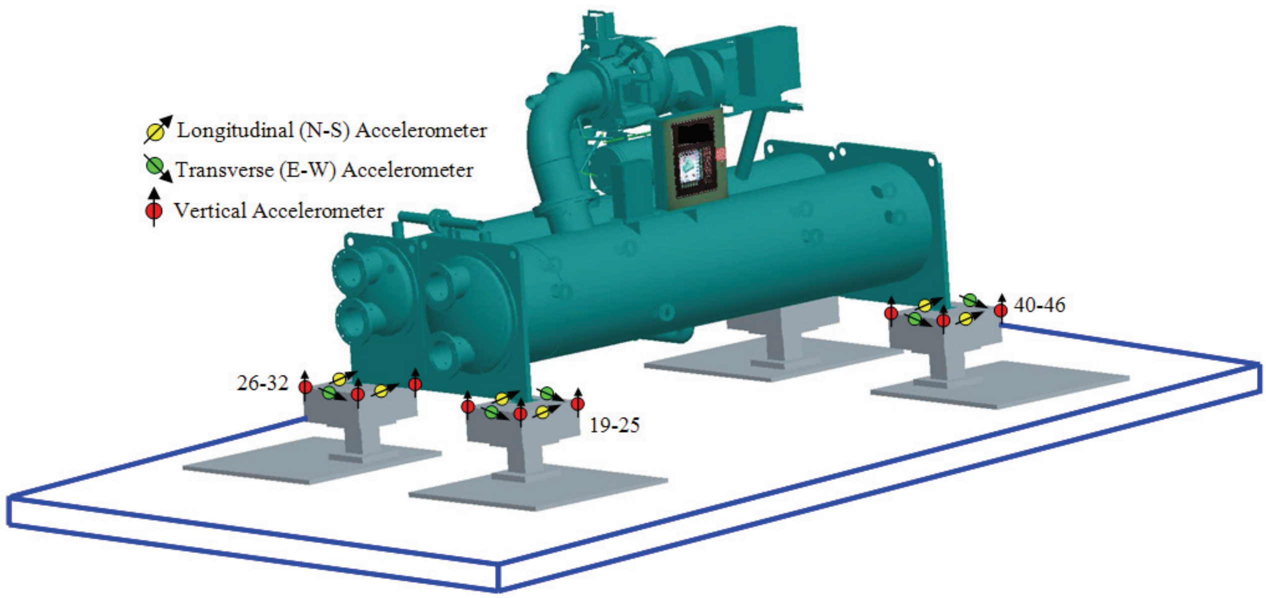

(c) Top Level of I/R Systems

Figure 4-6 Accelerometer Locations (cont'd)

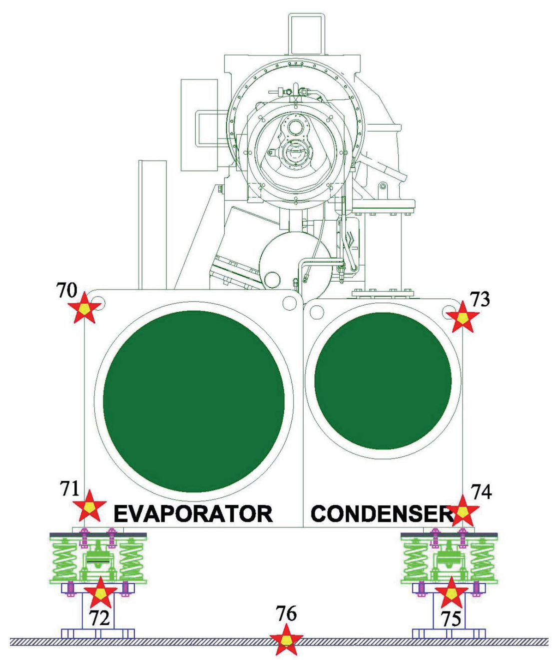

Figure 4-7 Light Emitting Diode (LED) Locations

Table 4-2 Instrumentation List: Accelerometers

Channel #	Quantity	Type	Symbol[1]	Direction	Location
1-3	3	Accelerometer		3 Axes	Center of Mass of Chiller
4-6	3	Accelerometer		3 Axes	Center of Shake Table Extension
7	1	Accelerometer		Transverse	Top Level of Load Cell No.1 (South East Corner)
8	1	Accelerometer		Longitudinal	
9	1	Accelerometer		Vertical	
10	1	Accelerometer		Transverse	Top Level of Load Cell No.2 (South West Corner)
11	1	Accelerometer		Longitudinal	
12	1	Accelerometer		Vertical	
13	1	Accelerometer		Transverse	Top Level of Load Cell No.3 (North West Corner)
14	1	Accelerometer		Longitudinal	
15	1	Accelerometer		Vertical	
16	1	Accelerometer		Transverse	Top Level of Load Cell No.4 (North East Corner)
17	1	Accelerometer		Longitudinal	
18	1	Accelerometer		Vertical	
19-20	2	Accelerometer		Transverse	Top Level of I/R System No.1 (South East Corner)
21-22	2	Accelerometer		Longitudinal	
23-25	3	Accelerometer		Vertical	
26-27	2	Accelerometer		Transverse	Top Level of I/R System No.2 (South West Corner)
28-29	2	Accelerometer		Longitudinal	
30-32	3	Accelerometer		Vertical	
33-34	2	Accelerometer		Transverse	Top Level of I/R System No.3 (North West Corner)
35-36	2	Accelerometer		Longitudinal	
37-39	3	Accelerometer		Vertical	
40-41	2	Accelerometer		Transverse	Top Level of I/R System No.4 (North East Corner)
42-43	2	Accelerometer		Longitudinal	
44-46	3	Accelerometer		Vertical	
47-49	3	Accelerometer		3 Axes	Center of Shake Table

1. Shown in figure 4-6

Table 4-3 Instrumentation List: Load Cells and Krypton LEDs

Channel #	Quantity	Type	Symbol[1]	Direction	Location
50	1	Load Cell (Shear Force)		Transverse	
51	1	Load Cell (Shear Force)		Longitudinal	
52	1	Load Cell (Axial Load)		Vertical	Load Cell No.1 (South East Corner)
53	1	Load Cell (Moment)		Transverse	
54	1	Load Cell (Moment)		Longitudinal	
55	1	Load Cell (Shear Force)		Transverse	
56	1	Load Cell (Shear Force)		Longitudinal	
57	1	Load Cell (Axial Load)		Vertical	Load Cell No.2 (South West Corner)
58	1	Load Cell (Moment)		Transverse	
59	1	Load Cell (Moment)		Longitudinal	
60	1	Load Cell (Shear Force)		Transverse	
61	1	Load Cell (Shear Force)		Longitudinal	
62	1	Load Cell (Axial Load)		Vertical	Load Cell No.3 (North West Corner)
63	1	Load Cell (Moment)		Transverse	
64	1	Load Cell (Moment)		Longitudinal	
65	1	Load Cell (Shear Force)		Transverse	
66	1	Load Cell (Shear Force)		Longitudinal	
67	1	Load Cell (Axial Load)		Vertical	Load Cell No.4 (North East Corner)
68	1	Load Cell (Moment)		Transverse	
69	1	Load Cell (Moment)		Longitudinal	
70	1	Displacement (Krypton)		3-D[2]	South Face of Chiller
71	1	Displacement (Krypton)		3-D	South Face of Chiller
72	1	Displacement (Krypton)		3-D	South Face of Chiller
73	1	Displacement (Krypton)		3-D	South Face of Chiller
74	1	Displacement (Krypton)		3-D	Top Level of Load Cell No.1
75	1	Displacement (Krypton)		3-D	Top Level of Load Cell No.2
76	1	Displacement (Krypton)		3-D	South Face of Shake Table

1. Shown in figure 4-7
2. 3 Dimensions

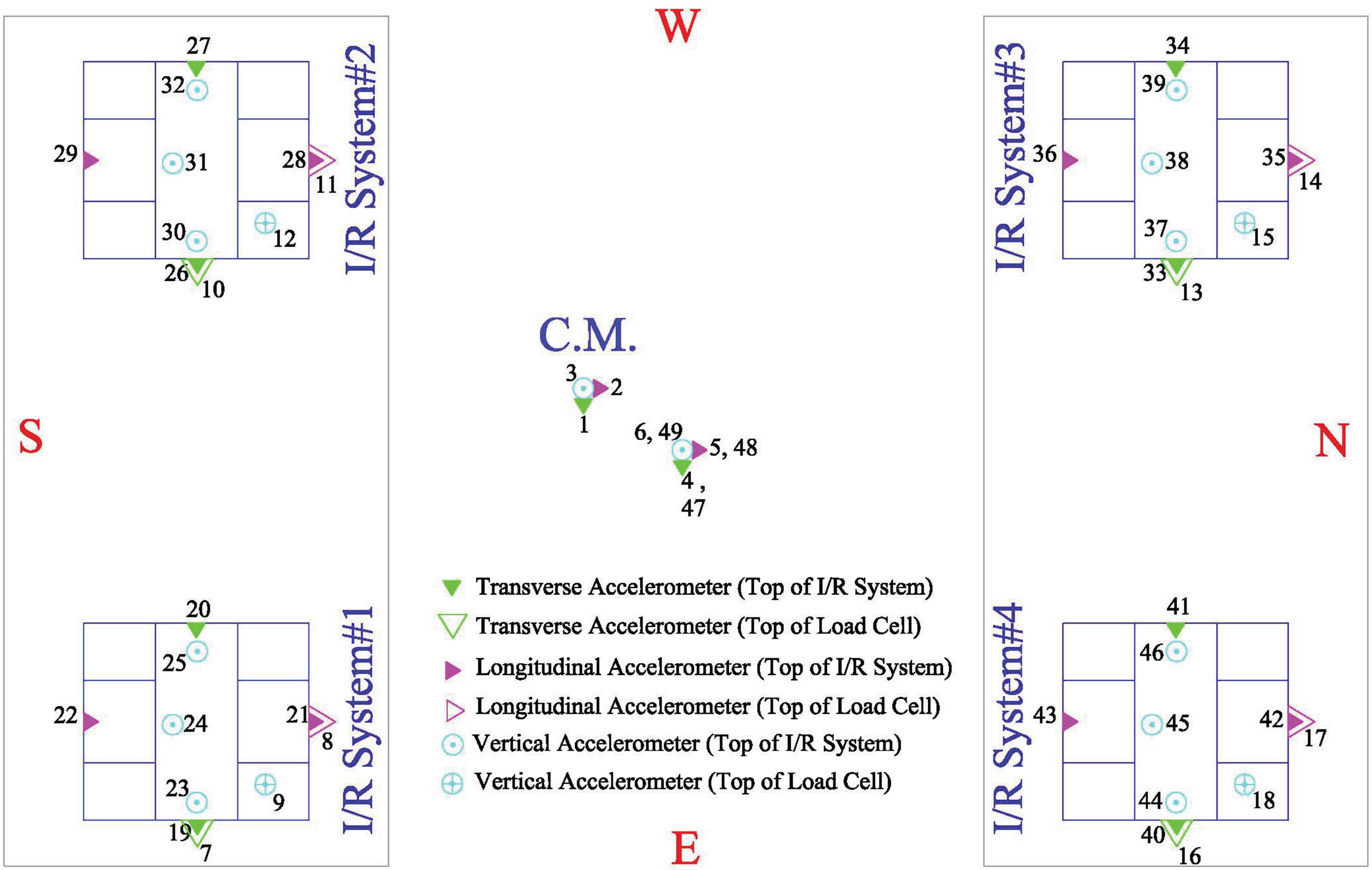

Figure 4-8 Accelerometers Arrangement and Associated Channel Numbers (Plan View)

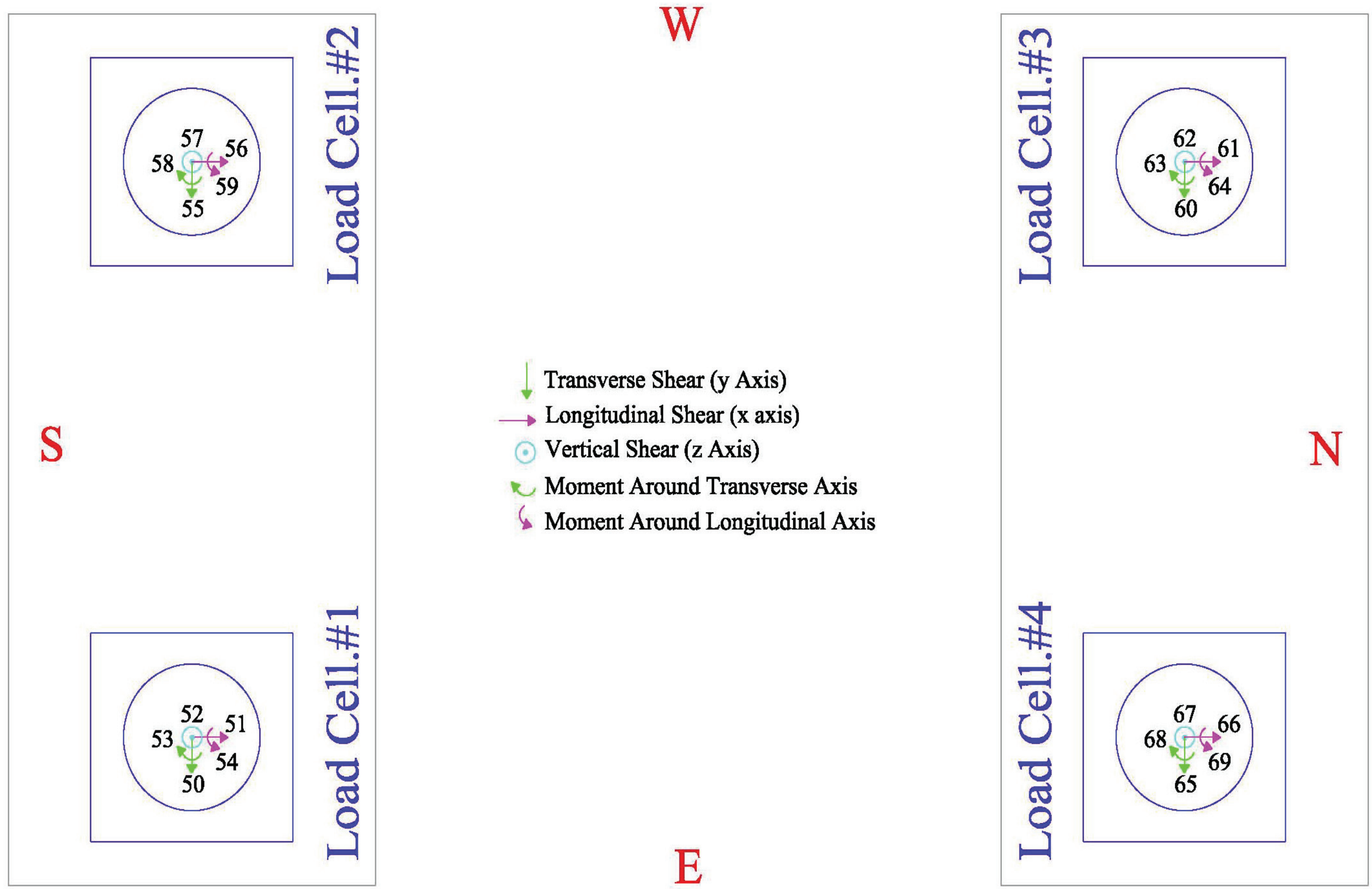

Figure 4-9 Load Cells Arrangement and Associated Channel Numbers (Plan View)

SECTION 5

SHAKE TABLE TESTS

5.1 Test Protocol

The chiller mounted on the I/R systems with different properties and configurations was subjected to a series of seismic and identification tests. The synthetic input motions of the seismic tests were generated based on the AC156 Testing Protocol (ICC-ES, 2004) and the IBC 2003 (ICC, 2003) requirements. The input motions were scaled to simulate various levels of ground or floor motion. In order to monitor the changes in dynamic (modal) properties of the test specimen throughout the experiments, each seismic test was preceded and followed by a tri-axial pulse-type system-identification test. Accelerations, displacements, and forces were measured by the 76 data acquisition channels described earlier in Section 4.

5.2 System-Identification Tests

Pulse-type system-identification tests were conducted before and after each seismic test to establish the dynamic properties (natural frequencies and mode shapes) of the chiller supported by the isolation component of the I/R systems, and to monitor the changes in the modal properties throughout the shake table test program. Since the established dynamic properties were associated to the test specimen supported only by the isolation component of the I/R systems (without engagement of the restraint components), the amplitude of the system-identification tests had to be calibrated to insure that no impact occurred against the snubbers of the restraint component of the I/R systems.

Equation 5-1 presents the desired input acceleration of the pulse tests and figure 5-1 shows the corresponding acceleration time-history for each of the three orthogonal directions, which includes the pulse.

$$a=\begin{cases}(0.05\,sin(20\pi t))g\ ; & t_s\leq t\leq t_s+0.1\\ 0\ ; & t\leq t_s\ or\ t\geq t_s+0.1\end{cases} \tag{5-1}$$

where:

a = input acceleration
g = acceleration due to gravity
t_s = 5 sec. for the transverse direction, 15 sec. for the longitudinal direction, and 25 sec. for the vertical direction

The ten second intervals between the individual pulses in each direction were considered to have the mounted chiller respond to each pulse from an initial at rest condition (no vibration). In other words, it was assumed that the response to the transverse and longitudinal pulses would damp out completely within the ten-second interval. From the response to the pulse in each direction, natural frequencies and mode shapes of the test specimen were established based on the procedure described in Section 6.1.

5.3 Seismic Tests

Based on Section 6.5.1 of the AC156 Testing Protocol (ICC-ES, 2004) and the seismic design requirements specified by the IBC 2003 (ICC, 2003) for architectural, mechanical, electrical, and other nonstructural components connected to building structures, two sets of tri-axial input motion were generated for the seismic tests: one set for the roof level (for the case where the test specimen was mounted

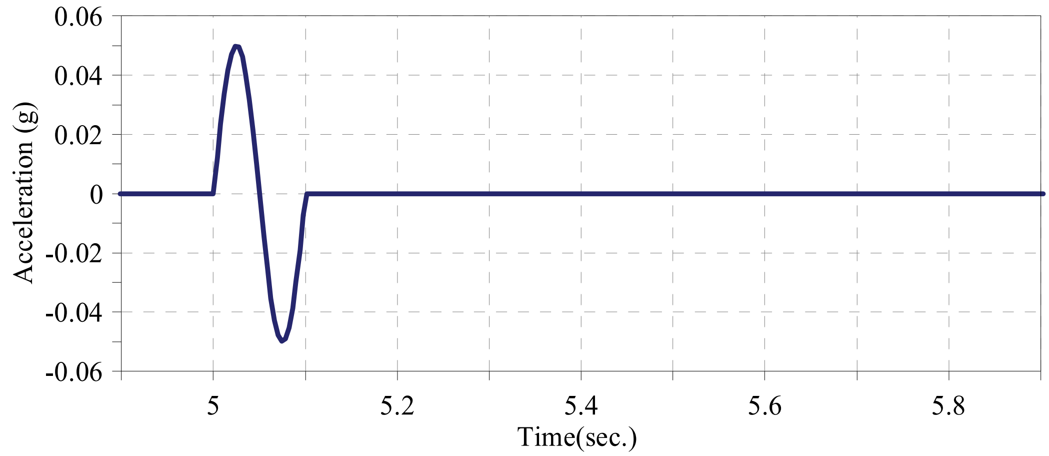

(a) Transverse Direction

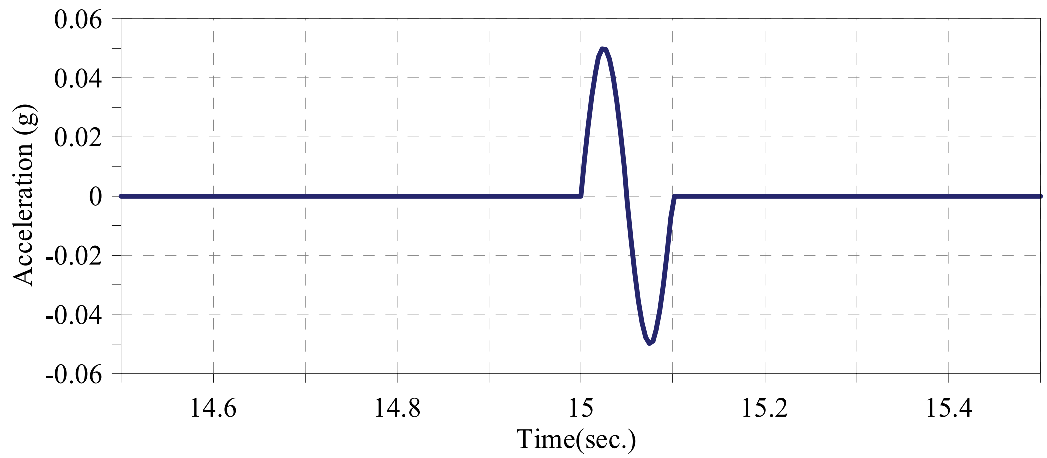

(b) Longitudinal Direction

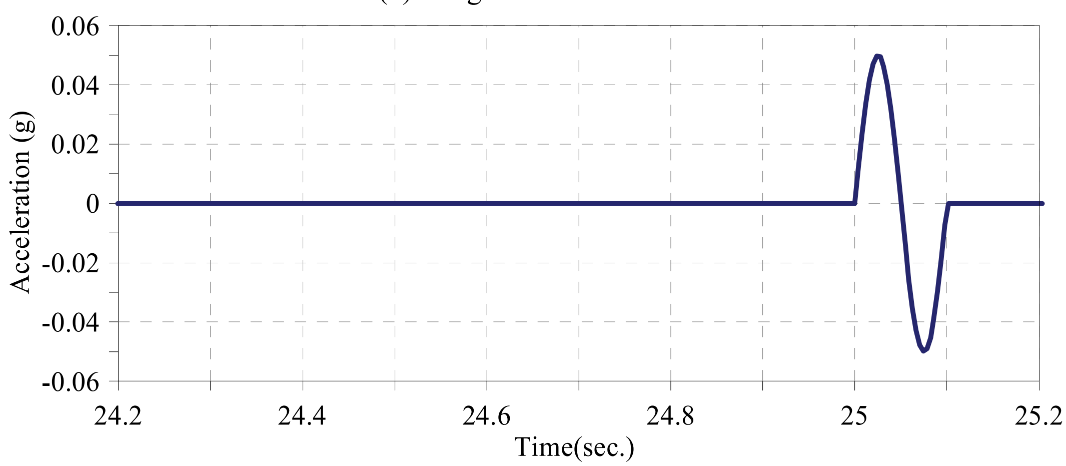

(b) Vertical Direction

Figure 5-1 Tri-axial Input Acceleration for Pulse-Type Identification Test

on the roof level of a structure) and one set for the base level of a building (for the case where the test specimen was mounted on the base level of a structure). It was assumed that the building structure containing the equipment (test specimen) was located on a class D site (according to the IBC 2003) in an area of high seismicity.

The response spectra of the generated input motions should match the required response spectra (RRS) specified by AC156 Testing Protocol (ICC-ES, 2004). Figure 5-2 is a parametric representation of the 5% damped horizontal and vertical required response spectra (RRS). As shown in this figure, for all frequencies, the amplitude of the vertical RRS is two third of the amplitude of the horizontal RSS.

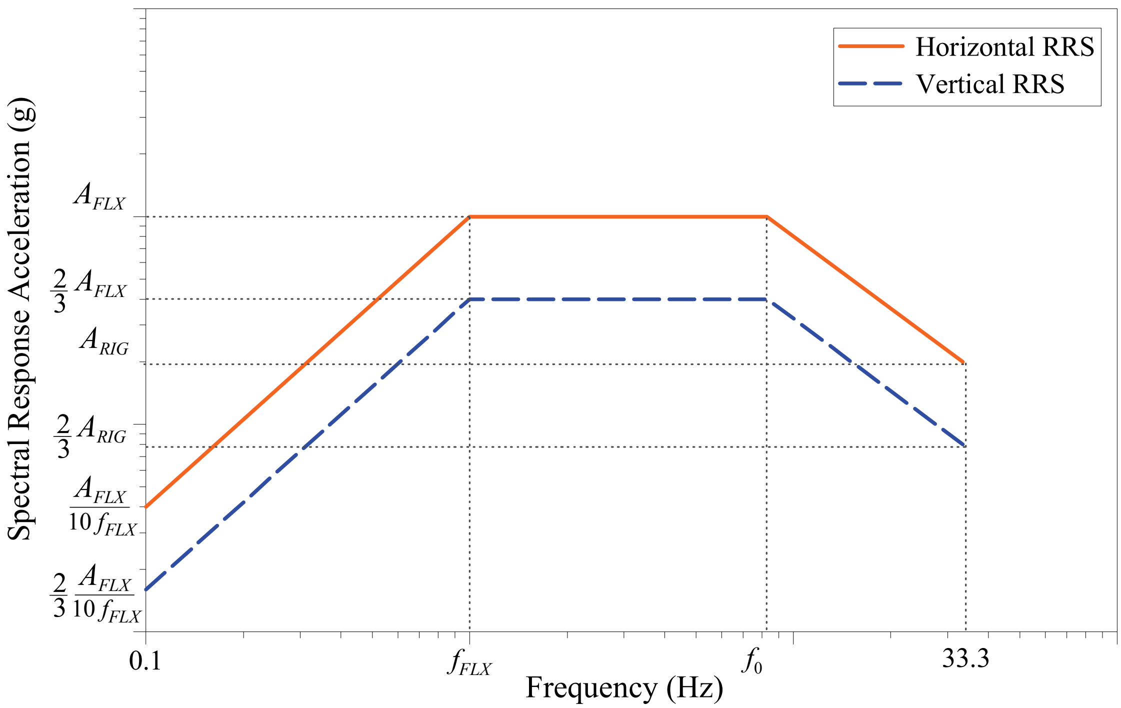

Figure 5-2 Required Response Spectrum (RRS)

According to the IBC 2003 and AC156 Testing Protocol, the horizontal spectral acceleration for a flexible equipment item (A_{FLX}), the horizontal spectral acceleration for a rigid equipment item (A_{RIG}), f_{FLX} , and f_0, shown in figure 5-2, were calculated by the following equations:

$$A_{FLX} = S_{DS}\left(1+2\frac{z}{h}\right) \leq 1.6S_{DS} \tag{5-2}$$

$$A_{RIG} = 0.4S_{DS}\left(1+2\frac{z}{h}\right) \tag{5-3}$$

$$f_{FLX} = \frac{S_{DS}}{S_{D1}\left(1+0.25\frac{z}{h}\right)} \tag{5-4}$$

$$f_0 = \frac{5\,S_{DS}}{S_{D1}} \tag{5-5}$$

where:

A_{FLX} = horizontal spectral acceleration calculated for a flexible equipment item
A_{RIG} = horizontal spectral acceleration calculated for a rigid equipment item
z = height of the level in the structure where the equipment is located with respect to base
h = average roof height of the structure with respect to base
S_{DS} = design 5-percent-damped spectral response acceleration at short period
S_{D1} = design 5-percent-damped spectral response acceleration at a period of one second

The height ratio $\frac{z}{h}$ was zero for the base level (equipment mounted on the base level), and was unity for the roof level (equipment mounted on the roof level). According to Section 1615.1.3 of IBC 2003, for a class D site in an area of high seismicity S_{DS} and S_{D1} were selected equal to 1.0g and 0.6g, respectively. Thus, A_{FLX}, A_{RIG}, f_0, and f_{FLX} were calculated by equations 5-2 through 5-5. Table 5-1 summarizes the values of the parameters required to construct the base and roof level RRS.

Figures 5-3 and 5-4 show the acceleration time-histories of the final tri-axial synthetic input motions for the base and roof level generated to match the corresponding RRS. Figure 5-5 compares the required response spectra (RRS) and the test response spectra (TRS) for the base and roof level input motions. The required response spectra and test response spectra of the generated input motions match quite well in the 0.5 to 10 Hz frequency range that includes all the natural frequencies of the chiller mounted on the I/R system. The sharp decrease of the spectral values for frequencies lower than 0.5 Hz is attributed to the high-pass filter with the 0.5 Hz corner frequency used by the shake table controller to accommodate the displacement capacity of the shake table.

Table 5-2 lists the peak accelerations of the two full-scale synthetic input motions in each of the three directions. As shown earlier in Section 2, the transverse component is associated with the short direction and the longitudinal component is associated with the long direction of the chiller.

Table 5-1 Parameters of Required Response Spectrum for Roof and Base Level

Equipment Location	A_{FLX}	A_{RIG}	f_{FLX}	f_0
Base Level	1.0g	0.4g	1.66 Hz	8.33 Hz
Roof Level	1.6g	1.2g	1.33 Hz	8.33 Hz

Table 5-2 Peak Accelerations of Full Scale Synthetic Input Motions

Synthetic Ground Motion	**Peak Acceleration (g)**		
	Transverse	Longitudinal	Vertical
Base Level	0.47	0.45	0.32
Roof Level	0.80	0.79	0.53

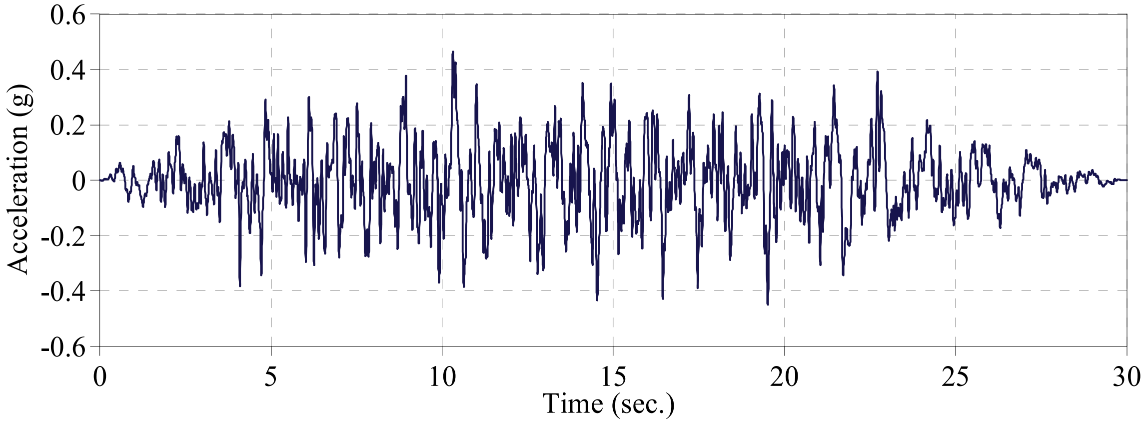

(a) Transverse Direction

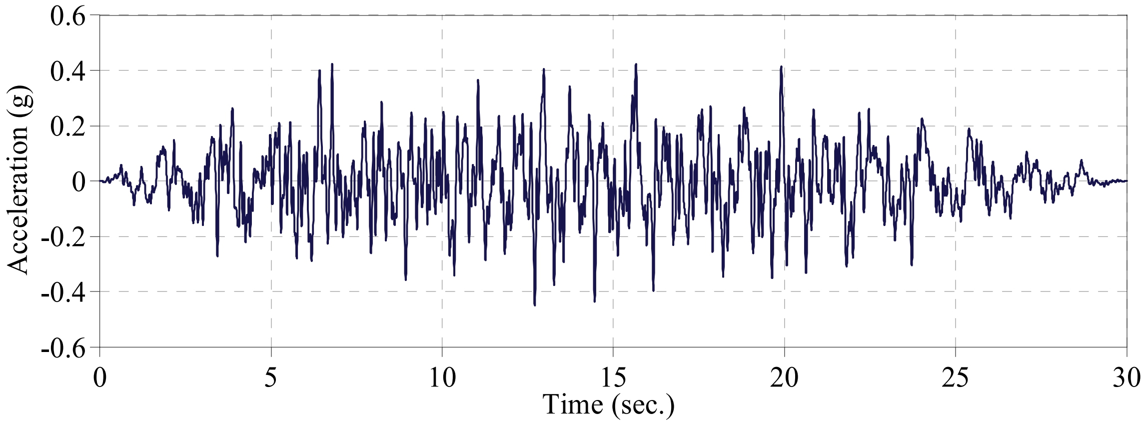

(b) Longitudinal Direction

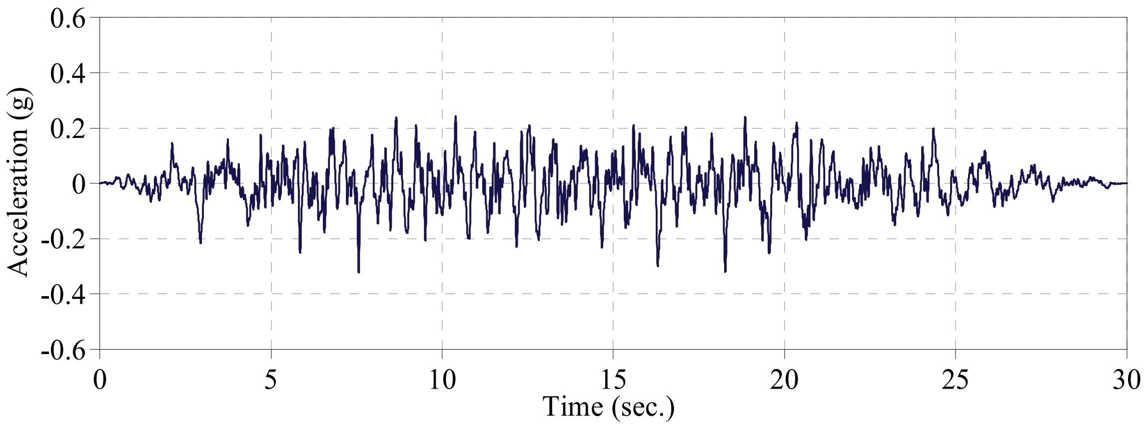

(c) Vertical Direction

Figure 5-3 Synthetic Input Motion for Base Level

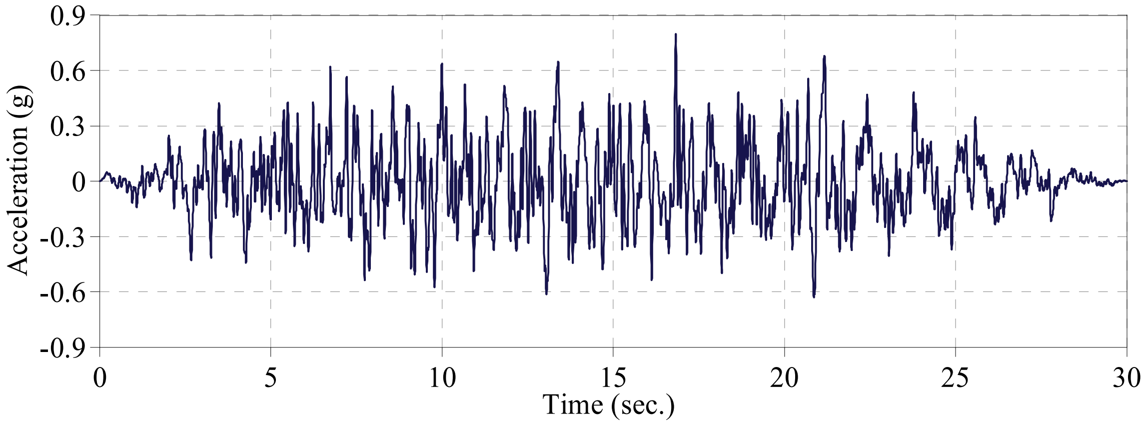

(a) Transverse Direction

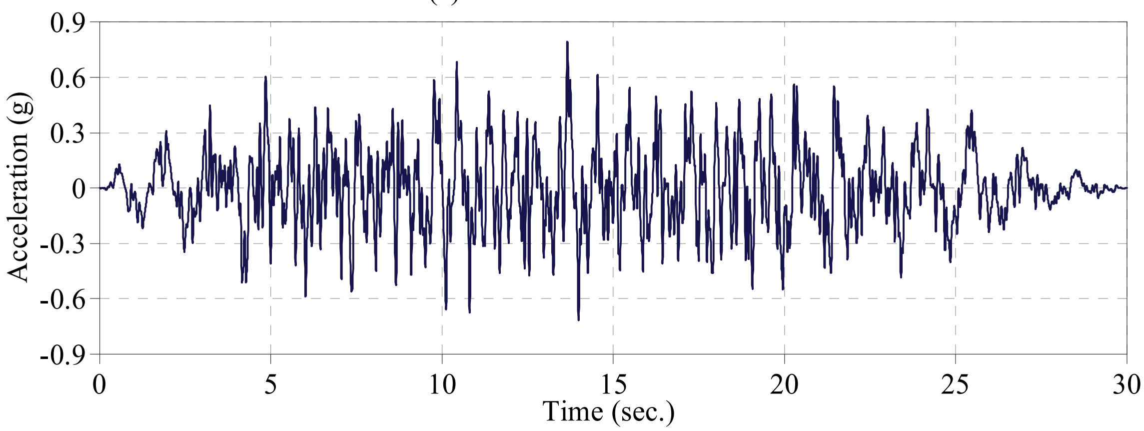

(b) Longitudinal Direction

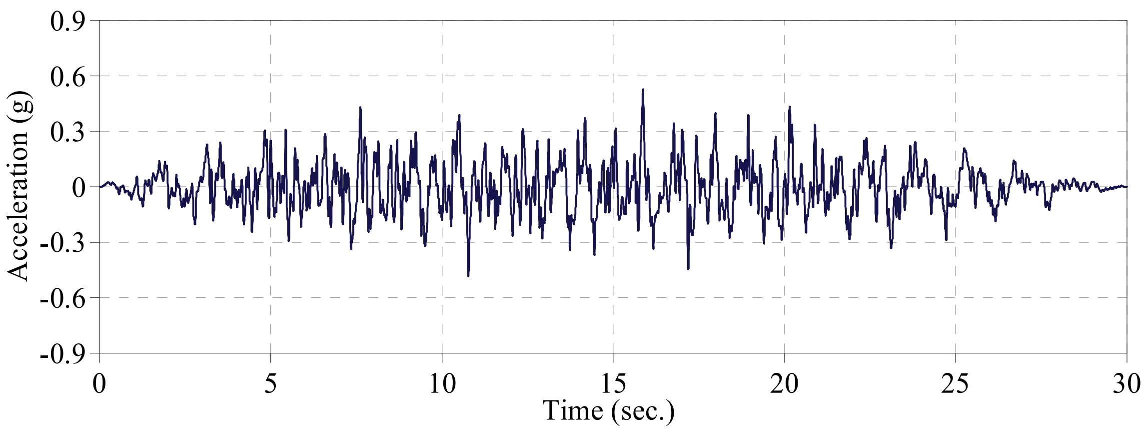

(c) Vertical Direction

Figure 5-4 Synthetic Input Motion for Roof Level

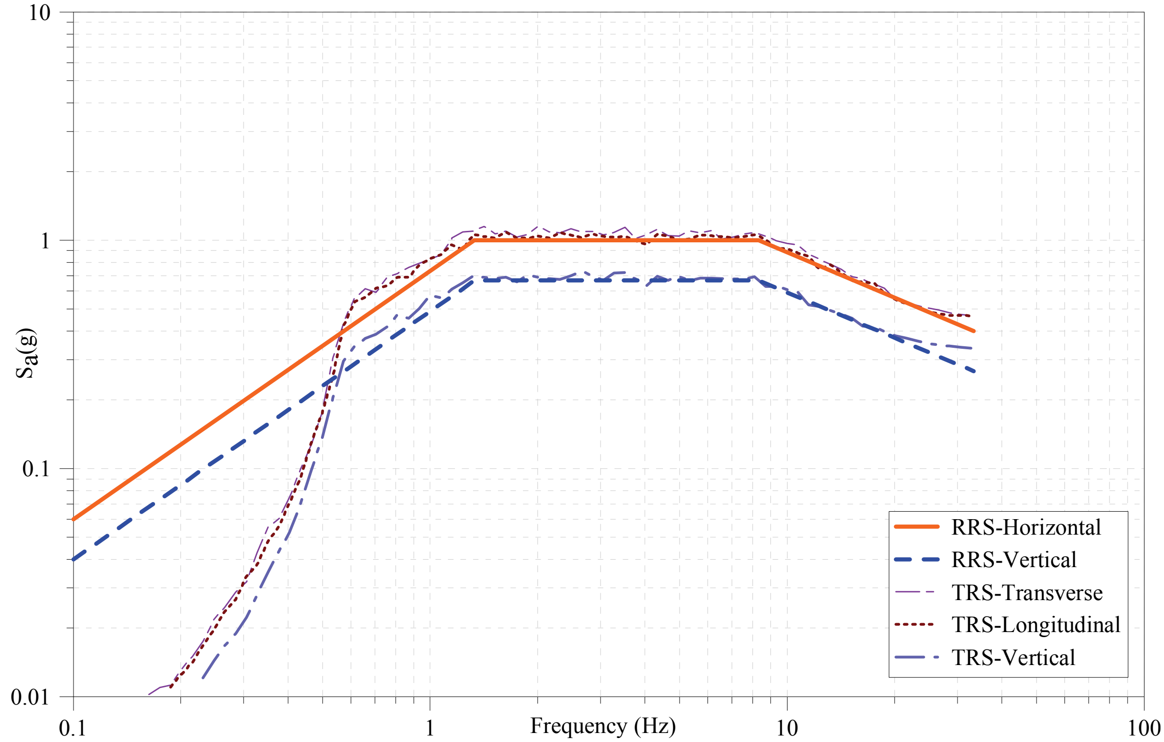

(a) Base Level

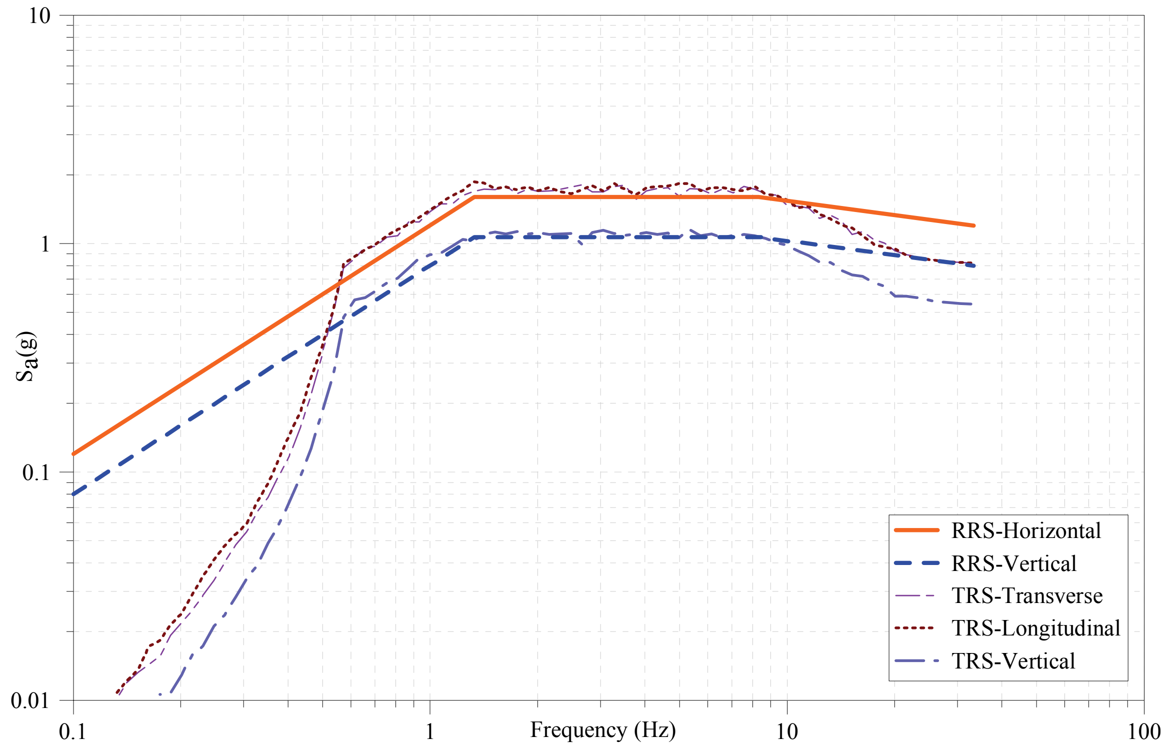

(b) Roof Level

Figure 5-5 Comparison of RRS and TRS for Base and Roof Level Input Motions

5.4 Test Plan

The test plan was elaborated by the authors in collaboration with the ASHRAE Technical Oversight Committee. The test plan initially included twelve different test series. As shown in table 5-3, each test series individually investigated four specific variables: 1) the design of the restraint component 2) the gap size of the restraint component (nominally identical for both of the horizontal and vertical gaps) 3) the thickness of the tubular rubber pads and 4) the hardness of the tubular rubber pads. As indicated in table 5-3, only ten of the twelve test series were conducted. For each test series, the chiller mounted on a specified configuration of the I/R systems was subjected to the two synthetic input motions scaled to different amplitudes (usually 10%, 25%, 50% and 100% of the full scale input motions presented in section 5-3).

Table 5-3 Definition of Seismic Test Series

Test Series No.	Restraint Component Design	Gap (mm [in])	Rubber Pad Thickness (mm [in])	Rubber Pad Hardness (Duro)	Test Date	Note
1	1.0 g	3 [1/8]	6 [1/4]	60	—	Not performed
2	1.0 g	6 [1/4]	6 [1/4]	60	12/12/2005	—
3	1.0 g	13 [1/2]	6 [1/4]	60	—	Not performed
4	3.0 g	3 [1/8]	6 [1/4]	60	12/14/2005	—
5	3.0 g	6 [1/4]	6 [1/4]	60	12/15/2005	—
6	3.0 g	13 [1/2]	6 [1/4]	60	01/06/2006	—
7	3.0 g	6 [1/4]	3 [1/8]	60	12/14/2005	—
8	3.0 g	6 [1/4]	13 [1/2]	60	01/06/2006	—
9	3.0 g	6 [1/4]	6 [1/4]	50	12/15/2005	—
10	1.0 g	11 [7/16]	19 [3/4]	60	12/12/2005	—
11	3.0 g	6 [1/4]	6 [1/4]	60	01/05/2006	Repeat of Test Series 9 and 5 with holes in base plates
12	3.0 g	6 [1/4]	6 [1/4]	50	01/05/2006	

The sequence of all seismic tests conducted in this project is presented in table 5-4. For brevity, the system-identification tests (see Section 5-2) have been omitted from this table. As mentioned previously, the experiments started with one identification test (just before TS10-S1) and each seismic test presented in table 5-4 was followed by one identification test. Therefore, a total of 73 identification tests and 72 seismic tests were conducted throughout the ten test series.

Table 5-4 Seismic Test Sequence

Test #	Test ID[1]	Restraint Component Design	Gap[2] (mm [in])	Tubular Rubber Pad		Input Motion	
				Thickness (mm [in])	Hardness (Duro)	Amplitude	Level
1	TS10-S1	1.0 g	11 [7/16]	19 [3/4]	60	10%	Base
2	TS10-S1a					10%	Roof
3	TS10-S2					25%	Base
4	TS10-S3					25%	Roof
5	TS10-S4					50%	Base
6	TS2-S1	1.0 g	6 [1/4]	6 [1/4]	60	10%	Base
7	TS2-S1a					10%	Roof
8	TS2-S2					25%	Base
9	TS2-S3					25%	Roof
10	TS2-S4					50%	Base
11	TS2-S5					50%	Roof
12	TS2-S6					100%	Base
13	TS2-S7					100%	Roof
14	TS2-S8					150%	Roof
15	TS2-S8a					150%	Roof
16	TS4-S1	3.0 g	3 [1/8]	6 [1/4]	60	10%	Roof
17	TS4-S3					25%	Roof
18	TS4-S5					50%	Roof
19	TS4-S7					100%	Roof
20	TS4-S8					100%	Roof
21	TS7-S1	3.0 g	6 [1/4]	3 [1/8]	70	10%	Roof
22	TS7-S3					25%	Roof
23	TS7-S5					50%	Roof
24	TS7-S7					100%	Roof

Table 5-4 (cont'd) Seismic Test Sequence

Test #	Test ID	Restraint Component Design	Gap (mm [in])	Tubular Rubber Pad		Input Motion	
				Thickness (mm [in])	Hardness (Duro)	Amplitude	Level
25	TS5-S1	3.0 g	6 [1/4]	6 [1/4]	60	10%	Base
26	TS5-S1a					10%	Roof
27	TS5-S2					25%	Base
28	TS5-S3					25%	Roof
29	TS5-S4					50%	Base
30	TS5-S5					50%	Roof
31	TS5-S6					100%	Base
32	TS5-S7					100%	Roof
33	TS9-S1	3.0 g	6 [1/4]	6 [1/4]	50	10%	Base
34	TS9-S1a					10%	Roof
35	TS9-S2					25%	Base
36	TS9-S3					25%	Roof
37	TS9-S4					50%	Base
38	TS9-S5					50%	Roof
39	TS9-S6					100%	Base
40	TS9-S7					100%	Roof
41	TS12-S1	3.0 g (Modified)[3]	6 [1/4]	6 [1/4]	50	10%	Base
42	TS12-S1a					10%	Roof
43	TS12-S2					25%	Base
44	TS12-S3					25%	Roof
45	TS12-S4					50%	Base
46	TS12-S5					50%	Roof
47	TS12-S6					100%	Base
48	TS12-S7					100%	Roof

Table 5-4 (cont'd) Seismic Test Sequence

Test #	Test ID	Restraint Component Design	Gap (mm [in])	Tubular Rubber Pad		Input Motion	
				Thickness (mm [in])	Hardness (Duro)	Amplitude	Level
49	TS11-S1	3.0 g (Modified)	6 [1/4]	6 [1/4]	60	10%	Base
50	TS11-S1a					10%	Roof
51	TS11-S2					25%	Base
52	TS11-S3					25%	Roof
53	TS11-S4					50%	Base
54	TS11-S5					50%	Roof
55	TS11-S6					100%	Base
56	TS11-S7					100%	Roof
57	TS6-S1	3.0 g (Modified)	13 [1/2]	6 [1/4]	60	10%	Base
58	TS6-S1a					10%	Roof
59	TS6-S2					25%	Base
60	TS6-S3					25%	Roof
61	TS6-S4					50%	Base
62	TS6-S5					50%	Roof
63	TS6-S6					75%	Base
64	TS6-S7					75%	Roof
65	TS8-S1	3.0 g (Modified)	6 [1/4]	13 [1/2]	60	10%	Base
66	TS8-S1a					10%	Roof
67	TS8-S2					25%	Base
68	TS8-S3					25%	Roof
69	TS8-S4					50%	Base
70	TS8-S5					50%	Roof
71	TS8-S6					100%	Base
72	TS8-S7					100%	Roof

1. Test Identification
2. For both the horizontal and vertical gaps
3. See Section 5.6 for details

5.5 Test Setup

The installation of the test setup was initiated by bolting two $275 \times 152 \times 5\,\text{cm}\,(108 \times 60 \times 2\,\text{in})$ steel plates to the shake table extension. Then, the load cells were bolted to the steel plates. Figure 5-6 shows the required dimensions to install the steel plates and the load cells. Then, the I/R systems were assembled and bolted to the load cells such that the orientation of the isolation component of the I/R systems be parallel to the transverse direction of the chiller. Thereafter, the chiller was mounted on top of the I/R systems. Finally, at each corner of the chiller, the top plate of the isolation and restraint component and the base plate of the chiller were all tied together by four grade 8 bolts. The sequence of the installation of the test setup is illustrated in figures 5-7(a) through 5-7(d).

Once the chiller was mounted on and bolted to the I/R systems, the leveling bolts that pass through the center of the coil springs and the two nuts on the rods of the restraint component were adjusted to provide the required vertical gaps in the restraint component according to the test plan requirements (figure 5-6(e)).

In order to modify the properties of the restraint component of the I/R systems between test series, as illustrated in figure 5-7(f), the restraint components were unbolted from the isolation components and sled out of the I/R systems. Modifications of the restraint component such as changing the tubular rubber pad and/or the steel bushing (figure 5-7(g)) could then take place. The modified restraint components could then be sled back into the I/R systems and bolted again to the I/R systems and to the chiller. At the end, the vertical gaps were adjusted according to the test plan.

The accelerometers and the other instrumentations were installed in the locations that were not affected by the modifications in the restraint components. However, between Test Series TS2 and TS4, the accelerometers above the top level of the load cells had to be detached and re-installed again. For reconfiguring the test setup from Test Series TS2 to Test Series TS4, as illustrated in figure 5-7(h), the whole I/R systems had to be changed. For that purpose, the chiller was mounted off the table and the 1.0 g design I/R systems were dismantled and replaced by the 3.0 g design I/R systems.

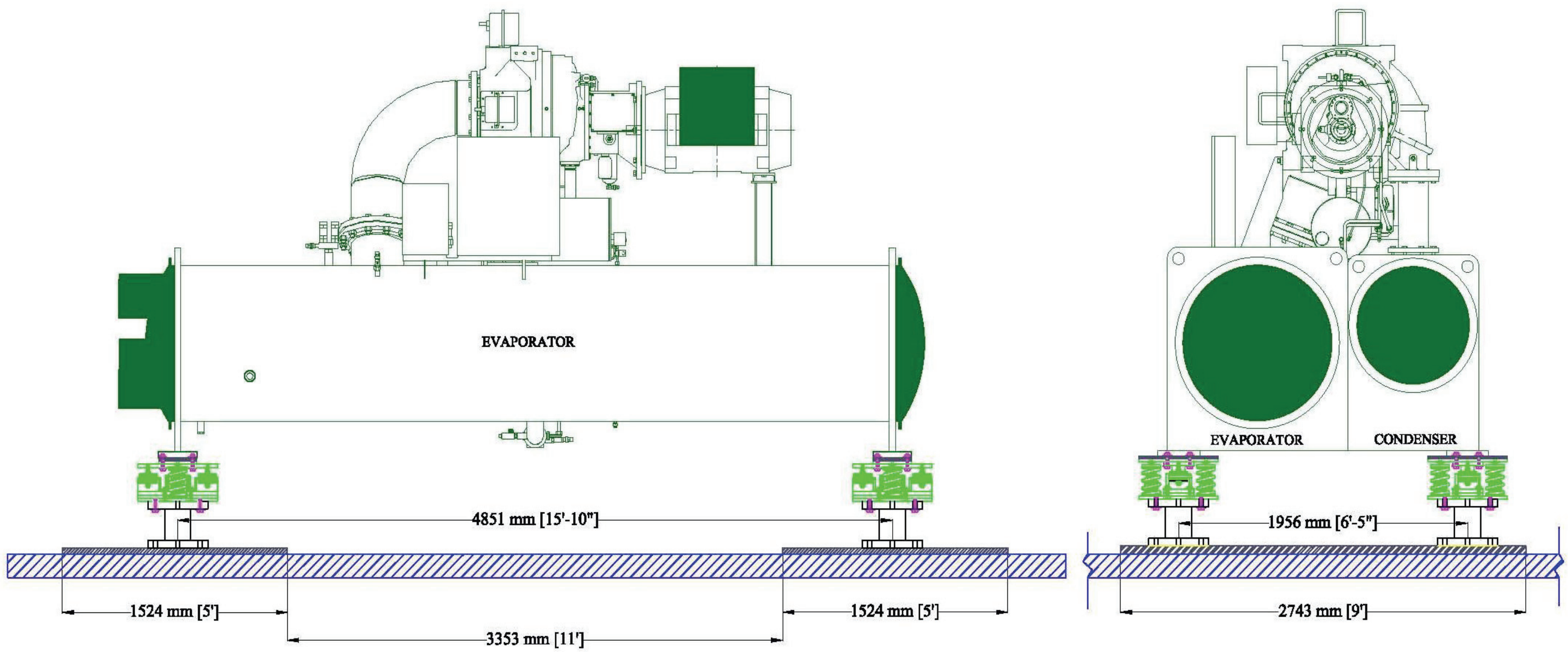

Figure 5-6 Dimensions Required for Test Setup

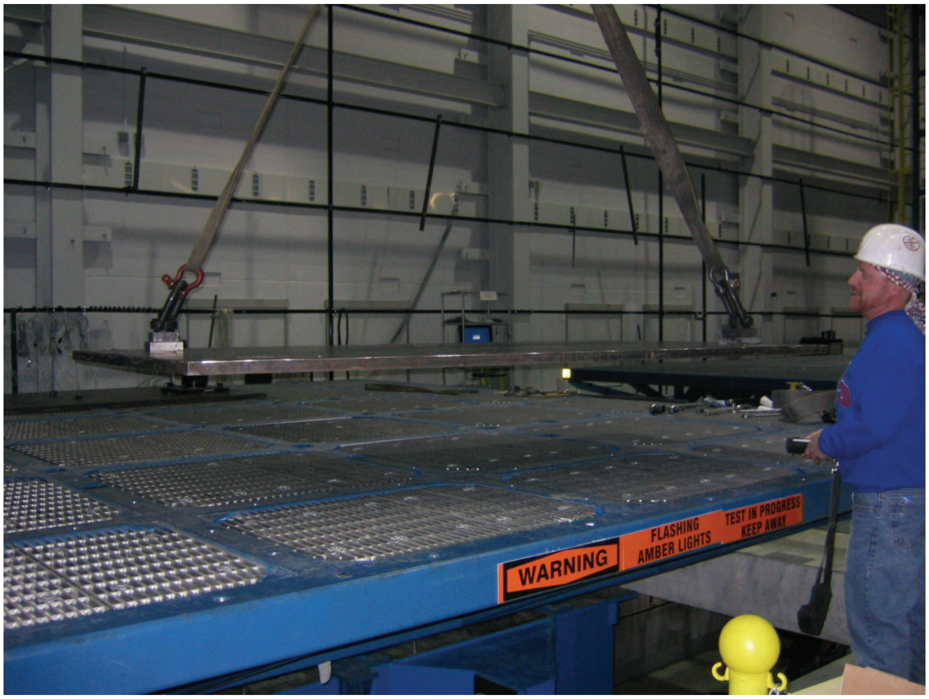

(a) 275×152×5 cm (108×60×2 in) Steel Plate Interfacing Load Cells and Table Extension

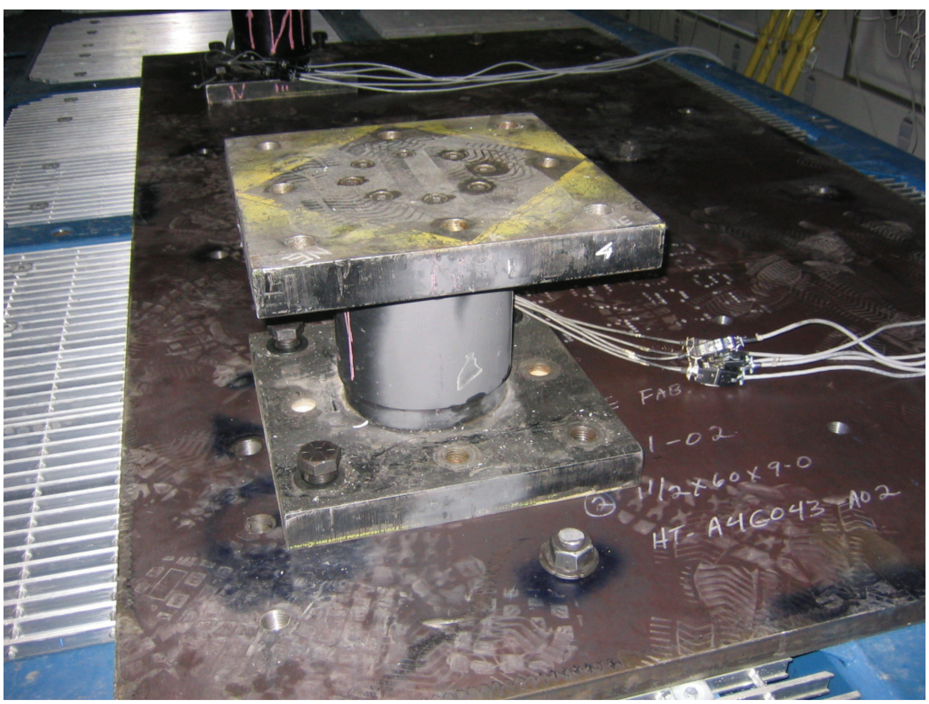

(b) Load Cells Bolted to Interfacing Plates

Figure 5-7 Test Setup Procedure

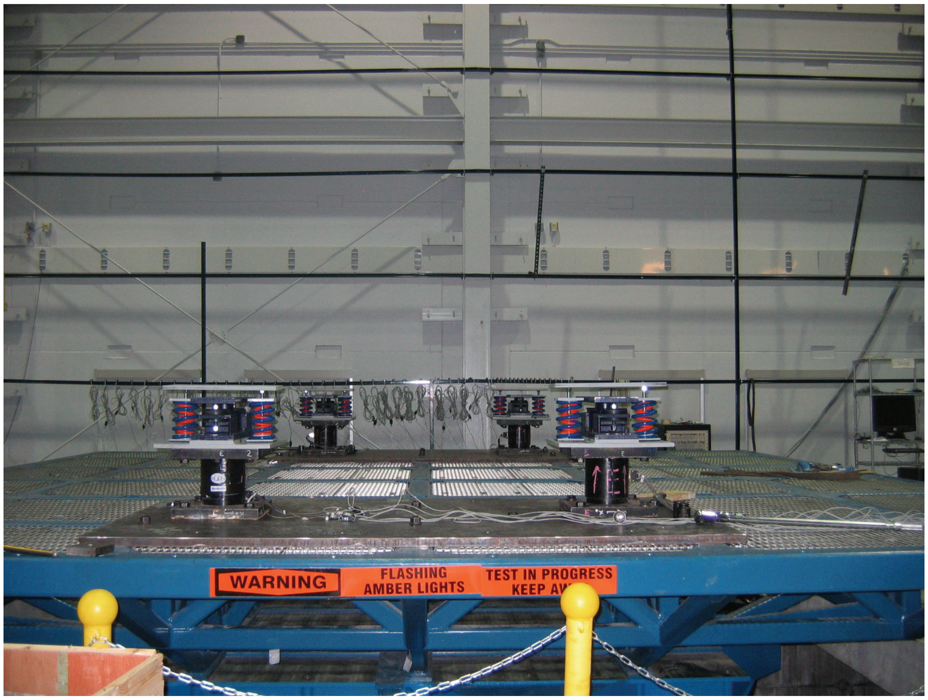

(c) I/R Systems Bolted to Load Cells

(d) Chiller Mounted on I/R Systems

Figure 5-7 (cont'd) Test Setup Procedure

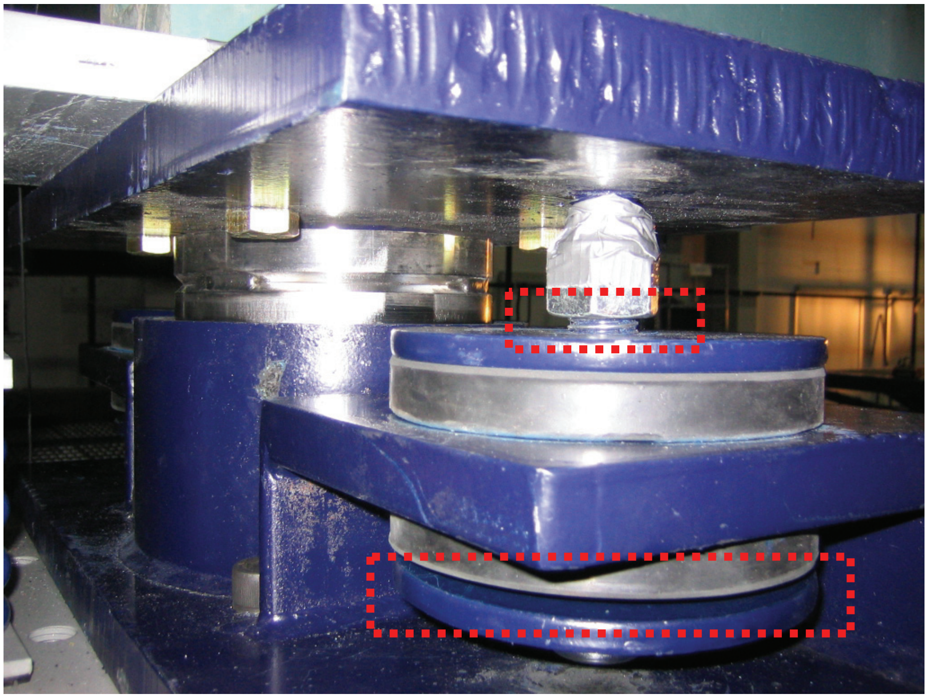

(e) Adjusting Vertical Gaps

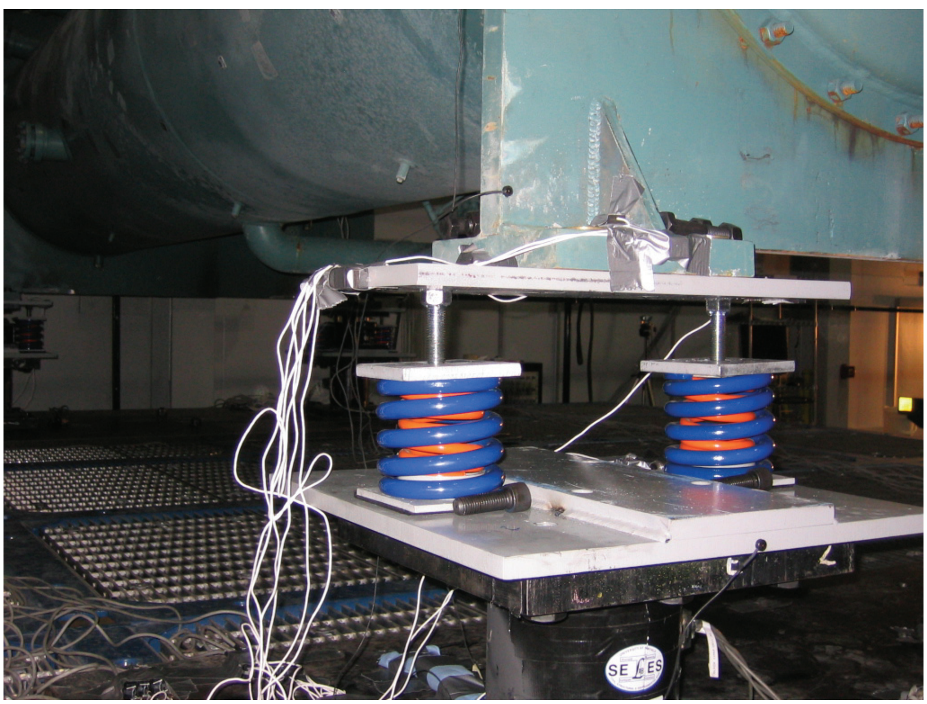

(f) Sliding Restraint Components out of I/R System for Modifications

Figure 5-7 (cont'd) Test Setup Procedure

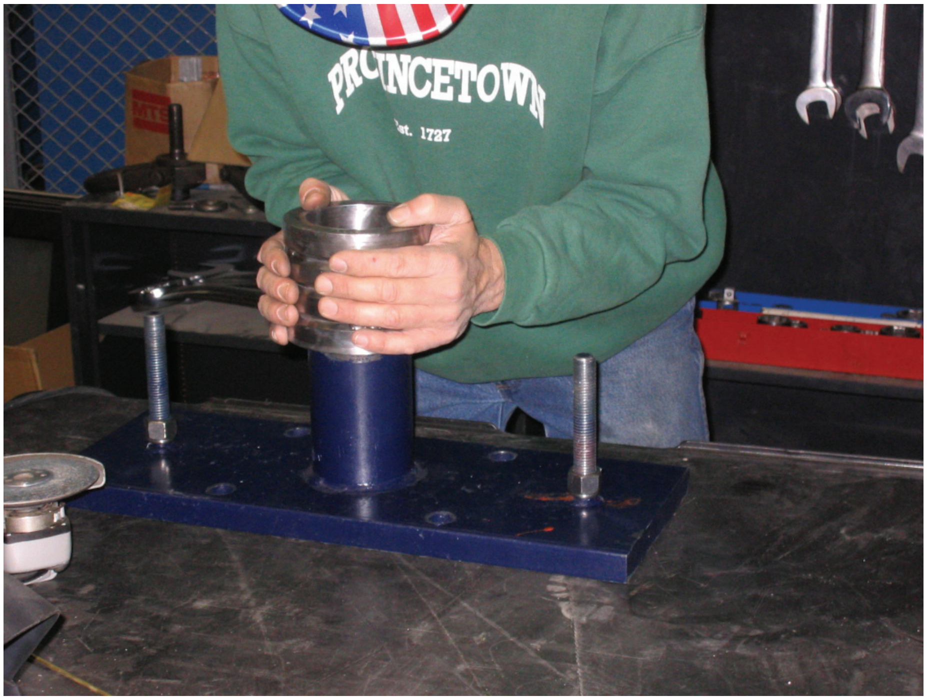

(g) Changing Steel Bushing to Adjust Horizontal Gap

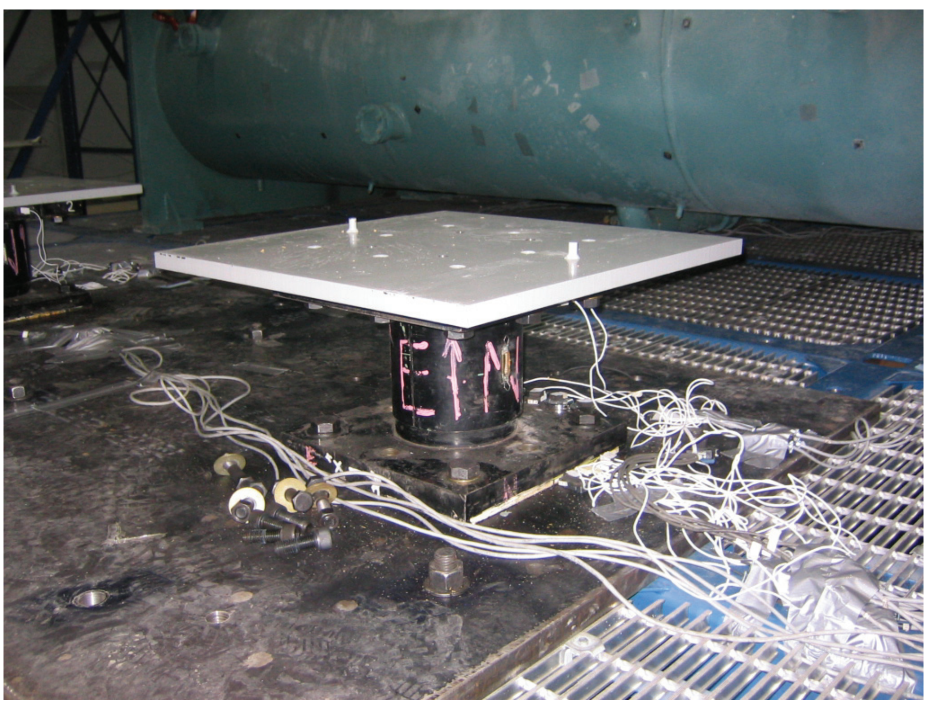

(h) Changing I/R Systems from 1.0 g Design to 3.0 g Design (between Test Series TS2 and TS4)

Figure 5-7 (cont'd) Test Setup Procedure

5.6 Isolation/Restraint System Installation Issues

Several installation issues affected the seismic response of the I/R systems. In particular, the three main issues that significantly affected the response are described in this section.

1) As described earlier and shown in figure 5-8(a), the horizontal gap of the I/R system is located in the hoop space left between the inner steel pipe (or the circumscribing steel bushing around it) and the tubular rubber pad. Theoretically, the inner steel pipe and the tubular rubber pad are coaxial, but in practice after mounting the chiller on top of the four I/R systems, the horizontal gaps in the restraint component of the I/R systems were not always uniform. In some of the test series with small nominal gap size, the offset between the axes of the tubular rubber pad and the inner steel pipe was larger than the nominal gap size and, therefore, the inner steel pipe was in contact with the tubular rubber pad, as illustrated in figure 5-8(b). In some cases throughout the test series, as the result of the severe shaking and impacts, the contact inside the restraint component was decreased or eliminated as shown in figure 5-8(c).

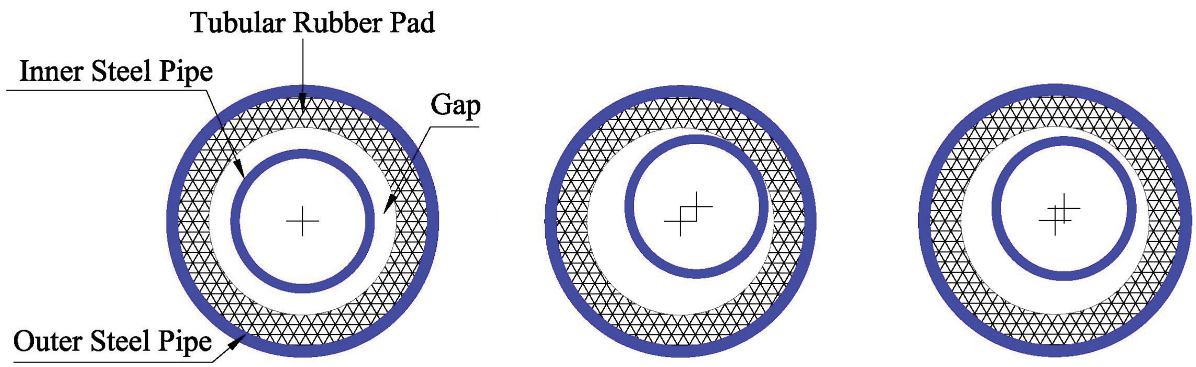

(a) Theoretical Configuration (Uniform Gap) (b) Practical Configuration (Offset with Contact) (c) Practical Configuration (Offset without Contact)

Figure 5-8 Horizontal Gap in At-Rest Condition after Installation (Top View)

2) Throughout Test Series TS5 and TS9 it was observed that after adjusting the vertical gaps at 6 mm (1/4 in), the distance left between the bottom nuts and the base plates had been smaller than the nominal gap size. Consequently, in the compression direction before the top nuts could hit the steel washer, the bottom nuts impacted with the base plate. In other words, in those two test series, the vertical restraint components were not working properly in one direction. The impacts between the bottom nuts and the base plates introduced large vertical acceleration responses to the chiller and, as shown in figure 5-9(a), slightly damaged the base plates.

To solve this problem and provide sufficient travel distance for the bottom nuts, two 51 mm (2 in) diameter holes were torched in the base plates of the 3.0 g design I/R systems, as shown in figure 5-9(b). The centers of the holes were aligned with the center of the grommets (axes of the rods). Figure 5-9(c) shows photographs of the modified 3.0 g design I/R systems.

Test Series TS12 and TS11 with the same specification assigned for the I/R systems tested in Test Series TS9 and TS5, respectively, were conducted to investigate the effect of the modification in the 3.0 g design I/R systems.

3) For Test Series TS7, the 3 mm (1/8 in) thick tubular rubber pads were formed by rolling two layers of 1.5 mm (1/16 in) thick rubber strips, as shown in figure 5-9. Initially only the tubular rubber pads with hardness of 50 or 60 Duro were included in the test plan, but in the laboratory, the hardness of the rolled rubber strips was measured as 70 Duro.

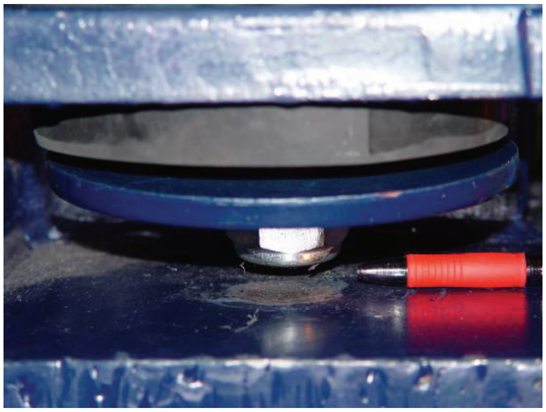

(a) Impacts of Bottom Nuts Damaging Base Plate

(b) Torching Holes in Base Plate

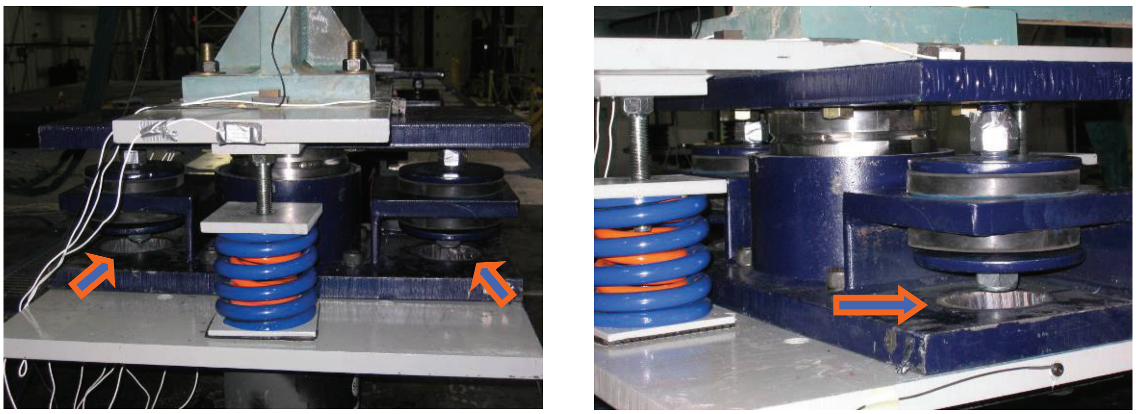

(c) Modified 3.0 g Design I/R Systems

Figure 5-9 Modification of 3.0 g Design I/R Systems

(a) 1.6 mm (1/16 in) Thick Rubber Role (Left) Cut to Strips (Right)

(b) Rubber Strips Rolled inside Pipe to Form Tubular Rubber Pad

Figure 5-10 Forming 3 mm (1/8 in) Thick Tubular Rubber Pad from 1.5 mm (1/16 in) Rubber Strips with 70 Duro Hardness for Test Series TS7

SECTION 6

TEST RESULTS

6.1 Dynamic Characteristics of Test Specimen Mounted on Isolation/Restraint Systems

The experimental study by Wanitkorkul and Filiatrault (2005) had shown that the first three modes of the same chiller in wet condition (full of water and refrigerant) and rigidly mounted to the floor had natural frequencies of 8.2, 8.5 and 10.0 Hertz (Hz) and were associated with the longitudinal, transverse, and vertical directions, respectively. Preliminary analyses based on the predicted mechanical properties of the isolation component of the I/R systems (coil springs) and mass of the chiller in wet condition predicted that, without engagement of the restraint component of the I/R systems (no impact), the chiller mounted on the I/R systems could be considered as a rigid body supported by four tri-axial flexible spring-dashpot elements.

Each point of the chiller mounted on the flexible elements has six degrees of freedom: one translational and one rotational degree of freedom for each of the transverse, longitudinal, and vertical directions. As a rigid body, the motions of all the points on the chiller can be related to each other by geometry-based kinematics equations. In other words, defining the motions of the six degrees of freedom at any point of the chiller (a reference point) along with the geometry-based kinematics equations can fully define the motion of the whole chiller. In this study, the center of mass of the chiller was selected as the reference point. Figure 6-1 shows the six reference degrees of freedom at the center of mass of the chiller.

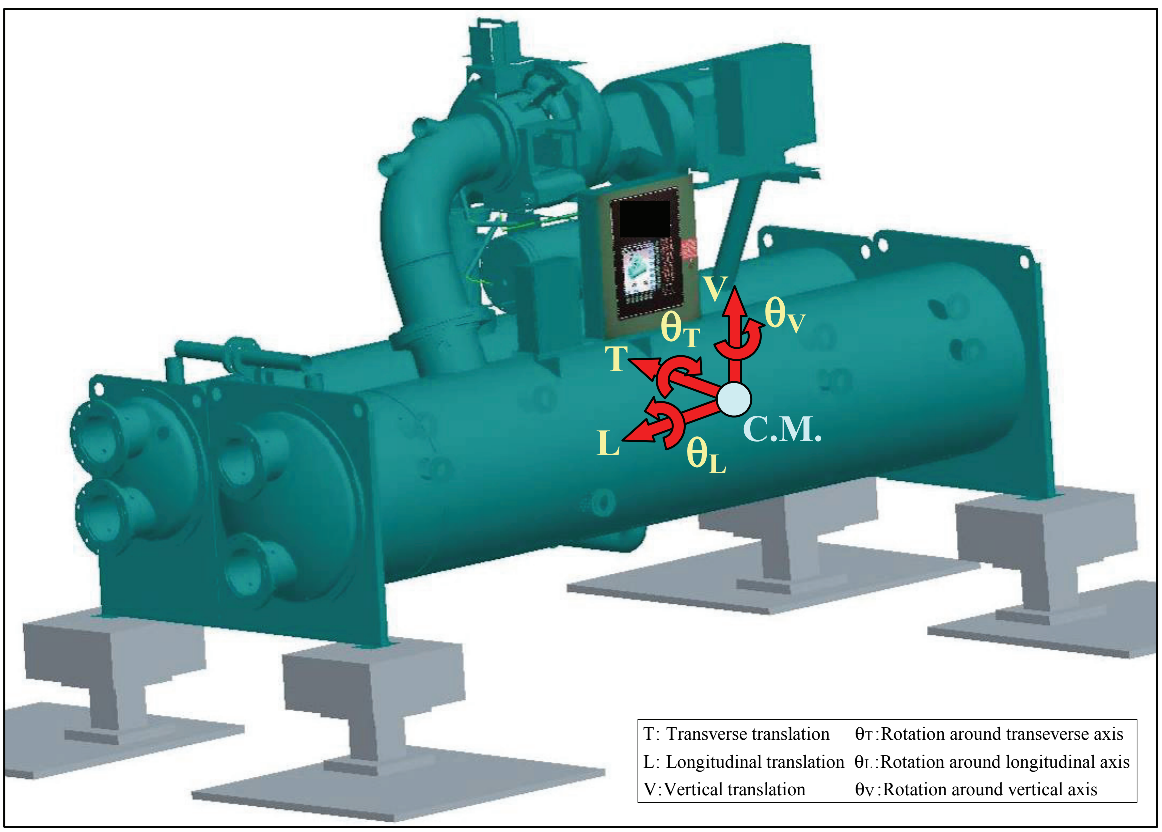

Figure 6-1 Six Reference Degrees of Freedom at Center of Mass of Chiller

The response of the chiller mounted on four I/R systems to any input motion can be fully described by the responses of the six degrees of freedom at the center of mass of the chiller, which were composed of the contribution of the six fundamental modal responses.

Each mode of vibration has a specific frequency, shape, and equivalent viscous damping ratio. In this section, the six natural frequencies and mode shapes of the test specimen supported by the isolation component of the I/R systems are established by processing the data obtained from the system-identification tests. In Section 6.2, the modal equivalent viscous damping ratios of the first three modes of vibration are estimated by processing the data obtained from the seismic tests.

The contribution of the six modal responses to the total displacement response of the six degrees of freedom at the center of mass of the chiller is represented by:

$$u(t)=\{T(t),L(t),V(t),\theta_T(t),\theta_L(t),\theta_V(t)\}^T=\sum_{n=1}^{6}\phi_n q_n(t) \tag{6-1}$$

$$\phi_n=\{T_n,L_n,V_n,\theta_{T_n},\theta_{L_n},\theta_{V_n}\}^T \tag{6-2}$$

where:

- $u(t)$ = displacement response vector at the center of mass of the chiller
- $T(t)$ = translational displacement response at the center of mass of the chiller at time t with respect to the transverse axis
- $L(t)$ = translational displacement response at the center of mass of the chiller at time t with respect to the longitudinal axis
- $V(t)$ = translational displacement response at the center of mass of the chiller at time t with respect to the vertical axis
- $\theta_T(t)$ = rotational displacement response at the center of mass of the chiller at time t around the transverse axis
- $\theta_L(t)$ = rotational displacement response at the center of mass of the chiller at time t around the longitudinal axis
- $\theta_V(t)$ = rotational displacement response at the center of mass of the chiller at time t around the vertical axis
- ϕ_n = the n^{th} mode shape
- n = 1,2,…,6
- T_n = translational displacement at the center of mass of the chiller in the n^{th} mode shape with respect to the transverse axis
- L_n = translational displacement at the center of mass of the chiller in the n^{th} mode shape with respect to the longitudinal axis
- V_n = translational displacement at the center of mass of the chiller in the n^{th} mode shape with respect to the vertical axis
- θ_{T_n} = rotational displacement at the center of mass of the chiller in the n^{th} mode shape around transverse axis
- θ_{L_n} = rotational displacement at the center of mass of the chiller in the n^{th} mode shape around the longitudinal axis
- θ_{V_n} = rotational displacement at the center of mass of the chiller in the n^{th} mode around the vertical axis
- $q_n(t)$ = time variant coefficient of the n^{th} mode

For a free vibration, the time variant coefficient of the n^{th} mode, $q_n(t)$, is defined by the following four equations (Chopra, 2000):

$$q_n(t)=e^{-\zeta_n\omega_n t}\left[q_n(0)\cos\omega_{nD}t+\frac{\dot{q}_n(0)+\zeta_n\omega_n q_n(0)}{\omega_{nD}}\sin\omega_{nD}t\right] \tag{6-3}$$

$$q_n(0)=\frac{\phi_n^T M u(0)}{\phi_n^T M \phi_n} \tag{6-4}$$

$$\dot{q}_n(0)=\frac{\phi_n^T M \dot{u}(0)}{\phi_n^T M \phi_n} \tag{6-5}$$

$$\omega_{nD}=\omega_n\sqrt{1-\zeta_n^2} \tag{6-6}$$

where:

ζ_n = equivalent viscous damping ratio of the n[th] mode
ω_n = undamped natural frequency of the n[th] mode
M = 6×6 global mass matrix of the chiller
ω_{nD} = damped natural frequency of the n[th] mode

For a free vibration starting from an at rest condition $(u(0)=\{0,0,0,0,0,0\}^T)$, according to equation 6-4:

$$q_n(0)=0 \tag{6-7}$$

Substituting equations 6-3 and 6-7 into equation 6-1 yields:

$$u(t)=\sum_{n=1}^{6}\phi_n e^{-\zeta_n\omega_n t}\left[\frac{\dot{q}_n(0)}{\omega_{nD}}\sin\omega_{nD}\,t\right] \tag{6-8}$$

For lightly damped modes ($\zeta_n \leq 10\%$) equation 6-6 indicates that the undamped and damped natural frequencies are almost equal and in equation 6-7, ω_{nD} can be replaced by ω_n :

$$u(t)=\sum_{n=1}^{6}\phi_n e^{-\zeta_n\omega_n t}\left[\frac{\dot{q}_n(0)}{\omega_n}\sin\omega_n\,t\right] \tag{6-9}$$

Equation 6-9 describes that the displacement response at the center of mass of the chiller in free vibration is a linear combination of six damped sinusoidal responses. Figure 6-2(a) is a schematic representation of a damped sinusoidal response defined by its frequency (ω_1), amplitude (A_0), and damping factor (B).

The second derivative of a damped sine wave is also a damped sine wave with the same frequency. Therefore, based on equation 6-9, the acceleration response (the second derivative of the displacement response) of the center of mass of the chiller in free vibration consists of six damped sinusoidal responses with frequencies equal to the six natural frequencies of the chiller supported by the isolation components of the I/R systems. Consequently, performing a Fast Fourier Transform (FFT) on the free vibration acceleration response measured at the center of mass would disclose the natural frequencies of the chiller supported by the isolation component of the I/R systems.

FFT technique transforms a set of data sampled in the time domain into the frequency domain. The result of FFT for each frequency is a complex number. One way to represent the FFT of a data set is using a power spectrum. A power spectrum shows the variation of the square of the amplitude per unit frequency versus frequency. Figure 6-2(b) is the power spectrum of the damped sinusoidal response of figure 6-2(a); as seen in figure 6-2(b), a peak exactly lies at the frequency ω_1, the natural frequency of the response. Likewise, as shown in figure 6-2(c), the power spectrum of a response combined by a number of damped sinusoidal responses, will have peaks exactly at the natural frequencies contributing to the total response. This characteristic of the power spectra make them a very expedient tool to identify the frequency content (the natural frequencies of the test specimen supported by the isolation component of the I/R system) of a data set (free vibration acceleration response at the center of mass of the test specimen).

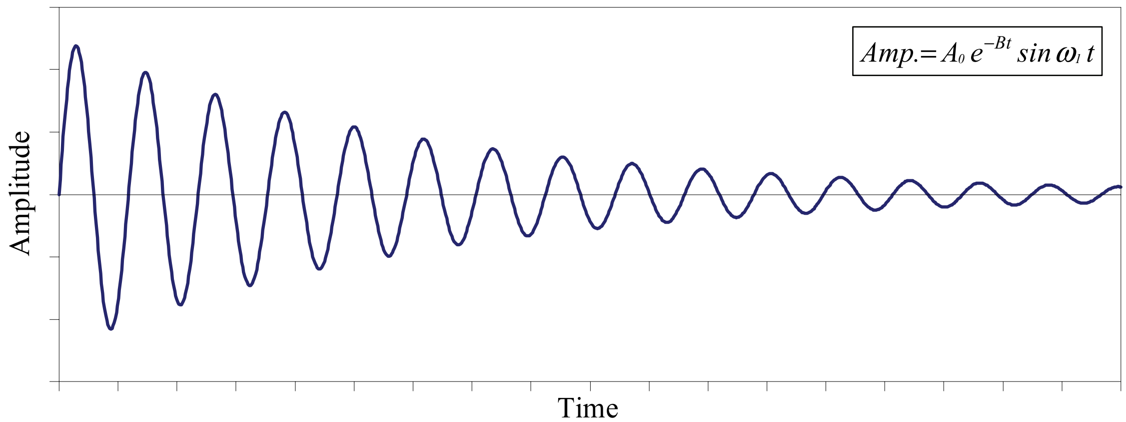

(a) Damped Sinusoidal Response with Frequency ω_l (A_0 and B: Conventional Coefficients)

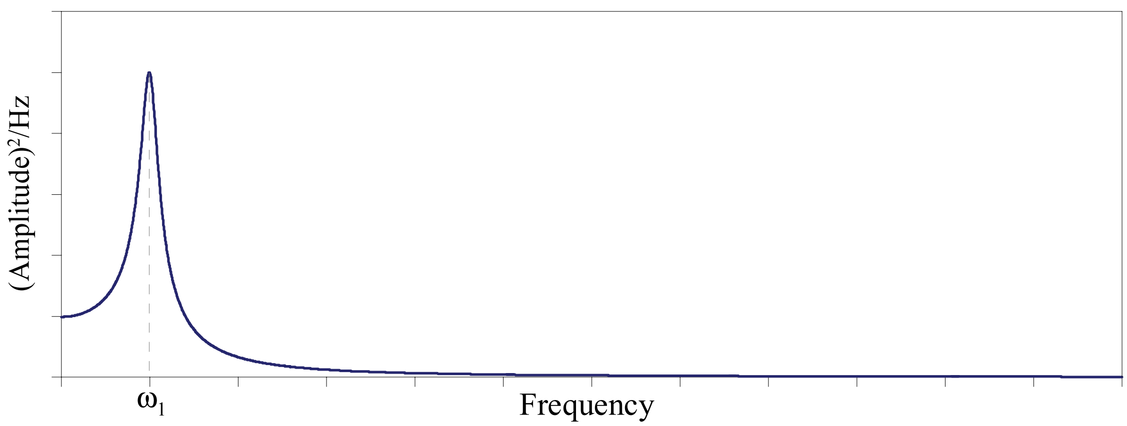

(b) Power Spectrum of a Damped Sinusoidal Response with Frequency ω_l

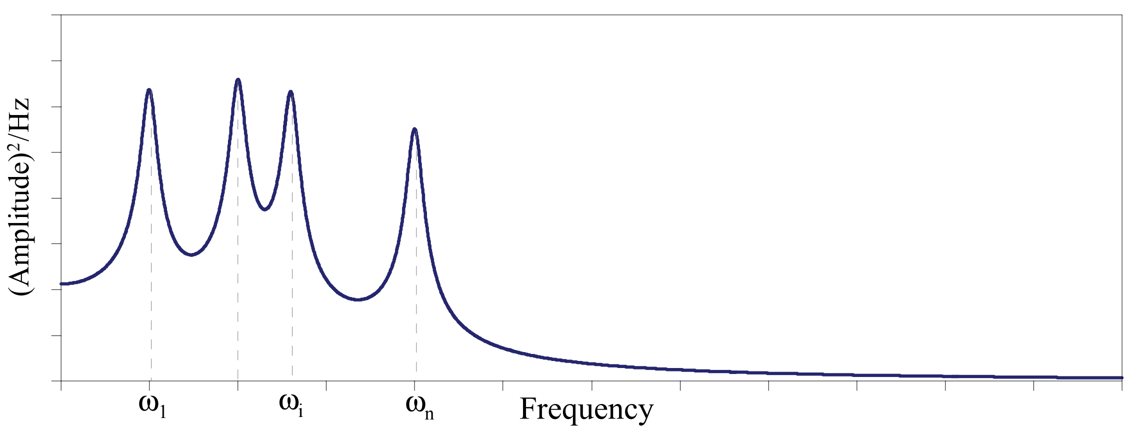

(c) Power Spectrum of a Linear Combination of a Number of Damped Sinusoidal Responses

Figure 6-2 Frequency Content Identification of Damped Sinusoidal Responses

The concept described above was used to evaluate the free vibration response at the center of mass of the chiller. Since all points of a rigid body oscillate at the same frequency, the concept can be extended to the other points of the chiller. In other words, the local peaks of the power spectrum of the acceleration response sampled through a free vibration at any point of the chiller would disclose the same natural frequencies.

The pulse tests were used to induce three different regimes of free vibration in the test specimen: (*i*) the free vibration starting after the first pulse was introduced to the chiller in the transverse direction at the 5th second (*ii*) the free vibration after the second pulse was introduced to the chiller in the longitudinal direction at the 15th second (*iii*) the free vibration after the third pulse was introduced to the chiller in the vertical direction at the 25th second. Therefore, each system-identification test provided three data sets of free vibration acceleration response. However, it should be noted that the data obtained from the pulse tests throughout the tests series in which the restraint components were engaged after installation (figure 5-7(b), Section 5.6) could not be used to identify the natural frequencies of the chiller supported only by the isolation component of the I/R systems.

Figures 6-3(a) and (b) show the power spectra of the transverse acceleration recorded at the center of mass of the chiller (channel #1) and top level of the I/R system #1 (channel #19), respectively, during the pulse-type system-identification test TS6-P1. Three natural frequencies corresponding to the three peaks in figures 6-3(a) and (b) can be easily identified as 1.17, 2.78 and 3.8 Hz. The presence of only three major peaks in figures 6-3(a) and (b) instead of six peaks (expected for six modes) is attributed to the contribution of only three modes to the total response through the first free vibration of the test TS6-P1. In other words, the first pulse of the system-identification test TS6-P1 (in the transverse direction) could only excite three modes of response. The other three modes of response would be excited by the second and third pulses in the longitudinal and vertical direction, respectively. As shown in figures 6-4 and 6-5, the power spectra of the acceleration response recorded by the longitudinal and vertical accelerometers through the second and third free vibrations of the same pulse test disclosed the other three natural frequencies as 1.54, 2.24, and 3.48 Hz.

Repeating the same procedure for the data acquired through the other system-identification tests resulted in six natural frequencies identical to those obtained from the system-identification test TS6-P1. Table 6-1 lists the six natural frequencies identified for the chiller supported by the isolation component of the I/R systems.

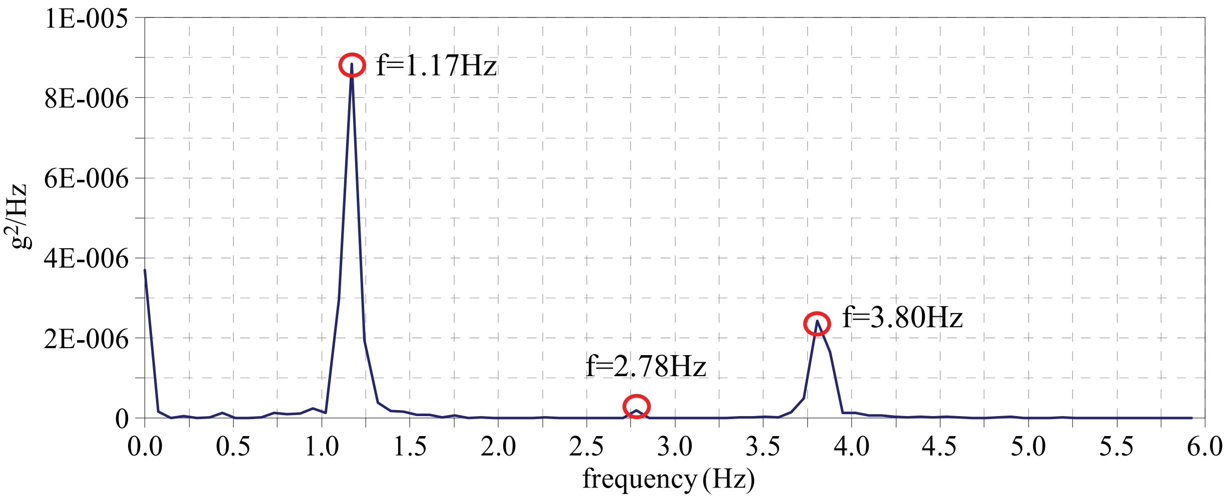

(a) Center of Mass of the Chiller (Channel #1)

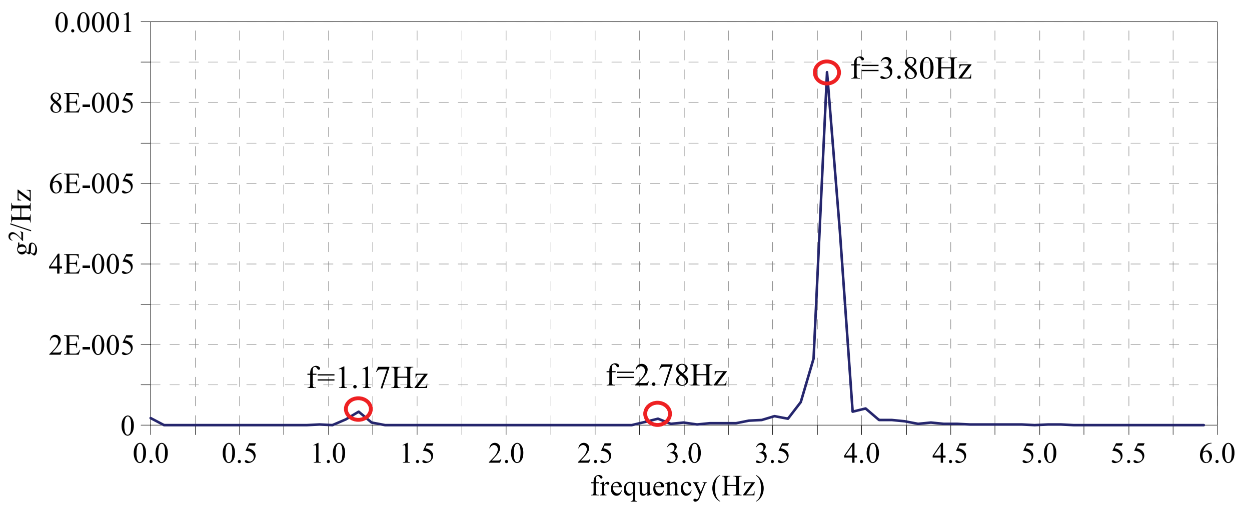

(b) Top Level of I/R System #1 (Channel #19)

Figure 6-3 Power Spectra of Transverse Acceleration Measured at Center of Mass and Corner #1 of the Chiller , Pulse Test TS6-P1

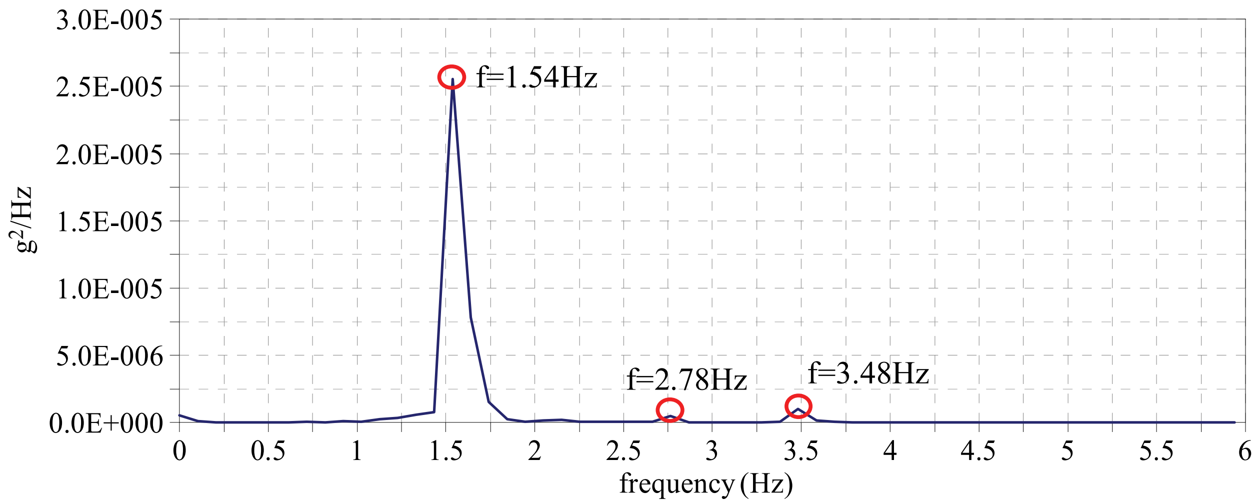

(a) Center of Mass of the Chiller (Channel #2)

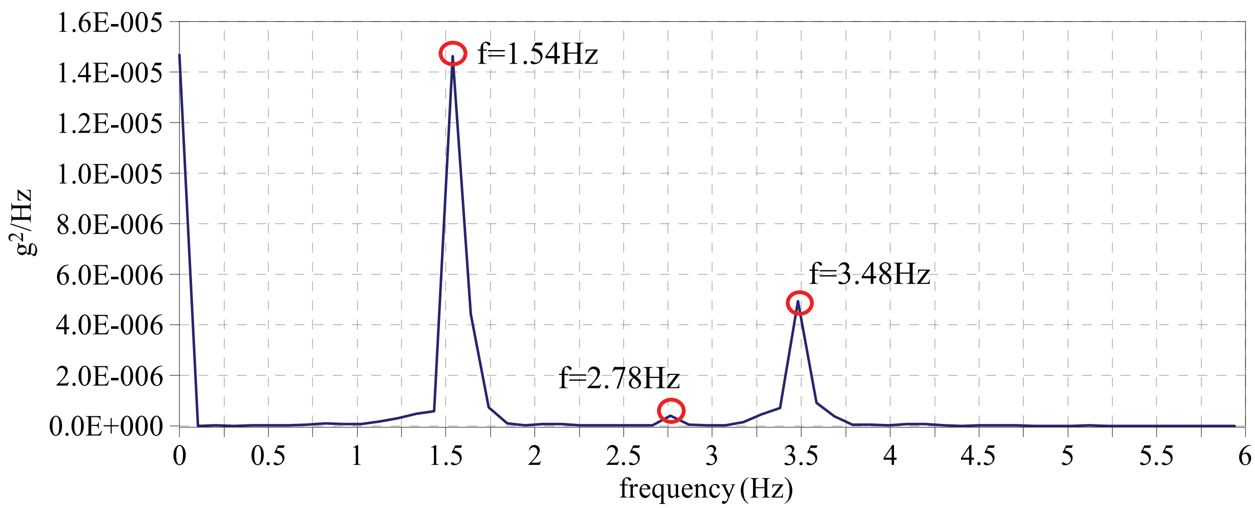

(b) Top Level of I/R System #1 (Channel #21)

Figure 6-4 Power Spectra of Longitudinal Acceleration Measured at Center of Mass and Corner #1, Pulse Test TS6-P1

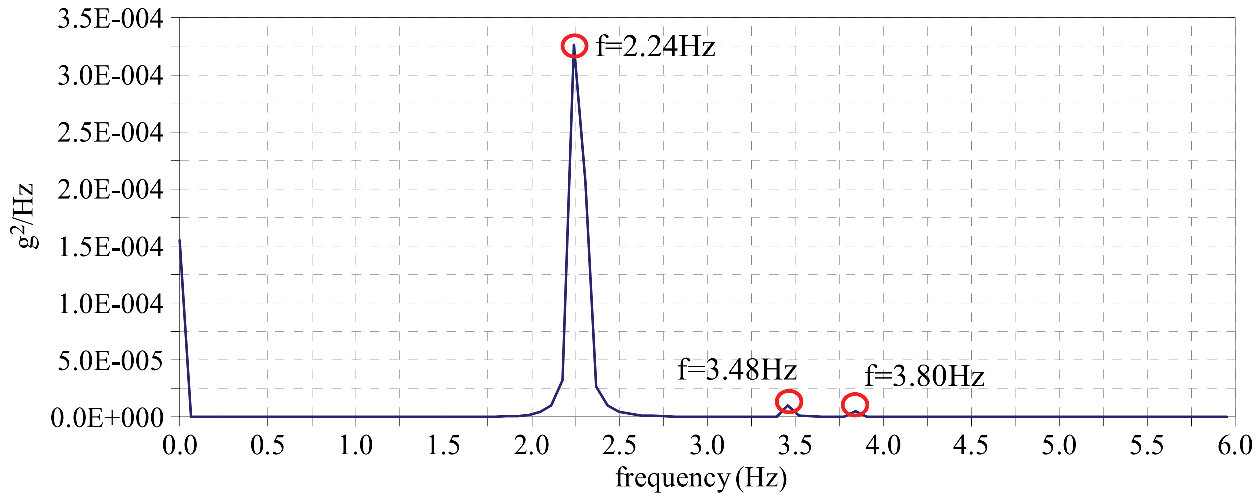

(a) Center of Mass of the Chiller (Channel #3)

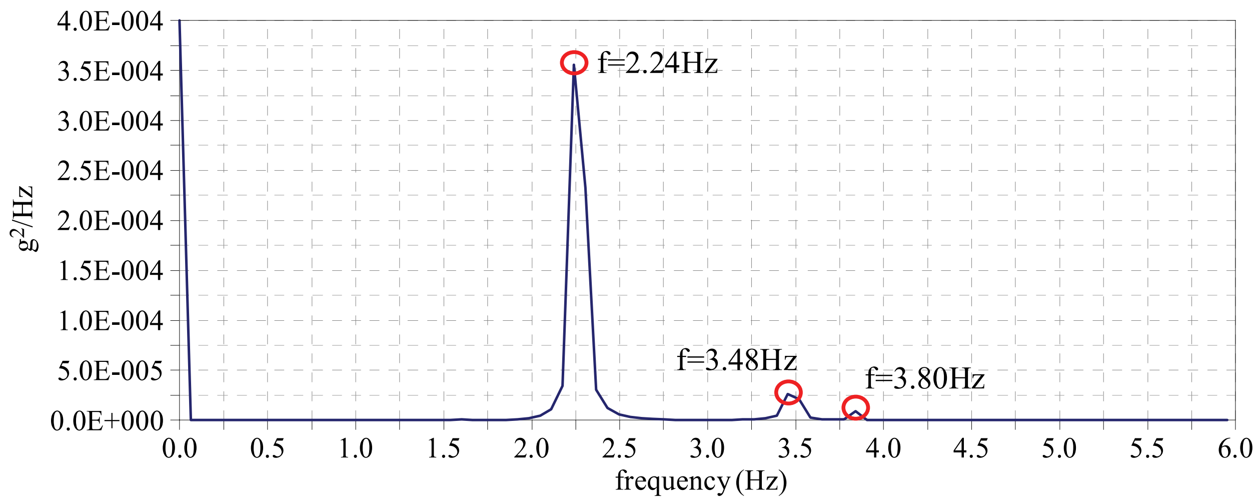

(b) Top Level of the I/R System #1 (Channel #24)

Figure 6-5 Power Spectra of Vertical Acceleration Measured at Center of Mass and Corner #1, Pulse Test TS6-P1

Table 6-1 Natural Frequencies/Periods of Chiller in Wet Condition Supported by Isolation Component of I/R Systems

Mode #	**1**	**2**	**3**	**4**	**5**	**6**
Frequency (Hz)	1.17	1.54	2.24	2.78	3.48	3.80
Period (sec)	0.85	0.65	0.45	0.36	0.29	0.26

Mode shapes are the other dynamic characteristics to be determined for the six modes of vibration. Mode shapes can be determined by comparing the modal response amplitude and phase of all degrees of freedom against the modal response amplitude and phase of a reference degree of freedom. Conventionally, for each mode of vibration, the degree of freedom with the largest modal response amplitude can be selected as the reference degree of freedom.

The comparison of the modal response amplitude is carried out by normalizing the modal response amplitude of each degree of freedom by the modal response amplitude of the reference degree of freedom. The unit of the vertical axis of power spectra is square of the response amplitude per unit frequency. Therefore, the square root of the ratio of the power spectrum amplitude of two degrees of freedom at the natural frequency of a given mode is equal to the ratio of the modal response amplitude of the two degrees of freedom.

As an example, for the third mode of vibration of the chiller supported by the isolation component of the I/R systems, if the vertical displacement at the center of mass of the chiller is considered as the reference degree of freedom, the modal response amplitude of the vertical displacement at the corner #1 of the chiller can be calculated based on the power spectra of figure 6-5. In this figure, at the natural frequency of the third mode of vibration (2.24 Hz), the power spectrum amplitudes of the vertical acceleration response at the center of mass and corner #1 of the chiller are 3.2614×10^{-4} g^2/Hz and 3.5591×10^{-4} g^2/Hz, respectively. Subsequently, the modal response amplitude of the vertical displacement at the corner #1 of the chiller is calculated as:

$$\sqrt{\frac{3.5591\times10^{-4}}{3.2614\times10^{-4}}}=1.045 \qquad (6\text{-}10)$$

This means that in the third mode of vibration, a unit vertical displacement at the center of mass of the chiller corresponds to a 1.045 unit vertical displacement at the corner #1.

The phase between the modal response of a given degree of freedom and the reference degree of freedom is shown by the sign of the normalized modal response. The positive sign is used for a degree of freedom in phase with the reference degree of freedom and the negative sign is used for a degree of freedom out of phase with the reference degree of freedom. As a result, the modal response of the reference degree of freedom is always taken as plus unity. Phase spectrum between two degrees of freedom is established based on the imaginary part of the FFTs of the response at the two degrees of freedom (Wheeler and Ganji, 2004).

As an example, figure 6-6 shows the phase spectrum between the vertical responses at the center of mass and corner #1 of the chiller throughout the system-identification test TS6-P1. As shown in this figure at the frequency of the third mode of vibration (2.24 Hz), the phase between the two responses is zero degree. In other words, in the third mode of vibration the two degrees of freedom are in phase.

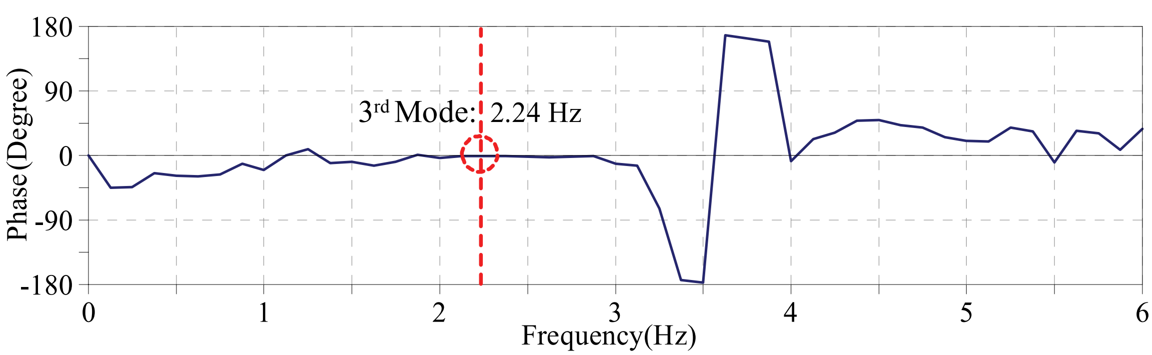

Figure 6-6 Phase Spectrum between Vertical Acceleration Responses at Center of Mass and Corner #1 of Chiller, Third Mode of Vibration (2.24 Hz), Pulse Test TS6-P1

The same procedure was repeated to establish the six modal amplitudes and phases of all of the degrees of freedom for which, the acceleration response was measured. However, since the six degrees of freedom at the center of mass (figure 6-1) were selected as the reference degrees of freedom to describe the motion of the chiller, the mode shapes had to represent the modal response of the same six degrees of freedom (three translational and three rotational degrees of freedom). For the three translational degrees of freedom at the center of mass of the chiller, the power and phase spectra of the measured acceleration responses could be used to calculate the normalized modal amplitudes and phases. For the three rotational degrees of freedom at the center of mass, on the other hand, since no response was measured, the normalized modal amplitudes and phases had to be calculated indirectly. The translational responses recorded at the center of mass and corners of the chiller could be used to calculate the modal response of the rotational degree of freedom at the center of mass of the chiller. The procedure for calculating the modal amplitudes of the rotational degrees of freedom at the center of mass of the chiller from the responses of the translational degrees of freedom at the center of mass and corners of the chiller is illustrated below by considering a general rigid body experiencing one of its modal vibrations.

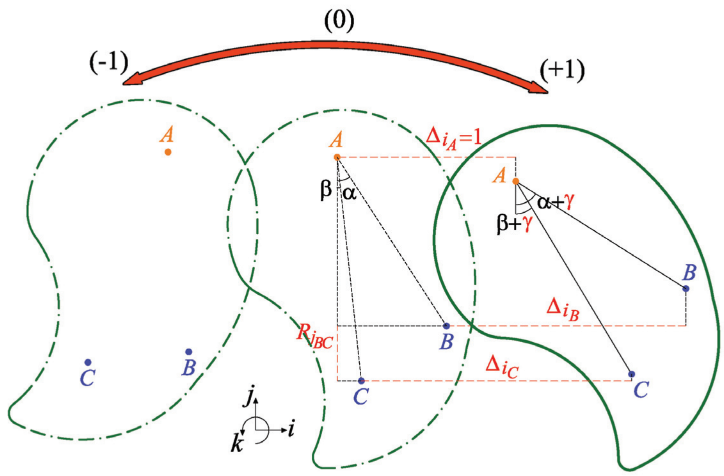

Figure 6-7 Rigid Body Modal Vibration

Figure 6-7 schematically shows a rigid body experiencing one of its modes of vibration, which is a combination of translation in the *i-j* plane and rotation around the *k* axis. In this figure, the rigid body is shown in at rest position (marked by (0)) and at maximum displacement positions (marked by ($\pm$1)) of the modal vibration. The acceleration responses in the *i* and *j* directions are measured at points *A, B,* and *C.* Points *B* and *C* have the same coordinate with respect to the *k* axis. The natural frequency of the considered mode is identified by the power spectra of the acceleration responses measured at points *A*, *B*, and *C.* The angle γ, which is the rotation around the *k* axis in the maximum displacement position, cannot be measured and needs to be calculated indirectly. If γ is small, the maximum displacement of points *B* and *C* with respect to the *i* axis can be related to each other by:

$$\left|\Delta_{iB}-\Delta_{iC}\right|=R_{jBC}\gamma \qquad (6\text{-}11)$$

where:

Δ_{iB} = modal displacement of point *B* with respect to the *i* axis
Δ_{iC} = modal displacement of point *C* with respect to the *i* axis
R_{jBC} = distance between points *B* and *C* with respect to the *j* axis
γ = modal rotation around the *k* axis

If the translational degree of freedom in direction of the *i* axis at point *A* is selected as the reference degree of freedom of the considered mode of vibration ($\Delta_{iA}=1$), Δ_{iB} and Δ_{iC} are calculated from the power spectra of the acceleration responses in direction of the *i* axis measured at points *B* and *C*:

$$\Delta_{iB} = \sqrt{\frac{PS_{iB}}{PS_{iA}}} \tag{6-12}$$

$$\Delta_{iC} = \sqrt{\frac{PS_{iC}}{PS_{iA}}} \tag{6-13}$$

where:

PS_{iA} = the power spectrum amplitude of the acceleration response at point *A* in direction of the *i* axis at the natural frequency of the considered mode

PS_{iB} = the power spectrum amplitude of the acceleration response at point *B* in direction of the *i* axis at the natural frequency of the considered mode

PS_{iC} = the power spectrum amplitude of the acceleration response at point *C* in direction of the *i* axis at the natural frequency of the considered mode

Substituting equations 6-12 and 6-13 into equation 6-11 and solving the resultant equation for γ will yield to:

$$\gamma = \frac{\left|\sqrt{PS_{iB}} - \sqrt{PS_{iC}}\right|}{R_{jBC}\sqrt{PS_{iA}}} \tag{6-14}$$

Analogously, if the center of mass of the chiller is assumed to be located at point *A* and its corners are assumed to be located at points *B* and *C*, the amplitude of the modal rotation at the center of mass of the chiller around any of the three axes ($\theta_{Tn}, \theta_{Ln}, \theta_{Vn}$) can be calculated based on the acceleration response measured at the center of mass and corners of the chiller with respect to one of the two other axes. For example, the longitudinal or vertical acceleration responses at the center of mass and two corners of the chiller with equal transversal coordinate are used to calculate the modal amplitude and phase of the rotational degree of freedom at the center of mass around the transverse axis (θ_{Tn}) .

For each mode of vibration, one of the six degrees of freedom at the center of mass of the chiller was considered as the reference degree of freedom (with the modal response amplitude of plus unity), and the procedure of finding the modal responses at the other degrees of freedom was repeated based on the data acquired in the same identification tests used earlier to establish the natural frequencies (tests without any contact in restraint component of the I/R systems). The mode shapes were calculated by averaging the results obtained from different system-identification tests. Table 6-2 presents the resulting six mode shapes of vibration for the test specimen supported by the isolation component of the I/R systems. The presented results indicate that the first three modes of vibration correspond to the pure translation of the chiller in the transverse, longitudinal, and vertical directions, respectively.

Table 6-2 Six Mode Shapes of Chiller in Wet Condition Supported by Isolation Component of I/R Systems

Translational DOFs at Center of Mass	T_n (cm)	L_n (cm)	V_n (cm)
	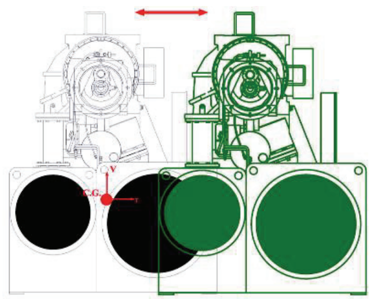	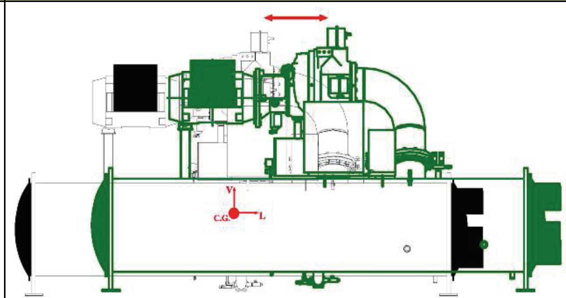	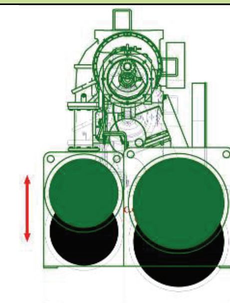
1st Mode (1.17 Hz)	1.0000	0.0606	-0.0641
2nd Mode (1.17 Hz)	0.0795	1.0000	-0.0562
3rd Mode (2.24 Hz)	-0.0784	-0.1069	1.0000
4th Mode (2.78 Hz)	-0.3258	-0.0730	1.0000
5th Mode (3.48 Hz)	0.3329	0.8059	1.0000
6th Mode (3.80 Hz)	1.0000	-0.1615	0.6556
Rotational DOFs at Center of Mass	θ_{T_n} (rad)	θ_{L_n} (rad)	θ_{V_n} (rad)
	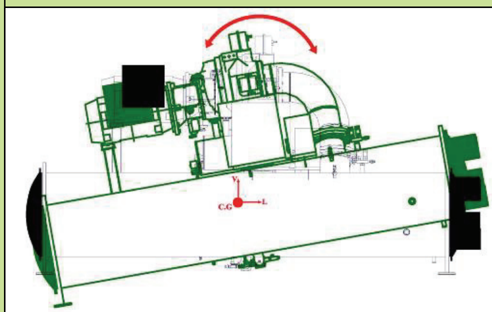	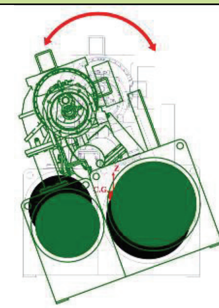	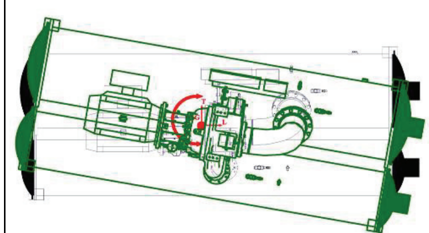
1st Mode (1.17 Hz)	0.0004	-0.0044	-0.0001
2nd Mode (1.17 Hz)	0.0023	0.0030	-0.0002
3rd Mode (2.24 Hz)	0.0003	4×10^{-05}	0.0008
4th Mode (2.78 Hz)	-0.0023	0.0027	-0.0098
5th Mode (3.48 Hz)	-0.0245	0.0144	-0.0034
6th Mode (3.80 Hz)	0.0030	0.0476	-0.0009

6.2 Seismic Tests Results

6.2.1 Estimation of Modal Equivalent Viscous Damping Ratios

Figure 6-8 shows a schematic representation of the free vibration response of a damped system. The decay of the response can be modeled by an equivalent viscous damping ratio. The equivalent damping ratio is usually quantified by measuring the decrement of the peak response amplitudes (Filiatrault, 1998). However, if the response is not symmetric with respect to the horizontal axis (time axis) double peak amplitudes can be used to eliminate the offset effect. As annotated in figure 6-8, the double amplitude response is defined as the difference between the maximum and minimum response within one response cycle.

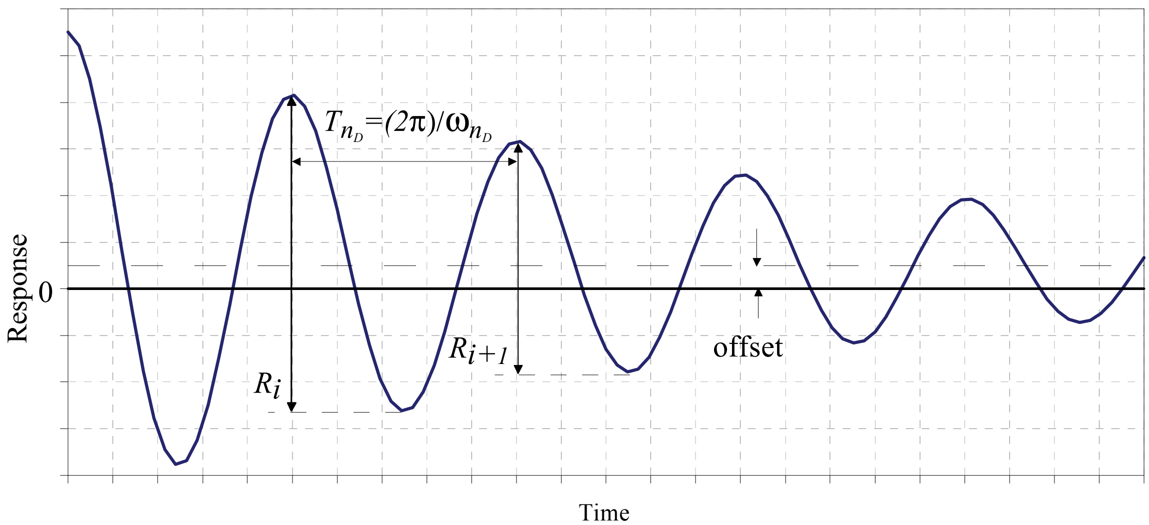

Figure 6-8 Decay of Response Attributed to Viscous Damping

In Section 6.1, it was shown that the amplitude of the modal free vibration response is characterized by an exponential decay. Therefore, R_i and R_{i+1} , the double amplitudes of two consecutive cycles (each cycle is a time interval equal to the damped natural period of vibration), are related to each other as:

$$\frac{R_i}{R_{i+1}}=e^{\zeta_n \omega_n T_{nD}} \qquad (6\text{-}15)$$

where:

R_i and R_{i+1} = double response amplitude of two consecutive cycles
ζ_n = equivalent viscous damping ratio of the nth mode
T_{nD} = damped natural period of the nth mode
ω_n = natural frequency of the nth mode

according to equation 6-6 :

$$T_{nD}=\frac{2\pi}{\omega_{nD}}=\frac{2\pi\zeta_n}{\sqrt{1-\zeta_n^2}} \qquad (6\text{-}16)$$

Substituting equation 6-16 into equation 6-15 and taking the natural logarithm of both sides of the equation yields:

$$ln(\frac{R_i}{R_{i+1}})=\frac{2\pi\zeta_n}{\sqrt{1-\zeta_n^2}} \qquad (6\text{-}17)$$

For small values of ζ_n (less than 0.1), equation 6-17 is simplified to:

$$ln(\frac{R_i}{R_{i+1}}) \simeq 2\pi\zeta_n \qquad (6\text{-}18)$$

Equation 6-18 is solved for ζ_n as:

$$\zeta_n \simeq \frac{1}{2\pi} ln(\frac{R_i}{R_{i+1}}) \qquad (6\text{-}19)$$

ζ_n varies with the amplitude of the response. The average of the peak amplitudes within two consecutive cycles used to calculate ζ_n can be considered as the response amplitude R corresponding to the calculated ζ_n :

$$R = \frac{(R_i + R_{i+1})}{4} \qquad (6\text{-}20)$$

Equations 6-19 and 6-20 are used to estimate the variation of the modal equivalent viscous damping ratio with the free vibration response amplitude.

Either of the system-identification tests or tale of the seismic tests provided free vibration response data sets, which could be processed to estimate the variation of modal equivalent viscous damping ratios with the free vibration response amplitudes. However, it was decided to calculate the modal damping ratios by processing the free vibration responses through the tale of the seismic tests so that variation of the equivalent viscous damping ratios over a larger response amplitude range could be considered.

By implementation of band-pass filters, the response quantities measured through the tale of the seismic tests were decomposed into six individual modal responses. The width of the band-pass filters were decided based on the natural frequencies established in Section 6.1. Figure 6-9 exhibits samples of band-pass filtered modal acceleration responses at the center of mass obtained from the tale of seismic test TS6-S1. In figure 6-9, the regions of the signals used to establish the equivalent viscous damping ratios are indicated by dotted lines on each response history.

After decomposing the responses into the six modal responses, it appeared clear that the contributions of the fourth, fifth and sixth modes to the measured responses were insignificant. Therefore, the modal equivalent viscous damping ratios were established only for the first three modes of vibration.

The variations of the modal equivalent viscous damping ratios with the amplitude of the acceleration response at the center of mass of the chiller for the first three modes of vibration are shown in figure 6-10. The results presented in this figure were obtained by processing the acceleration responses at the center of mass of the chiller in the tale of the seismic tests of Test Series TS6. Figure 6-11 presents similar results for the first two modes of vibration based on the displacement response at the top of the south-west edge of the chiller measured by the Krypton camera through channel # 70 (see figure 4-7).

The results show that in most cases, the equivalent viscous damping ratio increases with the response amplitude. The first three modes of vibration of the chiller in wet condition supported by the isolation component of the I/R systems are lightly damped with the equivalent viscous damping ratios less than three percents of the critical damping.

Since the first three modes of vibration could be associated with pure translations in the transverse, longitudinal and vertical directions, respectively, it can be concluded that the modal equivalent viscous damping ratios of the first three modes represent the damping ratios provided by the isolation components of the I/R systems in the transverse, longitudinal, and vertical directions, respectively. In other words, the results show that the isolation components of the I/R systems provided around three percents and one percent equivalent damping ratio in the horizontal and vertical directions, respectively.

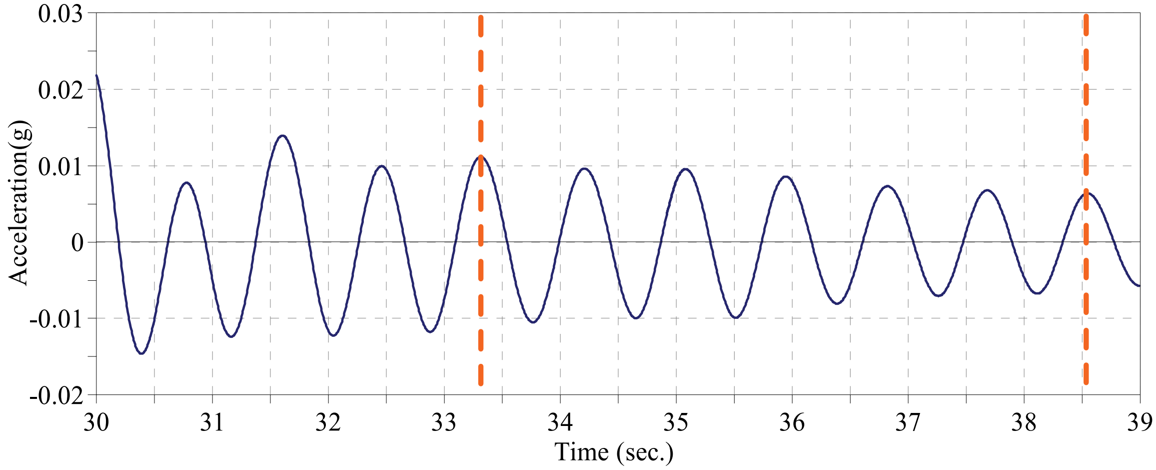

(a) Transverse Acceleration, First Mode

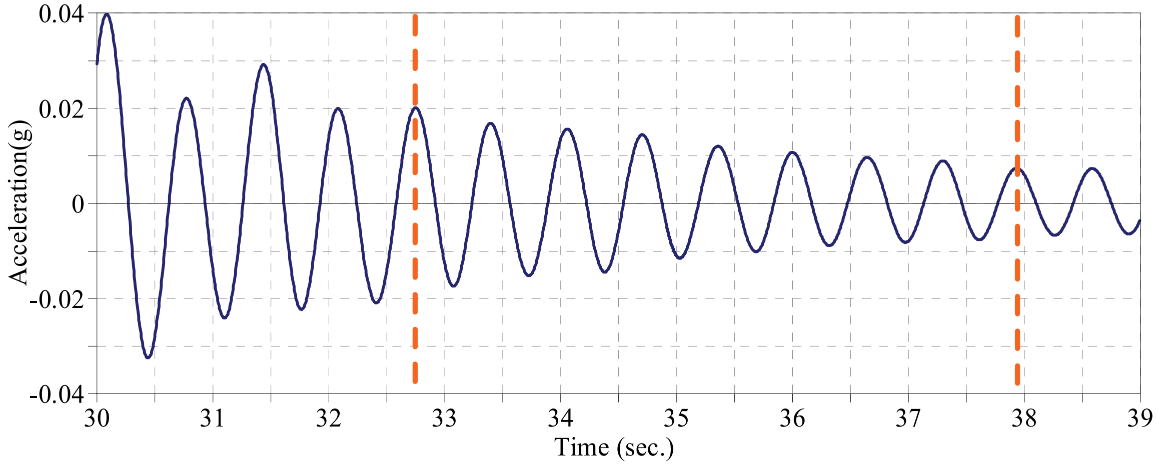

(b) Longitudinal Acceleration, Second Mode

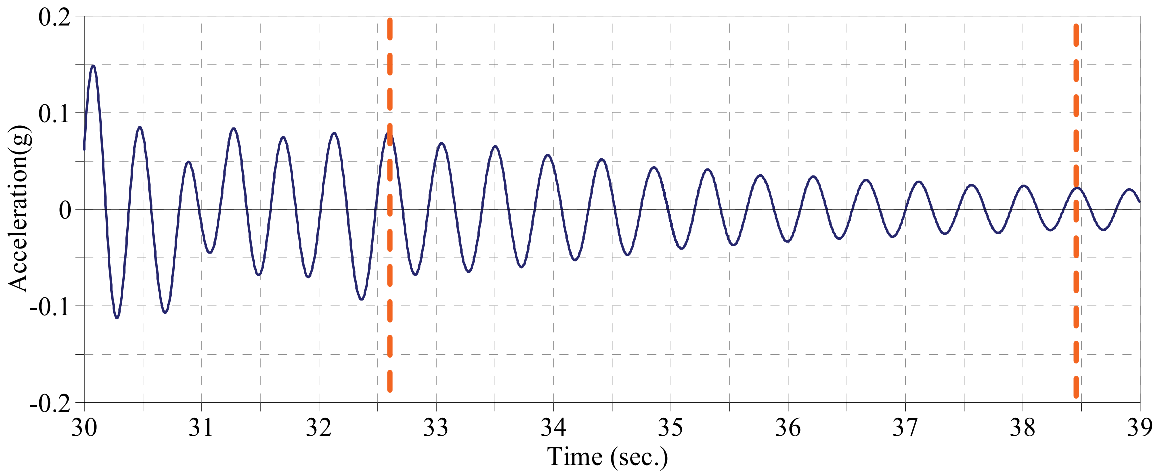

(c) Vertical Acceleration, Third Mode

Figure 6-9 Band-Pass Filtered Modal Acceleration Responses at Center of Mass, Tale of Seismic Test TS6-S1 Used to Establish Modal Damping Ratios

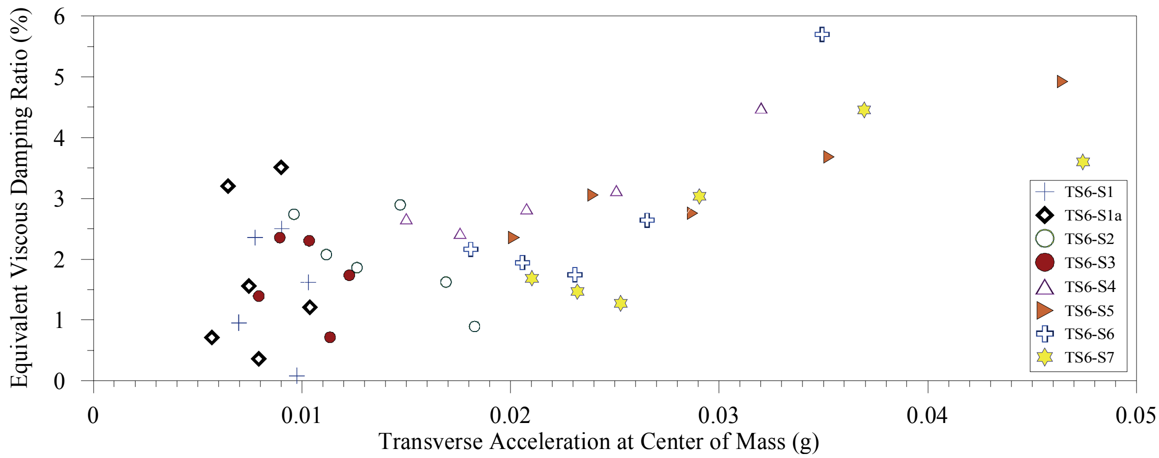

(a) First Mode

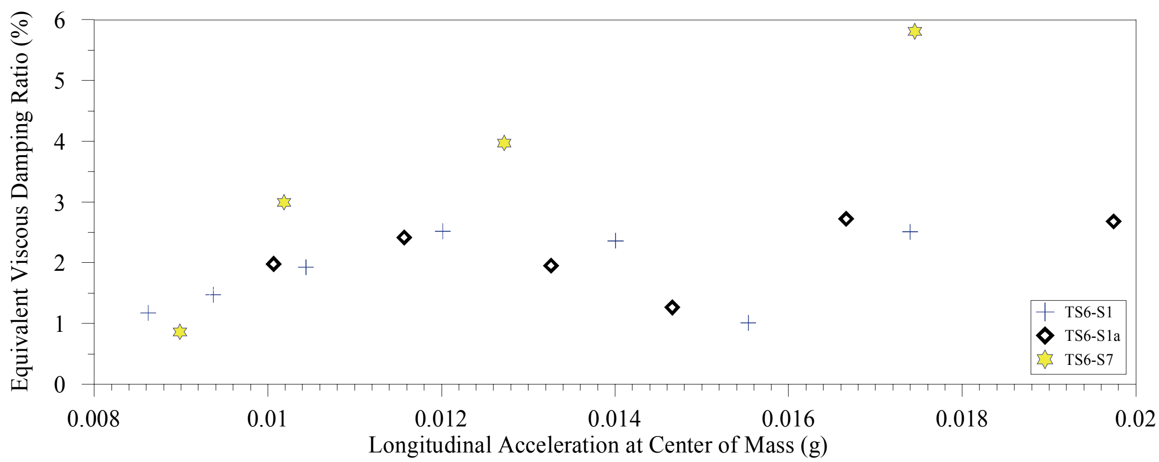

(b) Second Mode

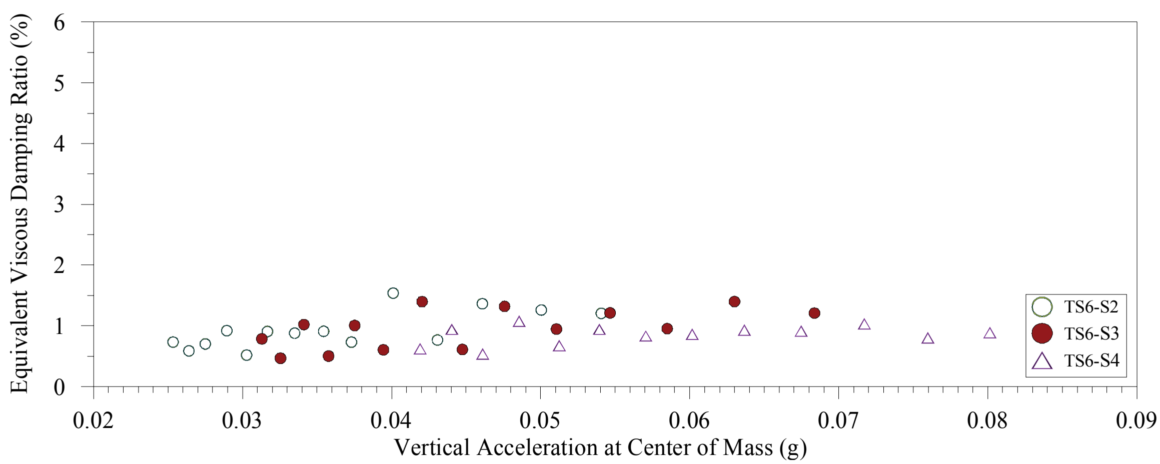

(c) Third Mode

Figure 6-10 Variation of Equivalent Viscous Damping Ratio with Acceleration Response Amplitude at Center of Mass for the First Three Modes of Vibration

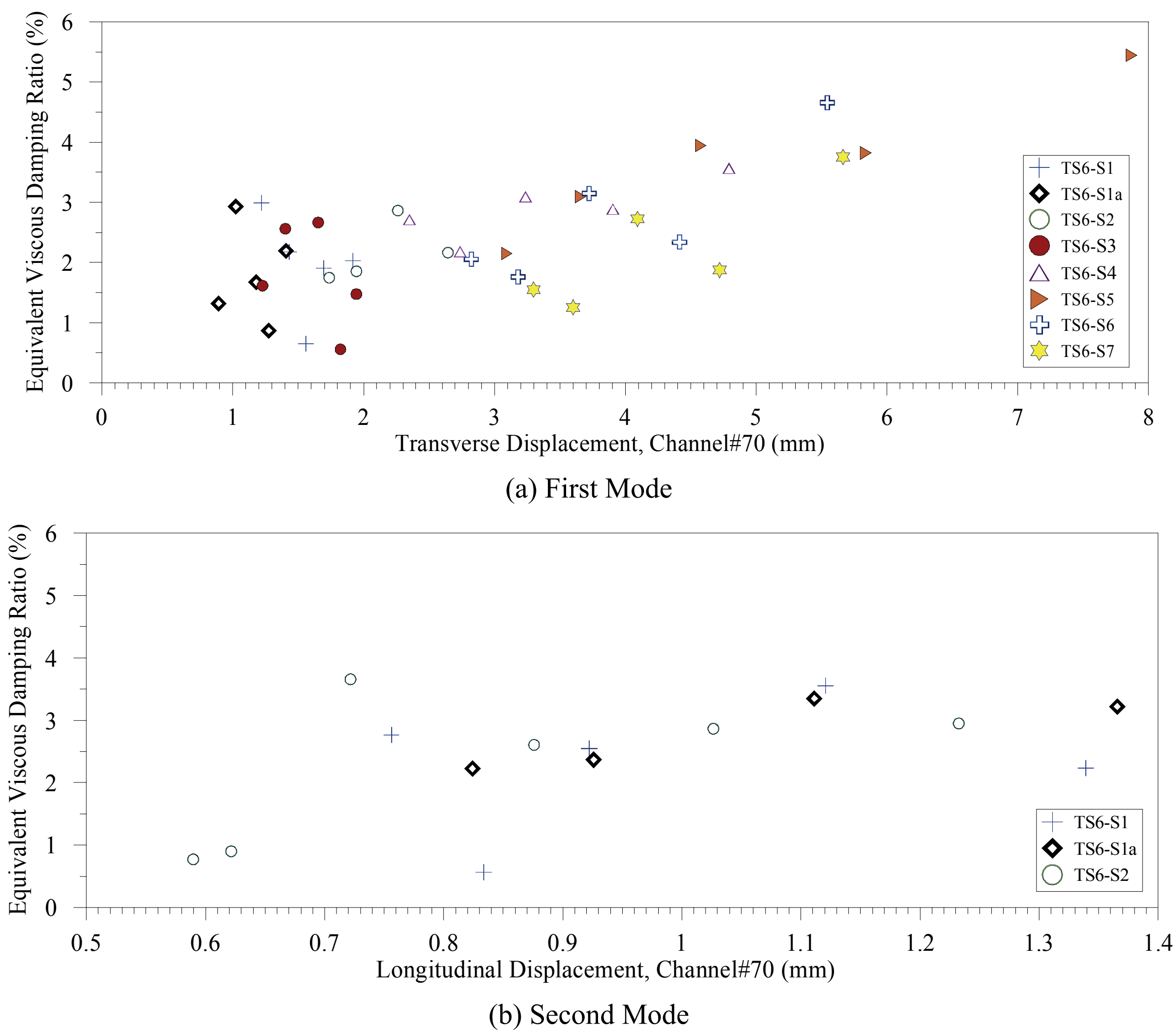

Figure 6-11 Variation of Equivalent Viscous Damping Ratio with Displacement Response Amplitude Measured by Channel #70 for the First Two Modes of Vibration

6.2.2 Damage Observations

During the 72 seismic tests conducted, the I/R systems were damaged only once in seismic test TS2-S8a. Inspection of the I/R systems after this seismic test, which corresponded to the roof level input motion scaled to 150% amplitude level, showed that all the bottom steel washers interfacing the grommets and bottom nuts were damaged and deformed into a conical shape. Figure 6-12 shows the photographs of one of the four I/R systems taken at the end of seismic test TS2-S8a. The only damaged component of the I/R systems were the steel washers, which could be easily replaced by new ones. However, because the displacement capacity of the earthquake simulator was almost reached during seismic test TS2-S8a, it was decided to end Test Series TS2 at that 150% amplitude level and start the next test series (TS4) with the 3.0 g design I/R systems.

Figure 6-12 Damage in Vertical Restraint Component of 1.0 g Design I/R Systems at the End of Seismic Test TS2-S8a

6.2.3 Response Envelopes

The peak acceleration responses at the center of mass of the chiller, the peak dynamic shear and normal forces induced in the I/R systems, and the peak relative displacement response of the four points on the south face of the chiller in all of the 72 seismic tests, are listed in tables 6-3, 6-4, 6-5, and 6-6, respectively. For brevity, the test setup characteristics are presented only in table 6-3. In few tests with strong input motion, because of the severe shaking some of the LEDs were detached from the chiller. Therefore, for those tests the peak relative displacement response was not available for all of the four points. In table 6-6, the corresponding cells are filled with N/A (Not Available). Analyses of the seismic test results will be presented in Section 7 of this report.

Table 6-3 Peak Acceleration Responses at Center of Mass of Chiller during Seismic Tests

Test #	Test ID[1]	Restraint Component Design	Gap[2] (mm[in])	Tubular Rubber Pad		Input Motion		Peak Acceleration at Center of Mass (g)		
				Thickness (mm[in])	Hardness (Duro)	Amplitude	Level	Transverse	Longitudinal	Vertical
1	TS10-S1	1.0 g	11 [7/16]	19 [3/4]	60	10%	Base	0.07	0.13	0.13
2	TS10-S1a					10%	Roof	0.22	0.17	0.19
3	TS10-S2					25%	Base	0.39	0.36	0.26
4	TS10-S3					25%	Roof	0.89	0.56	0.47
5	TS10-S4					50%	Base	0.64	0.50	0.56
6	TS2-S1	1.0 g	6 [1/4]	6 [1/4]	60	10%	Base	0.18	0.11	0.07
7	TS2-S1a					10%	Roof	0.29	0.20	0.18
8	TS2-S2					25%	Base	0.40	0.27	0.37
9	TS2-S3					25%	Roof	0.60	0.56	0.45
10	TS2-S4					50%	Base	0.69	0.60	0.60
11	TS2-S5					50%	Roof	1.31	0.91	1.13
12	TS2-S6					100%	Base	1.44	1.02	1.03
13	TS2-S7					100%	Roof	2.45	1.16	2.39
14	TS2-S8					150%	Roof	2.22	1.93	2.30
15	TS2-S8a					150%	Roof	2.98	2.36	3.29
16	TS4-S1	3.0 g	3 [1/8]	6 [1/4]	60	10%	Roof	0.26	0.21	0.20
17	TS4-S3					25%	Roof	0.51	0.48	0.43
18	TS4-S5					50%	Roof	0.95	0.62	0.93
19	TS4-S7					100%	Roof	1.62	1.62	1.41
20	TS4-S8					100%	Roof	1.33	1.43	1.38

Table 6-3 (cont'd) Peak Acceleration Responses at Center of Mass of Chiller during Seismic Tests

Test #	Test ID	Restraint Component Design	Gap (mm[in])	Tubular Rubber Pad		Input Motion		Peak Acceleration at Center of Mass (g)		
				Thickness (mm[in])	Hardness (Duro)	Amplitude	Level	Transverse	Longitudinal	Vertical
21	TS7-S1	3.0 g	6 [1/4]	3 [1/8]	70	10%	Roof	0.35	0.23	0.27
22	TS7-S3					25%	Roof	0.61	0.66	0.70
23	TS7-S5					50%	Roof	1.06	1.20	1.30
24	TS7-S7					100%	Roof	1.54	2.01	1.79
25	TS5-S1	3.0 g	6 [1/4]	6 [1/4]	60	10%	Base	0.12	0.12	0.10
26	TS5-S1a					10%	Roof	0.38	0.24	0.19
27	TS5-S2					25%	Base	0.42	0.36	0.44
28	TS5-S3					25%	Roof	0.81	0.69	0.67
29	TS5-S4					50%	Base	0.88	0.80	1.11
30	TS5-S5					50%	Roof	1.36	1.14	1.36
31	TS5-S6					100%	Base	1.61	1.27	1.83
32	TS5-S7					100%	Roof	2.03	1.88	1.90
33	TS9-S1	3.0 g	6 [1/4]	6 [1/4]	50	10%	Base	0.16	0.15	0.14
34	TS9-S1a					10%	Roof	0.35	0.26	0.24
35	TS9-S2					25%	Base	0.45	0.45	0.51
36	TS9-S3					25%	Roof	0.63	0.70	0.57
37	TS9-S4					50%	Base	0.59	0.78	0.81
38	TS9-S5					50%	Roof	1.34	1.20	1.17
39	TS9-S6					100%	Base	1.35	1.48	1.77
40	TS9-S7					100%	Roof	1.86	2.04	1.68

Table 6-3 (cont'd) Peak Acceleration Responses at Center of Mass of Chiller during Seismic Tests

Test #	Test ID	Restraint Component Design	Gap (mm [in])	Tubular Rubber Pad		Input Motion		Peak Acceleration at Center of Mass (g)		
				Thickness (mm [in])	Hardness (Duro)	Amplitude	Level	Transverse	Longitudinal	Vertical
41	TS12-S1	3.0 g (Modified)[3]	6 [1/4]	6 [1/4]	50	10%	Base	0.15	0.19	0.15
42	TS12-S1a					10%	Roof	0.34	0.28	0.20
43	TS12-S2					25%	Base	0.46	0.33	0.33
44	TS12-S3					25%	Roof	0.64	0.63	0.46
45	TS12-S4					50%	Base	0.62	0.77	0.52
46	TS12-S5					50%	Roof	1.39	1.07	1.06
47	TS12-S6					100%	Base	1.27	1.20	1.21
48	TS12-S7					100%	Roof	1.80	1.82	1.60
49	TS11-S1	3.0 g (Modified)	6 [1/4]	6 [1/4]	60	10%	Base	0.15	0.15	0.13
50	TS11-S1a					10%	Roof	0.28	0.22	0.20
51	TS11-S2					25%	Base	0.52	0.39	0.41
52	TS11-S3					25%	Roof	0.61	0.57	0.58
53	TS11-S4					50%	Base	0.66	0.76	0.55
54	TS11-S5					50%	Roof	1.16	1.19	1.05
55	TS11-S6					100%	Base	1.26	1.25	1.44
56	TS11-S7					100%	Roof	1.82	1.89	1.69
57	TS6-S1	3.0 g (Modified)	13 [1/2]	6 [1/4]	60	10%	Base	0.13	0.12	0.11
58	TS6-S1a					10%	Roof	0.19	0.30	0.16
59	TS6-S2					25%	Base	0.42	0.40	0.41
60	TS6-S3					25%	Roof	0.89	0.73	0.52

Table 6-3 (cont'd) Peak Acceleration Responses at Center of Mass of Chiller during Seismic Tests

Test #	Test ID	Restraint Component Design	Gap (mm [in])	Tubular Rubber Pad		Input Motion		Peak Acceleration at Center of Mass (g)		
				Thickness (mm [in])	Hardness (Duro)	Amplitude	Level	Transverse	Longitudinal	Vertical
61	TS6-S4	3.0 g (Modified)	13 [1/2]	6 [1/4]	60	50%	Base	0.73	0.69	0.90
62	TS6-S5					50%	Roof	1.29	1.47	1.11
63	TS6-S6					75%	Base	1.23	1.18	1.12
64	TS6-S7					75%	Roof	1.99	1.72	1.96
65	TS8-S1	3.0 g (Modified)	6 [1/4]	13 [1/2]	60	10%	Base	0.16	0.14	0.14
66	TS8-S1a					10%	Roof	0.31	0.21	0.19
67	TS8-S2					25%	Base	0.40	0.37	0.30
68	TS8-S3					25%	Roof	0.66	0.71	0.46
69	TS8-S4					50%	Base	0.72	0.75	0.64
70	TS8-S5					50%	Roof	1.33	1.11	1.09
71	TS8-S6					100%	Base	1.16	1.16	1.31
72	TS8-S7					100%	Roof	1.92	2.10	1.66

1. Test Identification
2. For both the horizontal and vertical gaps
3. See Section 5.6 for details

Table 6-4 Peak Dynamic Shear Forces Induced in I/R Systems during Seismic Tests

Test #	Test ID[1]	Peak Dynamic Shear Forces															
		Load Cell #1				Load Cell #2				Load Cell #3				Load Cell #4			
		Transverse		Longitudinal		Transverse		Longitudinal		Transverse		Longitudinal		Transverse		Longitudinal	
		(kips)	(kN)	(kips)	(kN)	(kips)	(kN)	(kips)	(kN)	(kips)	(kN)	(kips)	(kN)	(kips)	(kN)	(kips)	(kN)
1	TS10-S1	0.77	3.41	0.72	3.20	0.53	2.38	1.41	6.25	0.42	1.85	0.38	1.68	0.41	1.84	0.37	1.62
2	TS10-S1a	1.33	5.94	1.16	5.14	1.25	5.58	2.03	9.01	1.50	6.66	1.74	7.73	1.50	6.66	0.82	3.64
3	TS10-S2	3.26	14.51	2.35	10.46	3.07	13.65	3.95	17.59	3.75	16.69	4.43	19.70	2.79	12.41	1.22	5.42
4	TS10-S3	5.72	25.46	3.01	13.37	5.01	22.27	5.04	22.40	4.50	20.01	7.11	31.63	5.00	22.26	2.76	12.28
5	TS10-S4	5.36	23.84	2.70	12.00	6.20	27.58	5.46	24.27	4.20	18.68	5.11	22.74	4.32	19.21	2.76	12.28
6	TS2-S1	0.73	3.24	0.52	2.33	1.47	6.55	1.05	4.65	2.36	10.48	1.67	7.41	1.85	8.23	0.38	1.67
7	TS2-S1a	2.54	11.28	0.82	3.66	3.10	13.77	2.23	9.91	3.36	14.95	3.10	13.81	3.09	13.75	0.73	3.25
8	TS2-S2	5.45	24.23	1.27	5.63	4.42	19.67	4.15	18.46	4.43	19.69	3.68	16.36	3.92	17.43	1.65	7.35
9	TS2-S3	5.50	24.46	2.21	9.82	5.57	24.78	5.95	26.47	5.44	24.21	7.35	32.71	5.92	26.34	1.71	7.60
10	TS2-S4	5.95	26.47	2.51	11.18	5.12	22.79	7.14	31.74	6.97	31.00	7.70	34.27	6.11	27.19	3.11	13.84
11	TS2-S5	8.87	39.45	4.76	21.16	7.18	31.95	10.70	47.60	10.51	46.75	10.54	46.87	8.68	38.61	3.68	16.37
12	TS2-S6	8.59	38.20	4.92	21.90	8.91	39.62	10.49	46.64	10.93	48.62	10.50	46.70	8.05	35.82	4.27	18.98
13	TS2-S7	16.61	73.87	6.20	27.57	13.20	58.71	12.94	57.54	17.14	76.24	13.57	60.38	13.86	61.63	3.63	16.14
14	TS2-S8	12.19	54.21	9.63	42.85	15.43	68.63	23.04	102.50	12.93	57.54	15.41	68.55	11.88	52.87	8.30	36.92
15	TS2-S8a	31.13	138.45	11.78	52.42	30.21	134.36	23.78	105.78	35.61	158.41	34.21	152.19	24.44	108.72	11.73	52.16
16	TS4-S1	1.21	5.38	1.02	4.53	1.91	8.51	1.40	6.23	2.63	11.72	2.30	10.25	2.72	12.12	0.67	3.00
17	TS4-S3	4.85	21.58	2.71	12.07	4.29	19.07	3.83	17.04	5.52	24.56	4.33	19.25	4.36	19.40	1.93	8.60
18	TS4-S5	5.54	24.62	3.81	16.96	6.31	28.08	4.27	18.99	8.35	37.12	4.14	18.40	6.84	30.42	1.84	8.17
19	TS4-S7	8.10	36.02	10.87	48.36	12.09	53.76	14.29	63.57	12.49	55.56	11.26	50.09	10.05	44.72	5.29	23.54
20	TS4-S8	9.47	42.12	8.69	38.66	13.83	61.52	13.93	61.96	12.35	54.91	10.78	47.95	9.88	43.95	4.91	21.82

Table 6-4 (cont'd) Peak Dynamic Shear Forces Induced in I/R Systems during Seismic Tests

Test #	Test ID	Peak Dynamic Shear Forces															
		Load Cell #1				Load Cell #2				Load Cell #3				Load Cell #4			
		Transverse		Longitudinal		Transverse		Longitudinal		Transverse		Longitudinal		Transverse		Longitudinal	
		(kips)	(kN)	(kips)	(kN)	(kips)	(kN)	(kips)	(kN)	(kips)	(kN)	(kips)	(kN)	(kips)	(kN)	(kips)	(kN)
21	TS7-S1	2.94	13.07	0.88	3.89	4.03	17.93	3.23	14.38	2.44	10.87	2.70	12.00	3.88	17.26	1.50	6.68
22	TS7-S3	4.37	19.45	2.40	10.68	5.82	25.88	6.08	27.06	5.45	24.25	7.03	31.27	6.38	28.40	2.51	11.18
23	TS7-S5	6.58	29.27	4.85	21.58	7.81	34.76	9.43	41.94	10.16	45.17	9.73	43.28	7.53	33.48	4.38	19.49
24	TS7-S7	9.12	40.56	6.13	27.27	9.27	41.22	17.68	78.62	11.24	49.99	16.99	75.55	11.02	49.04	6.10	27.12
25	TS5-S1	1.32	5.87	0.72	3.20	1.63	7.25	1.52	6.75	1.63	7.24	1.46	6.47	1.30	5.78	0.79	3.52
26	TS5-S1a	2.08	9.26	1.24	5.53	2.96	13.15	2.87	12.75	3.19	14.18	3.44	15.29	4.52	20.11	1.16	5.15
27	TS5-S2	3.74	16.66	1.43	6.35	4.15	18.48	4.88	21.72	3.57	15.86	3.72	16.55	4.75	21.14	2.13	9.48
28	TS5-S3	4.49	19.96	2.63	11.69	6.67	29.66	7.79	34.66	6.25	27.80	7.82	34.78	5.30	23.58	2.59	11.52
29	TS5-S4	5.26	23.40	2.88	12.80	6.63	29.49	8.50	37.82	7.29	32.42	8.89	39.56	4.69	20.85	4.10	18.25
30	TS5-S5	7.73	34.41	4.81	21.40	8.17	36.35	11.11	49.41	11.64	51.76	11.10	49.39	6.52	29.00	4.77	21.22
31	TS5-S6	8.92	39.67	5.89	26.21	7.51	33.38	12.01	53.44	13.29	59.12	13.62	60.60	6.02	26.77	5.13	22.84
32	TS5-S7	12.21	54.32	6.41	28.52	12.16	54.10	24.90	110.76	17.80	79.18	18.17	80.84	11.50	51.14	5.79	25.76
33	TS9-S1	1.05	4.67	0.56	2.47	1.66	7.40	1.63	7.26	0.80	3.57	1.29	5.75	1.14	5.05	1.31	5.84
34	TS9-S1a	2.24	9.98	0.99	4.40	3.39	15.06	3.47	15.41	1.76	7.81	2.99	13.30	2.63	11.72	1.60	7.14
35	TS9-S2	3.49	15.52	1.95	8.65	5.14	22.84	6.25	27.81	3.07	13.66	4.81	21.39	4.23	18.82	2.56	11.37
36	TS9-S3	4.62	20.57	2.68	11.93	5.94	26.40	6.21	27.61	6.47	28.80	5.83	25.94	5.07	22.53	2.90	12.91
37	TS9-S4	3.73	16.61	3.00	13.33	6.69	29.77	8.78	39.07	4.90	21.78	7.23	32.16	4.85	21.58	4.54	20.19
38	TS9-S5	8.02	35.67	4.38	19.49	9.33	41.48	12.02	53.47	9.41	41.85	9.20	40.91	8.18	36.39	5.49	24.42
39	TS9-S6	8.31	36.98	5.48	24.37	9.73	43.28	11.72	52.12	10.33	45.94	12.79	56.91	6.50	28.91	5.80	25.79
40	TS9-S7	10.45	46.49	6.62	29.43	14.36	63.86	19.67	87.49	18.69	83.12	15.66	69.68	12.24	54.43	6.27	27.87

Table 6-4 (cont'd) Peak Dynamic Shear Forces Induced in I/R Systems during Seismic Tests

Test #	Test ID	Peak Dynamic Shear Forces															
		Load Cell #1				Load Cell #2				Load Cell #3				Load Cell #4			
		Transverse		Longitudinal		Transverse		Longitudinal		Transverse		Longitudinal		Transverse		Longitudinal	
		(kips)	(kN)	(kips)	(kN)	(kips)	(kN)	(kips)	(kN)	(kips)	(kN)	(kips)	(kN)	(kips)	(kN)	(kips)	(kN)
41	TS12-S1	0.711	3.16	0.534	2.38	1.832	8.15	1.862	8.28	1.316	5.85	2.340	10.41	1.148	5.11	0.861	3.83
42	TS12-S1a	2.101	9.35	1.026	4.56	4.413	19.63	3.492	15.53	2.430	10.81	3.983	17.72	3.263	14.51	1.529	6.80
43	TS12-S2	3.141	13.97	1.433	6.38	4.958	22.05	4.755	21.15	3.374	15.01	4.592	20.43	3.970	17.66	1.846	8.21
44	TS12-S3	4.233	18.83	3.123	13.89	4.757	21.16	7.305	32.50	6.408	28.50	7.429	33.05	5.569	24.77	2.673	11.89
45	TS12-S4	5.08	22.59	2.98	13.27	7.47	33.21	9.20	40.91	5.82	25.87	7.87	35.01	6.18	27.49	3.20	14.21
46	TS12-S5	8.96	39.84	4.66	20.71	11.05	49.14	12.88	57.28	8.17	36.35	10.50	46.70	8.60	38.24	4.55	20.22
47	TS12-S6	8.83	39.27	5.05	22.48	9.25	41.13	11.41	50.76	11.69	52.00	12.89	57.33	8.79	39.11	4.57	20.34
48	TS12-S7	13.96	62.07	8.59	38.20	14.55	64.73	22.61	100.56	15.12	67.28	16.95	75.40	17.23	76.63	6.53	29.06
49	TS11-S1	1.84	8.17	0.54	2.40	1.52	6.76	1.45	6.46	1.86	8.26	2.58	11.48	1.76	7.83	0.39	1.73
50	TS11-S1a	3.58	15.91	1.25	5.56	3.06	13.62	3.00	13.36	3.17	14.08	3.92	17.45	3.62	16.09	1.23	5.48
51	TS11-S2	4.91	21.85	1.55	6.90	5.62	24.98	4.71	20.97	4.59	20.43	5.07	22.54	4.60	20.44	1.53	6.81
52	TS11-S3	5.79	25.75	2.75	12.23	5.78	25.71	6.75	30.02	6.86	30.49	7.69	34.20	7.51	33.40	2.39	10.62
53	TS11-S4	6.09	27.09	3.42	15.23	6.61	29.38	8.83	39.28	6.63	29.48	8.22	36.55	7.17	31.89	2.93	13.05
54	TS11-S5	11.40	50.69	4.75	21.11	9.48	42.15	12.84	57.09	8.85	39.37	11.09	49.32	9.06	40.28	3.70	16.48
55	TS11-S6	10.09	44.88	5.95	26.48	9.89	43.97	11.02	49.00	12.31	54.74	12.87	57.24	10.12	45.02	4.13	18.38
56	TS11-S7	15.85	70.51	7.12	31.69	13.87	61.68	20.00	88.96	11.70	52.04	17.75	78.98	12.65	56.25	6.76	30.08
57	TS6-S1	1.68	7.48	0.71	3.15	0.72	3.22	1.47	6.55	0.44	1.96	0.37	1.64	1.34	5.95	1.39	6.19
58	TS6-S1a	3.13	13.90	2.30	10.24	1.71	7.59	4.26	18.94	2.32	10.30	1.82	8.09	2.04	9.09	2.84	12.64
59	TS6-S2	5.50	24.46	2.12	9.42	2.72	12.10	5.63	25.04	4.46	19.84	3.02	13.41	4.08	18.16	2.65	11.77
60	TS6-S3	8.32	37.03	3.83	17.04	5.59	24.87	7.25	32.23	7.38	32.82	6.59	29.33	7.92	35.24	3.33	14.82

Table 6-4 (cont'd) Peak Dynamic Shear Forces Induced in I/R Systems during Seismic Tests

Test #	Test ID	Peak Dynamic Shear Forces															
		Load Cell #1				Load Cell #2				Load Cell #3				Load Cell #4			
		Transverse		Longitudinal		Transverse		Longitudinal		Transverse		Longitudinal		Transverse		Longitudinal	
		(kips)	(kN)	(kips)	(kN)	(kips)	(kN)	(kips)	(kN)	(kips)	(kN)	(kips)	(kN)	(kips)	(kN)	(kips)	(kN)
61	TS6-S4	6.78	30.15	3.10	13.79	4.46	19.82	8.74	38.88	7.28	32.38	6.29	27.97	7.08	31.48	3.44	15.29
62	TS6-S5	10.30	45.82	6.48	28.82	6.01	26.72	12.16	54.10	10.83	48.16	11.96	53.22	8.79	39.10	5.70	25.36
63	TS6-S6	8.89	39.53	4.40	19.55	5.76	25.60	11.25	50.05	9.34	41.56	9.65	42.93	8.49	37.78	4.47	19.87
64	TS6-S7	12.65	56.26	8.54	38.00	9.21	40.97	18.38	81.75	11.01	48.98	13.48	59.97	13.75	61.17	5.96	26.49
65	TS8-S1	2.15	9.54	0.55	2.46	0.87	3.87	1.14	5.06	1.56	6.96	1.44	6.39	1.36	6.07	0.87	3.85
66	TS8-S1a	3.02	13.41	0.99	4.42	1.81	8.05	2.43	10.82	3.15	14.00	2.24	9.95	4.45	19.81	1.42	6.32
67	TS8-S2	3.24	14.40	1.69	7.51	2.35	10.45	3.66	16.30	3.25	14.45	2.84	12.65	5.10	22.68	1.95	8.69
68	TS8-S3	5.12	22.77	2.82	12.53	2.78	12.36	6.08	27.05	5.37	23.87	7.02	31.22	6.89	30.66	2.74	12.20
69	TS8-S4	5.21	23.20	3.11	13.82	3.27	14.56	7.49	33.32	5.95	26.46	8.09	35.99	7.66	34.05	3.84	17.07
70	TS8-S5	9.88	43.96	4.22	18.76	5.32	23.64	11.19	49.77	9.22	40.99	9.82	43.69	10.70	47.61	4.56	20.29
71	TS8-S6	9.79	43.54	4.50	20.00	4.89	21.74	10.32	45.91	7.17	31.89	11.00	48.92	8.36	37.20	4.50	20.04
72	TS8-S7	17.66	78.57	7.75	34.49	6.47	28.76	21.09	93.81	13.48	59.97	17.59	78.25	15.96	70.98	7.06	31.42

1. Test Identification

Table 6-5 Peak Dynamic Normal Forces Induced in I/R Systems during Seismic Tests

Test#	Test ID[1]	Peak Dynamic Normal Forces															
		Load Cell #1				Load Cell #2				Load Cell #3				Load Cell #4			
		Tension		Compression		Tension		Compression		Tension		Compression		Tension		Compression	
		(kips)	(kN)	(kips)	(kN)	(kips)	(kN)	(kips)	(kN)	(kips)	(kN)	(kips)	(kN)	(kips)	(kN)	(kips)	(kN)
1	TS10-S1	2.4	10.6	-1.2	-5.4	1.5	6.8	-1.4	-6.3	1.6	7.2	-1.3	-5.9	1.6	6.9	-1.4	-6.3
2	TS10-S1a	3.7	16.4	-3.3	-14.9	3.8	16.8	-2.5	-10.9	3.4	15.2	-3.5	-15.6	3.2	14.0	-3.0	-13.5
3	TS10-S2	3.8	17.1	-5.8	-25.9	4.6	20.2	-5.2	-23.1	4.5	20.2	-5.0	-22.3	5.0	22.5	-5.0	-22.2
4	TS10-S3	6.6	29.3	-8.1	-36.0	8.9	39.4	-9.7	-43.3	9.4	41.8	-9.8	-43.5	5.5	24.5	-7.4	-33.0
5	TS10-S4	7.5	33.2	-9.1	-40.3	10.8	48.0	-10.3	-45.8	13.2	58.7	-7.3	-32.5	7.0	31.1	-10.7	-47.8
6	TS2-S1	1.4	6.3	-1.1	-4.9	1.9	8.5	-1.0	-4.4	1.9	8.6	-1.5	-6.5	1.3	5.8	-1.7	-7.4
7	TS2-S1a	3.1	13.6	-3.7	-16.3	2.9	12.7	-3.8	-16.9	3.3	14.5	-3.8	-16.7	2.1	9.1	-3.6	-15.9
8	TS2-S2	4.4	19.7	-6.7	-30.0	5.2	23.2	-7.5	-33.3	3.7	16.6	-6.0	-26.6	5.5	24.6	-5.7	-25.4
9	TS2-S3	6.0	26.5	-9.3	-41.3	8.2	36.6	-6.9	-30.7	8.3	36.9	-9.0	-40.2	6.2	27.8	-7.4	-32.7
10	TS2-S4	16.2	72.2	-9.4	-42.0	10.1	45.0	-8.3	-36.8	8.5	37.7	-9.3	-41.5	10.2	45.5	-10.1	-45.1
11	TS2-S5	15.4	68.7	-18.5	-82.3	13.5	59.9	-18.8	-83.6	17.7	78.6	-19.2	-85.6	13.6	60.3	-17.6	-78.1
12	TS2-S6	17.1	76.0	-18.5	-82.1	19.3	85.7	-15.7	-69.9	21.6	95.9	-20.7	-91.9	17.4	77.3	-15.6	-69.5
13	TS2-S7	29.2	129.7	-33.5	-149.0	37.4	166.4	-26.8	-119.0	34.5	153.7	-30.9	-137.6	30.2	134.4	-41.2	-183.1
14	TS2-S8	30.8	137.2	-25.8	-114.6	92.1	409.9	-26.6	-118.1	43.4	193.1	-26.8	-119.1	23.8	105.7	-32.5	-144.6
15	TS2-S8a	106.4	473.4	-41.9	-186.2	105.0	467.3	-33.6	-149.3	106.5	473.5	-30.7	-136.4	49.4	219.9	-46.7	-207.5
16	TS4-S1	5.5	24.3	-3.5	-15.7	3.2	14.3	-2.5	-11.2	1.9	8.5	-2.4	-10.6	1.2	5.3	-2.4	-10.5
17	TS4-S3	9.4	41.8	-8.4	-37.4	10.6	47.0	-8.8	-39.0	5.9	26.0	-5.3	-23.8	5.8	26.0	-5.4	-24.2
18	TS4-S5	15.2	67.5	-18.0	-80.1	14.4	64.1	-14.6	-64.9	9.1	40.6	-9.8	-43.5	8.3	36.9	-11.5	-51.3
19	TS4-S7	52.8	234.8	-21.6	-96.1	24.0	106.9	-33.4	-148.7	13.8	61.4	-22.7	-101.1	24.0	106.9	-18.2	-80.8
20	TS4-S8	34.0	151.1	-22.6	-100.7	18.6	82.9	-32.0	-142.2	20.3	90.1	-18.7	-83.4	29.3	130.3	-23.7	-105.6

Table 6-5 (cont'd) Peak Dynamic Normal Forces Induced in I/R Systems during Seismic Tests

Test#	Test ID	Peak Dynamic Normal Forces															
		Load Cell #1				Load Cell #2				Load Cell #3				Load Cell #4			
		Tension		Compression		Tension		Compression		Tension		Compression		Tension		Compression	
		(kips)	(kN)	(kips)	(kN)	(kips)	(kN)	(kips)	(kN)	(kips)	(kN)	(kips)	(kN)	(kips)	(kN)	(kips)	(kN)
21	TS7-S1	4.3	19.0	-3.3	-14.9	5.2	22.9	-4.7	-20.9	5.2	23.2	-4.5	-19.8	2.9	13.0	-2.6	-11.5
22	TS7-S3	12.0	53.6	-8.2	-36.7	9.0	40.2	-10.0	-44.6	10.0	44.6	-8.4	-37.2	10.2	45.2	-8.1	-35.9
23	TS7-S5	19.6	87.1	-18.4	-82.0	15.6	69.5	-16.8	-74.6	21.4	95.1	-14.9	-66.3	13.1	58.4	-14.0	-62.1
24	TS7-S7	22.4	99.5	-24.3	-108.2	31.0	137.8	-29.7	-132.1	40.3	179.3	-20.1	-89.6	23.0	102.3	-19.6	-87.3
25	TS5-S1	1.8	7.9	-1.9	-8.6	2.6	11.7	-1.3	-5.9	1.5	6.8	-1.9	-8.5	1.9	8.6	-1.0	-4.6
26	TS5-S1a	4.7	20.7	-3.7	-16.4	4.0	17.8	-4.8	-21.2	4.8	21.4	-3.4	-15.0	3.8	16.8	-3.9	-17.4
27	TS5-S2	6.2	27.8	-7.6	-33.9	6.3	28.0	-7.6	-33.6	7.7	34.1	-5.7	-25.3	6.8	30.2	-6.3	-27.8
28	TS5-S3	11.2	49.6	-6.8	-30.2	11.3	50.5	-8.7	-38.7	14.0	62.4	-7.8	-34.6	8.6	38.1	-9.1	-40.3
29	TS5-S4	16.4	73.1	-9.0	-39.9	14.0	62.3	-10.0	-44.5	14.5	64.3	-9.1	-40.3	16.2	72.2	-9.7	-43.0
30	TS5-S5	16.7	74.1	-20.2	-89.8	21.9	97.6	-19.1	-84.9	21.5	95.6	-16.6	-73.8	22.5	100.0	-18.7	-83.0
31	TS5-S6	22.3	99.3	-16.9	-75.4	25.3	112.4	-19.1	-85.0	29.0	128.8	-17.8	-79.0	22.6	100.7	-15.6	-69.2
32	TS5-S7	30.1	133.8	-34.9	-155.3	99.6	442.9	-15.3	-68.1	32.9	146.4	-31.0	-137.9	26.3	116.8	-24.4	-108.5
33	TS9-S1	1.9	8.6	-1.9	-8.2	2.4	10.8	-1.1	-4.8	2.6	11.5	-2.2	-9.6	2.4	10.7	-2.2	-9.9
34	TS9-S1a	5.9	26.0	-3.1	-13.7	4.6	20.6	-4.3	-19.3	5.9	26.1	-5.1	-22.6	4.4	19.5	-4.2	-18.6
35	TS9-S2	8.6	38.2	-6.6	-29.1	9.9	44.1	-8.2	-36.3	5.3	23.5	-5.7	-25.3	7.8	34.9	-7.2	-32.0
36	TS9-S3	13.1	58.2	-10.7	-47.8	10.5	46.7	-10.4	-46.1	10.3	45.9	-9.5	-42.3	8.5	37.9	-9.3	-41.2
37	TS9-S4	10.0	44.3	-8.6	-38.4	12.9	57.6	-7.3	-32.7	13.2	58.5	-11.4	-50.6	10.2	45.5	-11.4	-50.6
38	TS9-S5	18.6	82.7	-18.9	-83.9	20.6	91.8	-19.3	-85.6	19.6	87.0	-17.7	-78.8	17.3	77.1	-18.1	-80.6
39	TS9-S6	18.9	84.2	-15.7	-69.9	24.4	108.4	-19.0	-84.5	25.8	114.9	-18.1	-80.6	22.7	100.9	-15.6	-69.3
40	TS9-S7	31.8	141.3	-26.6	-118.2	53.4	237.7	-21.0	-93.3	32.2	143.4	-29.1	-129.5	24.6	109.3	-24.1	-107.2

Table 6-5 (cont'd) Peak Dynamic Normal Forces Induced in I/R Systems during Seismic Tests

Test#	Test ID	Peak Dynamic Normal Forces															
		Load Cell #1				Load Cell #2				Load Cell #3				Load Cell #4			
		Tension		Compression		Tension		Compression		Tension		Compression		Tension		Compression	
		(kips)	(kN)	(kips)	(kN)	(kips)	(kN)	(kips)	(kN)	(kips)	(kN)	(kips)	(kN)	(kips)	(kN)	(kips)	(kN)
41	TS12-S1	1.9	8.6	-1.9	-8.5	2.6	11.3	-1.6	-6.9	2.0	8.9	-2.6	-11.6	2.3	10.3	-2.1	-9.3
42	TS12-S1a	4.0	17.9	-3.8	-17.0	3.1	14.0	-4.1	-18.1	4.3	19.2	-4.2	-18.6	3.5	15.6	-4.0	-17.7
43	TS12-S2	6.1	27.4	-7.0	-31.4	6.2	27.7	-7.4	-32.9	5.2	23.2	-4.5	-20.1	5.0	22.2	-7.0	-31.2
44	TS12-S3	8.9	39.7	-8.9	-39.5	7.1	31.7	-9.7	-43.1	9.3	41.5	-8.9	-39.6	7.0	31.3	-8.2	-36.3
45	TS12-S4	7.8	34.7	-9.1	-40.4	9.3	41.2	-9.1	-40.5	8.8	39.0	-11.0	-48.9	9.6	42.7	-10.8	-48.2
46	TS12-S5	14.8	66.0	-18.8	-83.6	14.6	64.7	-20.8	-92.4	14.0	62.4	-19.1	-84.8	10.0	44.5	-23.0	-102.4
47	TS12-S6	14.8	65.9	-18.9	-84.2	18.2	81.0	-20.2	-89.8	21.0	93.2	-16.5	-73.4	19.0	84.3	-17.5	-77.7
48	TS12-S7	21.9	97.6	-51.3	-228.2	65.1	289.7	-19.1	-84.7	25.5	113.6	-25.2	-112.2	22.3	99.4	-28.5	-126.7
49	TS11-S1	2.5	11.1	-2.2	-9.8	2.7	12.1	-1.8	-8.2	2.4	10.6	-2.1	-9.5	2.3	10.3	-1.9	-8.3
50	TS11-S1a	3.7	16.3	-4.8	-21.6	2.7	12.1	-5.0	-22.3	3.9	17.4	-3.8	-17.1	2.7	11.8	-4.0	-18.0
51	TS11-S2	5.9	26.0	-7.2	-32.0	6.6	29.5	-8.6	-38.2	4.5	20.1	-5.1	-22.6	5.8	25.9	-6.3	-28.2
52	TS11-S3	8.3	37.1	-9.5	-42.4	6.7	29.7	-9.3	-41.2	9.0	40.2	-8.2	-36.3	6.8	30.3	-9.4	-41.9
53	TS11-S4	9.0	40.2	-11.6	-51.4	8.9	39.5	-9.8	-43.8	8.4	37.4	-9.4	-42.0	7.7	34.3	-9.1	-40.5
54	TS11-S5	18.0	80.0	-17.6	-78.3	13.9	61.8	-18.8	-83.5	13.9	61.9	-17.8	-79.0	13.8	61.3	-19.6	-87.1
55	TS11-S6	15.8	70.5	-16.8	-74.9	18.4	82.0	-20.7	-91.9	21.5	95.8	-16.1	-71.8	17.3	77.0	-14.7	-65.2
56	TS11-S7	25.2	112.2	-38.1	-169.5	51.7	229.8	-36.5	-162.6	21.6	96.3	-27.3	-121.4	24.0	106.7	-24.0	-106.5
57	TS6-S1	2.2	9.7	-1.8	-7.9	1.6	6.9	-1.5	-6.6	1.8	7.8	-1.6	-7.3	1.6	6.9	-1.5	-6.7
58	TS6-S1a	2.0	8.9	-3.2	-14.1	2.3	10.4	-2.7	-12.0	1.7	7.4	-4.2	-18.6	3.6	15.9	-2.5	-11.0
59	TS6-S2	4.9	21.8	-4.3	-19.0	7.6	33.7	-2.6	-11.4	4.6	20.5	-5.8	-25.8	6.1	27.3	-3.5	-15.7
60	TS6-S3	13.1	58.3	-10.8	-48.1	10.8	48.2	-12.0	-53.5	12.0	53.3	-12.1	-53.8	6.7	29.8	-10.3	-45.7

Table 6-5 (cont'd) Peak Dynamic Normal Forces Induced in I/R Systems during Seismic Tests

Test#	Test ID	Peak Dynamic Normal Forces															
		Load Cell #1				Load Cell #2				Load Cell #3				Load Cell #4			
		Tension		Compression		Tension		Compression		Tension		Compression		Tension		Compression	
		(kips)	(kN)	(kips)	(kN)	(kips)	(kN)	(kips)	(kN)	(kips)	(kN)	(kips)	(kN)	(kips)	(kN)	(kips)	(kN)
61	TS6-S4	11.0	49.0	-11.3	-50.4	15.9	70.8	-11.3	-50.1	11.7	52.1	-10.1	-44.7	8.6	38.4	-9.8	-43.5
62	TS6-S5	18.0	80.3	-20.0	-88.9	15.0	66.6	-19.3	-86.1	17.6	78.1	-17.3	-76.8	23.5	104.7	-15.0	-66.7
63	TS6-S6	17.8	79.0	-18.1	-80.6	18.3	81.2	-23.6	-105.1	13.7	61.1	-14.2	-63.2	13.8	61.2	-22.3	-99.4
64	TS6-S7	24.4	108.6	-36.4	-162.1	18.2	80.9	-34.9	-155.3	24.6	109.4	-23.5	-104.5	21.6	96.2	-27.5	-122.1
65	TS8-S1	3.1	13.7	-1.7	-7.6	3.0	13.3	-1.5	-6.8	1.9	8.5	-1.5	-6.9	6.7	29.8	-1.3	-5.7
66	TS8-S1a	4.6	20.4	-5.0	-22.1	4.4	19.4	-5.0	-22.3	5.2	23.0	-3.7	-16.7	4.2	18.7	-3.7	-16.3
67	TS8-S2	5.7	25.5	-6.6	-29.5	6.7	29.6	-7.7	-34.4	4.1	18.4	-5.0	-22.1	5.6	24.7	-6.2	-27.6
68	TS8-S3	9.6	42.5	-8.7	-38.7	7.0	31.2	-10.3	-45.9	9.1	40.5	-7.6	-34.0	8.3	36.9	-7.0	-31.4
69	TS8-S4	10.6	47.1	-10.5	-46.7	10.9	48.5	-10.5	-46.7	9.3	41.3	-9.4	-41.7	9.8	43.4	-10.2	-45.4
70	TS8-S5	14.1	62.9	-22.0	-97.9	12.8	56.9	-19.9	-88.4	13.5	60.1	-18.7	-83.2	11.2	49.7	-18.2	-81.2
71	TS8-S6	17.8	79.3	-17.5	-77.8	19.3	85.7	-18.8	-83.4	19.6	87.1	-17.1	-76.0	15.5	68.8	-17.5	-78.0
72	TS8-S7	36.0	160.2	-51.3	-228.4	76.6	340.8	-32.4	-144.2	22.3	99.0	-25.9	-115.0	28.2	125.6	-22.5	-100.0

1. Test Identification

Table 6-6 Peak Relative Displacement at South Face of Chiller during Seismic Tests

Test#	Test ID[1]	Peak Relative Displacement (mm)											
		West-Top			West-Bottom			East-Top			East-Bottom		
		Trans.[2]	Long.[3]	Vert.[4]	Trans.	Long.	Vert.	Trans.	Long.	Vert.	Trans.	Long.	Vert.
1	TS10-S1	12.9	11.3	8.8	9.2	10.7	8.6	12.7	11.5	9.0	9.3	10.2	9.0
2	TS10-S1a	20.3	17.5	11.5	13.6	16.0	11.3	20.1	20.3	10.8	13.4	17.5	10.6
3	TS10-S2	33.6	20.9	12.5	21.1	18.8	12.5	33.0	21.0	13.9	20.8	17.5	14.0
4	TS10-S3	41.9	23.6	16.5	26.3	20.1	16.4	41.1	29.8	16.6	25.9	24.5	16.7
5	TS10-S4	40.0	22.0	17.1	27.0	19.3	17.1	39.4	24.3	18.5	26.8	21.0	18.5
6	TS2-S1	16.2	6.5	6.9	11.5	5.2	7.0	16.0	5.8	6.7	11.3	4.5	6.8
7	TS2-S1a	23.0	8.3	12.9	15.3	6.7	12.7	22.6	9.2	10.1	15.1	7.9	10.2
8	TS2-S2	26.8	10.9	16.6	17.1	8.0	16.6	26.3	12.1	13.3	16.7	8.7	13.3
9	TS2-S3	28.9	14.3	16.2	17.2	10.2	16.0	28.3	15.4	15.7	16.9	11.3	15.7
10	TS2-S4	32.8	15.8	17.6	18.3	11.3	17.5	32.1	18.5	16.5	18.0	12.5	16.4
11	TS2-S5	42.8	20.8	26.0	20.8	13.5	26.1	41.6	21.7	23.4	20.2	14.3	23.6
12	TS2-S6	44.6	21.0	25.0	21.6	14.0	25.4	43.8	40.3	25.3	20.9	15.3	23.4
13	TS2-S7	61.6	24.5	38.3	28.0	15.7	38.8	N/A[5]	N/A	N/A	27.0	14.3	39.2
14	TS2-S8	N/A	N/A	N/A	24.0	23.1	38.2	N/A	N/A	N/A	23.2	19.5	36.2
15	TS2-S8a	66.5	35.8	49.0	34.9	23.2	49.7	N/A	39.9	50.1	33.5	22.1	50.3
16	TS4-S1	8.4	4.8	4.4	5.8	3.8	4.4	8.4	5.7	6.3	5.9	4.6	6.2
17	TS4-S3	12.8	8.2	8.4	8.7	6.0	8.5	12.8	9.2	9.2	8.9	7.0	9.1
18	TS4-S5	16.5	9.8	12.6	9.8	6.3	12.7	16.9	9.2	14.2	10.2	7.3	14.2
19	TS4-S7	24.5	19.6	17.1	13.7	13.5	17.2	25.0	23.9	23.2	14.2	16.5	23.0
20	TS4-S8	30.8	19.7	17.6	16.5	13.6	17.9	31.6	24.9	22.7	17.0	16.3	22.5

Table 6-6 (cont'd) Peak Relative Displacement at South Face of Chiller during Seismic Tests

Test#	Test ID	Peak Relative Displacement (mm)											
		West-Top			West-Bottom			East-Top			East-Bottom		
		Trans.	Long.	Vert.	Trans.	Long.	Vert.	Trans.	Long.	Vert.	Trans.	Long.	Vert.
21	TS7-S1	17.6	9.8	11.1	12.6	8.1	11.2	17.7	10.5	9.5	12.7	8.9	9.4
22	TS7-S3	21.2	13.7	12.0	13.9	10.9	12.1	21.7	16.3	14.1	14.2	12.0	14.0
23	TS7-S5	25.5	17.7	15.5	15.1	13.4	15.6	26.1	21.8	17.9	15.6	15.2	17.9
24	TS7-S7	29.4	N/A	N/A	16.8	42.0	43.4	29.9	N/A	32.8	17.5	N/A	33.6
25	TS5-S1	14.3	7.0	8.2	10.0	5.5	8.2	14.5	7.4	8.3	10.2	6.2	8.3
26	TS5-S1a	17.5	7.5	10.0	11.2	6.6	10.2	17.9	11.3	10.1	11.4	8.9	10.0
27	TS5-S2	18.8	10.5	12.4	12.0	7.9	12.5	19.2	12.9	12.8	12.2	11.1	12.7
28	TS5-S3	19.9	14.2	12.9	11.7	10.6	13.0	20.4	17.8	13.2	12.0	14.1	13.2
29	TS5-S4	21.3	16.1	13.7	12.5	11.2	14.0	21.7	18.5	14.7	12.9	14.5	14.6
30	TS5-S5	26.1	20.5	18.9	14.5	15.5	19.2	26.3	23.6	18.7	14.8	17.4	18.6
31	TS5-S6	26.9	21.0	18.5	16.0	15.9	18.8	27.5	23.2	16.7	16.5	17.4	16.6
32	TS5-S7	31.8	28.9	21.8	18.3	22.0	22.1	32.5	33.3	21.7	19.1	22.6	21.6
33	TS9-S1	12.8	8.4	7.6	8.2	7.4	7.7	12.9	7.5	8.4	8.2	6.3	8.4
34	TS9-S1a	17.4	9.5	9.8	10.2	8.7	9.9	17.5	10.2	9.8	10.2	8.8	9.6
35	TS9-S2	17.8	13.3	12.3	10.9	11.6	12.4	18.1	15.0	10.7	10.9	10.6	10.6
36	TS9-S3	19.7	14.3	14.2	11.8	11.7	14.3	19.9	16.0	14.1	12.2	11.9	13.8
37	TS9-S4	20.1	16.0	12.6	12.1	13.4	12.5	20.5	17.3	11.8	12.4	12.5	11.7
38	TS9-S5	27.2	19.6	17.1	15.9	14.6	17.4	27.8	23.7	17.2	16.7	16.7	17.0
39	TS9-S6	27.3	21.3	17.1	16.2	17.4	17.5	27.5	23.2	14.7	16.7	16.7	14.6
40	TS9-S7	33.9	30.2	21.7	20.6	23.9	22.0	34.5	35.1	20.7	21.3	23.2	20.6

Table 6-6 (cont'd) Peak Relative Displacement at South Face of Chiller during Seismic Tests

Test#	Test ID	Peak Relative Displacement (mm)											
		West-Top			West-Bottom			East-Top			East-Bottom		
		Trans.	Long.	Vert.	Trans.	Long.	Vert.	Trans.	Long.	Vert.	Trans.	Long.	Vert.
41	TS12-S1	13.1	7.5	8.7	8.4	6.3	8.8	13.2	8.4	8.6	8.6	7.1	8.6
42	TS12-S1a	16.0	9.2	8.9	9.5	7.5	9.0	16.2	12.2	10.3	9.8	10.1	10.2
43	TS12-S2	18.9	12.4	11.2	10.7	9.1	11.2	19.2	13.1	11.7	11.0	10.9	11.6
44	TS12-S3	20.2	15.2	12.0	11.4	12.0	12.1	20.7	18.0	12.9	11.8	12.8	12.8
45	TS12-S4	20.8	16.4	13.1	12.9	11.8	13.3	21.3	18.1	15.1	13.2	13.2	14.8
46	TS12-S5	30.5	20.6	18.6	16.5	14.4	18.9	30.8	23.7	21.2	16.8	16.9	21.0
47	TS12-S6	30.2	21.4	19.7	16.1	16.2	19.7	30.6	23.3	21.4	16.3	16.2	21.2
48	TS12-S7	40.8	29.0	25.5	22.2	20.0	25.8	42.3	32.9	31.0	23.2	21.1	30.7
49	TS11-S1	11.5	8.8	7.5	7.5	7.5	7.6	11.8	8.5	8.3	7.7	7.0	8.3
50	TS11-S1a	15.2	10.1	9.8	9.7	8.7	10.0	15.5	12.0	10.2	10.1	9.1	10.1
51	TS11-S2	17.8	13.9	12.1	11.4	10.4	12.3	18.2	14.7	12.1	11.9	10.8	12.0
52	TS11-S3	19.5	15.9	12.0	11.6	11.8	12.2	20.1	17.5	14.1	12.0	12.2	14.0
53	TS11-S4	20.5	16.8	13.0	12.7	11.8	13.3	20.9	19.3	14.2	12.9	13.4	14.1
54	TS11-S5	28.7	21.4	18.3	15.2	15.3	18.6	28.9	24.0	20.4	15.9	15.9	20.3
55	TS11-S6	28.4	20.0	18.9	15.8	14.3	19.3	28.8	23.4	18.6	16.5	15.3	18.5
56	TS11-S7	36.9	29.7	23.8	20.4	21.1	24.0	38.1	32.9	24.4	21.4	21.2	24.2
57	TS6-S1	19.7	12.0	10.5	13.4	10.8	10.5	20.0	12.7	13.4	13.7	10.8	13.3
58	TS6-S1a	22.0	16.5	14.8	14.7	14.7	14.8	22.4	17.8	15.1	15.0	14.8	15.0
59	TS6-S2	28.6	18.4	17.8	17.4	16.2	17.8	29.0	20.3	16.8	17.7	17.6	16.7
60	TS6-S3	37.2	22.2	20.9	21.7	18.6	21.0	37.5	25.7	21.2	22.0	20.4	21.0

Table 6-6 (cont'd) Peak Relative Displacement at South Face of Chiller during Seismic Tests

Test#	Test ID	Peak Relative Displacement (mm)											
		West-Top			West-Bottom			East-Top			East-Bottom		
		Trans.	Long.	Vert.	Trans.	Long.	Vert.	Trans.	Long.	Vert.	Trans.	Long.	Vert.
61	TS6-S4	33.9	21.9	20.5	19.0	18.2	20.4	34.9	26.8	21.3	20.0	21.6	21.3
62	TS6-S5	39.1	29.6	24.3	22.1	21.8	24.7	40.3	33.4	25.9	23.2	24.9	25.8
63	TS6-S6	39.0	26.7	25.6	21.9	21.7	26.2	40.3	29.9	26.9	22.9	23.2	26.7
64	TS6-S7	44.6	34.5	32.2	25.5	25.8	32.6	45.0	39.4	33.1	25.9	29.2	33.3
65	TS8-S1	13.9	7.2	9.0	9.5	6.4	9.0	14.1	7.7	8.5	9.6	6.5	8.5
66	TS8-S1a	17.1	9.1	10.3	10.6	8.0	10.3	17.3	10.8	9.9	10.7	9.3	9.8
67	TS8-S2	18.3	10.9	11.4	11.1	9.5	11.4	18.6	13.0	11.2	11.4	10.6	11.1
68	TS8-S3	22.0	15.4	12.5	13.2	12.7	12.6	22.5	16.8	12.7	13.6	12.8	12.6
69	TS8-S4	22.1	16.3	13.9	12.8	13.2	13.8	22.6	18.3	13.2	13.2	13.7	13.2
70	TS8-S5	29.7	20.3	17.8	17.0	15.8	18.1	30.6	24.9	18.9	17.7	17.6	18.9
71	TS8-S6	28.6	20.8	19.7	16.5	16.5	19.5	29.6	23.5	16.4	17.1	16.5	16.4
72	TS8-S7	39.0	29.7	22.0	22.4	22.9	22.3	40.1	33.5	23.5	23.4	22.2	23.3

1. Test Identification
2. Transverse Direction
3. Longitudinal Direction
4. Vertical Direction
5. Not Available

SECTION 7

SEISMIC TEST RESULTS ANALYSES

The seismic test results presented in Section 6 are analyzed in this section. Sensitivity analyses for various variables are conducted in order to identify specific trends in the seismic performance of the I/R systems supporting the chiller.

7.1 Seismic Response at Test Specimen Center of Mass

The peak acceleration response at the center of mass of a rigidly mounted chiller in each direction is almost equal to the peak input acceleration in the corresponding direction. In other words, for a rigidly mounted chiller, there is little-to-no acceleration amplification. For a chiller mounted on I/R systems, on the other hand, compared to the peak input acceleration, the peak acceleration responses at the center of mass of the chiller can be amplified up to several times. There are several reasons for the amplification of acceleration response at the center of mass of the chiller including the vertical distance between the center of mass and the supports plane and the impacts in the restraint component of I/R systems. An acceleration amplification factor at the center of mass of the chiller can be defined as:

$$A.A.F. = \frac{a_{max,CM}}{a_{max,Inp}} \qquad (7\text{-}1)$$

where:

$A.A.F.$ = the acceleration amplification factor
$a_{max,CM}$ = the peak acceleration response at the center of mass of the chiller
$a_{max,Inp}$ = the corresponding input peak acceleration

The $A.A.F.$ can be defined for acceleration response in any directions (longitudinal, transverse, and vertical) of the response, as well as for the horizontal and resultant acceleration response. The acceleration response histories at the center of mass of the chiller in the transverse, longitudinal, and vertical directions (measured directly by the accelerometers) were used in equations 7-2 and 7-3 to calculate the horizontal and resultant acceleration response histories at the center of mass of the chiller:

$$|a_H(t)| = \sqrt{a_T(t)^2 + a_L(t)^2} \qquad (7\text{-}2)$$

$$|a_R(t)| = \sqrt{a_T(t)^2 + a_L(t)^2 + a_V(t)^2} \qquad (7\text{-}3)$$

where:

$a_T(t)$ = the transverse acceleration response
$a_L(t)$ = the longitudinal acceleration response
$a_V(t)$ = the vertical acceleration response
$a_H(t)$ = the horizontal acceleration response
$a_R(t)$ = the resultant acceleration response

The variation of the transverse, longitudinal, horizontal, vertical, and resultant acceleration response amplification factors at the center of mass of the chiller with the corresponding peak input acceleration during the 72 seismic tests are presented in figures 7-1(a) through 7-1(e). For any given seismic test, according to equation 7-1, multiplying the peak input acceleration (the horizontal axis) by the corresponding acceleration amplification factor (the vertical axis) directly gives the peak acceleration response experienced at the center of mass of the chiller.

In most of the tests with peak input accelerations larger than 0.15g, the acceleration amplification factor reduces with an increase of the peak input acceleration. The maximum and minimum amplification factors for each of the transverse, longitudinal, vertical, horizontal, and resultant acceleration responses are listed in tables 7-1 through 7-4. During all the 72 seismic tests conducted, the acceleration amplification factor varies between 1.8 and 4.5 for the horizontal acceleration response, between 2.2 and 4.5 for the vertical acceleration response, and between 2.2 and 4.3 for the resultant acceleration response.

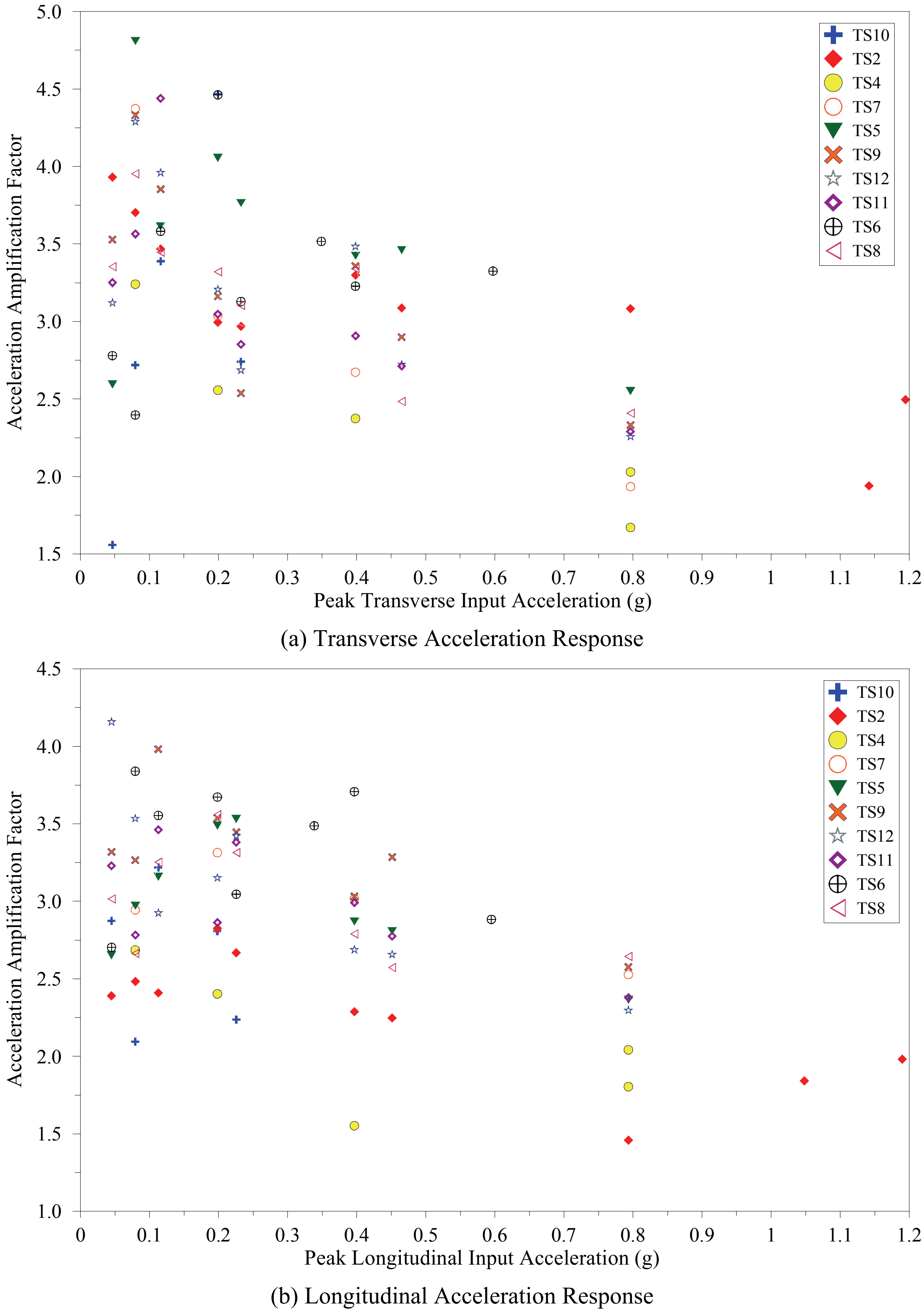

(a) Transverse Acceleration Response

(b) Longitudinal Acceleration Response

Figure 7-1 Variations of Acceleration Amplification Factors at Center of Mass of Chiller with Peak Input Acceleration

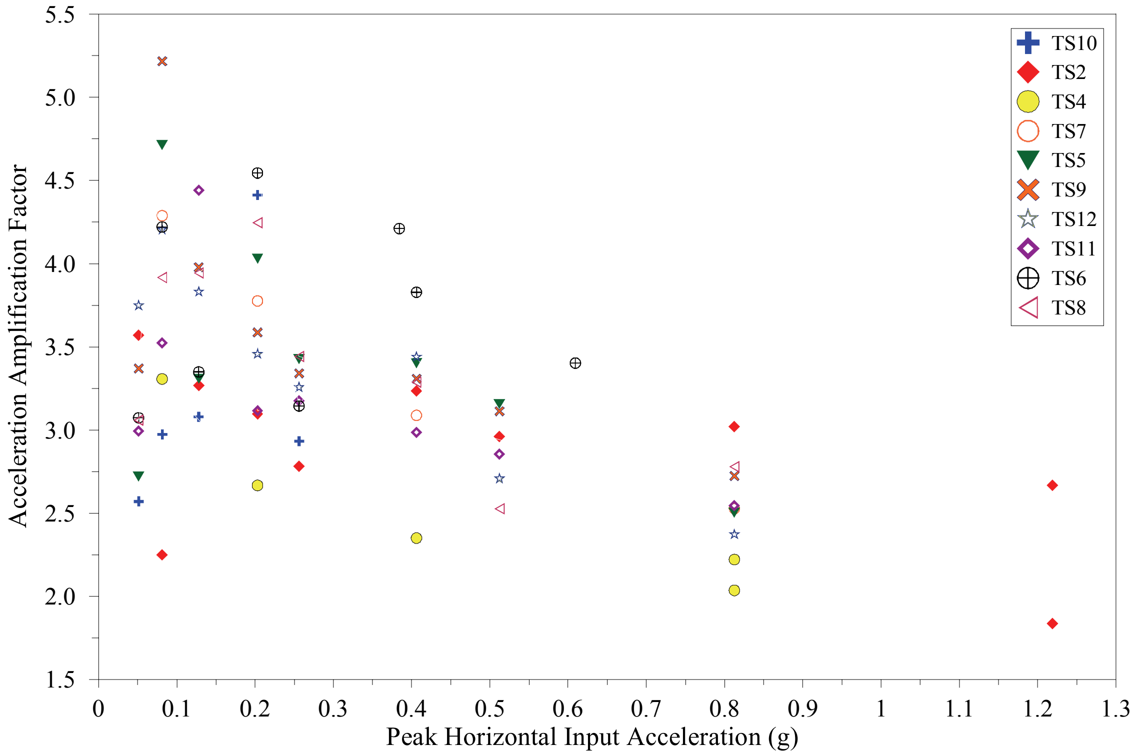

(c) Horizontal Acceleration Response

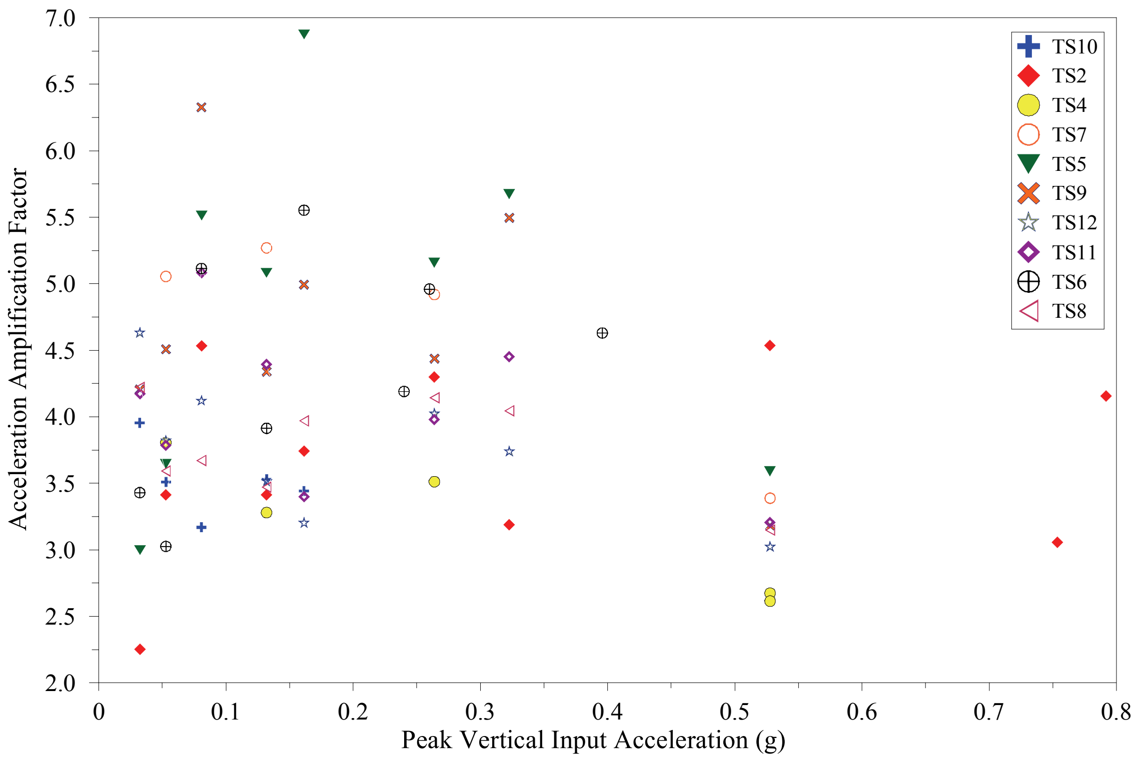

(d) Vertical Acceleration Response

Figure 7-1 (cont'd) Variations of Acceleration Amplification Factors at Center of Mass of Chiller with Peak Input Acceleration

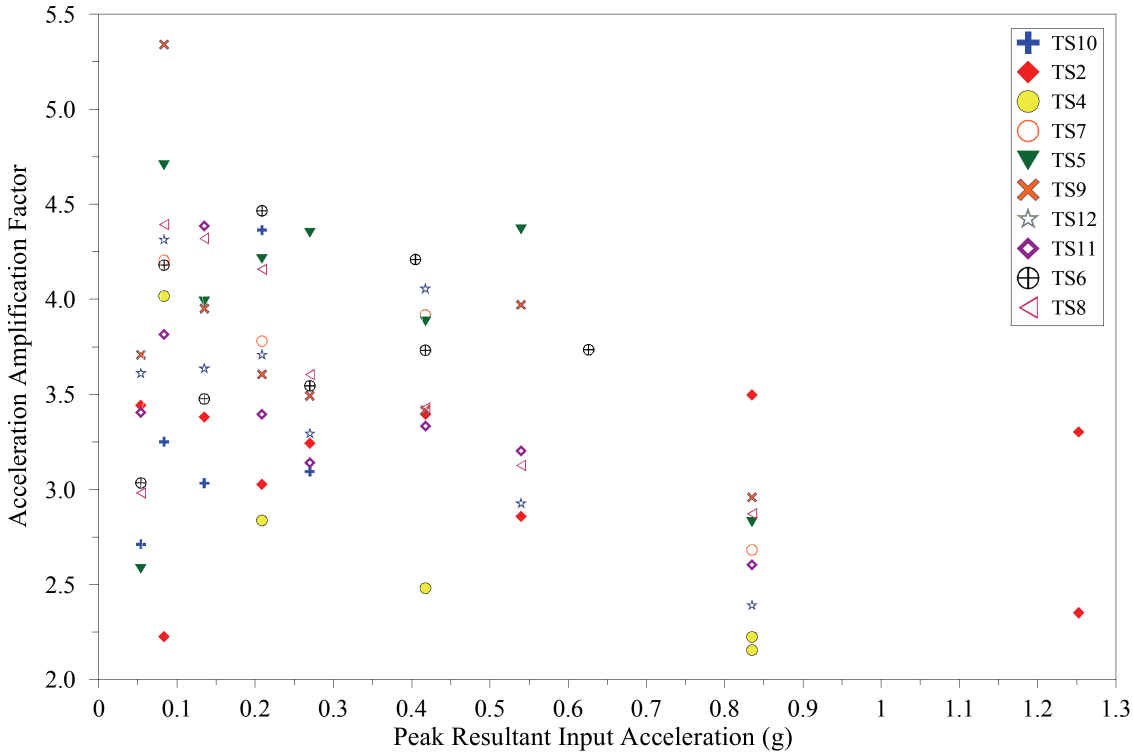

(e) Resultant Acceleration Response

Figure 7-1 (cont'd) Variations of Acceleration Amplification Factors at Center of Mass of Chiller with Peak Input Acceleration

From the two different 1.0 g design I/R systems tested, the system tested in Test Series TS10 (with the larger gap size and thicker rubber pad) induced the larger acceleration amplification factors at the center of mass of the chiller and therefore exhibited the poorer seismic performance. Among the 3.0 g design I/R systems, those tested in Test Series TS4 induced the smallest acceleration amplification factors and those tested in Test Series TS5, TS6, and TS9 induced the largest. Therefore, the 3.0 g design I/R systems tested in Test Series TS4 exhibited the best seismic performance, and the 3.0 g design I/R systems tested in Test Series TS5, TS6, and TS9 exhibited the poorest. However, considering the fact that the seismic performance of the I/R systems tested in Test Series TS5 and TS9 were significantly affected by the malfunctioning of their vertical restraint component (see Section 5.6), leaves the I/R systems tested in Test Series TS6 as the sole nominee for the poorest seismic performance.

The maximum acceleration responses at the center of mass of the chiller during all of the 72 seismic tests conducted are listed in tables 7-5 and 7-6. As predicted, the maximum acceleration responses have occurred in the tests with the maximum input motion amplitudes. The center of mass of the chiller mounted on the 1.0 g and 3.0 g design I/R systems experienced resultant peak accelerations up to 4.14g and 2.47g, respectively.

Table 7-1 Maximum Acceleration Amplification Factors at Center of Mass of Chiller Mounted on 1.0 g Design I/R Systems

Acceleration Component	Maximum A.A.F.	Test ID	Input Motion		Peak Response at Center of Mass (g)
			Amplitude / Level	Peak Acceleration (g)	
Transverse	4.5	TS10-S3	25% / Roof	0.20	0.89
Longitudinal	3.3	TS10-S2	25% / Base	0.11	0.36
Horizontal	4.5	TS10-S3	25% / Roof	0.20	0.90
Vertical	4.5	TS2-S7	100% / Roof	0.53	2.39
Resultant	4.3	TS10-S3	25% / Roof	0.21	0.91

Table 7-2 Maximum Acceleration Amplification Factors at Center of Mass of Chiller Mounted on 3.0 g Design I/R Systems

Acceleration Component	Maximum A.A.F.	Test ID	Input Motion		Peak Response at Center of Mass (g)
			Amplitude / Level	Peak Acceleration (g)	
Transverse	4.8	TS5-S1a	10% / Roof	0.08	0.38
Longitudinal	4.2	TS12-S1	10% / Base	0.05	0.19
Horizontal	4.5	TS9-S1a	10% / Roof	0.20	0.90
Vertical	6.9	TS5-S4	50% / Base	0.16	1.11
Resultant	4.3	TS9-S1a	10% / Roof	0.21	0.91

Table 7-3 Minimum Acceleration Amplification Factors at Center of Mass of Chiller Mounted on 1.0 g Design I/R Systems

Acceleration Component	Minimum A.A.F.	Test ID	Input Motion		Peak Response at Center of Mass (g)
			Amplitude / Level	Peak Acceleration (g)	
Transverse	1.6	TS10-S1	10% / Base	0.05	0.07
Longitudinal	1.5	TS2-S7	100% / Roof	0.79	1.16
Horizontal	1.8	TS2-S8	150% / Roof	1.22	2.24
Vertical	2.3	TS2-S1	10% / Base	0.03	0.07
Resultant	2.2	TS2-S1a	10% / Roof	0.08	0.19

Table 7-4 Minimum Acceleration Amplification Factors at Center of Mass of Chiller Mounted on 3.0 g Design I/R Systems

Acceleration Component	Minimum A.A.F.	Test ID	Input Motion		Peak Response at Center of Mass (g)
			Amplitude / Level	Peak Acceleration (g)	
Transverse	1.7	TS4-S8	100% / Roof	0.80	1.33
Longitudinal	1.6	TS4-S5	50% / Roof	0.40	0.62
Horizontal	2.0	TS4-S8	100% / Roof	0.81	1.66
Vertical	2.6	TS4-S8	100% / Roof	0.53	1.38
Resultant	2.2	TS4-S8	100% / Roof	0.83	1.80

Table 7-5 Maximum Acceleration Responses at Center of Mass of Chiller Mounted on 1.0 g Design I/R Systems

Acceleration Component	Maximum Response at Center of Mass (g)	Test ID	Input Motion		A.A.F.
			Amplitude/ Level	Peak Acceleration (g)	
Transverse	2.98	TS2-S8a	150% / Roof	1.19	2.5
Longitudinal	2.36	TS2-S8a	150% / Roof	1.19	2.0
Horizontal	3.25	TS2-S8a	150% / Roof	1.22	2.7
Vertical	3.29	TS2-S8a	150% / Roof	0.79	4.2
Resultant	4.14	TS2-S8a	150% / Roof	1.25	3.3

Table 7-6 Maximum Acceleration Responses at Center of Mass of Chiller Mounted on 3.0 g Design I/R Systems

Acceleration Component	Maximum Response at Center of Mass (g)	Test ID	Input Motion		A.A.F.
			Amplitude/ Level	Peak Acceleration (g)	
Transverse	2.03	TS5-S7	100% / Roof	0.80	2.6
Longitudinal	2.10	TS8-S7	100% / Roof	0.80	2.7
Horizontal	2.26	TS8-S7	100% / Roof	0.81	2.8
Vertical	1.96	TS6-S7	75% / Roof	0.40	5.0
Resultant	2.47	TS9-S7	100% / Roof	0.83	3.0

7.2 Seismic Response at Support Locations

The response quantities measured at the support locations during the seismic tests included the peak acceleration responses at the four corners of the chiller (top level of the I/R systems), and the peak dynamic forces introduced into the I/R systems. These response quantities are analyzed in this section.

Similar to the peak acceleration responses at the center of mass, the acceleration amplification factors is an expedient representation of the results for the peak acceleration responses at the four corners of the chiller. Figures 7-2 through 7-4 show the amplification factors of the peak transverse, longitudinal, and vertical acceleration responses at the four corners of the chiller during the 72 seismic tests conducted. For peak input accelerations larger than 0.15g (when severe impacts occurred in the restraint component of the I/R systems), the acceleration amplification factors quickly decrease with an increase of the peak input acceleration.

Tables 7-7 through 7-10 summarize the maximum and minimum amplification of the acceleration responses at the corners of the chiller mounted on the 1.0 g and 3.0 g design I/R systems. The amplification of the acceleration response for the 1.0 g design I/R systems varies between 1.9 and 10.5 in the transverse direction, between 1.5 and 21 in the longitudinal direction, and between 2.9 and 10.5 in the vertical direction. The amplification of the acceleration response for the 3.0 g design I/R systems varies between 2.2 and 10.3 in the transverse direction, between 2.0 and 27.7 in the longitudinal direction, and between 3.0 and 13.8 in the vertical direction.

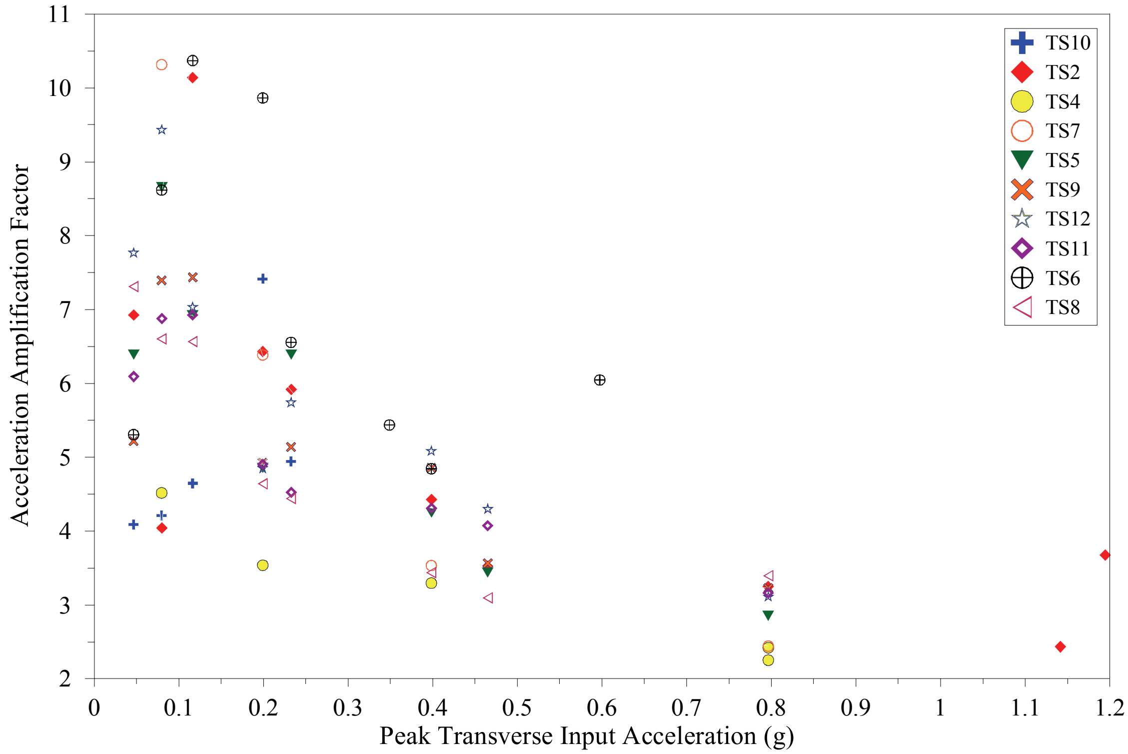

(a) Corner # 1

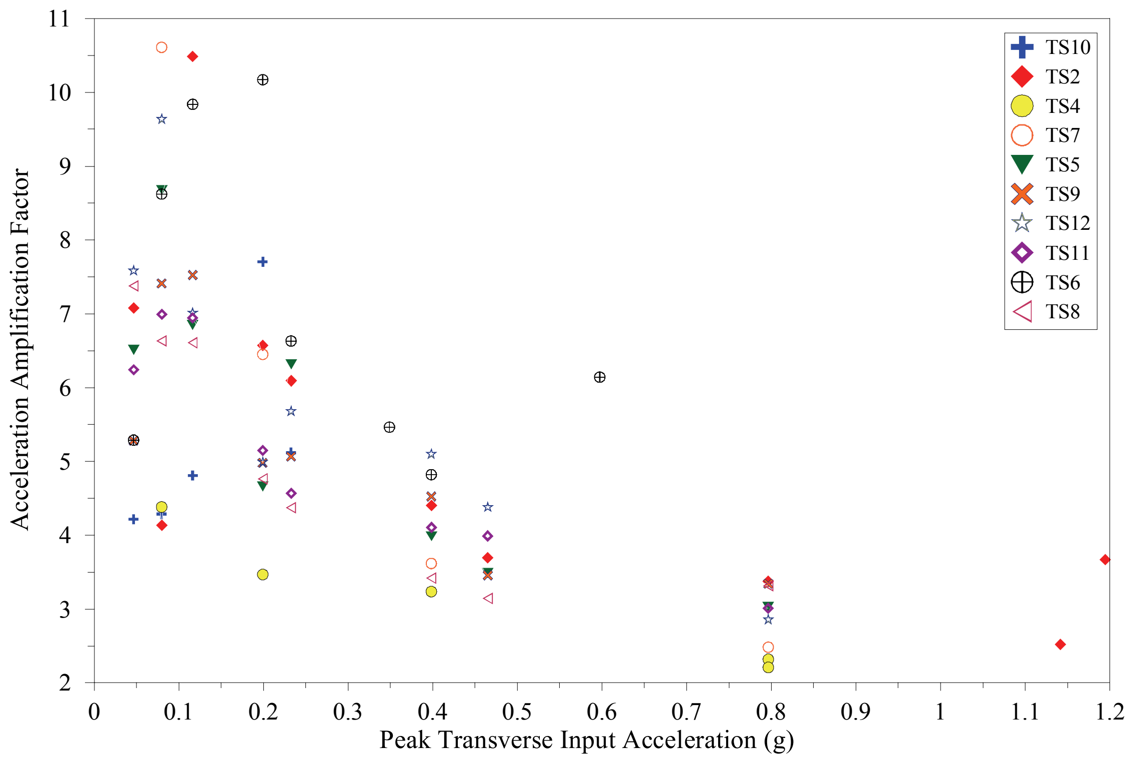

(b) Corner # 2

Figure 7-2 Variations of Acceleration Amplification Factor at Corners of Chiller (I/R Systems) with Peak Transverse Input Acceleration

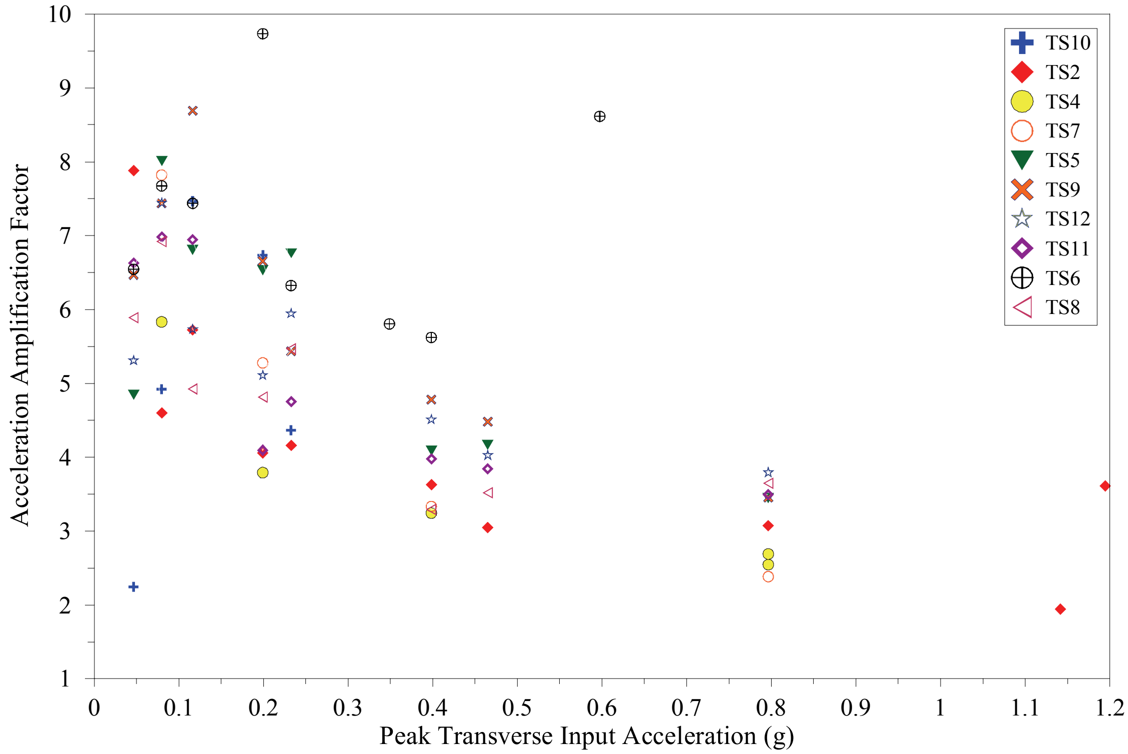

(c) Corner # 3

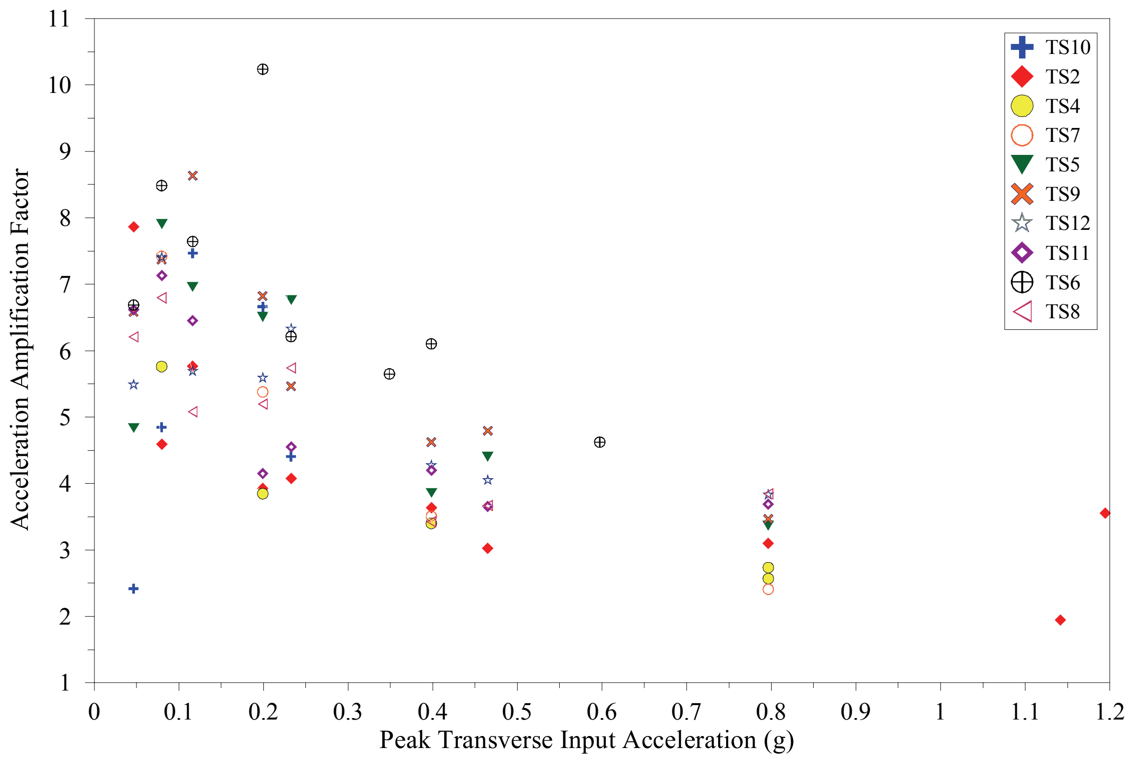

(d) Corner # 4

Figure 7-2 (cont'd) Variations of Acceleration Amplification Factor at Corners of Chiller (I/R Systems) with Peak Transverse Input Acceleration

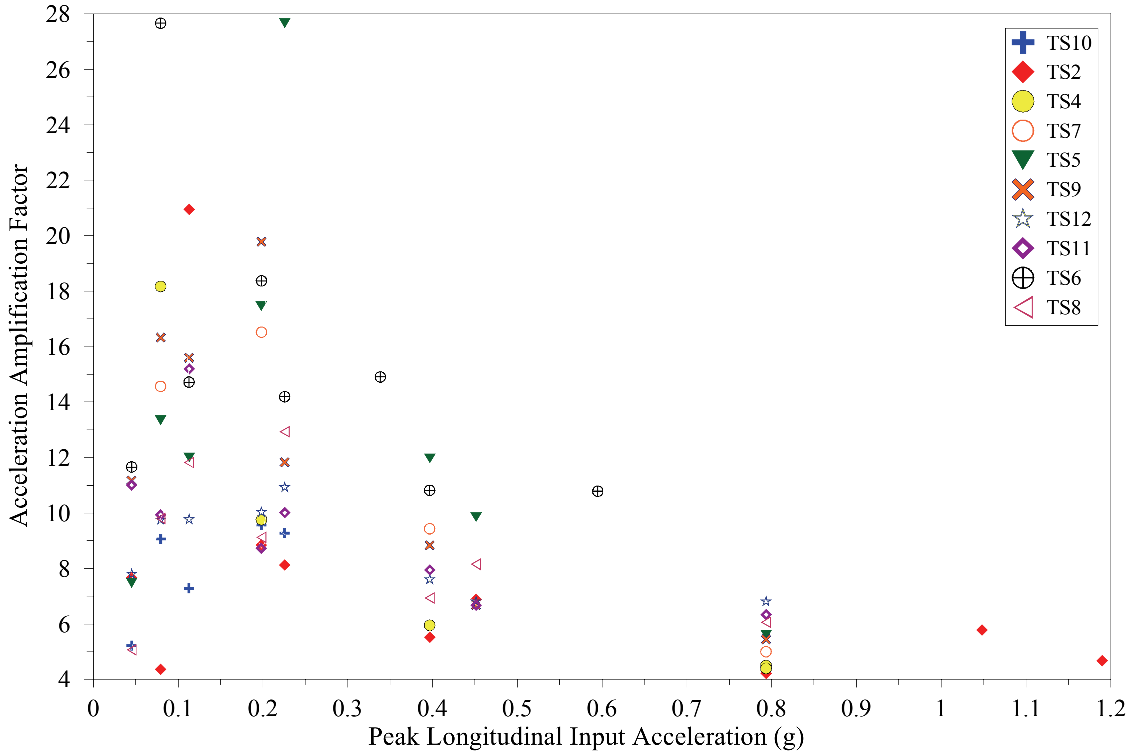

(a) Corner # 1

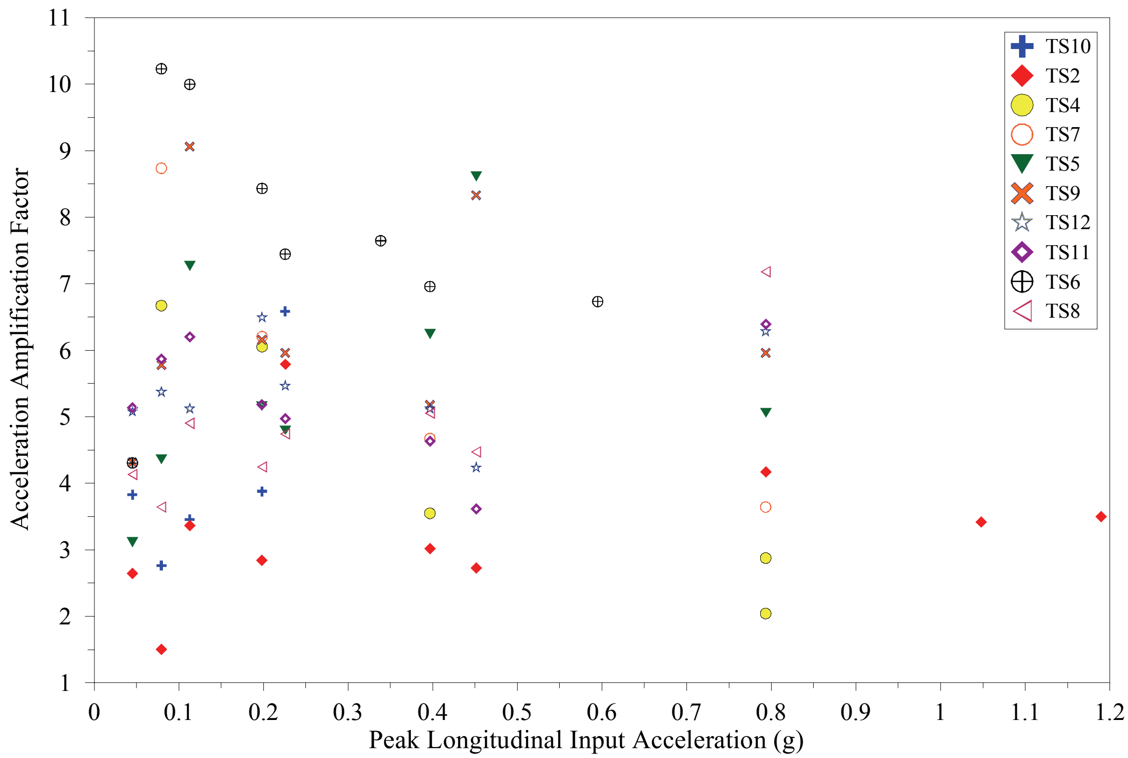

(b) Corner # 2

Figure 7-3 Variations of Acceleration Amplification Factor at Corners of Chiller (I/R Systems) with Peak Longitudinal Input Acceleration

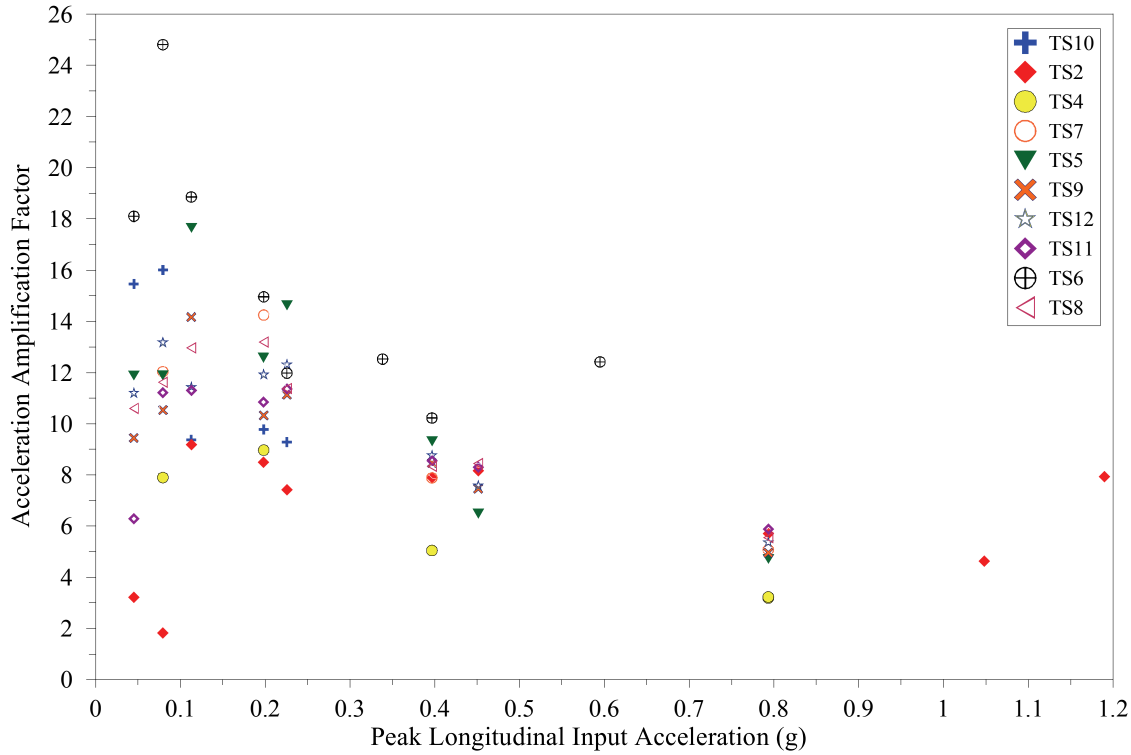

(c) Corner # 3

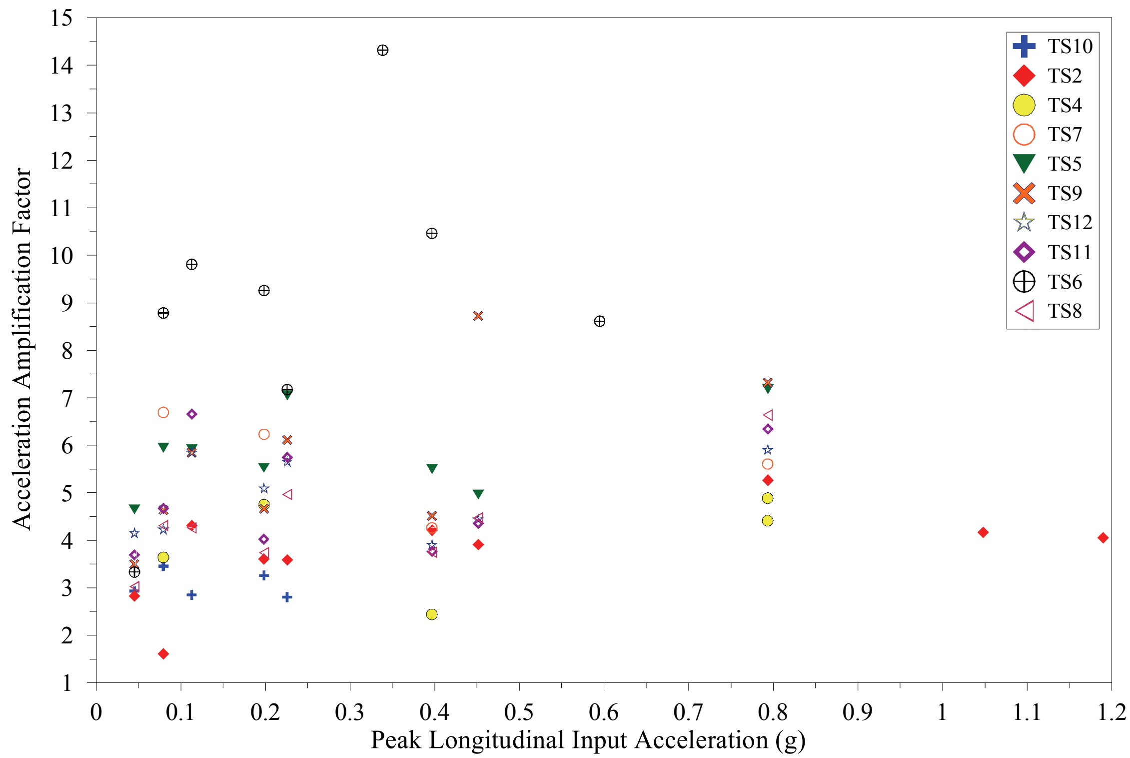

(d) Corner # 4

Figure 7-3 (cont'd) Variations of Acceleration Amplification Factor at Corners of Chiller (I/R Systems) with Peak Longitudinal Input Acceleration

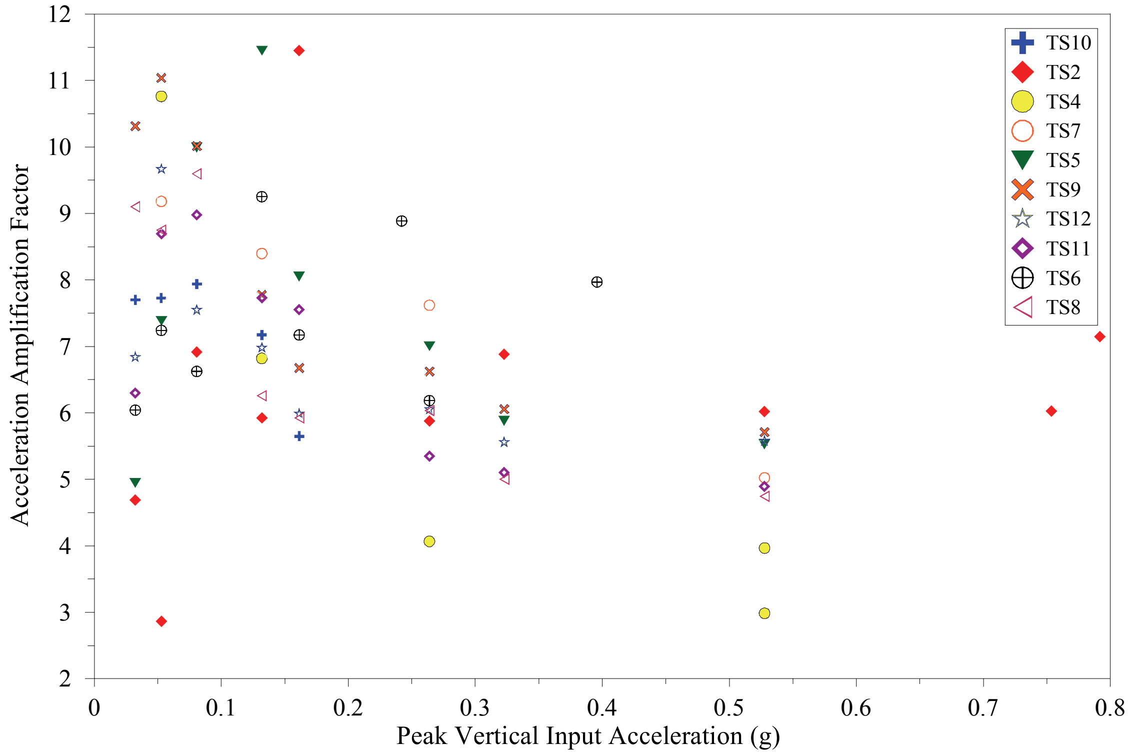

(a) Corner # 1

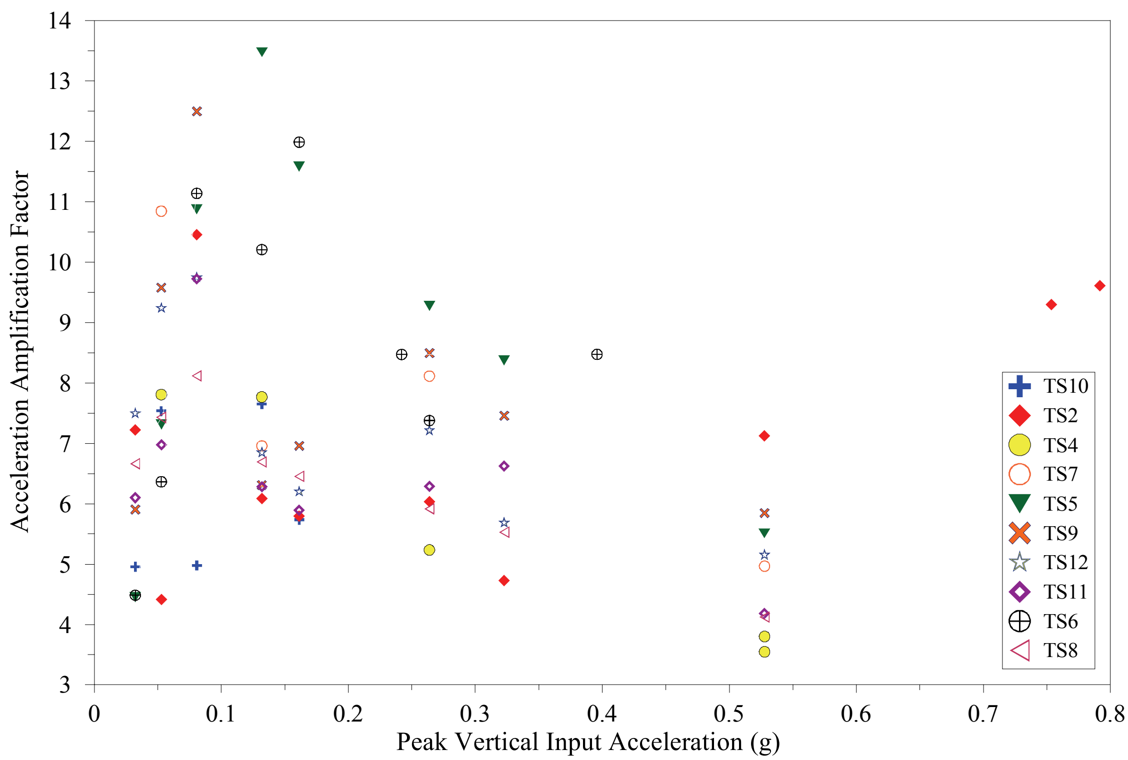

(b) Corner # 2

Figure 7-4 Variations of Acceleration Amplification Factor at Corners of Chiller (I/R Systems) with Peak Vertical Input Acceleration

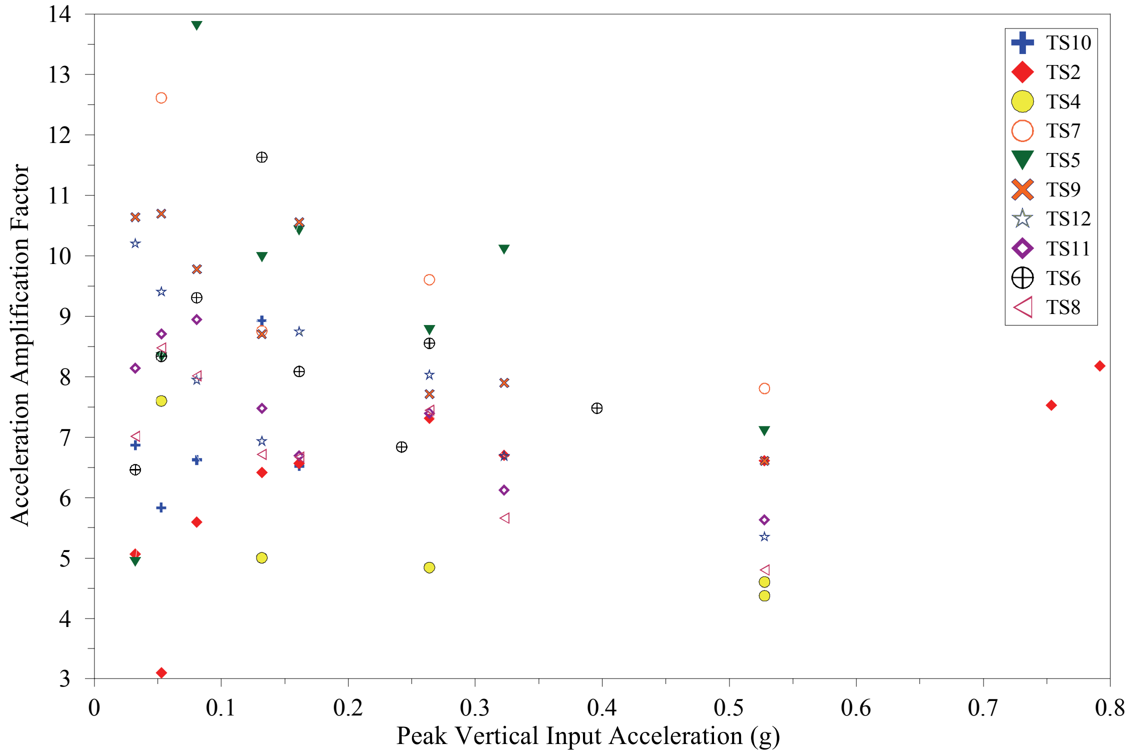

(c) Corner # 3

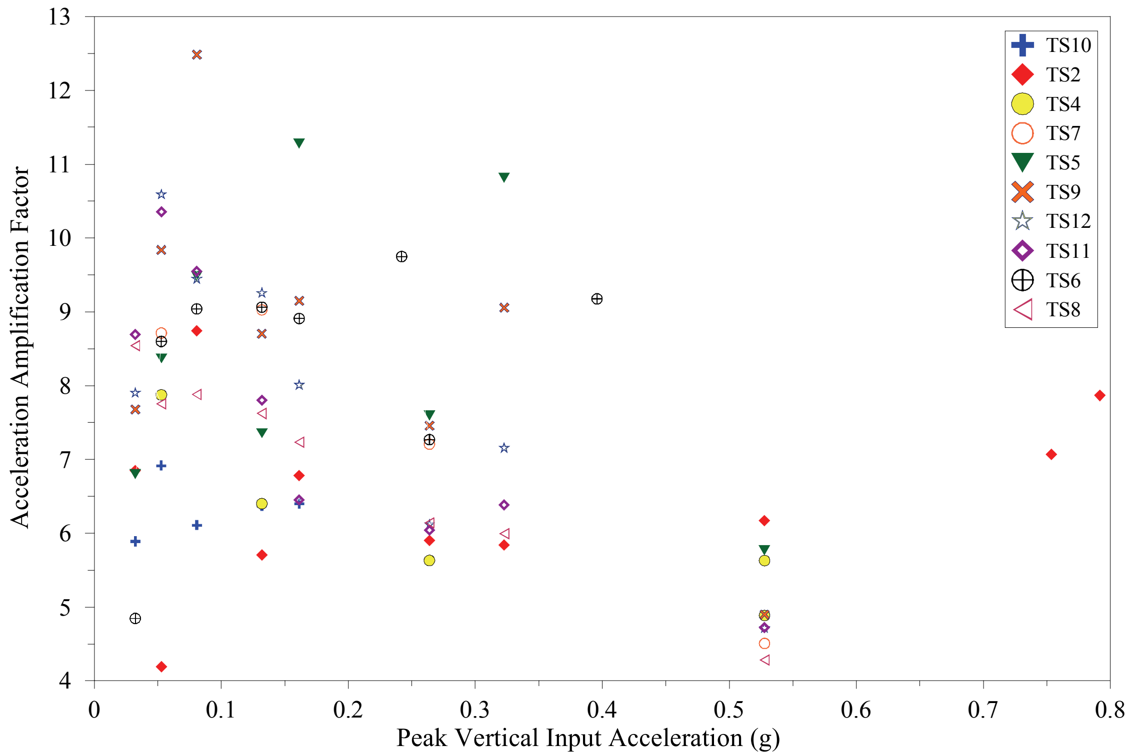

(d) Corner # 4

Figure 7-4 (cont'd) Variations of Acceleration Amplification Factor at Corners of Chiller (I/R Systems) with Peak Vertical Input Acceleration

Table 7-7 Maximum Acceleration Amplification Factors in 1.0 g Design I/R Systems

Acceleration Component	Maximum A.A.F.	Corner #	Test ID	Input Motion		Peak Response at Corners of Chiller (g)
				Amplitude / Level	Peak Acceleration (g)	
Transverse	10.5	2	TS2-S2	25% / Base	0.12	1.18
Longitudinal	21.0	1	TS2-S2	25% / Base	0.11	2.36
Horizontal	11.5	1	TS2-S4	50% / Base	0.16	1.85

Table 7-8 Maximum Acceleration Amplification Factors in 3.0 g Design I/R Systems

Acceleration Component	Maximum A.A.F.	Corner #	Test ID	Input Motion		Peak Response at Corners of Chiller (g)
				Amplitude / Level	Peak Acceleration (g)	
Transverse	10.3	1	TS7-S1	10% / Roof	0.08	0.82
Longitudinal	27.7	1	TS6-S1a	10% / Roof	0.08	2.19
Vertical	13.8	3	TS5-S2	25% / Base	0.08	1.11

Table 7-9 Minimum Acceleration Amplification Factors in 1.0 g Design I/R Systems

Acceleration Component	Minimum A.A.F.	Corner #	Test ID	Input Motion		Peak Response at Corners of Chiller (g)
				Amplitude / Level	Peak Acceleration (g)	
Transverse	1.9	3.0	TS2-S8	150% / Roof	1.14	1.94
Longitudinal	1.5	2.0	TS2-S1a	10% / Roof	0.08	0.12
Vertical	2.9	1.0	TS2-S1a	10% / Roof	0.05	0.15

Table 7-10 Minimum Acceleration Amplification Factors in 3.0 g Design I/R Systems

Acceleration Component	Minimum A.A.F.	Corner #	Test ID	Input Motion		Peak Response at Corners of Chiller (g)
				Amplitude / Level	Peak Acceleration (g)	
Transverse	2.2	2	TS4-S8	100% / Roof	0.80	1.76
Longitudinal	2.0	2	TS4-S8	100% / Roof	0.79	1.62
Vertical	3.0	1	TS4-S7	100% / Roof	0.53	1.58

The acceleration amplification factors at the corners of the chiller are larger than those at the center of mass of the chiller. The differences between the acceleration amplification factors at the center of mass and corners of the chiller are attributed to the distance between the center of mass and the corners of the chiller, at which the impacts occur. While propagating towards the center of mass, the impact shocks generated at the corners of the chiller are damped and absorbed by the body of the chiller and the liquid inside it. The slighter the impacts in the restraint components of the I/R systems are, the larger portion of them is absorbed by the body of the chiller. In other words, as the results confirm, the differences between the amplification of the acceleration responses at the corners and the center of mass of the chiller are more significant for the tests with the lower amplitude input motions.

Tables 7-11 and 7-12 summarize the maximum acceleration responses at the four corners of the chiller mounted on the 1.0 g and 3.0 g design I/R systems, respectively. In Test TS2-S8a, the 1.0 g design I/R systems experienced maximum transverse, longitudinal, and vertical acceleration responses of 4.39g, 9.44g, and 5.66g, respectively. In Test TS6-S7, the 3.0 g design I/R systems experienced maximum transverse and longitudinal acceleration responses of 5.15g and 7.39g, respectively. In Test TS7-S7, the 3.0 g design I/R systems experienced maximum vertical acceleration response of 4.12g.

Table 7-11 Maximum Acceleration Responses at Corners of Chiller Mounted on 1.0 g Design I/R Systems

Acceleration Component	Maximum Response at Corners of Chiller (g)	Corner #	Test ID	Input Motion		A.A.F.
				Amplitude / Level	Peak Acceleration (g)	
Transverse	4.39	1	TS2-S8a	150% / Roof	1.19	3.7
Longitudinal	9.44	4	TS2-S8a	150% / Roof	1.19	7.9
Vertical	5.66	1	TS2-S8a	150% / Roof	0.79	7.2

Table 7-12 Maximum Acceleration Responses at Corners of Chiller Mounted on 3.0 g Design I/R Systems

Acceleration Component	Maximum Response at Corners of Chiller(g)	Corner #	Test ID	Input Motion		A.A.F.
				Amplitude / Level	Peak Acceleration (g)	
Transverse	5.15	3	TS6-S7	75% / Roof	0.60	8.6
Longitudinal	7.39	4	TS6-S7	75% / Roof	0.59	12.4
Vertical	4.12	3	TS7-S7	100% / Roof	0.53	7.8

The maximum dynamic forces (including the longitudinal, transverse, and horizontal shear forces and the normal force) experienced by the 1.0 g and 3.0 g design I/R systems are listed in tables 7-13 and 7-14, respectively. Based on the results obtained from all the 72 seismic tests, the 1.0 g design I/R systems were able to withstand dynamic shear and normal forces of 205 and 474 kN, respectively. The 3.0 g design I/R systems were able to withstand dynamic shear and normal forces of 121 and 443 kN, respectively.

The dynamic forces introduced into the I/R systems are carried by both of the isolation and restraint component of the I/R systems. Based on the stiffness of the coil springs (see Section 3.5), the isolation component of an I/R system with the largest gap size considered (13 mm), carries a dynamic shear force of only 2.6 kN and a dynamic normal force of only 7.8 kN:

$$206\ (\frac{kN}{m}) \times 0.013\ (m) = 2.6\ (kN) \qquad (7\text{-}4)$$

$$613\ (\frac{kN}{m}) \times 0.013\ (m) = 7.8\ (kN) \qquad (7\text{-}5)$$

Compared to the maximum dynamic forces introduced into the I/R systems (listed in tables 7-13 and 7-14), the maximum dynamic forces carried by the isolation component of the I/R systems are quite insignificant. Therefore, it can be assumed that all the maximum dynamic forces introduced to the I/R systems are carried by their restraint component. In Section 3, it was shown that the static design capacities of the restraint component of the 1.0 g and 3.0 g design I/R systems were 29 and 88 kN, respectively. Therefore, the I/R systems were able to withstand dynamic forces much stronger than their static design capacities without any major damage.

Table 7-13 Maximum Dynamic Forces Introduced into 1.0 g Design I/R Systems (Static Design Capacity = 29 kN)

Dynamic Force	Direction	Maximum Response (kN)	I/R System #	Test ID	Input Motion	
					Amplitude / Level	Corresponding Peak Acceleration (g)
Shear	Transverse	158	3	TS2-S8a	150% / Roof	1.19
	Longitudinal	152	3	TS2-S8a	150% / Roof	1.19
	Horizontal	205	3	TS2-S8a	150% / Roof	1.22
Normal	Vertical	474	3	TS2-S8a	150% / Roof	0.79

Table 7-14 Maximum Dynamic Forces Introduced into 3.0 g Design I/R Systems (Static Design Capacity = 88 kN)

Dynamic Force	Direction	Maximum Response (kN)	I/R System #	Test ID	Input Motion	
					Amplitude / Level	Corresponding Peak Acceleration (g)
Shear	Transverse	83	3	TS9-S7	100% / Roof	0.80
	Longitudinal	111	2	TS5-S7	100% / Roof	0.79
	Horizontal	121	2	TS5-S7	100% / Roof	0.81
Normal	Vertical	443	2	TS5-S7	100% / Roof	0.53

The peak dynamic forces and the corresponding peak acceleration responses at the I/R systems were used to perform serenity checks on the test results. As an example, the peak dynamic longitudinal shear force of 111 kN (table 7-14) and the corresponding peak longitudinal acceleration response of 4.02g at I/R system #2 in Test TS5-S7 meant that the I/R system #2 had been carrying an equivalent seismic weight of 27.6 kN (around 25% of weight of the chiller), which is quite reasonable.

Figures 7-5 through 7-8 show the variations of the peak dynamic forces introduced into the I/R systems with the corresponding peak input acceleration during the 72 seismic tests conducted. The results suggest as a general trend that the dynamic forces (both shear and normal forces) introduced into the I/R systems increase almost linearly with the corresponding peak input acceleration.

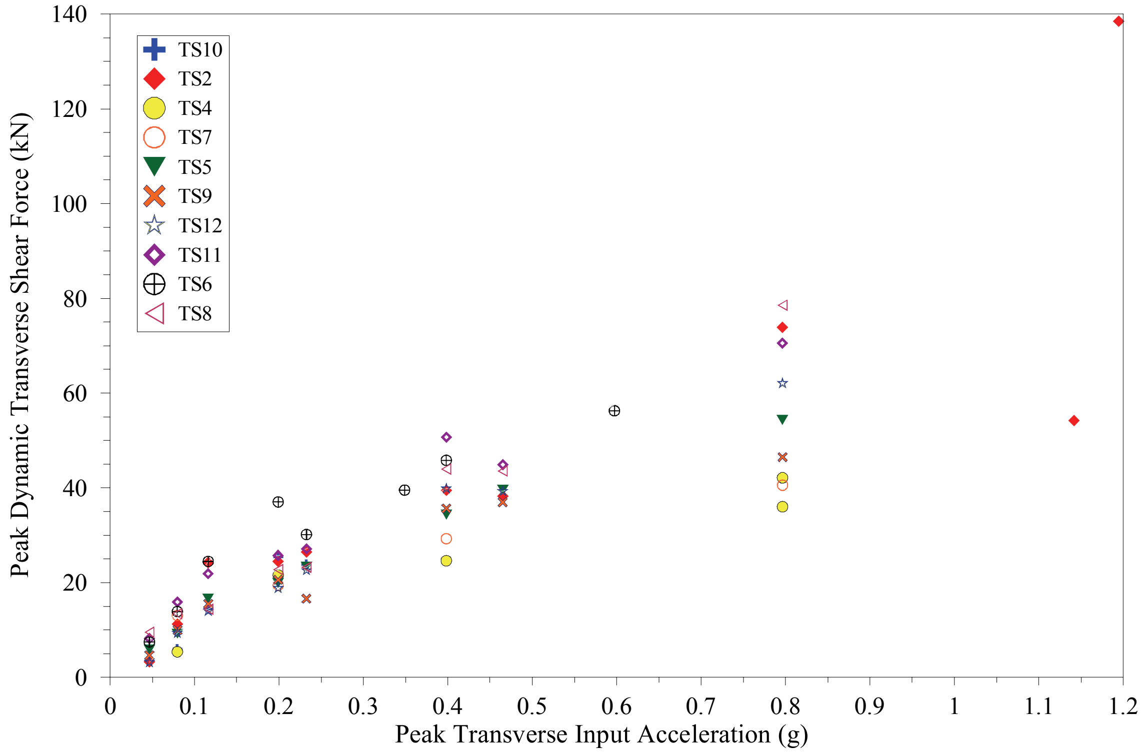

(a) Transverse Shear Force

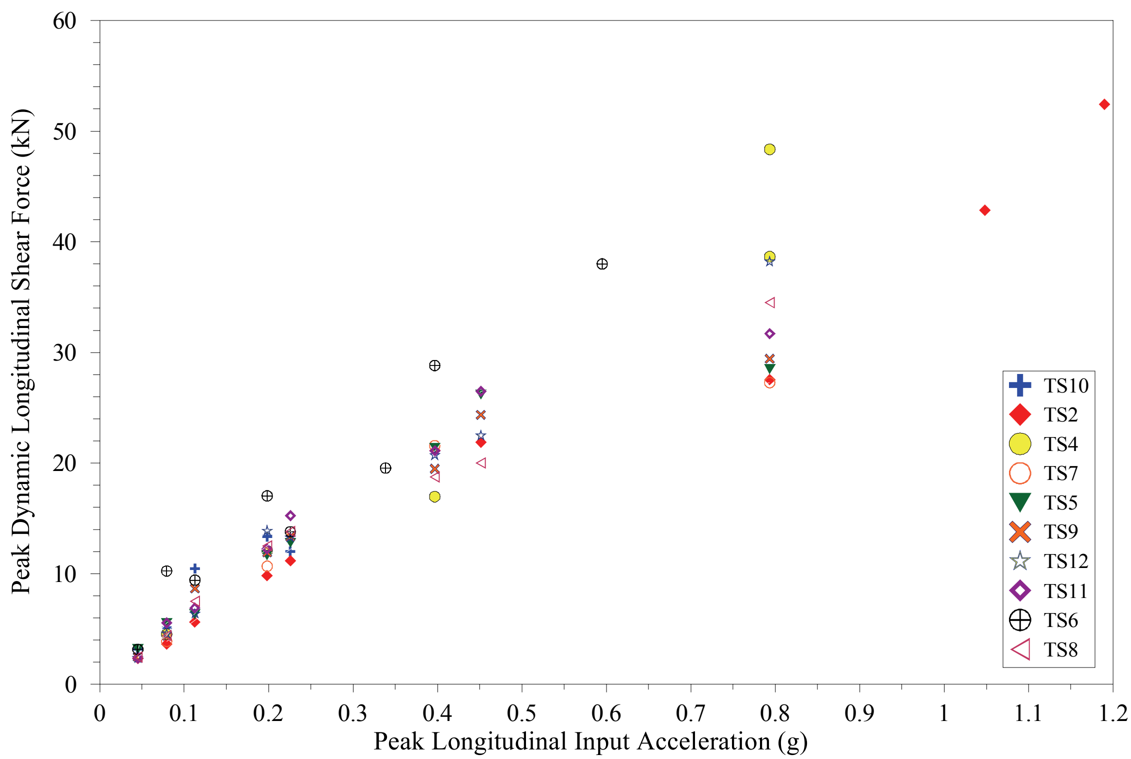

(b) Longitudinal Shear Force

Figure 7-5 Variations of Peak Dynamic Forces Introduced into I/R System Located at Corner #1 with Peak Base Acceleration

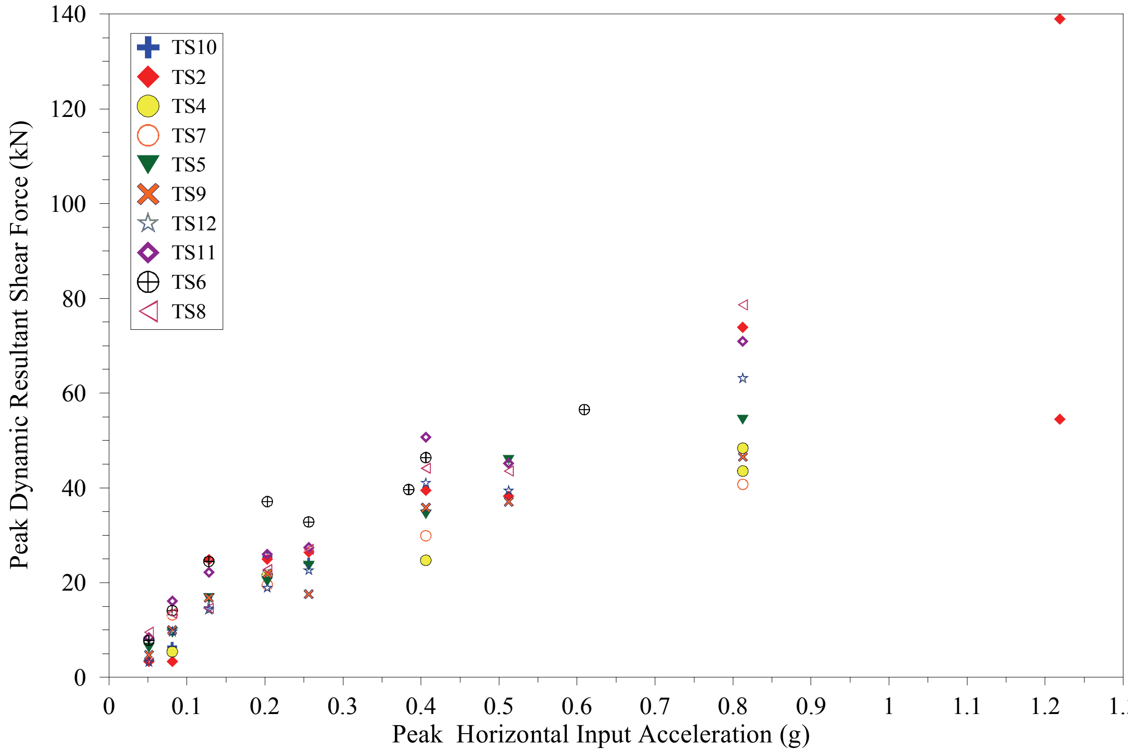

(c) Resultant Shear Force

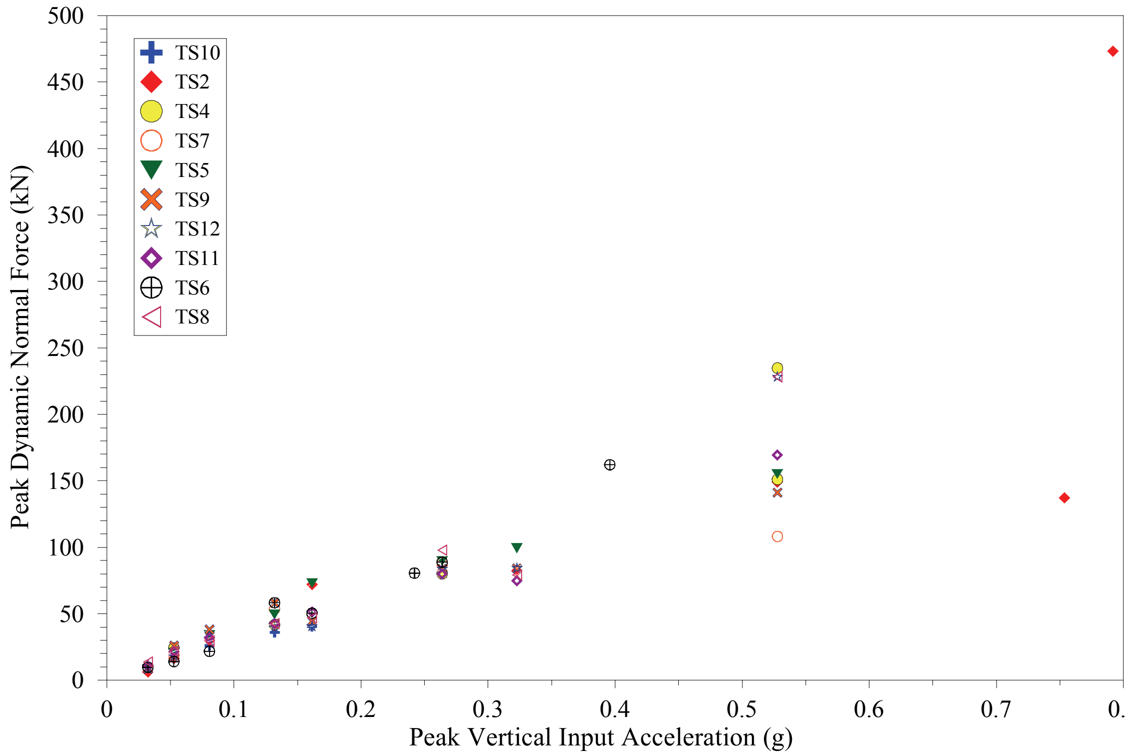

(d) Normal Force

Figure 7-5 (cont'd) Variations of Peak Dynamic Forces Introduced into I/R System Located at Corner #1 with Peak Base Acceleration

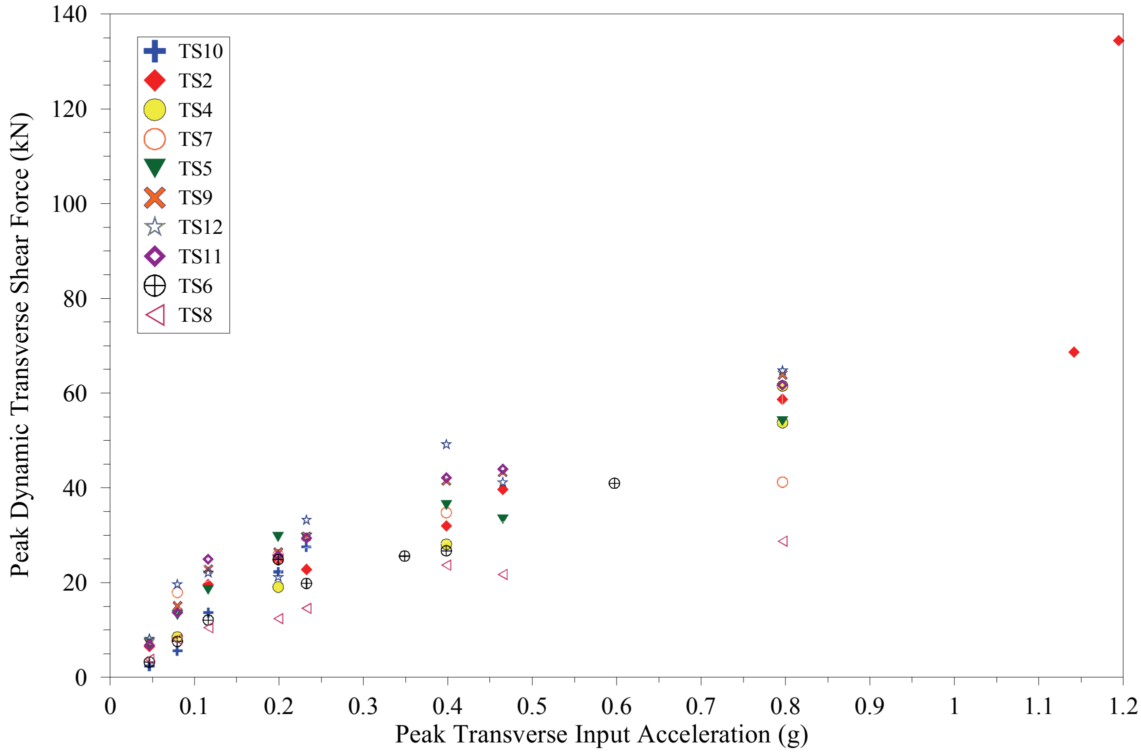

(a) Transverse Shear Force

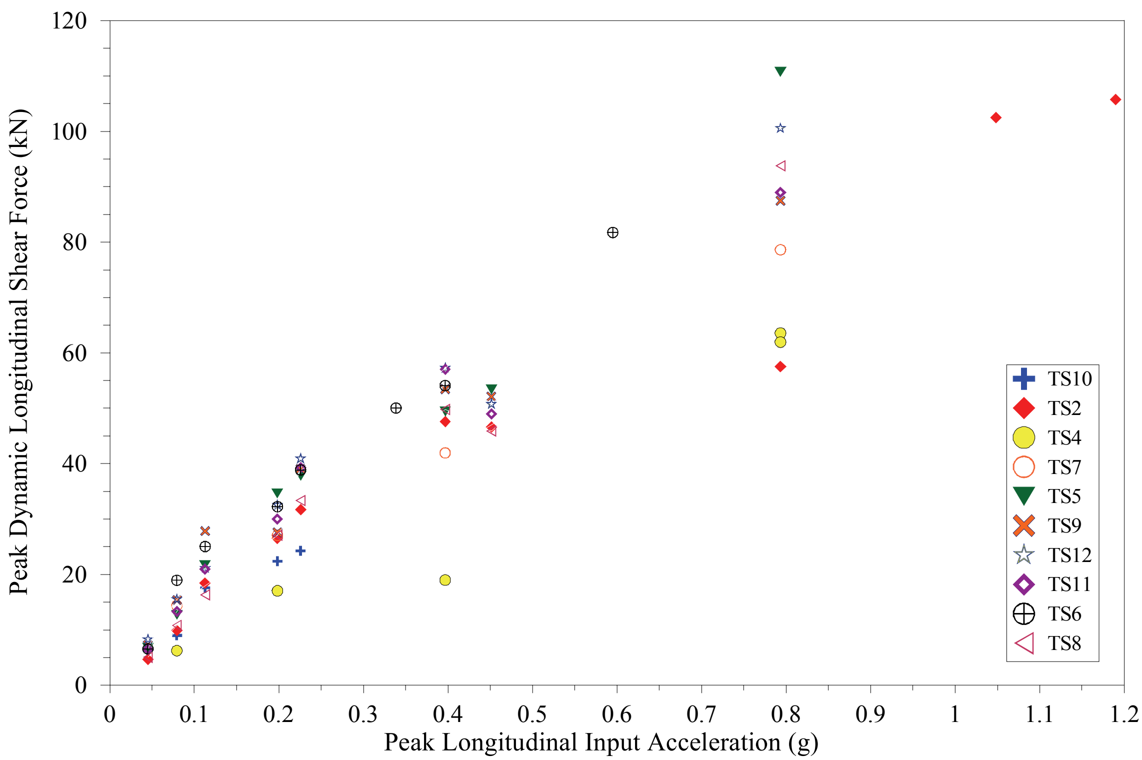

(b) Longitudinal Shear Force

Figure 7-6 Variations of Peak Dynamic Forces Introduced into I/R System Located at Corner #2 with Peak Base Acceleration

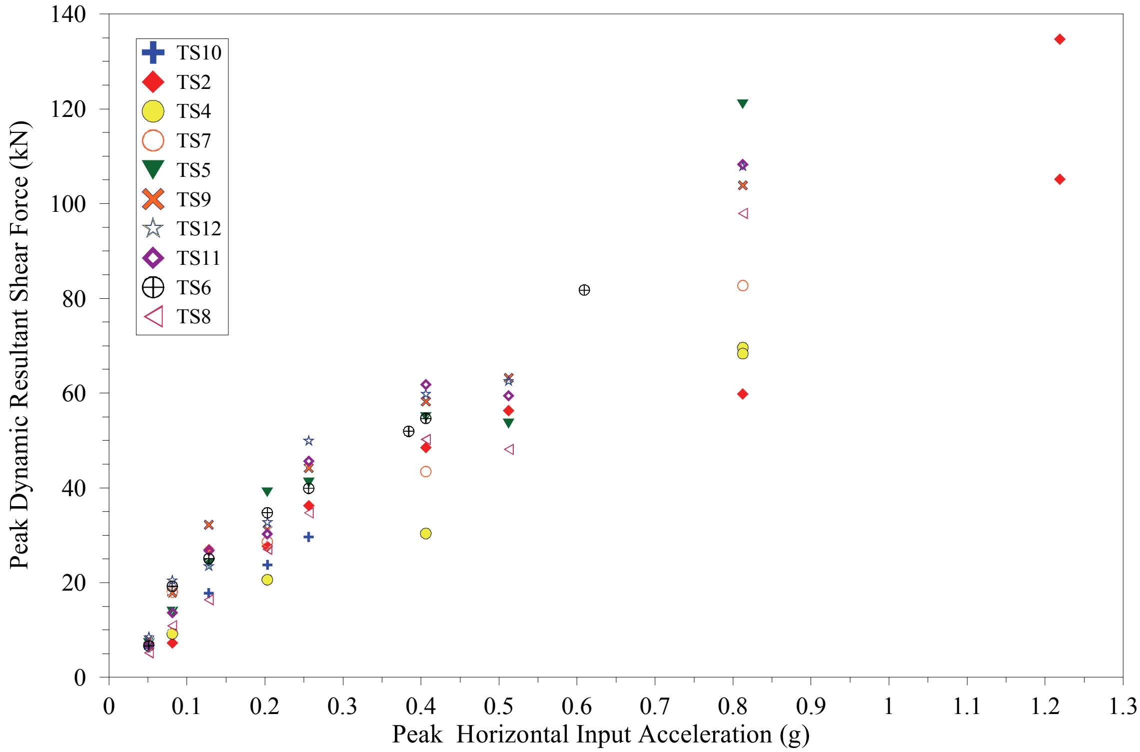

(c) Resultant Shear Force

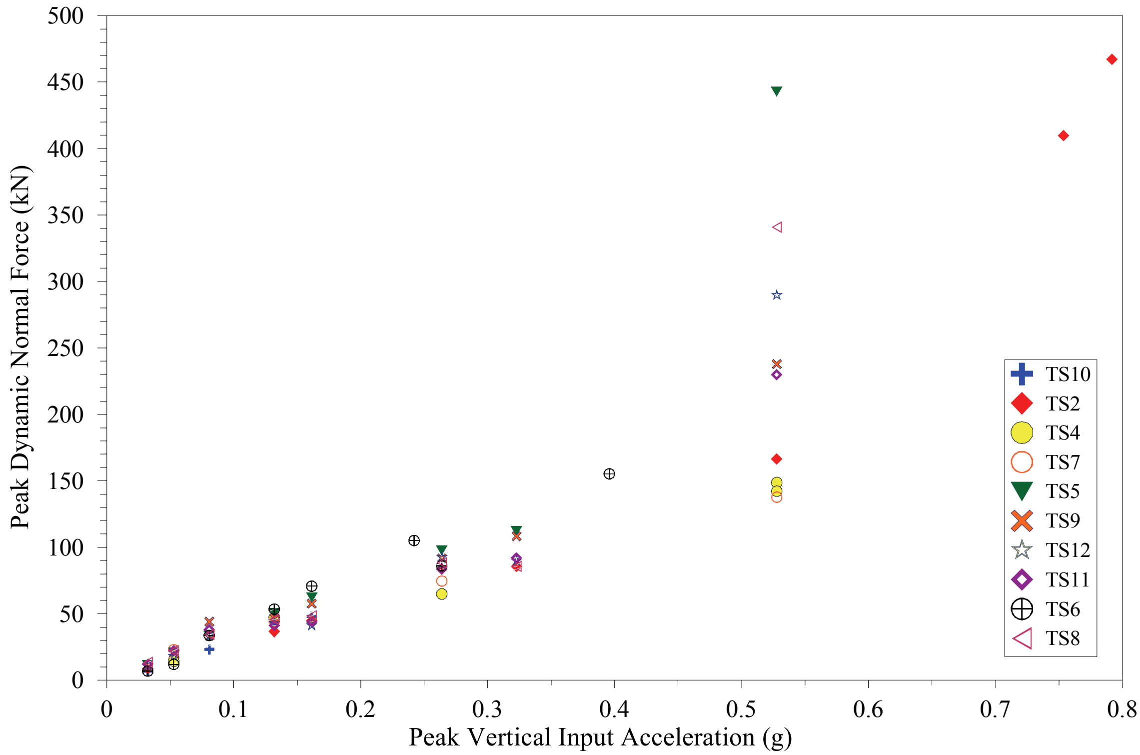

(d) Normal Force

Figure 7-6 (cont'd) Variations of Peak Dynamic Forces Introduced into I/R System Located at Corner #2 with Peak Base Acceleration

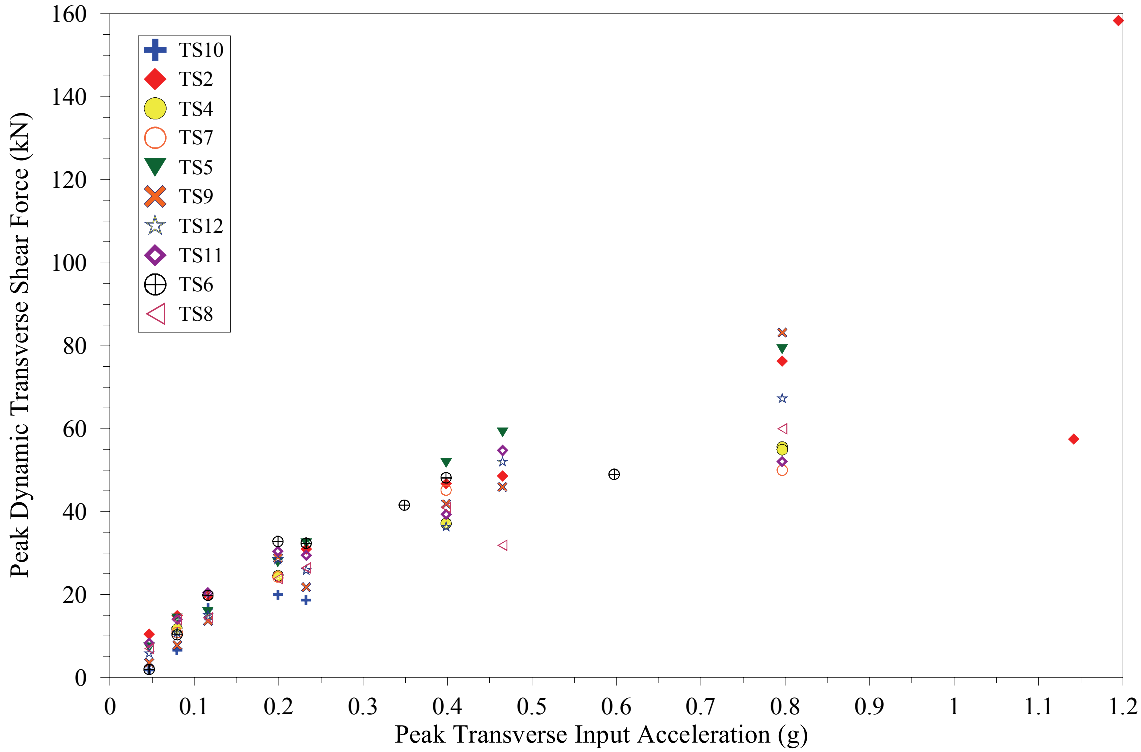

(a) Transverse Shear Force

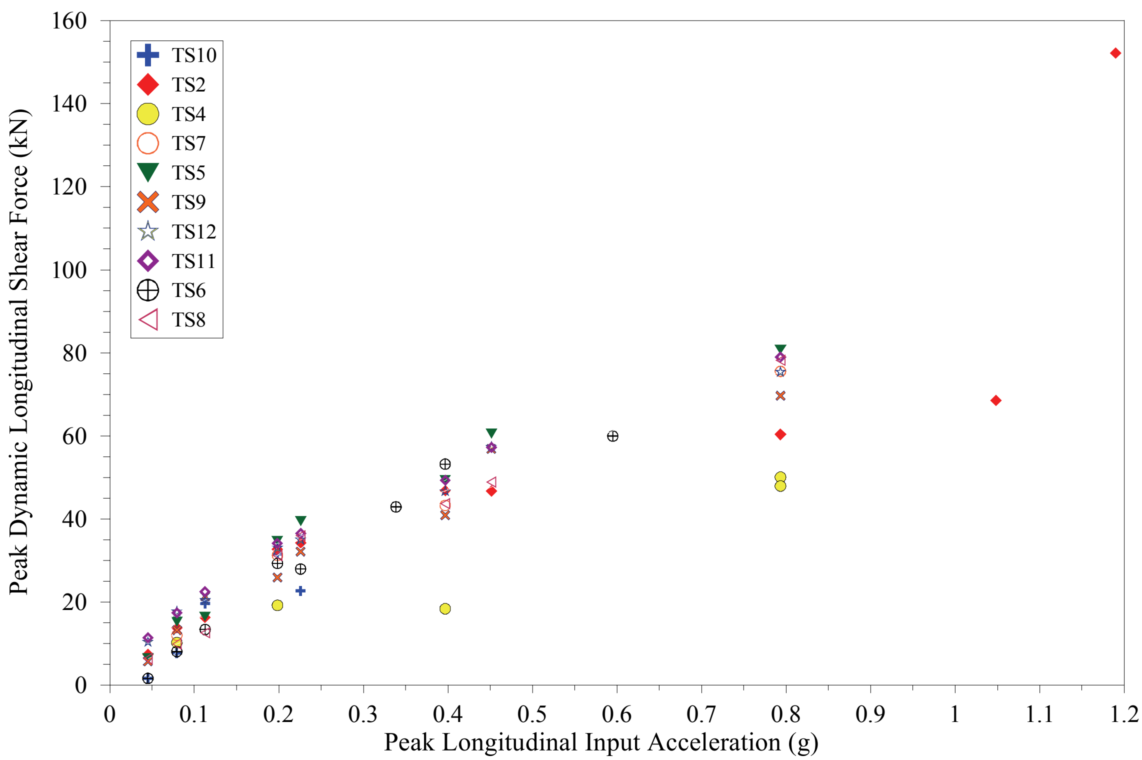

(b) Longitudinal Shear Force

Figure 7-7 Variations of Peak Dynamic Forces Introduced into I/R System Located at Corner #3 with Peak Base Acceleration

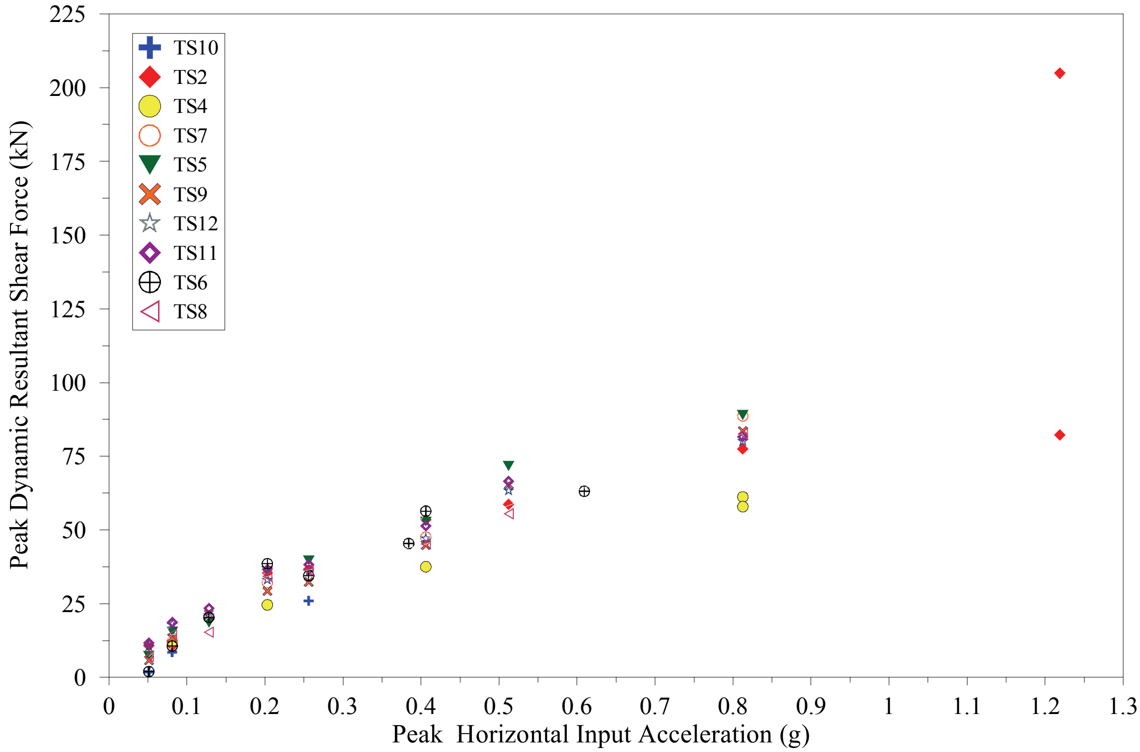

(c) Resultant Shear Force

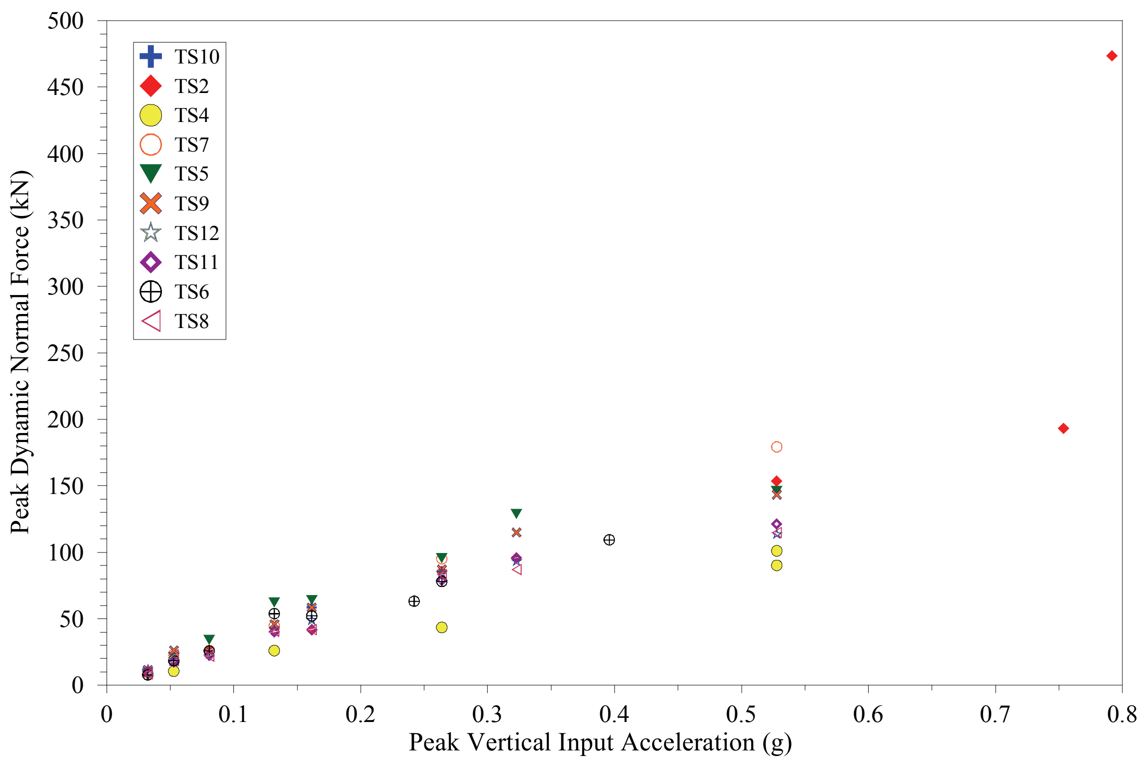

(d) Normal Force

Figure 7-7 (cont'd) Variations of Peak Dynamic Forces Introduced into I/R System Located at Corner #3 with Peak Base Acceleration

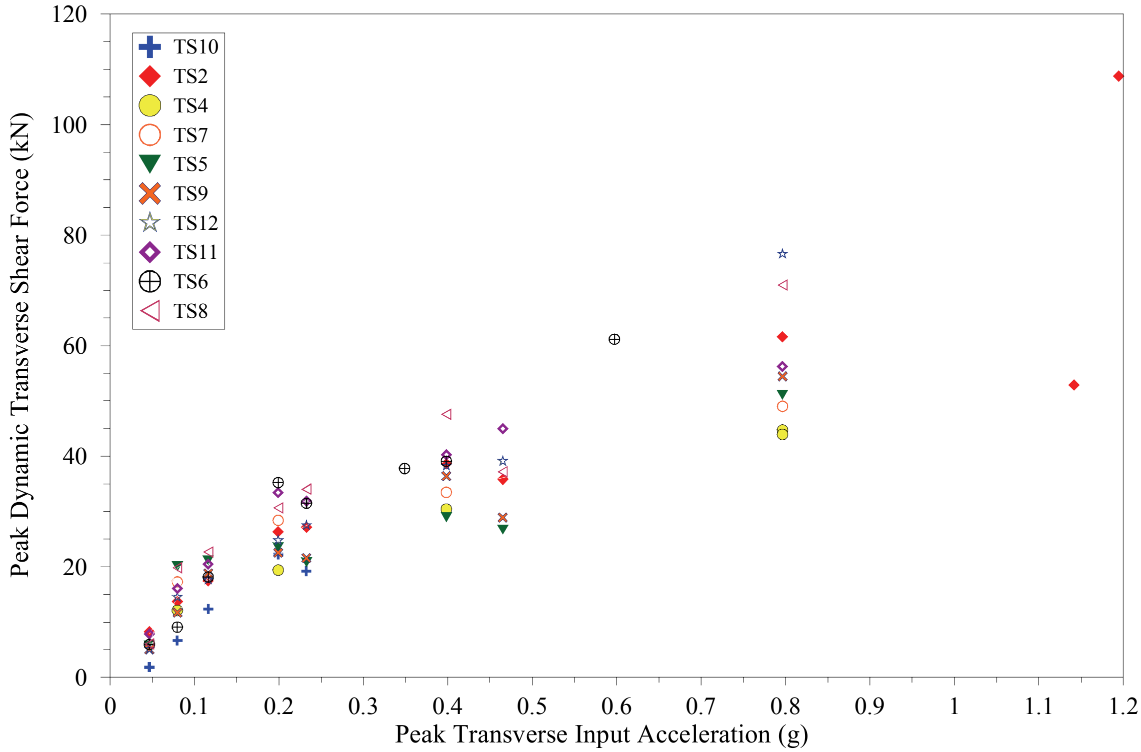

(a) Transverse Shear Force

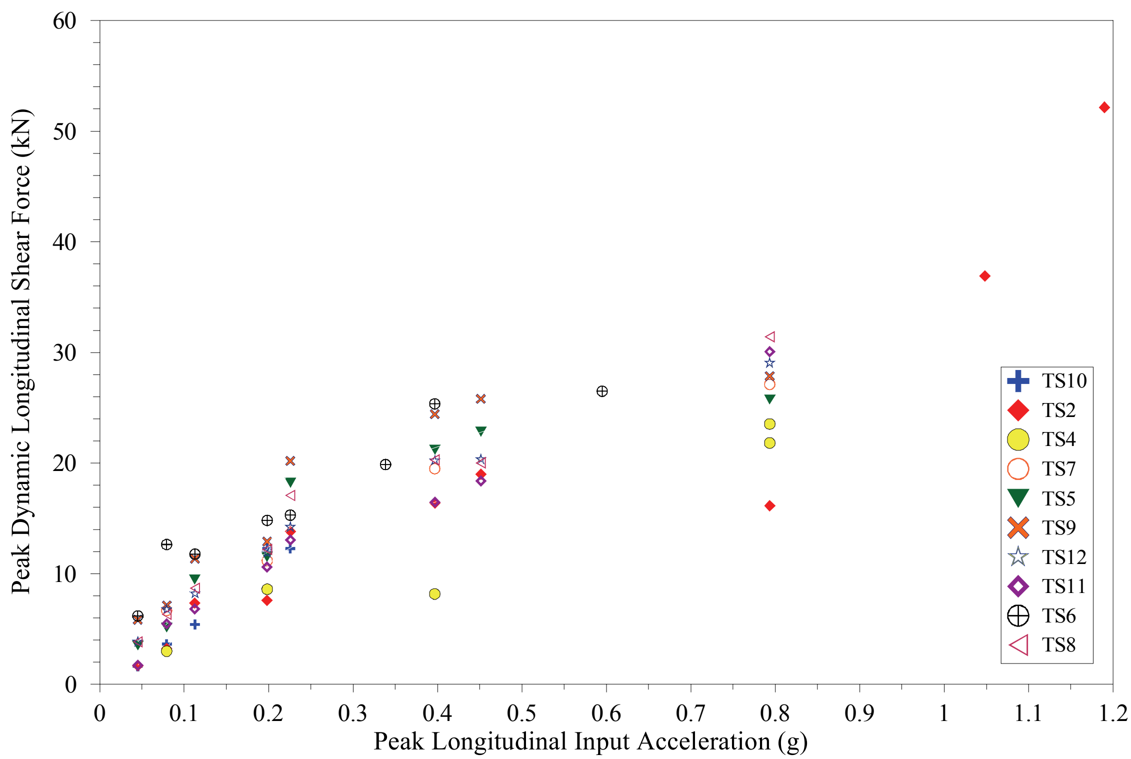

(b) Longitudinal Shear Force

Figure 7-8 Variations of Peak Dynamic Forces Introduced into I/R System Located at Corner #4 with Peak Base Acceleration

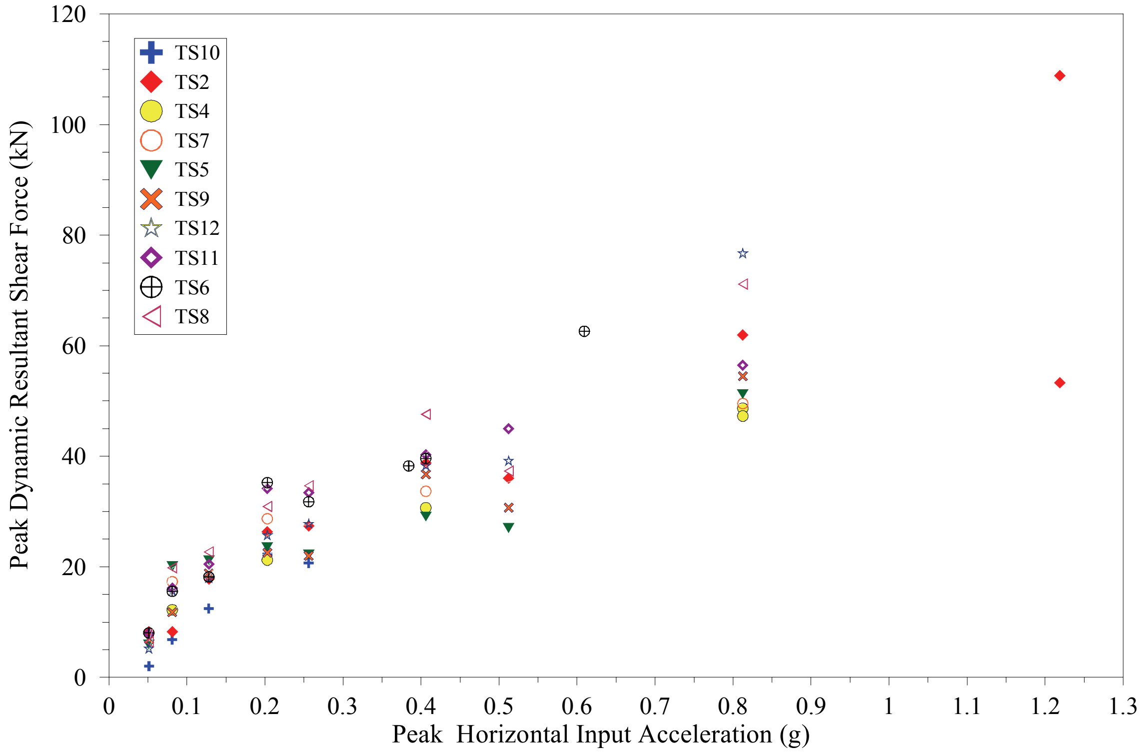

(c) Resultant Shear Force

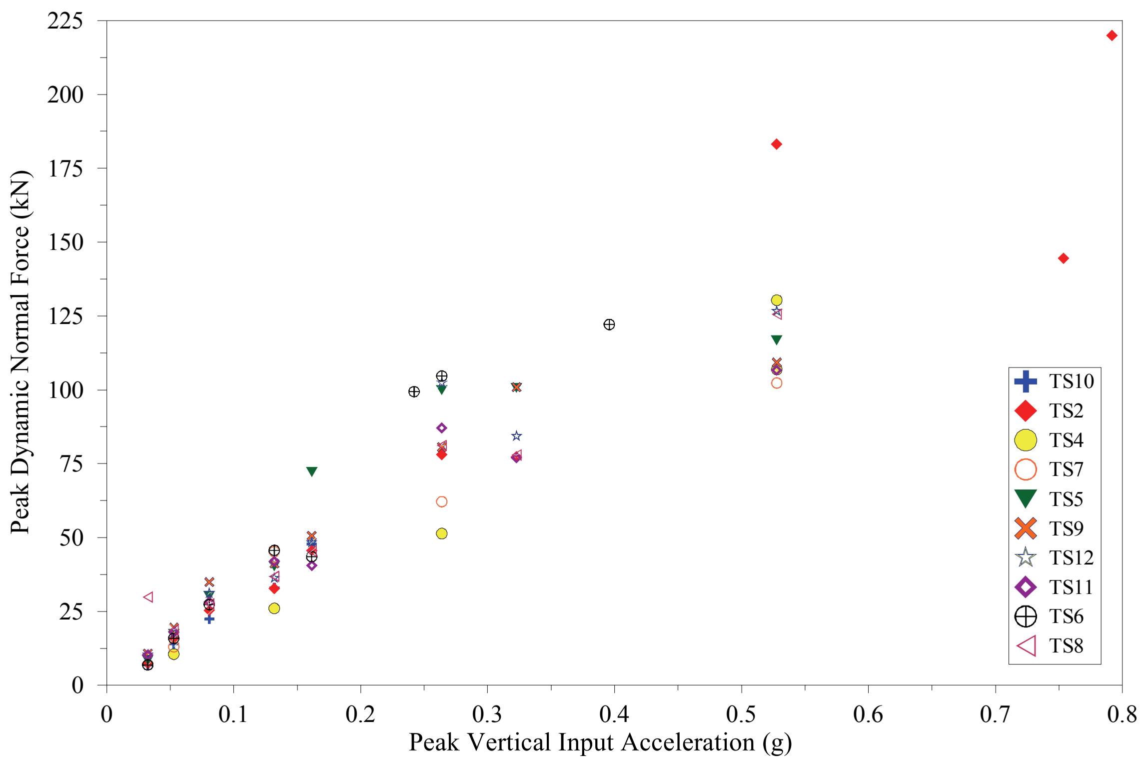

(d) Normal Force

Figure 7-8 (cont'd) Variations of Peak Dynamic Forces Introduced into I/R System Located at Corner #4 with Peak Base Acceleration

7.3 Relative Displacement Response of Test Specimen

As indicated earlier in Section 4.2, throughout the tests the absolute displacement response of four points on the south face of the chiller and one point on the shake table extension were measured by the KRYPTON coordinate measurement machine. Subtracting the absolute displacement of the table extension from the absolute displacement response of a point on the chiller would yeild the relative displacement response of that point. Figures 7-9 and 7-10 show the relative displacement response histories of the top-west point on the south face of the chiller (channel#70, as shown in Figure 4-7 and listed in Table 4-3) in seismic tests TS6-S1 and TS4-S8, respectively. In these figures the dashed lines represent the displacement associated with the gap size of the restraint component of the I/R systems. It is noteworthy that the displacement histories in figure 7-9 were obtained in a test with very low-intensity input motion (10% of the base level input motion), whereas the displacement histories in figure 7-10 were obtained in a test with the strongest input motion (full scale of the roof level input motion).

If the chiller experienced only pure translation and the snubber elements were uncompressible, the relative displacement histories of Figures 7-9 and 7-10 would have been limited to the dashed lines. However, in the seismic tests and particularly in those with strong input motion and large gap size, the chiller experienced combination of translation and rotation. In addition, as a result of the impacts that occurred in the restraint components of the I/R systems the rubber snubbers were compressed. Therefore, the relative displacement response of the four points on the south face of the chiller in most of the seismic tests exceeded the gap size.

In order to compare the peak relative displacement response of the test specimen to the gap size, a dimensionless Relative Displacement Response Ratio (*R.D.R.R.*) can be defined as:

$$R.D.R.R. = \frac{\text{Peak Relative Displacement}}{\text{Gap Size}} \tag{7-4}$$

For each seismic test, the *R.D.R.R.* was calculated in the transverse, longitudinal, and vertical direction. Figures 7-11 through 7-13 exhibit the variation of the *R.D.R.R.* at the west-top and west-bottom points located on the south face of the chiller with the peak input acceleration obtained in the 72 seismic tests. As shown in these figures, the peak relative displacement response at the south face of the chiller in some tests has been as large as ten times of the gap size. The comparison of the *R.D.R.R* of the top and bottom point on the south face of the chiller confirms that the peak relative displacement response is proportionate to the distance from the support locations.

Tables 7-15 through 7-18 list the maximum and minimum relative displacement response of the south face of the chiller mounted on the 1.0 g and 3.0 g design I/R systems obtained in all the 72 seismic tests. In the seismic test series TS2 with the chiller mounted on the 1.0 g design I/R systems and the gap size of 6 mm (1/4 in), the south face of the chiller has experienced peak relative displacement response of 66.5, 40.3, and 50.1 mm in the transverse, longitudinal, and vertical direction respectively. In the seismic test series TS6 with 3.0 g design I/R systems and 13 mm (1/2 in) gap size, the peak relative displacement response at south face of the chiller has been 45.0, 39.4, and 33.1 mm in the transverse, longitudinal, and vertical direction, respectively.

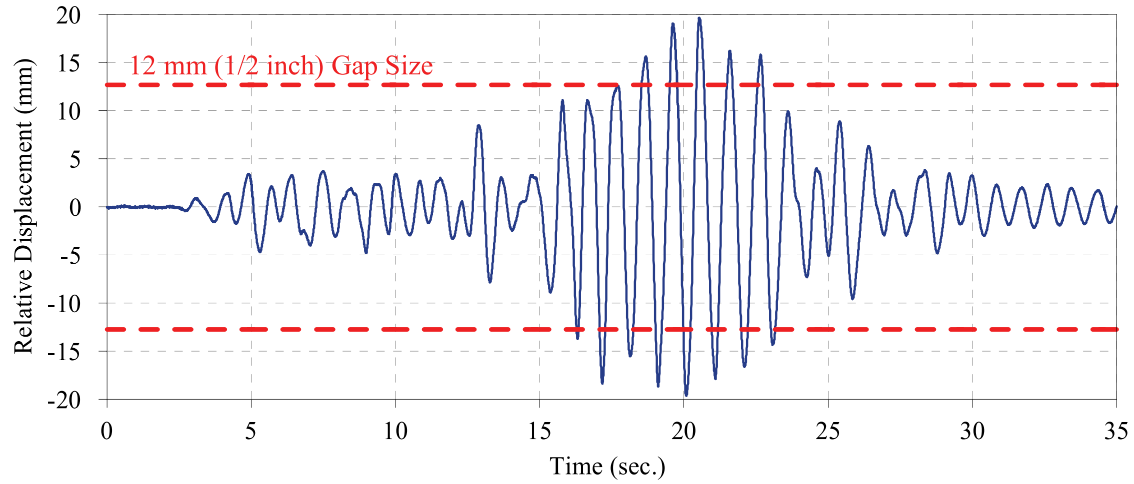

(a) Transverse

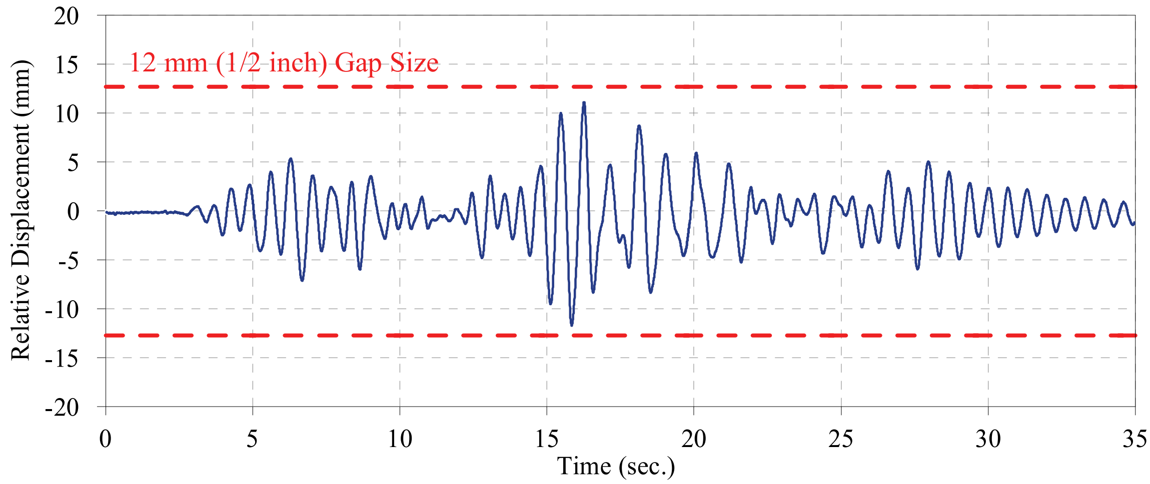

(b) Longitudinal

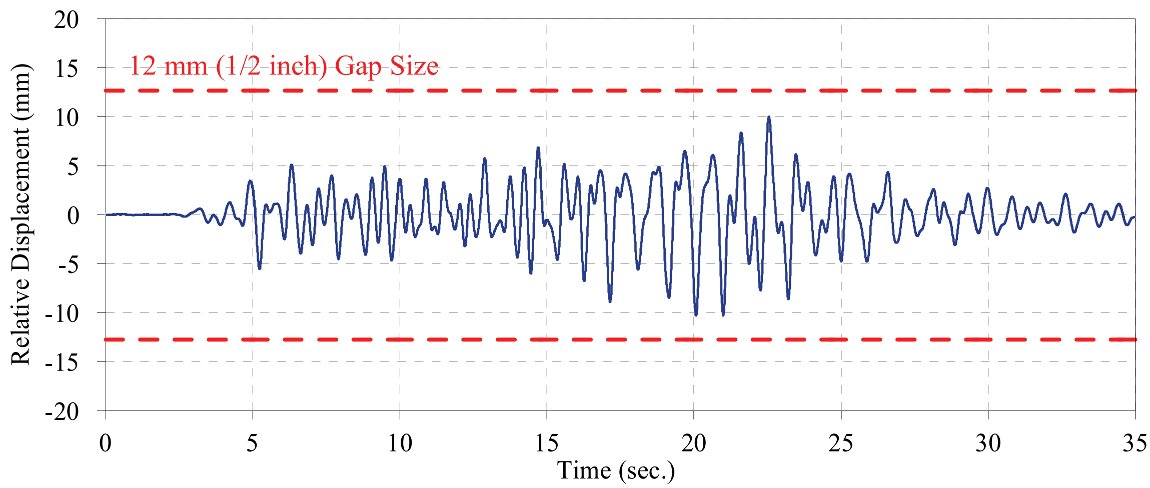

(c) Vertical

Figure 7-9 Relative Displacement Response History of Top-West Point on South Face of Chiller, Seismic Test TS6-S1

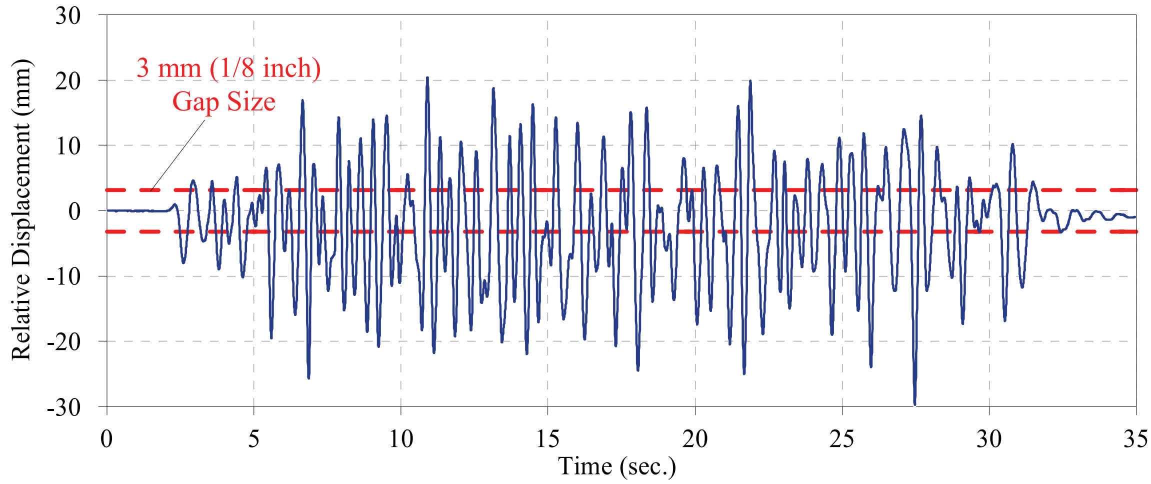

(a) Transverse

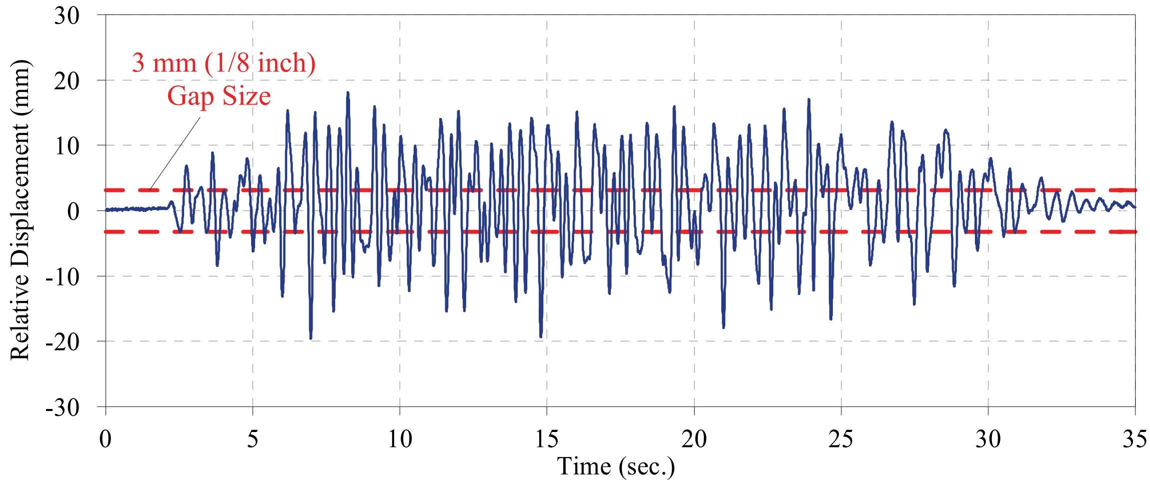

(b) Longitudinal

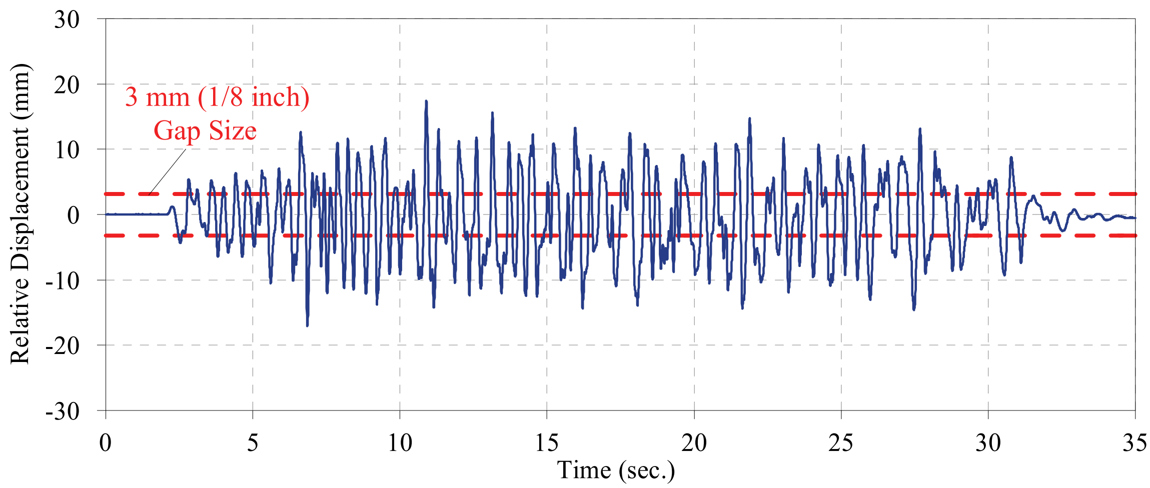

(c) Vertical

Figure 7-10 Relative Displacement Response History of Top-West Point on South Face of Chiller, Seismic Test TS4-S8

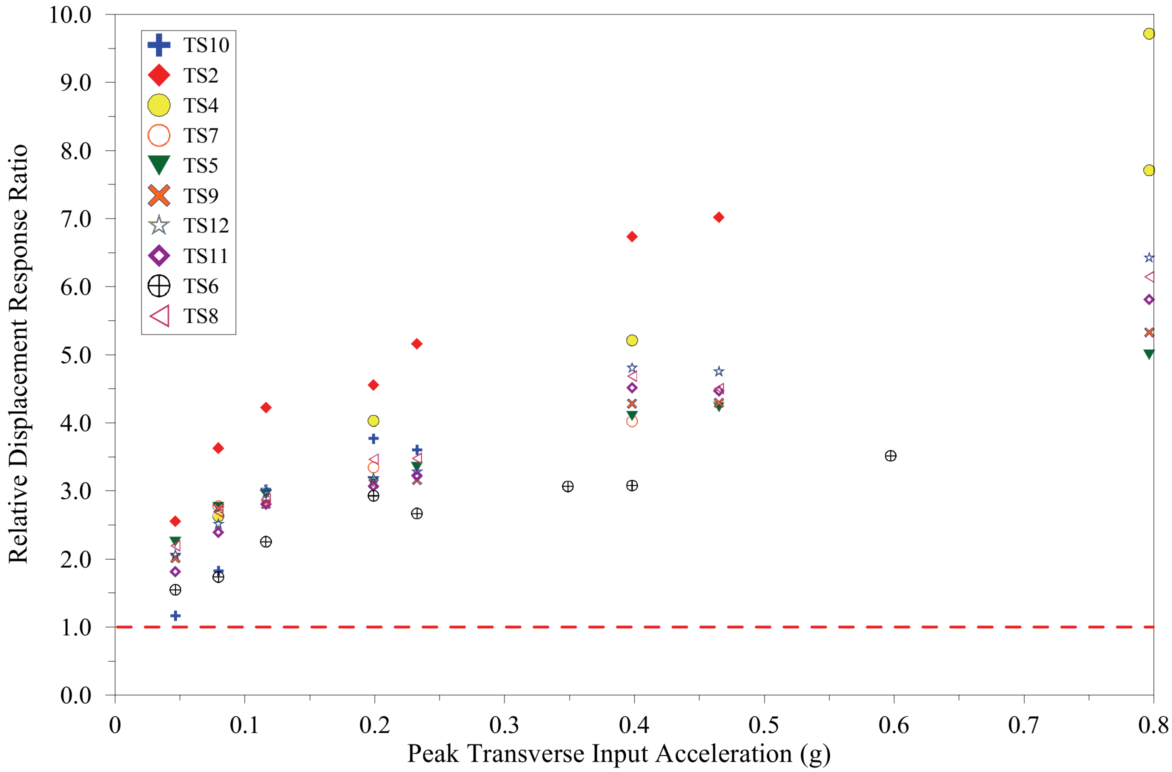

(a) Top-West Point

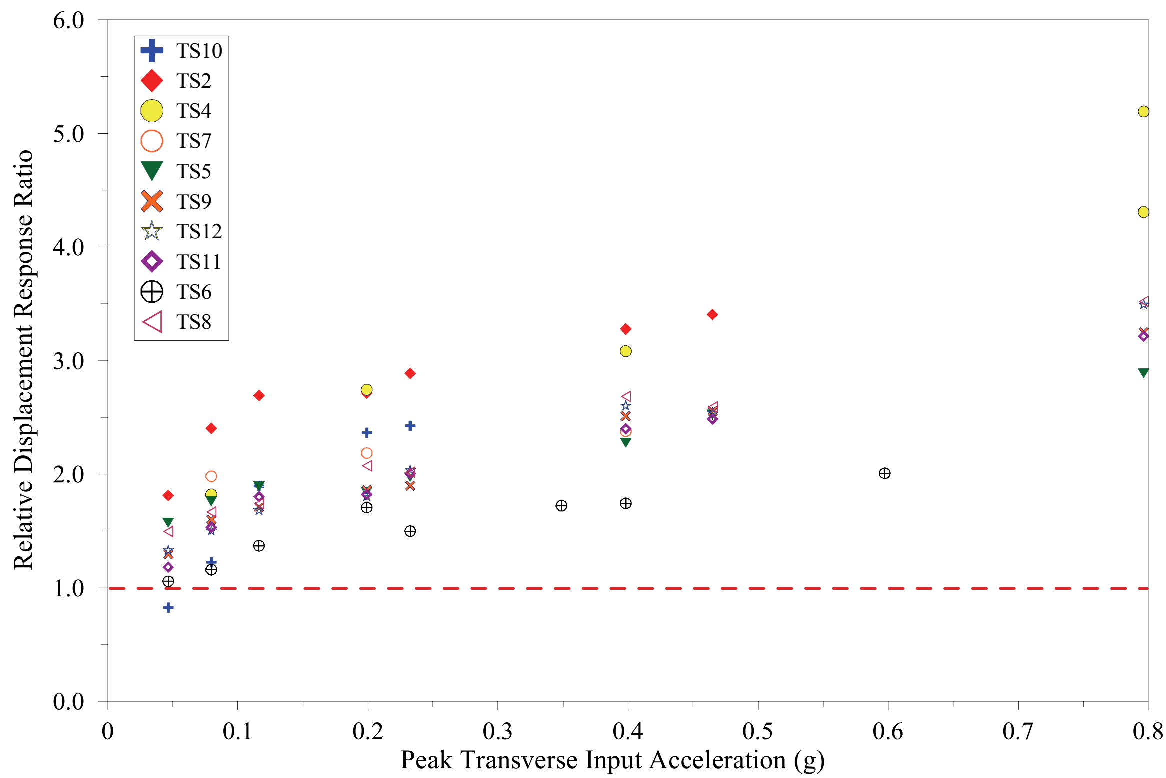

(b) Bottom-West Point

Figure 7-11 Variation of Relative Displacement Response Ratio at West Points on Chiller South Face with Peak Base Acceleration, Transverse Direction

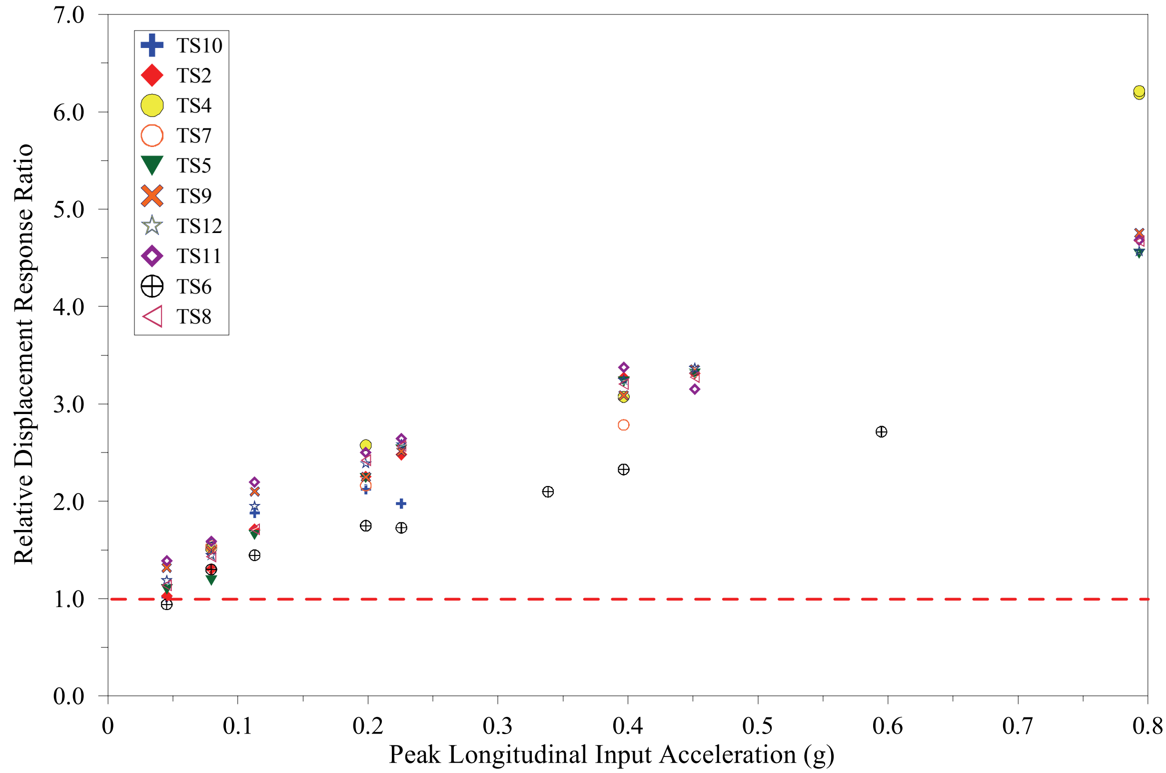

(a) Top-West Point

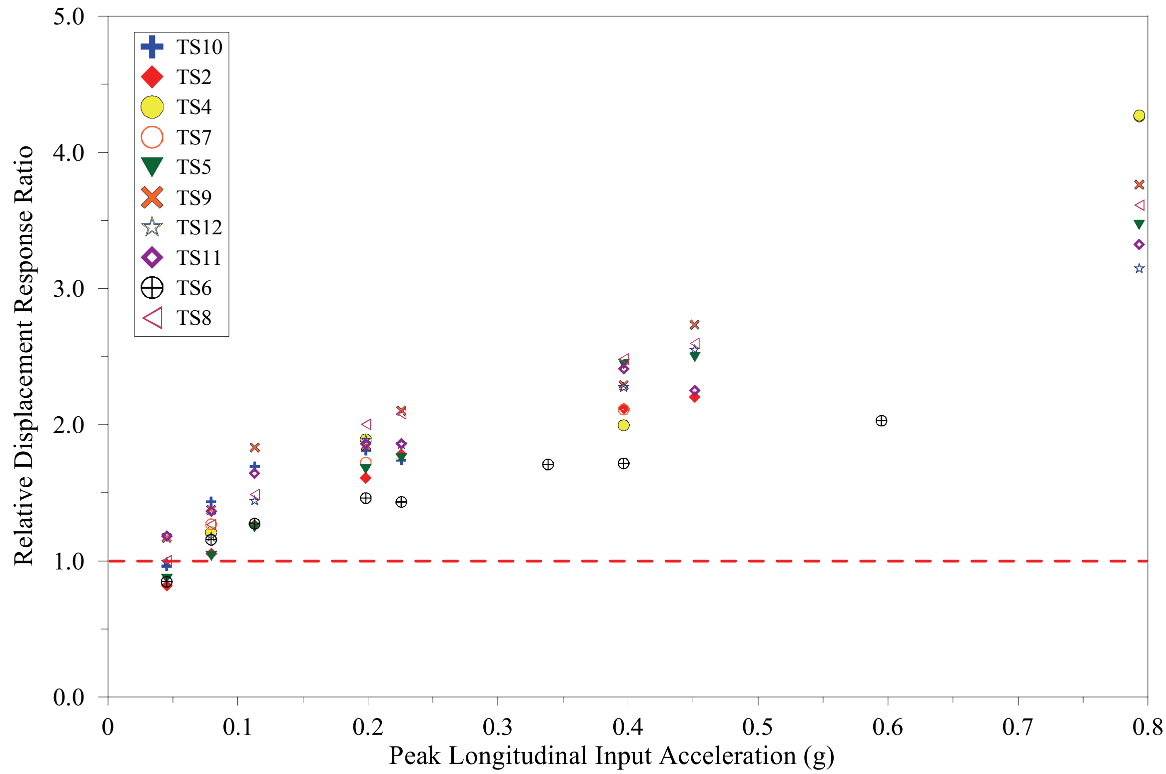

(b) Bottom-West Point

Figure 7-12 Variation of Relative Displacement Response Ratio at West Points on Chiller South Face with Peak Base Acceleration, Longitudinal Direction

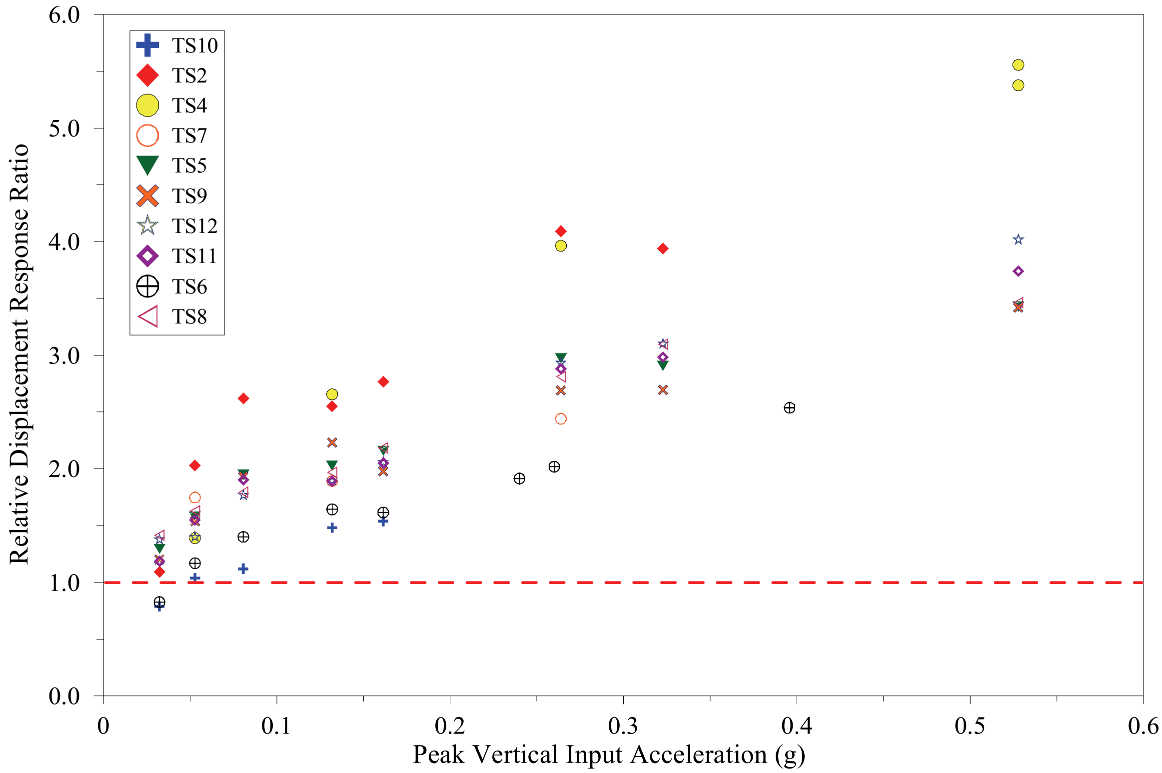

(a) Top-West Point

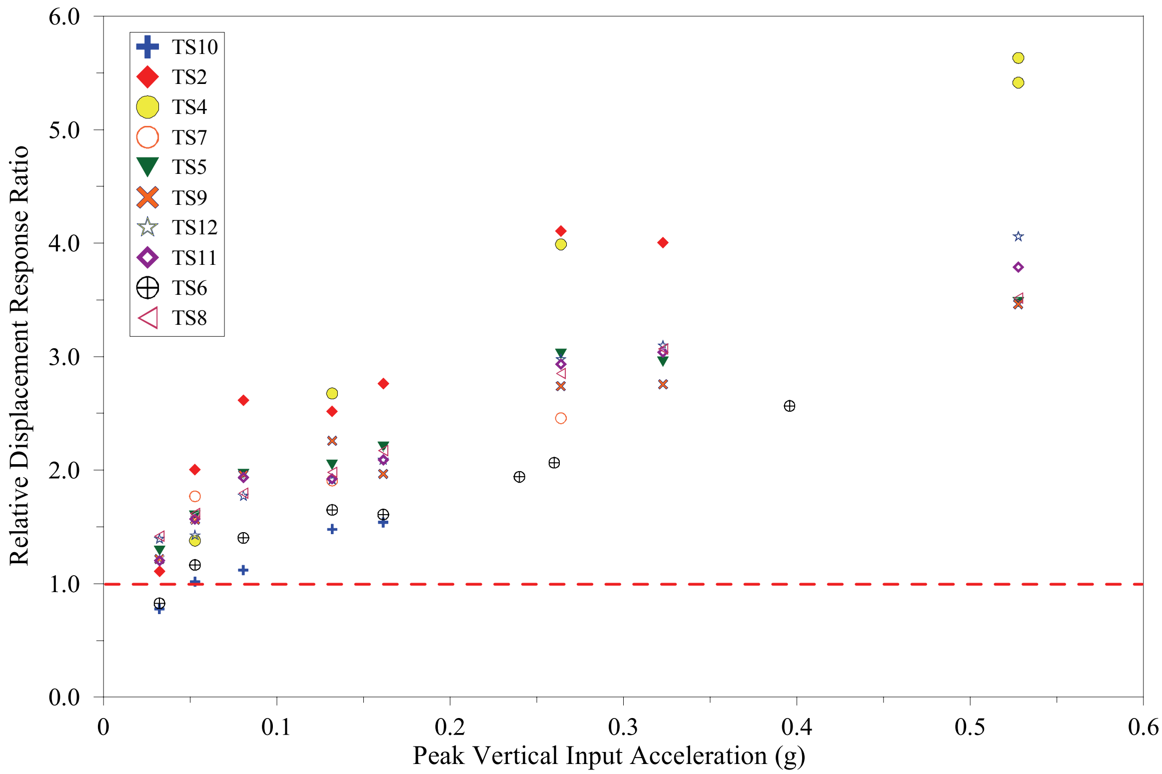

(b) Bottom-West Point

Figure 7-13 Variation of Relative Displacement Response Ratio at West Points on Chiller South Face with Peak Base Acceleration, Vertical Direction

Table 7-15 Minimum Relative Displacement Response at Top Level of South Face of Chiller Mounted on 1.0 g Design I/R Systems

Direction	Peak Relative Displacement Response (mm)	Test ID	Input Motion	
			Amplitude/ Level	Corresponding Peak Acceleration (g)
Transverse	12.7	TS10-S1	10%-Base	0.05
Longitudinal	5.8	TS2-S1	10%-Base	0.05
Vertical	6.7	TS2-S1	10%-Base	0.03

Table 7-16 Maximum Relative Displacement Response at Top Level of South Face of Chiller Mounted on 1.0 g Design I/R Systems

Direction	Peak Relative Displacement Response (mm)	Test ID	Input Motion	
			Amplitude/ Level	Corresponding Peak Acceleration (g)
Transverse	66.5	TS2-S8a	150%-Roof	1.19
Longitudinal	40.3	TS2-S6	100%-Base	0.45
Vertical	50.1	TS2-S8a	150%-Roof	0.80

Table 7-17 Minimum Relative Displacement Response at Top Level of South Face of Chiller Mounted on 3.0 g Design I/R Systems

Direction	Peak Relative Displacement Response (mm)	Test ID	Input Motion	
			Amplitude/ Level	Corresponding Peak Acceleration (g)
Transverse	8.4	TS4-S1	10%-Roof	0.08
Longitudinal	4.8	TS4-S1	10%-Roof	0.08
Vertical	4.4	TS4-S1	10%-Roof	0.05

Table 7-18 Maximum Relative Displacement Response at Top Level of South Face of Chiller Mounted on 3.0 g Design I/R Systems

Direction	Peak Relative Displacement Response (mm)	Test ID	Input Motion	
			Amplitude/ Level	Corresponding Peak Acceleration (g)
Transverse	45.0	TS6-S7	75%-Roof	0.60
Longitudinal	39.4	TS6-S7	75%-Roof	0.59
Vertical	33.1	TS6-S7	75%-Roof	0.40

7.4 Experimental Sensitivity Analysis

Conducting several test series with different design specifications for the 3.0 g design I/R systems provided the required data to investigate experimentally the sensitivity in the seismic performance of the I/R systems to the changes in their design specifications. The lower amplifications of the horizontal, vertical, and resultant acceleration responses at the center of mass of the chiller were selected as the indicators for the better seismic performance of the I/R systems.

The rubber pad thickness and hardness, gap size, and modification in the base plate of the I/R systems (see Section 5.6) were the four variables considered in the design specifications of the I/R systems. Tables 7-15 through 7-20 provide a list of the test series grouped together based on common and variable specifications. Figures 7-9 through 7-13 show the comparisons of the peak horizontal, vertical, and resultant acceleration response amplifications at the center of mass of the chiller for each of the groups of test series listed in the tables 7-15 through 7-20.

Table 7-19 Test Series Involving Variation of Rubber Pad Thickness in Presence of Identical Gap Size

Variable Specification	rubber pad thickness	**Variation**	**Test Series**
		3 mm (1/8 in)	TS7
		6 mm (1/4 in)	TS5
		6 mm (1/4 in)	TS11
		13 mm (1/2 in)	TS8
Common Specification(s)	gap size: 6 mm (1/4 in)		

Table 7-20 Test Series Involving Variation of Gap Size in Presence of Identical Rubber Pad Thickness

Variable Specification	gap size	**Variation**	**Test Series**
		3 mm (1/8 in)	TS4
		6 mm (1/4 in)	TS5
		6 mm (1/4 in)	TS11
		13 mm (1/2 in)	TS6
Common Specification(s)	rubber pad thickness: 6 mm (1/4 in)		

Table 7-21 Test Series Involving Variation of Rubber Pad Hardness in Presence of Identical Rubber Pad Thickness and Gap Size for Original 3.0 g Design I/R Systems

Variable Specification	rubber pad hardness	**Variation**	**Test Series**
		60 Duro	TS5
		50 Duro	TS9
Common Specification(s)	rubber pad thickness and gap size: 6 mm (1/4 in) (original 3.0 g design I/R systems)		

Table 7-22 Test Series Involving Variation of Rubber Pad Hardness in Presence of Identical Rubber Pad Thickness and Gap Size for Modified 3.0 g Design I/R Systems

Variable Specification	rubber pad hardness	**Variation**	**Test Series**
		60 Duro	TS11
		50 Duro	TS12
Common Specification(s)	rubber pad thickness and gap size: 6 mm (1/4 in) (modified 3.0 g design I/R systems)		

Table 7-23 Test Series Involving Modification of 3.0 g Design I/R Systems in Presence of Identical Gap Size, Rubber Pad Thickness, and 60 Duro Hardness

Variable Specification	modification in 3.0 g design I/R systems	**Variation**	**Test Series**
		original 3.0 g design	TS5
		modified 3.0 g design	TS11
Common Specification(s)	rubber pad thickness and gap size: 6 mm (1/4 in), rubber pad hardness: 60 Duro		

Table 7-24 Test Series Involving Modification of 3.0 g Design I/R Systems in Presence of Identical Gap Size, Rubber Pad Thickness, and 50 Duro Hardness

Variable Specification	modification in 3.0 g design I/R systems	**Variation**	**Test Series**
		original 3.0 g design	TS9
		modified 3.0 g design	TS12
Common Specification(s)	rubber pad thickness and gap size: 6 mm (1/4 in), rubber pad hardness: 50 Duro		

In figure 7-9, which is used to investigate the effect of the rubber pad thickness on the seismic performance of the I/R systems, the results of Test Series TS5 should be directly compared to the results of Test Series TS7 (both test series were conducted with the original I/R systems). Similarly, the results of Test Series TS11 should be directly compared to the results of Test Series TS8 (both test series were conducted with the modified I/R systems). Despite the significant scatter in the results shown in figure 7-9, the test series with the thinner rubber pad generally exhibit lower amplification of the peak acceleration response at the center of mass of the chiller. Based on the results obtained, it can be stated that although the thicker rubber pads might reduce the peak dynamic forces introduced into the I/R systems, in terms of the amplification of the peak acceleration response at the center of mass of the chiller, the thicker rubber pad does not necessarily mean the better seismic performance. In an over all comparison among the four 3.0 g design I/R systems tested with gap size of 6 mm (1/4 in), the modified I/R systems with the rubber pad thickness of 6 mm (1/4 in) exhibited the best seismic performance.

Although the rubber pad thickness is a property of the horizontal restraint component of the I/R systems, variations of the rubber pad thickness caused different seismic responses in the vertical direction, as shown in figure 7-9(b). In fact, these results confirm that there is an interaction between the horizontal and vertical seismic responses of the I/R systems.

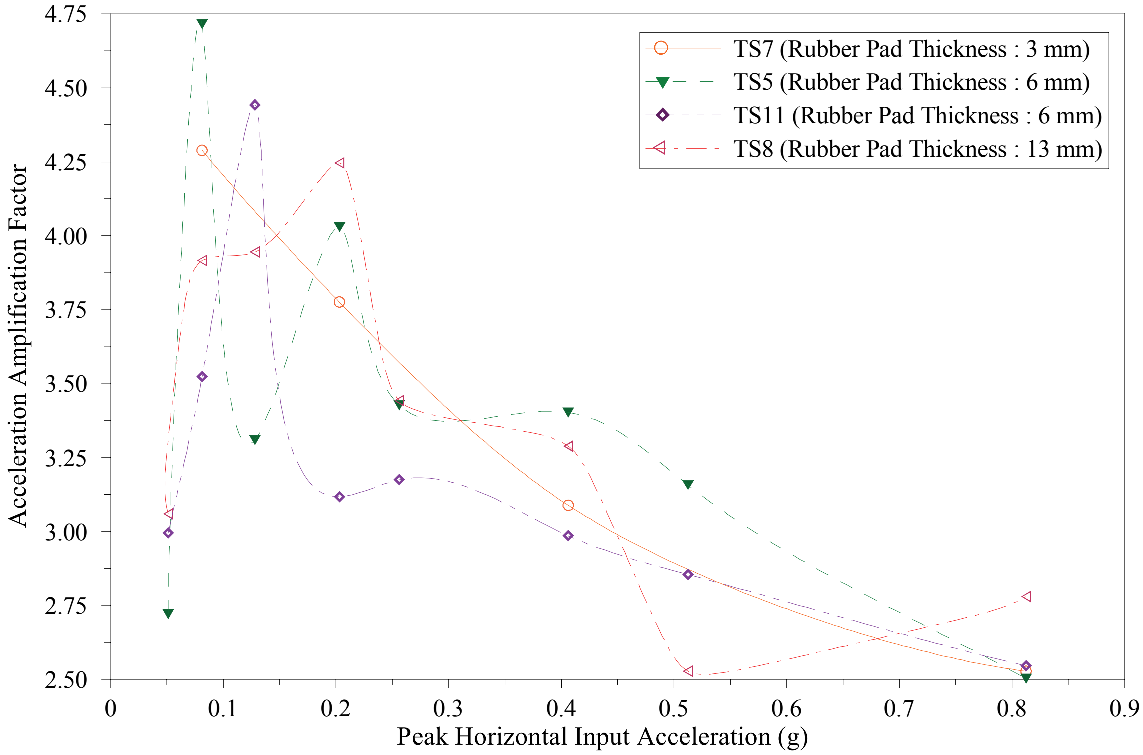

(a) Horizontal Acceleration Response at the Center of Mass

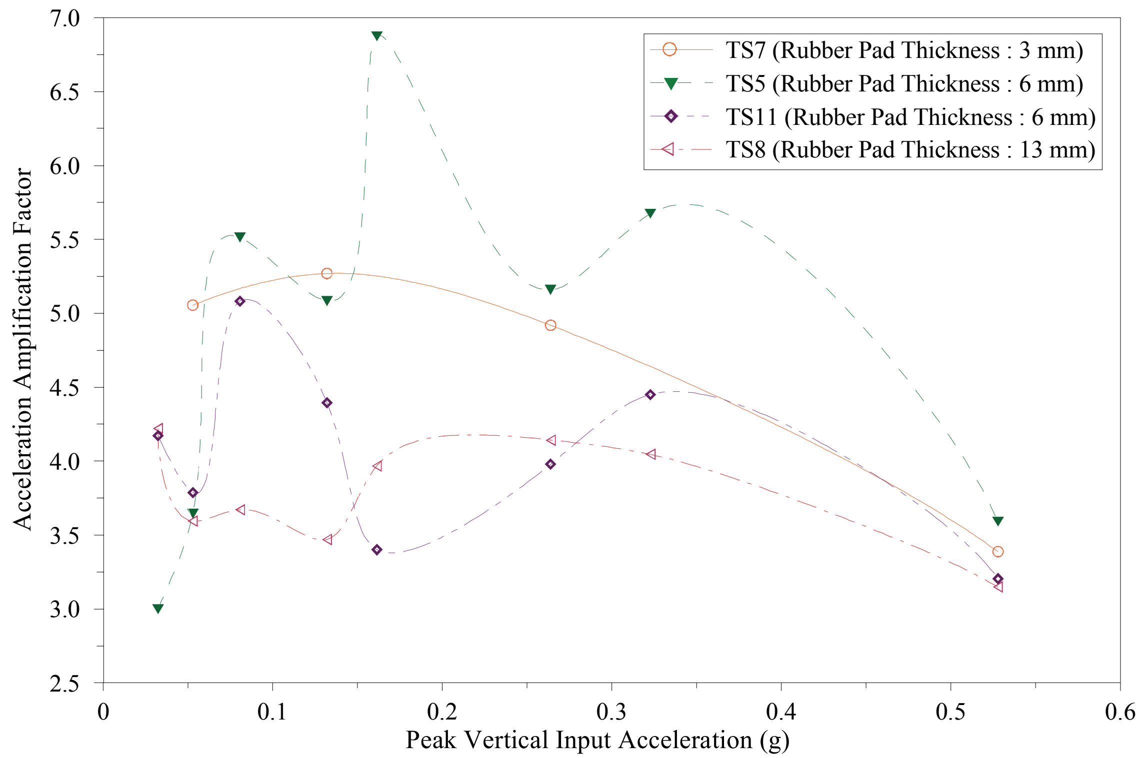

(b)Vertical Acceleration Response at the Center of Mass

Figure 7-14 Effect of Rubber Pad Thickness on Peak Acceleration Responses at Center of Mass of Chiller, 3.0 g Design I/R Systems

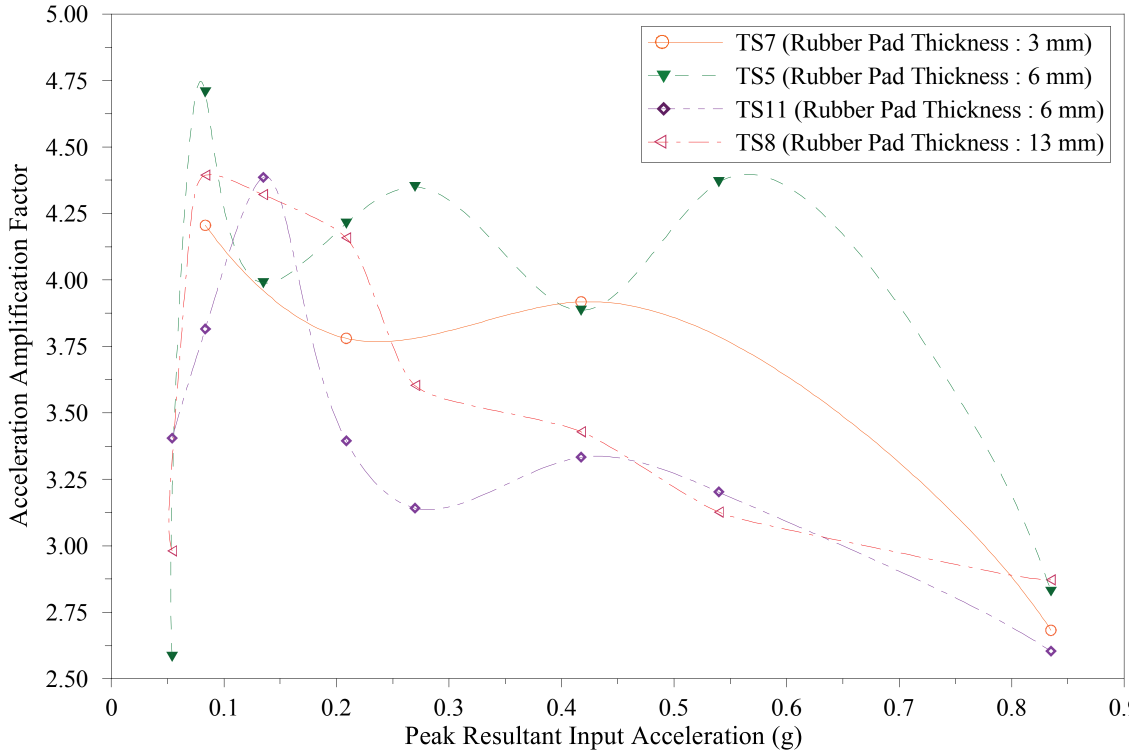

(c) Resultant Acceleration Response at the Center of Mass

Figure 7-14 (cont'd) Effect of Rubber Pad Thickness on Peak Acceleration Responses at Center of Mass of Chiller, 3.0 g Design I/R Systems

The effect of the gap size on the seismic performance of four 3.0 g design I/R systems with identical rubber pad thickness of 6 mm (1/4 in) is presented in figure 7-10. The results of Test Series TS5 should be directly compared to the result of Test Series TS4 (both test series were conducted with the original I/R systems). Similarly, the results of Test Series TS11 should be directly compared to the results of Test Series TS6 (both test series were conducted with the modified I/R systems).

The results shown in figure 7-10 indicate that for input motions with peak acceleration larger than 0.15 g, the I/R systems with smaller gap sizes show significantly better seismic performance. Incidentally, the large gap size of the I/R systems in the tests with low amplitude input motion could preclude the impacts in the restraint components and could lower the amplification of the acceleration responses at the center of mass of the chiller. For the tests with intense input motions, the I/R systems with the large gap size clearly exhibited unsatisfactorily performance. Furthermore, the large gap size of the I/R systems has resulted in introduction of significant peak dynamic forces into the I/R systems. Note that throughout Test Series TS6, because the capacity of the load cells was reached, testing of the I/R systems with largest gap size (13 mm [0.5 in]) was halted at only 75% amplitude of the input motions.

Overall, among all the I/R systems with rubber pad thickness of 6 mm (1/4 in), the original I/R systems with a gap size of 3 mm (1/8 in) exhibited the best seismic performance. Compared to the rubber pad thickness, the gap size seems to have a more direct influence on the seismic performance of the I/R systems. For severe input motions, the results confirm that the smaller gap size always corresponds to a better seismic performance.

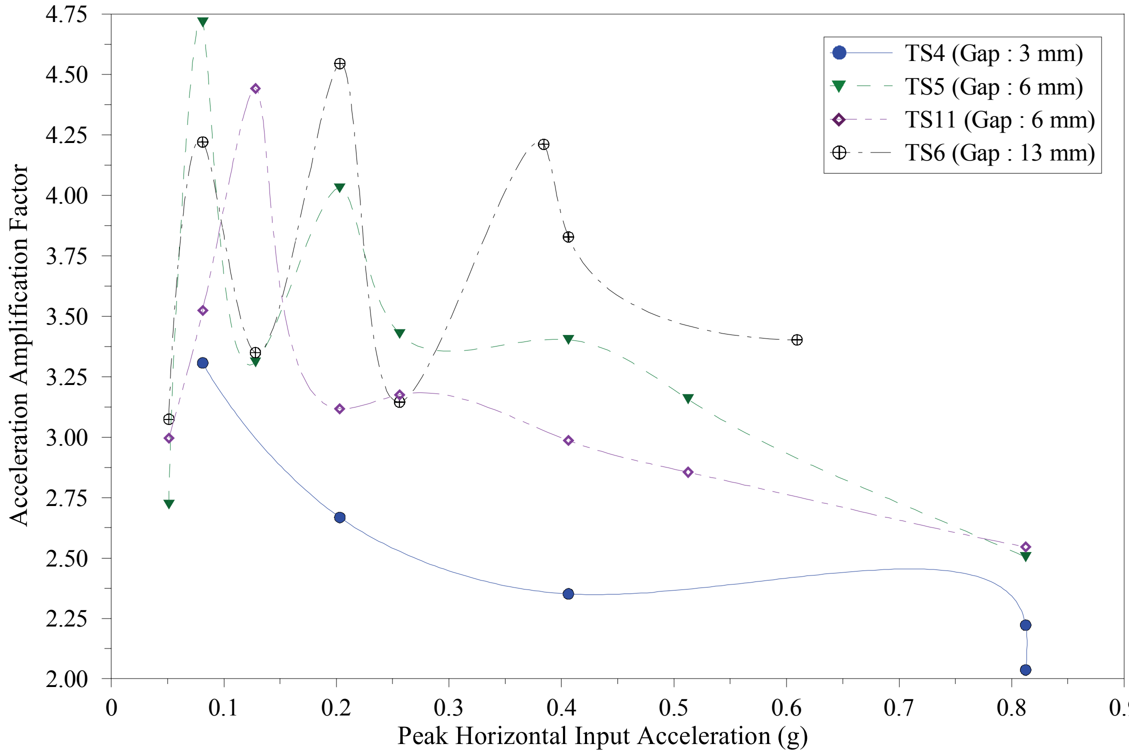

(a) Horizontal Acceleration Response at the Center of Mass

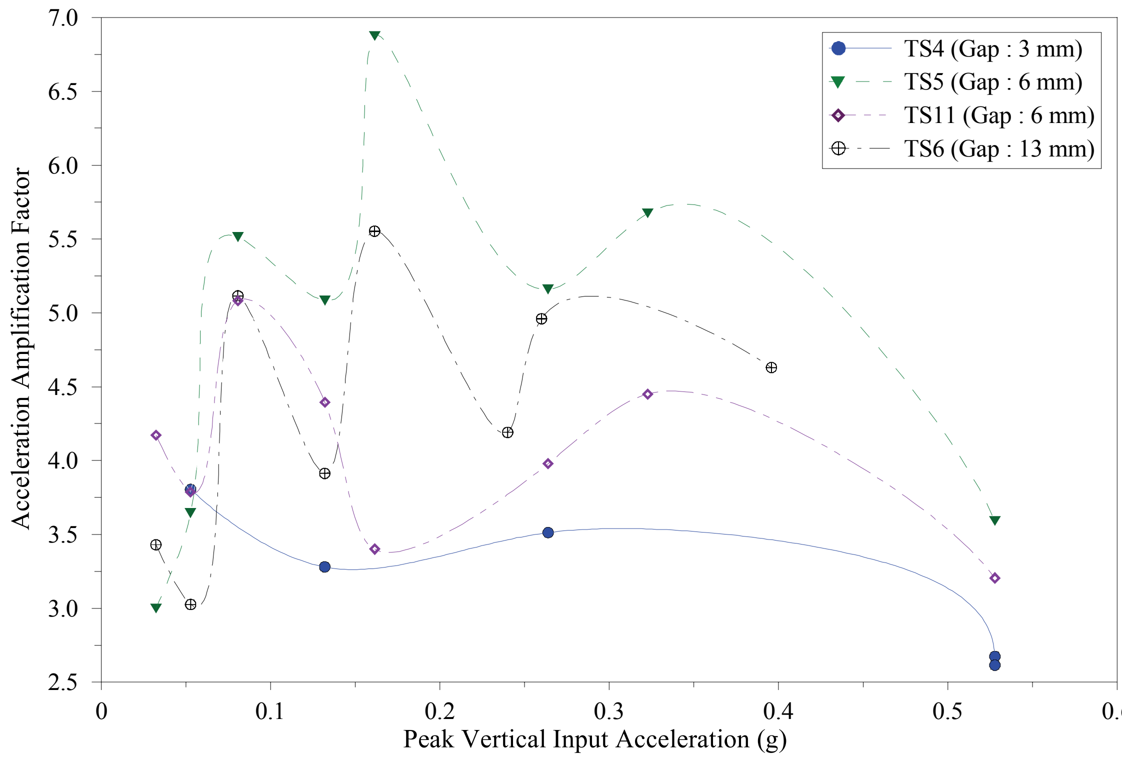

(b) Vertical Acceleration Response at the Center of Mass

Figure 7-15 Effect of Gap Size on Peak Acceleration Responses at Center of Mass of Chiller, 3.0 g Design I/R Systems

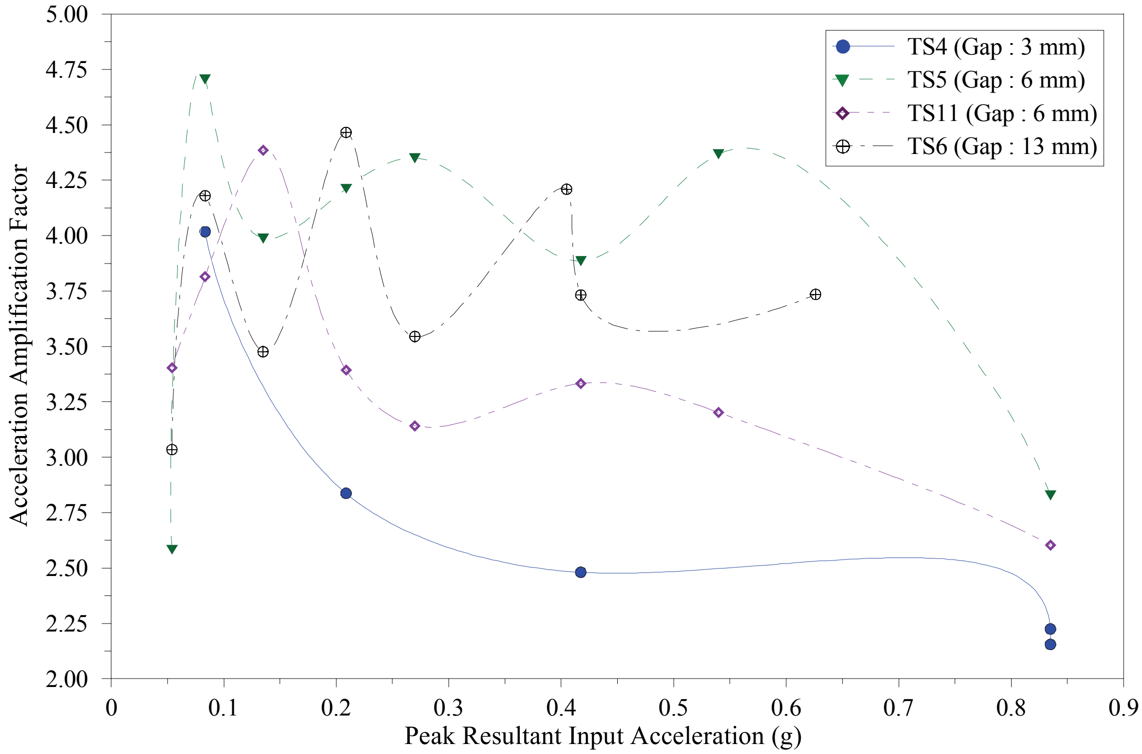

(c) Resultant Acceleration Response at the Center of Mass

Figure 7-15 (cont'd) Effect of Gap Size on Peak Acceleration Responses at Center of Mass of Chiller, 3.0 g Design I/R Systems

The effect of the rubber pad hardness on the seismic performance of two different I/R systems with identical rubber pad thickness and gap size of 6 mm (1/4 inch) is shown in figures 7-11 and 7-12 for the original and modified 3.0 g design I/R systems, respectively. The results shown in figures 7-11 and 7-12 are too scattered to conclude any general trend from them. In presence of other effects like malfunctioning of the vertical restraint component of the I/R systems in Test Series TS5 and TS9, it can only be stated that the seismic performance of the I/R systems does not seem to be highly sensitive to the change in rubber pad hardness from 50 to 60 Duro.

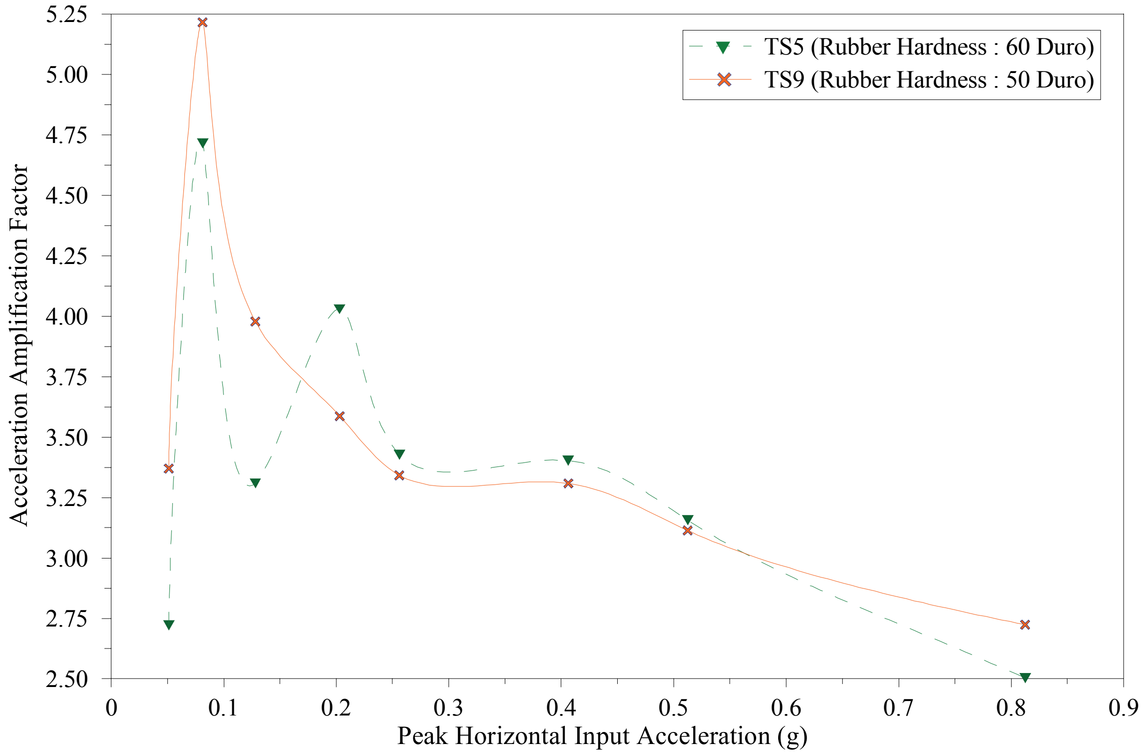

(a) Horizontal Acceleration Response at the Center of Mass

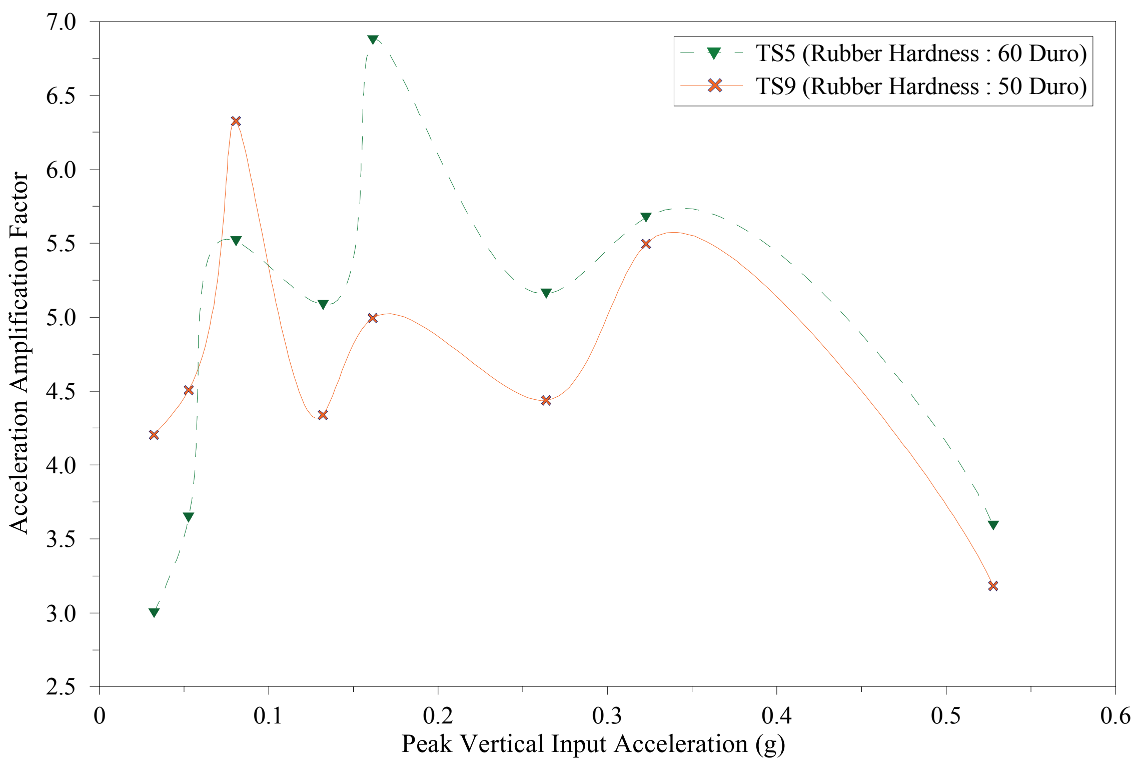

(b) Vertical Acceleration Response at the Center of Mass

Figure 7-16 Effect of Rubber Pad Hardness on Peak Acceleration Responses at Center of Mass of Chiller, Original 3.0 g Design I/R Systems

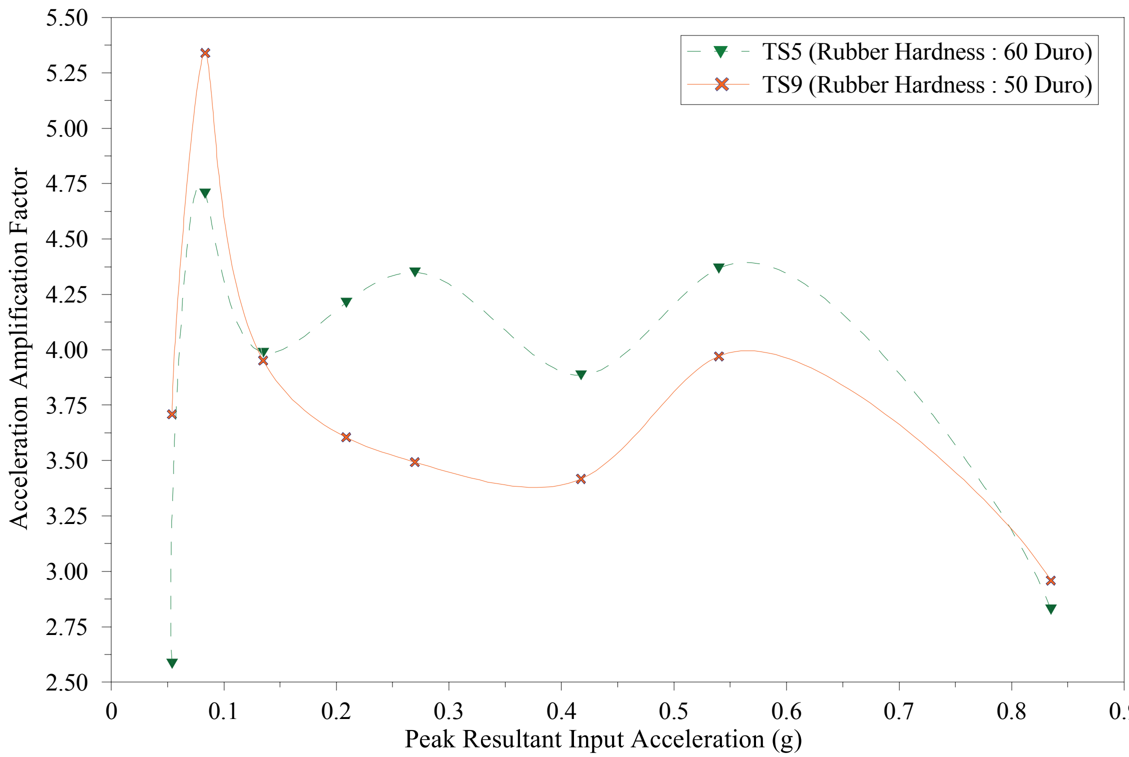

(c) Resultant Acceleration Response at the Center of Mass

Figure 7-16 (cont'd) Effect of Rubber Pad Hardness on Peak Acceleration Responses at Center of Mass of Chiller, Original 3.0 g Design I/R Systems

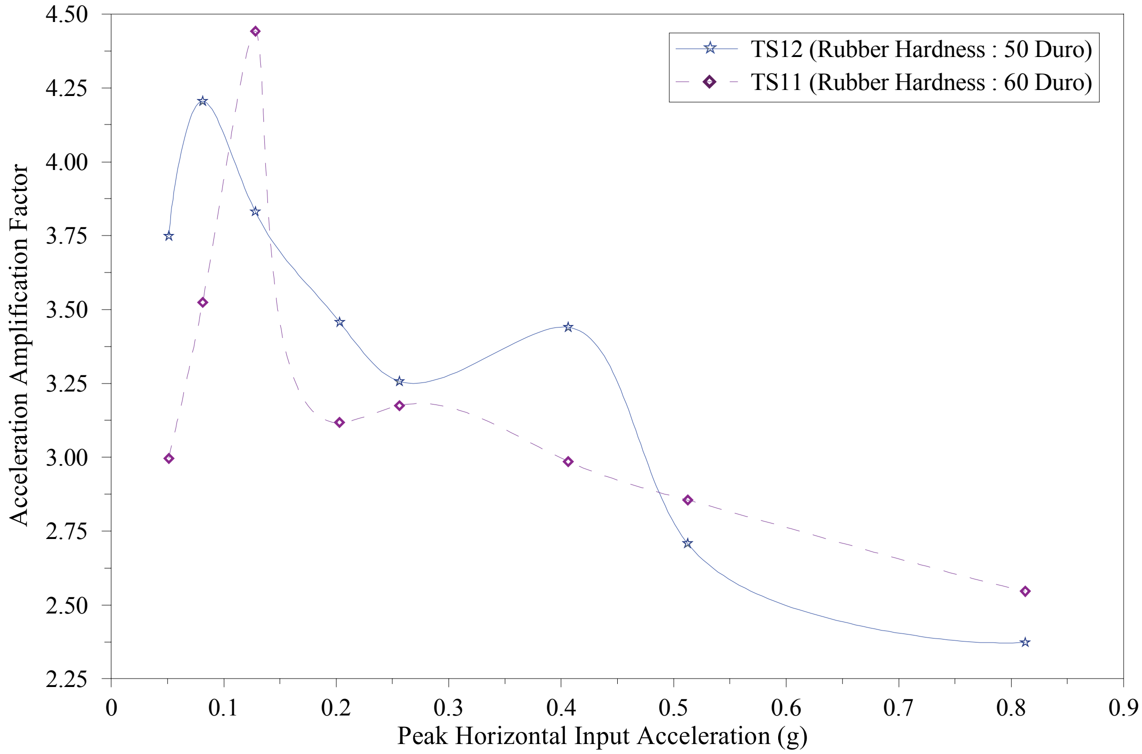

(a) Horizontal Acceleration Response at the Center of Mass

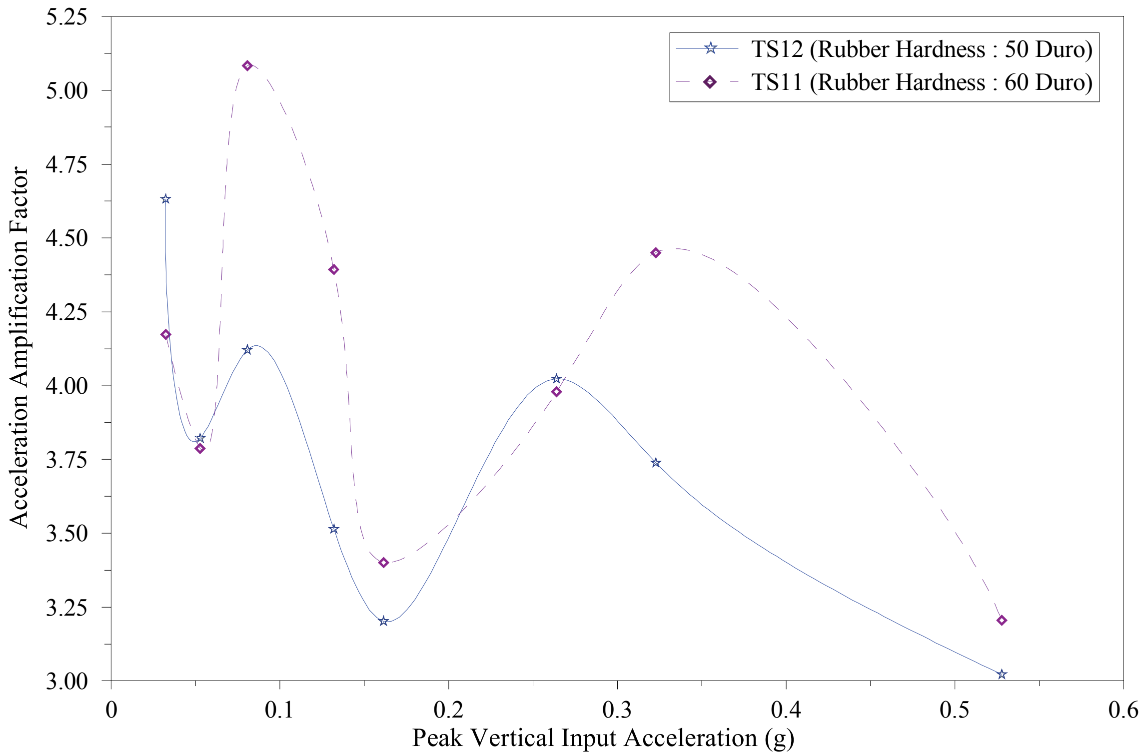

(b) Amplification Factors for the Vertical Acceleration Response the Center of Mass

Figure 7-17 Effect of Rubber Pad Hardness on Peak Acceleration Responses at Center of Mass of Chiller, Modified 3.0 g Design I/R Systems

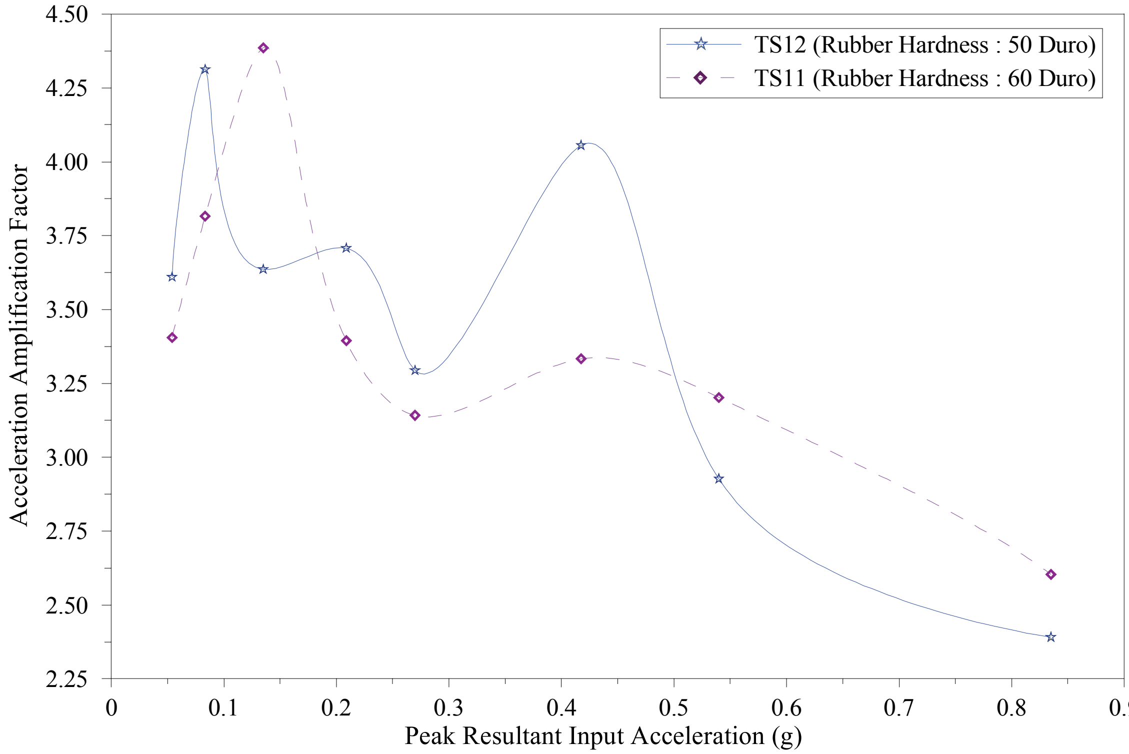

(c) Resultant Acceleration Response at the Center of Mass

Figure 7-17 (cont'd) Effect of Rubber Pad Hardness on Peak Acceleration Responses at Center of Mass of Chiller, Modified 3.0 g Design I/R Systems

The effect of the malfunctioning of the vertical restraint component on the seismic performance of the original I/R systems in Tests Series TS5 and TS9 were shown earlier in figures 7-9 and 7-10. This issue is investigated more specifically in figure 7-13. In this figure, the results of Test Series TS5 are directly compared to the results of Test Series TS11 (gap size and rubber pad thickness of 6 mm, rubber hardness of 60 Duro). Similarly, the results of Test Series TS9 are compared directly to the results of Test Series TS12 (gap size and rubber pad thickness of 6 mm, rubber hardness of 50 Duro). The results confirm that in Test Series TS5 and TS9 (before modification if the I/R systems), the impacts between the steel rod and base plate (see figure 5-9(a)) have dramatically degraded the seismic performance of the I/R systems. It was expected that the malfunctioning of the vertical restraint component affect mainly the vertical response at the center of mass of the chiller. However, because of the interaction between the horizontal and vertical seismic responses of the I/R systems, the horizontal and resultant acceleration responses at the center of mass of the chiller were also affected by the malfunctioning of the vertical restraint components.

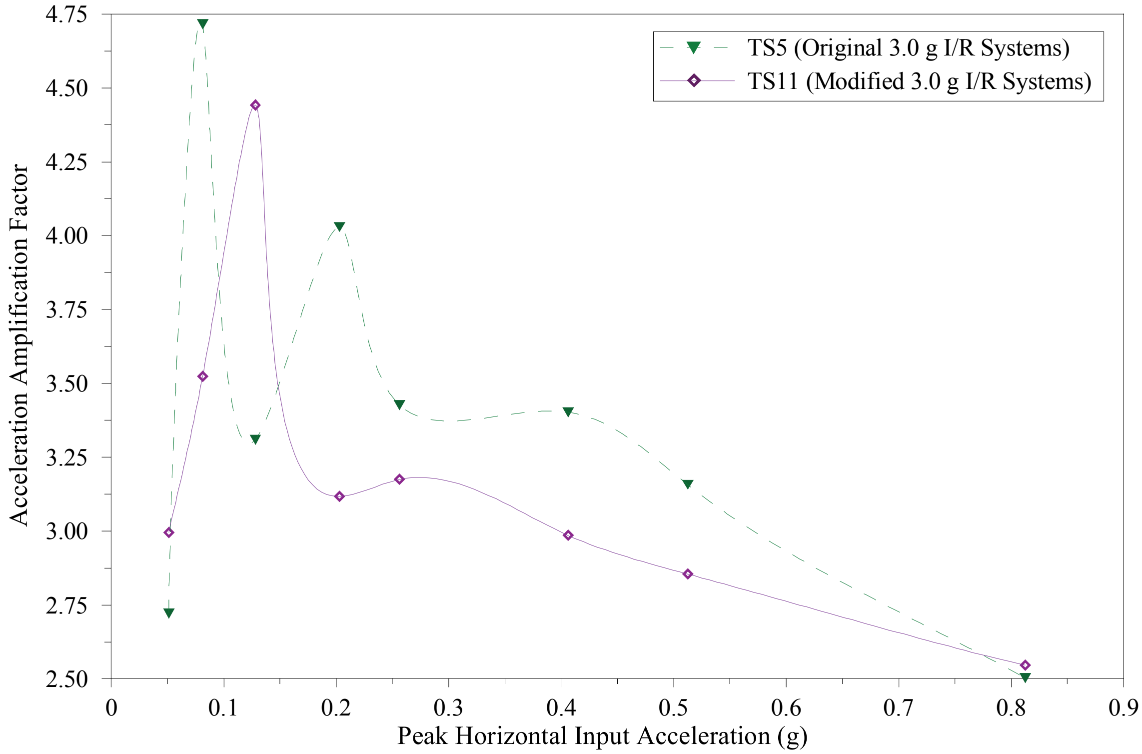

(a) Horizontal Acceleration Response at the Center of Mass

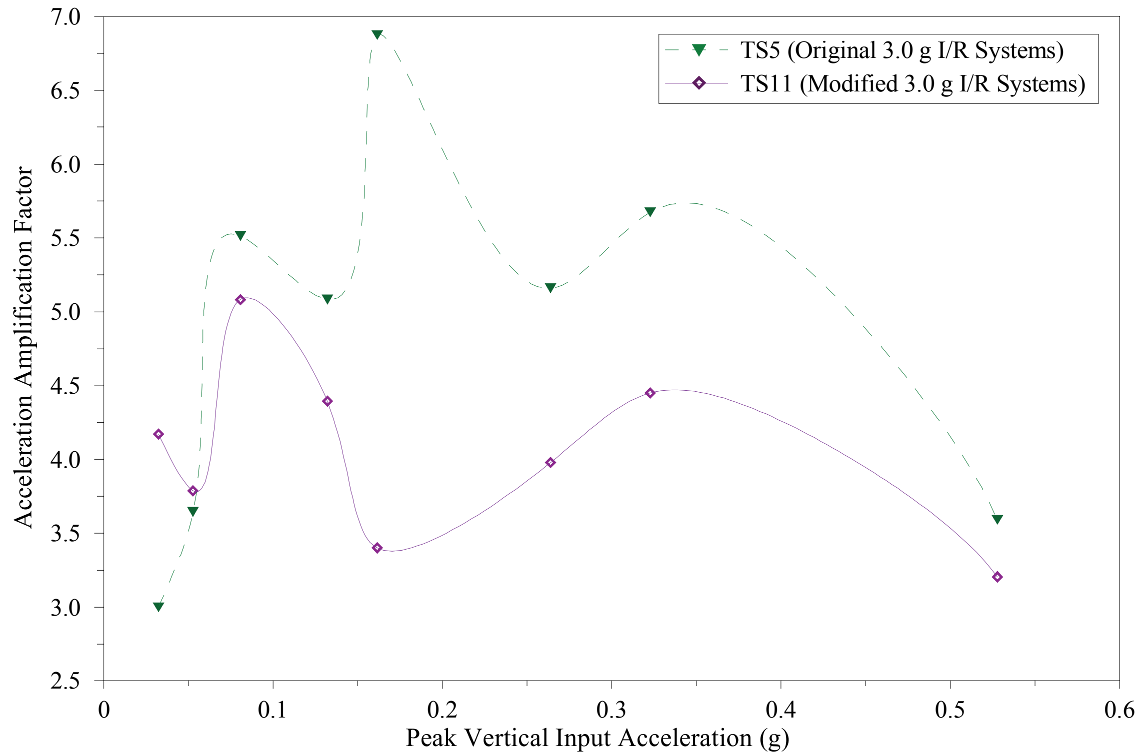

(b) Vertical Acceleration Response at the Center of Mass

Figure 7-18 Effect of Modification in 3.0 g Design I/R Systems on Peak Acceleration Responses at Center of Mass of Chiller

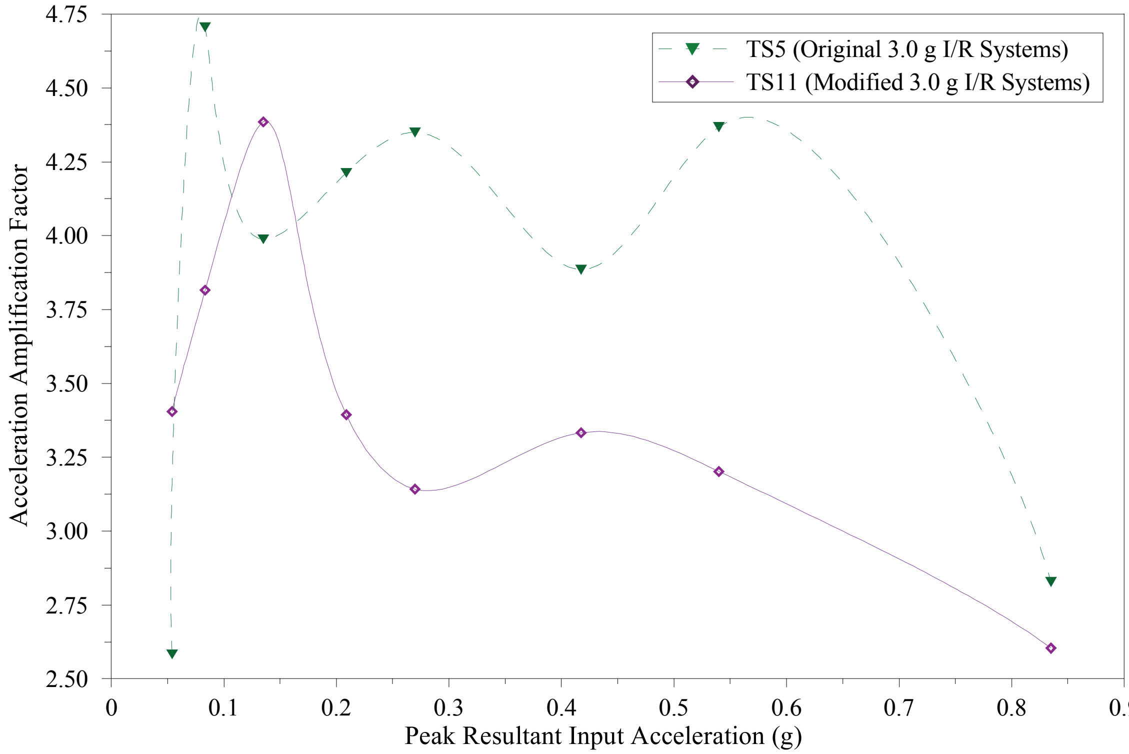

(c) Resultant Acceleration Response at the Center of Mass

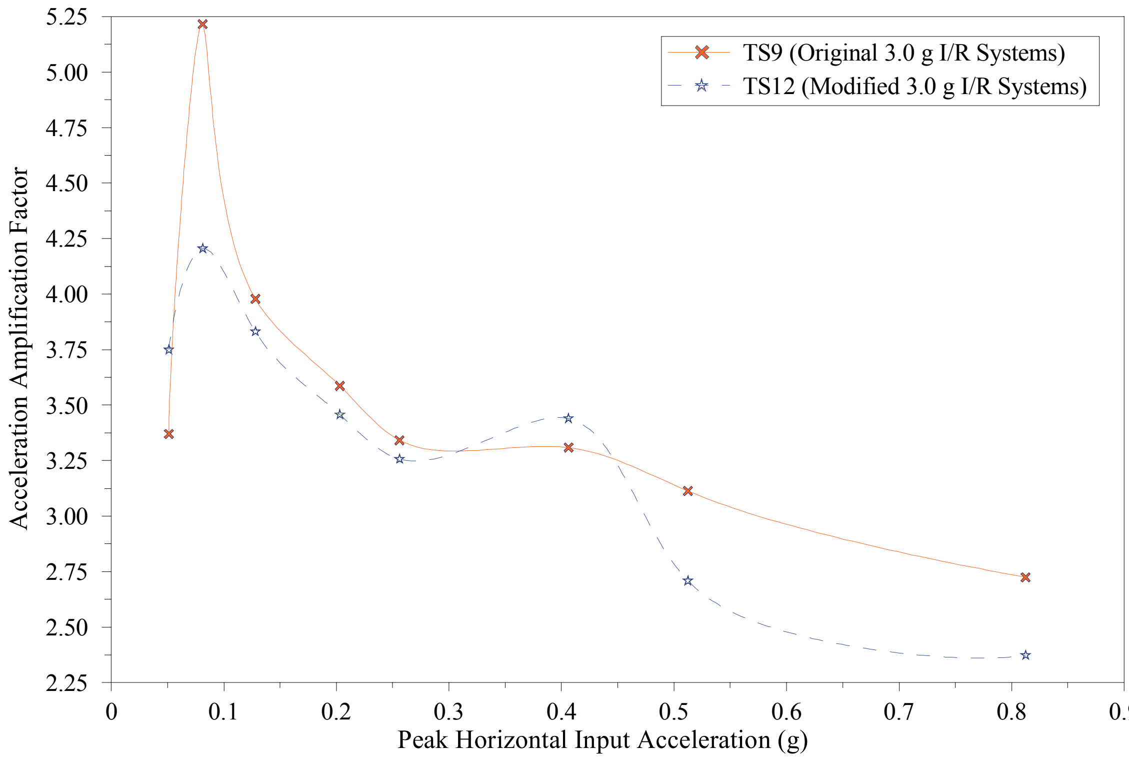

(d) Horizontal Acceleration Response at the Center of Mass

Figure 7-18 (cont'd) Effect of Modification in 3.0 g Design I/R Systems on Peak Acceleration Responses at Center of Mass of Chiller

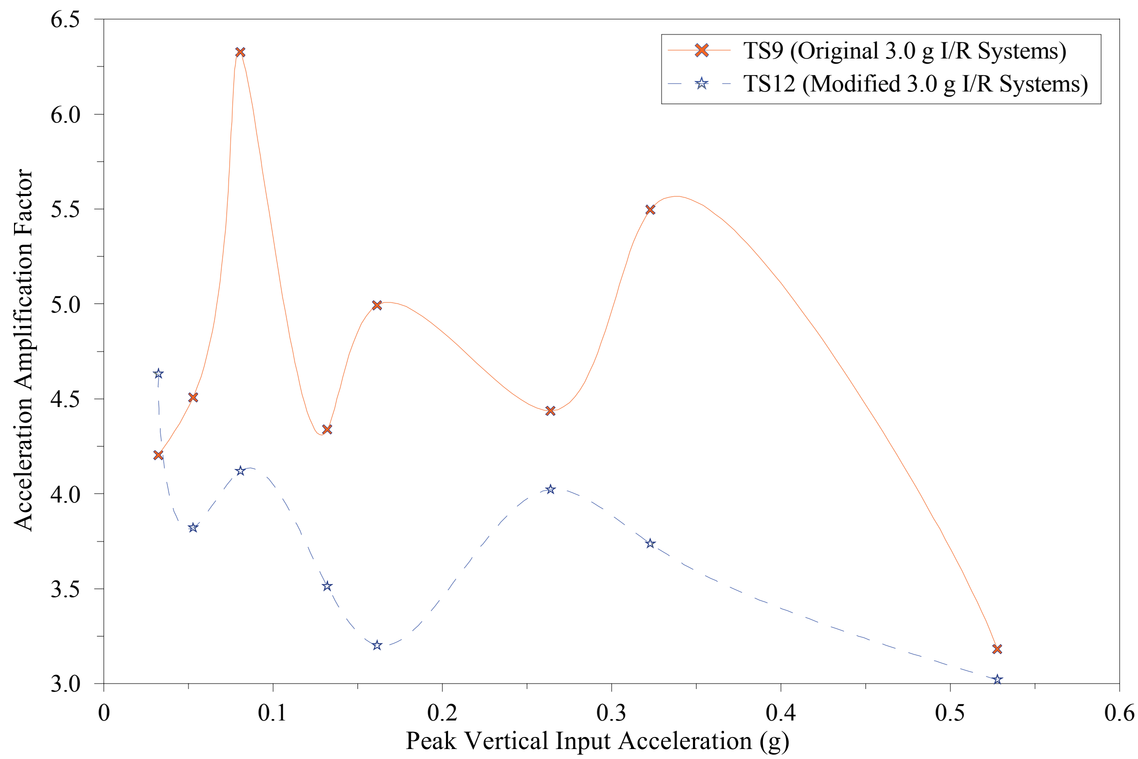

(e) Vertical Acceleration Response at the Center of Mass

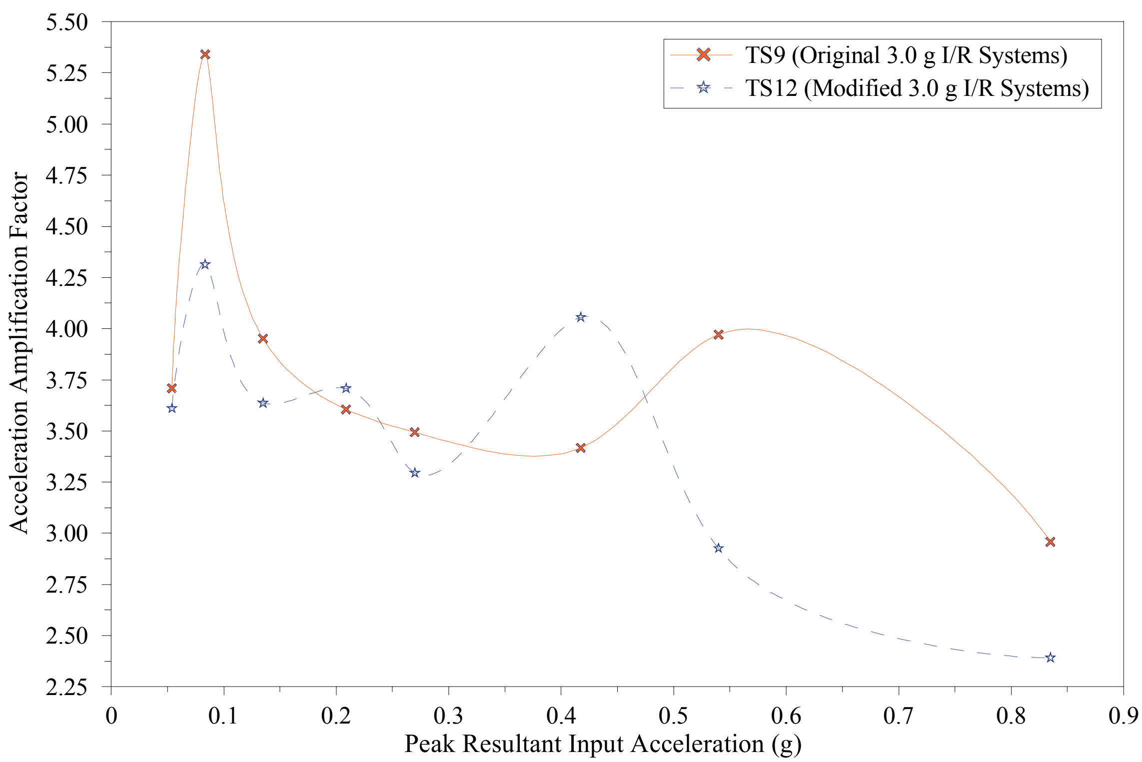

(f) Resultant Acceleration Response at the Center of Mass

Figure 7-18 (cont'd) Effect of Modification in 3.0 g Design I/R Systems on Peak Acceleration Responses at Center of Mass of Chiller

SECTION 8

CONCLUSIONS

The experimental research presented in this report evaluated the seismic performance of an isolation/restraint (I/R) system supporting a heavy mechanical equipment item. The studied I/R system was typical of the systems designed by the members of the American Society of Heating, Refrigerating, and Air-Conditioning Engineers. The heavy HVAC-type test specimen was a centrifugal liquid chiller weighing 11997 kg (26450 lb). The chiller was supported by four of the I/R systems. The main conclusions obtained from the 73 system-identification and 72 seismic tests are described in this section.

The results of the system-identification tests showed that the first three natural frequencies of the chiller (filled with water and refrigerant), supported by the isolation component of the I/R system at its four corners, were 1.17, 1.54, and 2.24 Hz. These natural frequencies were significantly smaller than even the first natural frequency of the rigidly mounted chiller (8.33 Hz). The first three mode shapes of the chiller supported by the isolation component of the I/R systems were almost pure translation in the transverse, longitudinal, and vertical direction, respectively.

Analyses of the decay of response at the end of the seismic tests (free vibration without engagement of the restraint components) showed that the isolation component of the I/R system provided only around one and three percents of the critical equivalent viscous damping ratio in the vertical and horizontal direction, respectively. Therefore, the isolation component of the I/R system can hardly reduce the response by energy dissipation.

The acceleration response measured at the center of mass and corners of the chiller during the seismic tests verified that the restraint component of the I/R systems limited the displacement response at the expanse of amplification of the acceleration response. During the 72 seismic tests conducted with different designs and specifications of the I/R systems, the peak acceleration response at the center of mass of the chiller was amplified between 1.8 and 4.5 times in the horizontal direction and between 2.2 and 4.5 times in the vertical direction.

In most of the tests with peak input accelerations high enough (higher than nearly 0.15g) to engage the restraint components, the amplification of the peak acceleration response at the center of mass of the chiller reduced with an increase of the peak input acceleration. Regardless of the I/R system design and specifications, for the high amplitude input motions (full-scale input motions), the acceleration amplification factor at the center of mass of the chiller varied only between 2.0 and 3.0.

Despite the reduction in the amplification of the peak acceleration response with an increase of the peak input acceleration, the maximum acceleration responses yet occurred in the tests with the maximum input motion amplitude. The center of mass of the chiller mounted on the 1.0 g and 3.0 g design I/R systems experienced peak resultant acceleration response as large as 4.14g and 2.47g, respectively.

The energy generated by the impacts occurring in the restraint component of the I/R systems was partially absorbed by the body of the chiller and the liquid inside it. Therefore, the amplification of the peak acceleration response at the corners was larger than that at the center of mass of the chiller. The amplification of the peak acceleration response at the corners of the chiller varied between 1.9 and 10.5 in the transverse direction, between 1.5 and 27.7 in the longitudinal direction, and between 2.9 and 13.8 in the vertical direction. Throughout the 72 seismic tests conducted, the corners of the chiller experienced maximum acceleration responses of 5.15g, 9.44g, and 5.66g in the transverse, longitudinal, and vertical direction, respectively.

The restraint component of the 1.0 g design I/R systems, designed for a static force of 29 kN, could withstand dynamic shear and normal forces larger than 200 and 450 kN, respectively. The bottom steel washers of the vertical restraint components were the only damaged elements of the 1.0 g design I/R systems during the seismic tests. After the seismic test with the input motion corresponding to the roof level and scaled to 150% amplitude, all the bottom steel washers were deformed into a conical shape. The 3.0 g design restraint component of the I/R systems, designed for a static load of only 88 kN, without any damage experienced dynamic shear and normal forces larger than 120 and 440 kN, respectively.

Withstanding the forces induced by acceleration responses as large as 10.0 g by the 1.0 g design restraint component of the I/R systems showed that the static design capacity is an extremely conservative estimation for the actual dynamic capacity of the restraint component of the I/R systems.

The maximum relative displacement response of mechanical equipment is very important for designing the ducts and pipes connected to the equipment. The results showed that because of the rotational response of the equipment and deformation of the snubber elements, the peak relative displacement response of the mounted equipment can be much larger than the gap size of the I/R systems. The effect of the rotational response in increasing the peak relative displacement response depends on the geometry of the test specimen. However, this effect is certainly higher for the response at the locations elevated from the I/R systems level. While the largest gap size in the seismic tests was 12 mm (0.5 in), the top level of the south face of the chiller experienced relative displacement response as large as 45 mm (1.77 in). The relative displacement response at top level of the south face of the chiller in some of the tests was as large as ten times of the gap size of the I/R systems.

The comparison of the seismic performance of four 3.0 g design I/R systems with the identical gap size and different rubber pad thickness showed that the application of the thicker rubber snubber had not always resulted in a reduction in the amplified acceleration response at the center of mass of the chiller and dynamic forces induced into the I/R systems. The rubber pad thickness is a property of the horizontal restraint component of the I/R systems. Therefore, the sensitivity of the seismic performance of the I/R systems in the vertical direction to the change in the rubber pad thickness confirmed that there is a considerable interaction between the horizontal and vertical seismic performance of the I/R systems.

The comparison of the seismic performance of four 3.0 g design I/R systems with the identical rubber pad thickness and different gap size showed that for the low amplitude input motions (with peak acceleration less than nearly 0.15g), the large gap size of the I/R systems could preclude the engagement of the restraint components and result in better seismic performance. However, for the input motions with peak acceleration high enough to engage the restraint components, the large gap size resulted in inducing significant peak dynamic forces into the I/R systems and amplifying the acceleration response at the center of mass of the chiller. For instance, increasing the gap size from 3mm (1/8 in) to 13mm (1/2 in) resulted in almost doubling of the acceleration response at the center of mass and the forces induced into the I/R systems. For high amplitude input motions, the smaller gap size always corresponded to a substantially better seismic performance.

In presence of the influential specifications such as the gap size and rubber pad thickness, the seismic performance of the I/R system showed little sensitivity to the change of the rubber pad hardness from 60 to 50 Duro.

The inadequate space left between the tip of the steel rods and the base plate of the original 3.0 g design I/R systems with large gap size resulted in malfunctioning of the vertical restraint components and consequently resulted in the poor seismic performance. The modification of the 3.0 g design I/R systems by creating holes in their base plates completely removed this issue and improved the seismic performance of the I/R systems.

Among all the specifications, the gap size had the most influence on the seismic performance of the I/R systems. Based on the results obtained in this study, in areas of high seismicity, it is strongly recommended to limit the gap size of the I/R systems to the gap size necessary for noise and operational vibration control.

SECTION 9

REFERENCES

[1] ASHRAE, (2003), ”Seismic and Wind Restraint Design”, 2003 ASHRAE Application Handbook, Chapter 54, American Society of Heating, Refrigerating and Air-Conditioning Engineers, Atlanta, GA.

[2] Chopra, A.K., (2000), “Dynamics of Structures: Theory and Applications to Earthquake Engineering”, Prentice Hall, Upper Saddle River, NJ.

[3] Filiatrault, A., (1998), “Elements of Earthquake Engineering and Structural Dynamics”, Polytechnic International Press, Montreal, Canada

[4] Filiatrault, A., Uang, C-M., Folz, B., Christopoulos, C. and Gatto, K., (2001), “Reconnaissance Report of the February 28, 2001 Nisqually (Seattle-Olympia) Earthquake”, Structural Systems Research Project Report No. SSRP-2000/15, Department of Structural Engineering, University of California, San Diego, La Jolla, CA.

[5] Gould, M. J., N. C. Griffin, (2003), “The Value of Seismically Installing and Strengthening Nonstructural Equipment and Systems to Significantly Reduce Business Interruption Losses”, in the Proceedings of Seminar on Seismic Design, Performance, and Retrofit of Nonstructural Components in Critical Facilities, ATC-29-2, Newport Beach, CA.

[6] ICC: International Code Council, (2003), “International Building Code”, International Code Council, Whittier, CA.

[7] ICC-ES: International Code Council-Evaluation Service Inc., (2004), “Acceptance Criteria for Seismic Qualification by Shake Table Testing of Nonstructural Components and Systems”, AC 156, Effective July 2004, ICC-ES Inc., International Code Council, Whittier, CA.

[8] Kinetics Noise Control, (2006), < http://www.kineticsnoise.com >

[9] Kircher, C. A., (2003), “Make Dollars and Sense to Improve Nonstructural System Performance”, in the Proceedings of Seminar on Seismic Design, Performance, and Retrofit of Nonstructural Components in Critical Facilities, ATC-29-2, Newport Beach, CA.

[10] Mason Industries Inc., (2006), < http://www.mason-ind.com >

[11] Tauby J. R., (2005), Personal Communications

[12] Wanitkorkul, A. and Filiatrault, A., (2005), “Seismic Qualification of a Centrifugal Liquid Chiller by Shake Table Testing”, CSEE-SEESL-2005-05, Department of Civil, Structural, and Environmental Engineering, University at Buffalo, the State University of New York, Buffalo, NY.

[13] Wheeler, A. and Ganji, A. R., (2004), “Introduction to Engineering Experimentation”, Prentice Hall, Upper Saddle River, NJ.

[14] York International Corporation, (2005), < http://www.york.com >

MCEER Technical Reports

MCEER publishes technical reports on a variety of subjects written by authors funded through MCEER. These reports are available from both MCEER Publications and the National Technical Information Service (NTIS). Requests for reports should be directed to MCEER Publications, MCEER, University at Buffalo, State University of New York, Red Jacket Quadrangle, Buffalo, New York 14261. Reports can also be requested through NTIS, 5285 Port Royal Road, Springfield, Virginia 22161. NTIS accession numbers are shown in parenthesis, if available.

NCEER-87-0001 "First-Year Program in Research, Education and Technology Transfer," 3/5/87, (PB88-134275, A04, MF-A01).

NCEER-87-0002 "Experimental Evaluation of Instantaneous Optimal Algorithms for Structural Control," by R.C. Lin, T.T. Soong and A.M. Reinhorn, 4/20/87, (PB88-134341, A04, MF-A01).

NCEER-87-0003 "Experimentation Using the Earthquake Simulation Facilities at University at Buffalo," by A.M. Reinhorn and R.L. Ketter, to be published.

NCEER-87-0004 "The System Characteristics and Performance of a Shaking Table," by J.S. Hwang, K.C. Chang and G.C. Lee, 6/1/87, (PB88-134259, A03, MF-A01). This report is available only through NTIS (see address given above).

NCEER-87-0005 "A Finite Element Formulation for Nonlinear Viscoplastic Material Using a Q Model," by O. Gyebi and G. Dasgupta, 11/2/87, (PB88-213764, A08, MF-A01).

NCEER-87-0006 "Symbolic Manipulation Program (SMP) - Algebraic Codes for Two and Three Dimensional Finite Element Formulations," by X. Lee and G. Dasgupta, 11/9/87, (PB88-218522, A05, MF-A01).

NCEER-87-0007 "Instantaneous Optimal Control Laws for Tall Buildings Under Seismic Excitations," by J.N. Yang, A. Akbarpour and P. Ghaemmaghami, 6/10/87, (PB88-134333, A06, MF-A01). This report is only available through NTIS (see address given above).

NCEER-87-0008 "IDARC: Inelastic Damage Analysis of Reinforced Concrete Frame - Shear-Wall Structures," by Y.J. Park, A.M. Reinhorn and S.K. Kunnath, 7/20/87, (PB88-134325, A09, MF-A01). This report is only available through NTIS (see address given above).

NCEER-87-0009 "Liquefaction Potential for New York State: A Preliminary Report on Sites in Manhattan and Buffalo," by M. Budhu, V. Vijayakumar, R.F. Giese and L. Baumgras, 8/31/87, (PB88-163704, A03, MF-A01). This report is available only through NTIS (see address given above).

NCEER-87-0010 "Vertical and Torsional Vibration of Foundations in Inhomogeneous Media," by A.S. Veletsos and K.W. Dotson, 6/1/87, (PB88-134291, A03, MF-A01). This report is only available through NTIS (see address given above).

NCEER-87-0011 "Seismic Probabilistic Risk Assessment and Seismic Margins Studies for Nuclear Power Plants," by Howard H.M. Hwang, 6/15/87, (PB88-134267, A03, MF-A01). This report is only available through NTIS (see address given above).

NCEER-87-0012 "Parametric Studies of Frequency Response of Secondary Systems Under Ground-Acceleration Excitations," by Y. Yong and Y.K. Lin, 6/10/87, (PB88-134309, A03, MF-A01). This report is only available through NTIS (see address given above).

NCEER-87-0013 "Frequency Response of Secondary Systems Under Seismic Excitation," by J.A. HoLung, J. Cai and Y.K. Lin, 7/31/87, (PB88-134317, A05, MF-A01). This report is only available through NTIS (see address given above).

NCEER-87-0014 "Modelling Earthquake Ground Motions in Seismically Active Regions Using Parametric Time Series Methods," by G.W. Ellis and A.S. Cakmak, 8/25/87, (PB88-134283, A08, MF-A01). This report is only available through NTIS (see address given above).

NCEER-87-0015 "Detection and Assessment of Seismic Structural Damage," by E. DiPasquale and A.S. Cakmak, 8/25/87, (PB88-163712, A05, MF-A01). This report is only available through NTIS (see address given above).

NCEER-87-0016 "Pipeline Experiment at Parkfield, California," by J. Isenberg and E. Richardson, 9/15/87, (PB88-163720, A03, MF-A01). This report is available only through NTIS (see address given above).

NCEER-87-0017 "Digital Simulation of Seismic Ground Motion," by M. Shinozuka, G. Deodatis and T. Harada, 8/31/87, (PB88-155197, A04, MF-A01). This report is available only through NTIS (see address given above).

NCEER-87-0018 "Practical Considerations for Structural Control: System Uncertainty, System Time Delay and Truncation of Small Control Forces," J.N. Yang and A. Akbarpour, 8/10/87, (PB88-163738, A08, MF-A01). This report is only available through NTIS (see address given above).

NCEER-87-0019 "Modal Analysis of Nonclassically Damped Structural Systems Using Canonical Transformation," by J.N. Yang, S. Sarkani and F.X. Long, 9/27/87, (PB88-187851, A04, MF-A01).

NCEER-87-0020 "A Nonstationary Solution in Random Vibration Theory," by J.R. Red-Horse and P.D. Spanos, 11/3/87, (PB88-163746, A03, MF-A01).

NCEER-87-0021 "Horizontal Impedances for Radially Inhomogeneous Viscoelastic Soil Layers," by A.S. Veletsos and K.W. Dotson, 10/15/87, (PB88-150859, A04, MF-A01).

NCEER-87-0022 "Seismic Damage Assessment of Reinforced Concrete Members," by Y.S. Chung, C. Meyer and M. Shinozuka, 10/9/87, (PB88-150867, A05, MF-A01). This report is available only through NTIS (see address given above).

NCEER-87-0023 "Active Structural Control in Civil Engineering," by T.T. Soong, 11/11/87, (PB88-187778, A03, MF-A01).

NCEER-87-0024 "Vertical and Torsional Impedances for Radially Inhomogeneous Viscoelastic Soil Layers," by K.W. Dotson and A.S. Veletsos, 12/87, (PB88-187786, A03, MF-A01).

NCEER-87-0025 "Proceedings from the Symposium on Seismic Hazards, Ground Motions, Soil-Liquefaction and Engineering Practice in Eastern North America," October 20-22, 1987, edited by K.H. Jacob, 12/87, (PB88-188115, A23, MF-A01). This report is available only through NTIS (see address given above).

NCEER-87-0026 "Report on the Whittier-Narrows, California, Earthquake of October 1, 1987," by J. Pantelic and A. Reinhorn, 11/87, (PB88-187752, A03, MF-A01). This report is available only through NTIS (see address given above).

NCEER-87-0027 "Design of a Modular Program for Transient Nonlinear Analysis of Large 3-D Building Structures," by S. Srivastav and J.F. Abel, 12/30/87, (PB88-187950, A05, MF-A01). This report is only available through NTIS (see address given above).

NCEER-87-0028 "Second-Year Program in Research, Education and Technology Transfer," 3/8/88, (PB88-219480, A04, MF-A01).

NCEER-88-0001 "Workshop on Seismic Computer Analysis and Design of Buildings With Interactive Graphics," by W. McGuire, J.F. Abel and C.H. Conley, 1/18/88, (PB88-187760, A03, MF-A01). This report is only available through NTIS (see address given above).

NCEER-88-0002 "Optimal Control of Nonlinear Flexible Structures," by J.N. Yang, F.X. Long and D. Wong, 1/22/88, (PB88-213772, A06, MF-A01).

NCEER-88-0003 "Substructuring Techniques in the Time Domain for Primary-Secondary Structural Systems," by G.D. Manolis and G. Juhn, 2/10/88, (PB88-213780, A04, MF-A01).

NCEER-88-0004 "Iterative Seismic Analysis of Primary-Secondary Systems," by A. Singhal, L.D. Lutes and P.D. Spanos, 2/23/88, (PB88-213798, A04, MF-A01).

NCEER-88-0005 "Stochastic Finite Element Expansion for Random Media," by P.D. Spanos and R. Ghanem, 3/14/88, (PB88-213806, A03, MF-A01).

NCEER-88-0006 "Combining Structural Optimization and Structural Control," by F.Y. Cheng and C.P. Pantelides, 1/10/88, (PB88-213814, A05, MF-A01).

NCEER-88-0007 "Seismic Performance Assessment of Code-Designed Structures," by H.H-M. Hwang, J-W. Jaw and H-J. Shau, 3/20/88, (PB88-219423, A04, MF-A01). This report is only available through NTIS (see address given above).

NCEER-88-0008 "Reliability Analysis of Code-Designed Structures Under Natural Hazards," by H.H-M. Hwang, H. Ushiba and M. Shinozuka, 2/29/88, (PB88-229471, A07, MF-A01). This report is only available through NTIS (see address given above).

NCEER-88-0009 "Seismic Fragility Analysis of Shear Wall Structures," by J-W Jaw and H.H-M. Hwang, 4/30/88, (PB89-102867, A04, MF-A01).

NCEER-88-0010 "Base Isolation of a Multi-Story Building Under a Harmonic Ground Motion - A Comparison of Performances of Various Systems," by F-G Fan, G. Ahmadi and I.G. Tadjbakhsh, 5/18/88, (PB89-122238, A06, MF-A01). This report is only available through NTIS (see address given above).

NCEER-88-0011 "Seismic Floor Response Spectra for a Combined System by Green's Functions," by F.M. Lavelle, L.A. Bergman and P.D. Spanos, 5/1/88, (PB89-102875, A03, MF-A01).

NCEER-88-0012 "A New Solution Technique for Randomly Excited Hysteretic Structures," by G.Q. Cai and Y.K. Lin, 5/16/88, (PB89-102883, A03, MF-A01).

NCEER-88-0013 "A Study of Radiation Damping and Soil-Structure Interaction Effects in the Centrifuge," by K. Weissman, supervised by J.H. Prevost, 5/24/88, (PB89-144703, A06, MF-A01).

NCEER-88-0014 "Parameter Identification and Implementation of a Kinematic Plasticity Model for Frictional Soils," by J.H. Prevost and D.V. Griffiths, to be published.

NCEER-88-0015 "Two- and Three- Dimensional Dynamic Finite Element Analyses of the Long Valley Dam," by D.V. Griffiths and J.H. Prevost, 6/17/88, (PB89-144711, A04, MF-A01).

NCEER-88-0016 "Damage Assessment of Reinforced Concrete Structures in Eastern United States," by A.M. Reinhorn, M.J. Seidel, S.K. Kunnath and Y.J. Park, 6/15/88, (PB89-122220, A04, MF-A01). This report is only available through NTIS (see address given above).

NCEER-88-0017 "Dynamic Compliance of Vertically Loaded Strip Foundations in Multilayered Viscoelastic Soils," by S. Ahmad and A.S.M. Israil, 6/17/88, (PB89-102891, A04, MF-A01).

NCEER-88-0018 "An Experimental Study of Seismic Structural Response With Added Viscoelastic Dampers," by R.C. Lin, Z. Liang, T.T. Soong and R.H. Zhang, 6/30/88, (PB89-122212, A05, MF-A01). This report is available only through NTIS (see address given above).

NCEER-88-0019 "Experimental Investigation of Primary - Secondary System Interaction," by G.D. Manolis, G. Juhn and A.M. Reinhorn, 5/27/88, (PB89-122204, A04, MF-A01).

NCEER-88-0020 "A Response Spectrum Approach For Analysis of Nonclassically Damped Structures," by J.N. Yang, S. Sarkani and F.X. Long, 4/22/88, (PB89-102909, A04, MF-A01).

NCEER-88-0021 "Seismic Interaction of Structures and Soils: Stochastic Approach," by A.S. Veletsos and A.M. Prasad, 7/21/88, (PB89-122196, A04, MF-A01). This report is only available through NTIS (see address given above).

NCEER-88-0022 "Identification of the Serviceability Limit State and Detection of Seismic Structural Damage," by E. DiPasquale and A.S. Cakmak, 6/15/88, (PB89-122188, A05, MF-A01). This report is available only through NTIS (see address given above).

NCEER-88-0023 "Multi-Hazard Risk Analysis: Case of a Simple Offshore Structure," by B.K. Bhartia and E.H. Vanmarcke, 7/21/88, (PB89-145213, A05, MF-A01).

NCEER-88-0024 "Automated Seismic Design of Reinforced Concrete Buildings," by Y.S. Chung, C. Meyer and M. Shinozuka, 7/5/88, (PB89-122170, A06, MF-A01). This report is available only through NTIS (see address given above).

NCEER-88-0025 "Experimental Study of Active Control of MDOF Structures Under Seismic Excitations," by L.L. Chung, R.C. Lin, T.T. Soong and A.M. Reinhorn, 7/10/88, (PB89-122600, A04, MF-A01).

NCEER-88-0026 "Earthquake Simulation Tests of a Low-Rise Metal Structure," by J.S. Hwang, K.C. Chang, G.C. Lee and R.L. Ketter, 8/1/88, (PB89-102917, A04, MF-A01).

NCEER-88-0027 "Systems Study of Urban Response and Reconstruction Due to Catastrophic Earthquakes," by F. Kozin and H.K. Zhou, 9/22/88, (PB90-162348, A04, MF-A01).

NCEER-88-0028 "Seismic Fragility Analysis of Plane Frame Structures," by H.H-M. Hwang and Y.K. Low, 7/31/88, (PB89-131445, A06, MF-A01).

NCEER-88-0029 "Response Analysis of Stochastic Structures," by A. Kardara, C. Bucher and M. Shinozuka, 9/22/88, (PB89-174429, A04, MF-A01).

NCEER-88-0030 "Nonnormal Accelerations Due to Yielding in a Primary Structure," by D.C.K. Chen and L.D. Lutes, 9/19/88, (PB89-131437, A04, MF-A01).

NCEER-88-0031 "Design Approaches for Soil-Structure Interaction," by A.S. Veletsos, A.M. Prasad and Y. Tang, 12/30/88, (PB89-174437, A03, MF-A01). This report is available only through NTIS (see address given above).

NCEER-88-0032 "A Re-evaluation of Design Spectra for Seismic Damage Control," by C.J. Turkstra and A.G. Tallin, 11/7/88, (PB89-145221, A05, MF-A01).

NCEER-88-0033 "The Behavior and Design of Noncontact Lap Splices Subjected to Repeated Inelastic Tensile Loading," by V.E. Sagan, P. Gergely and R.N. White, 12/8/88, (PB89-163737, A08, MF-A01).

NCEER-88-0034 "Seismic Response of Pile Foundations," by S.M. Mamoon, P.K. Banerjee and S. Ahmad, 11/1/88, (PB89-145239, A04, MF-A01).

NCEER-88-0035 "Modeling of R/C Building Structures With Flexible Floor Diaphragms (IDARC2)," by A.M. Reinhorn, S.K. Kunnath and N. Panahshahi, 9/7/88, (PB89-207153, A07, MF-A01).

NCEER-88-0036 "Solution of the Dam-Reservoir Interaction Problem Using a Combination of FEM, BEM with Particular Integrals, Modal Analysis, and Substructuring," by C-S. Tsai, G.C. Lee and R.L. Ketter, 12/31/88, (PB89-207146, A04, MF-A01).

NCEER-88-0037 "Optimal Placement of Actuators for Structural Control," by F.Y. Cheng and C.P. Pantelides, 8/15/88, (PB89-162846, A05, MF-A01).

NCEER-88-0038 "Teflon Bearings in Aseismic Base Isolation: Experimental Studies and Mathematical Modeling," by A. Mokha, M.C. Constantinou and A.M. Reinhorn, 12/5/88, (PB89-218457, A10, MF-A01). This report is available only through NTIS (see address given above).

NCEER-88-0039 "Seismic Behavior of Flat Slab High-Rise Buildings in the New York City Area," by P. Weidlinger and M. Ettouney, 10/15/88, (PB90-145681, A04, MF-A01).

NCEER-88-0040 "Evaluation of the Earthquake Resistance of Existing Buildings in New York City," by P. Weidlinger and M. Ettouney, 10/15/88, to be published.

NCEER-88-0041 "Small-Scale Modeling Techniques for Reinforced Concrete Structures Subjected to Seismic Loads," by W. Kim, A. El-Attar and R.N. White, 11/22/88, (PB89-189625, A05, MF-A01).

NCEER-88-0042 "Modeling Strong Ground Motion from Multiple Event Earthquakes," by G.W. Ellis and A.S. Cakmak, 10/15/88, (PB89-174445, A03, MF-A01).

NCEER-88-0043 "Nonstationary Models of Seismic Ground Acceleration," by M. Grigoriu, S.E. Ruiz and E. Rosenblueth, 7/15/88, (PB89-189617, A04, MF-A01).

NCEER-88-0044 "SARCF User's Guide: Seismic Analysis of Reinforced Concrete Frames," by Y.S. Chung, C. Meyer and M. Shinozuka, 11/9/88, (PB89-174452, A08, MF-A01).

NCEER-88-0045 "First Expert Panel Meeting on Disaster Research and Planning," edited by J. Pantelic and J. Stoyle, 9/15/88, (PB89-174460, A05, MF-A01).

NCEER-88-0046 "Preliminary Studies of the Effect of Degrading Infill Walls on the Nonlinear Seismic Response of Steel Frames," by C.Z. Chrysostomou, P. Gergely and J.F. Abel, 12/19/88, (PB89-208383, A05, MF-A01).

NCEER-88-0047 "Reinforced Concrete Frame Component Testing Facility - Design, Construction, Instrumentation and Operation," by S.P. Pessiki, C. Conley, T. Bond, P. Gergely and R.N. White, 12/16/88, (PB89-174478, A04, MF-A01).

NCEER-89-0001 "Effects of Protective Cushion and Soil Compliancy on the Response of Equipment Within a Seismically Excited Building," by J.A. HoLung, 2/16/89, (PB89-207179, A04, MF-A01).

NCEER-89-0002 "Statistical Evaluation of Response Modification Factors for Reinforced Concrete Structures," by H.H-M. Hwang and J-W. Jaw, 2/17/89, (PB89-207187, A05, MF-A01).

NCEER-89-0003 "Hysteretic Columns Under Random Excitation," by G-Q. Cai and Y.K. Lin, 1/9/89, (PB89-196513, A03, MF-A01).

NCEER-89-0004 "Experimental Study of `Elephant Foot Bulge' Instability of Thin-Walled Metal Tanks," by Z-H. Jia and R.L. Ketter, 2/22/89, (PB89-207195, A03, MF-A01).

NCEER-89-0005 "Experiment on Performance of Buried Pipelines Across San Andreas Fault," by J. Isenberg, E. Richardson and T.D. O'Rourke, 3/10/89, (PB89-218440, A04, MF-A01). This report is available only through NTIS (see address given above).

NCEER-89-0006 "A Knowledge-Based Approach to Structural Design of Earthquake-Resistant Buildings," by M. Subramani, P. Gergely, C.H. Conley, J.F. Abel and A.H. Zaghw, 1/15/89, (PB89-218465, A06, MF-A01).

NCEER-89-0007 "Liquefaction Hazards and Their Effects on Buried Pipelines," by T.D. O'Rourke and P.A. Lane, 2/1/89, (PB89-218481, A09, MF-A01).

NCEER-89-0008 "Fundamentals of System Identification in Structural Dynamics," by H. Imai, C-B. Yun, O. Maruyama and M. Shinozuka, 1/26/89, (PB89-207211, A04, MF-A01).

NCEER-89-0009 "Effects of the 1985 Michoacan Earthquake on Water Systems and Other Buried Lifelines in Mexico," by A.G. Ayala and M.J. O'Rourke, 3/8/89, (PB89-207229, A06, MF-A01).

NCEER-89-R010 "NCEER Bibliography of Earthquake Education Materials," by K.E.K. Ross, Second Revision, 9/1/89, (PB90-125352, A05, MF-A01). This report is replaced by NCEER-92-0018.

NCEER-89-0011 "Inelastic Three-Dimensional Response Analysis of Reinforced Concrete Building Structures (IDARC-3D), Part I - Modeling," by S.K. Kunnath and A.M. Reinhorn, 4/17/89, (PB90-114612, A07, MF-A01). This report is available only through NTIS (see address given above).

NCEER-89-0012 "Recommended Modifications to ATC-14," by C.D. Poland and J.O. Malley, 4/12/89, (PB90-108648, A15, MF-A01).

NCEER-89-0013 "Repair and Strengthening of Beam-to-Column Connections Subjected to Earthquake Loading," by M. Corazao and A.J. Durrani, 2/28/89, (PB90-109885, A06, MF-A01).

NCEER-89-0014 "Program EXKAL2 for Identification of Structural Dynamic Systems," by O. Maruyama, C-B. Yun, M. Hoshiya and M. Shinozuka, 5/19/89, (PB90-109877, A09, MF-A01).

NCEER-89-0015 "Response of Frames With Bolted Semi-Rigid Connections, Part I - Experimental Study and Analytical Predictions," by P.J. DiCorso, A.M. Reinhorn, J.R. Dickerson, J.B. Radziminski and W.L. Harper, 6/1/89, to be published.

NCEER-89-0016 "ARMA Monte Carlo Simulation in Probabilistic Structural Analysis," by P.D. Spanos and M.P. Mignolet, 7/10/89, (PB90-109893, A03, MF-A01).

NCEER-89-P017 "Preliminary Proceedings from the Conference on Disaster Preparedness - The Place of Earthquake Education in Our Schools," Edited by K.E.K. Ross, 6/23/89, (PB90-108606, A03, MF-A01).

NCEER-89-0017 "Proceedings from the Conference on Disaster Preparedness - The Place of Earthquake Education in Our Schools," Edited by K.E.K. Ross, 12/31/89, (PB90-207895, A012, MF-A02). This report is available only through NTIS (see address given above).

NCEER-89-0018 "Multidimensional Models of Hysteretic Material Behavior for Vibration Analysis of Shape Memory Energy Absorbing Devices, by E.J. Graesser and F.A. Cozzarelli, 6/7/89, (PB90-164146, A04, MF-A01).

NCEER-89-0019 "Nonlinear Dynamic Analysis of Three-Dimensional Base Isolated Structures (3D-BASIS)," by S. Nagarajaiah, A.M. Reinhorn and M.C. Constantinou, 8/3/89, (PB90-161936, A06, MF-A01). This report has been replaced by NCEER-93-0011.

NCEER-89-0020 "Structural Control Considering Time-Rate of Control Forces and Control Rate Constraints," by F.Y. Cheng and C.P. Pantelides, 8/3/89, (PB90-120445, A04, MF-A01).

NCEER-89-0021 "Subsurface Conditions of Memphis and Shelby County," by K.W. Ng, T-S. Chang and H-H.M. Hwang, 7/26/89, (PB90-120437, A03, MF-A01).

NCEER-89-0022 "Seismic Wave Propagation Effects on Straight Jointed Buried Pipelines," by K. Elhmadi and M.J. O'Rourke, 8/24/89, (PB90-162322, A10, MF-A02).

NCEER-89-0023 "Workshop on Serviceability Analysis of Water Delivery Systems," edited by M. Grigoriu, 3/6/89, (PB90-127424, A03, MF-A01).

NCEER-89-0024 "Shaking Table Study of a 1/5 Scale Steel Frame Composed of Tapered Members," by K.C. Chang, J.S. Hwang and G.C. Lee, 9/18/89, (PB90-160169, A04, MF-A01).

NCEER-89-0025 "DYNA1D: A Computer Program for Nonlinear Seismic Site Response Analysis - Technical Documentation," by Jean H. Prevost, 9/14/89, (PB90-161944, A07, MF-A01). This report is available only through NTIS (see address given above).

NCEER-89-0026 "1:4 Scale Model Studies of Active Tendon Systems and Active Mass Dampers for Aseismic Protection," by A.M. Reinhorn, T.T. Soong, R.C. Lin, Y.P. Yang, Y. Fukao, H. Abe and M. Nakai, 9/15/89, (PB90-173246, A10, MF-A02). This report is available only through NTIS (see address given above).

NCEER-89-0027 "Scattering of Waves by Inclusions in a Nonhomogeneous Elastic Half Space Solved by Boundary Element Methods," by P.K. Hadley, A. Askar and A.S. Cakmak, 6/15/89, (PB90-145699, A07, MF-A01).

NCEER-89-0028 "Statistical Evaluation of Deflection Amplification Factors for Reinforced Concrete Structures," by H.H.M. Hwang, J-W. Jaw and A.L. Ch'ng, 8/31/89, (PB90-164633, A05, MF-A01).

NCEER-89-0029 "Bedrock Accelerations in Memphis Area Due to Large New Madrid Earthquakes," by H.H.M. Hwang, C.H.S. Chen and G. Yu, 11/7/89, (PB90-162330, A04, MF-A01).

NCEER-89-0030 "Seismic Behavior and Response Sensitivity of Secondary Structural Systems," by Y.Q. Chen and T.T. Soong, 10/23/89, (PB90-164658, A08, MF-A01).

NCEER-89-0031 "Random Vibration and Reliability Analysis of Primary-Secondary Structural Systems," by Y. Ibrahim, M. Grigoriu and T.T. Soong, 11/10/89, (PB90-161951, A04, MF-A01).

NCEER-89-0032 "Proceedings from the Second U.S. - Japan Workshop on Liquefaction, Large Ground Deformation and Their Effects on Lifelines, September 26-29, 1989," Edited by T.D. O'Rourke and M. Hamada, 12/1/89, (PB90-209388, A22, MF-A03).

NCEER-89-0033 "Deterministic Model for Seismic Damage Evaluation of Reinforced Concrete Structures," by J.M. Bracci, A.M. Reinhorn, J.B. Mander and S.K. Kunnath, 9/27/89, (PB91-108803, A06, MF-A01).

NCEER-89-0034 "On the Relation Between Local and Global Damage Indices," by E. DiPasquale and A.S. Cakmak, 8/15/89, (PB90-173865, A05, MF-A01).

NCEER-89-0035 "Cyclic Undrained Behavior of Nonplastic and Low Plasticity Silts," by A.J. Walker and H.E. Stewart, 7/26/89, (PB90-183518, A10, MF-A01).

NCEER-89-0036 "Liquefaction Potential of Surficial Deposits in the City of Buffalo, New York," by M. Budhu, R. Giese and L. Baumgrass, 1/17/89, (PB90-208455, A04, MF-A01).

NCEER-89-0037 "A Deterministic Assessment of Effects of Ground Motion Incoherence," by A.S. Veletsos and Y. Tang, 7/15/89, (PB90-164294, A03, MF-A01).

NCEER-89-0038 "Workshop on Ground Motion Parameters for Seismic Hazard Mapping," July 17-18, 1989, edited by R.V. Whitman, 12/1/89, (PB90-173923, A04, MF-A01).

NCEER-89-0039 "Seismic Effects on Elevated Transit Lines of the New York City Transit Authority," by C.J. Costantino, C.A. Miller and E. Heymsfield, 12/26/89, (PB90-207887, A06, MF-A01).

NCEER-89-0040 "Centrifugal Modeling of Dynamic Soil-Structure Interaction," by K. Weissman, Supervised by J.H. Prevost, 5/10/89, (PB90-207879, A07, MF-A01).

NCEER-89-0041 "Linearized Identification of Buildings With Cores for Seismic Vulnerability Assessment," by I-K. Ho and A.E. Aktan, 11/1/89, (PB90-251943, A07, MF-A01).

NCEER-90-0001 "Geotechnical and Lifeline Aspects of the October 17, 1989 Loma Prieta Earthquake in San Francisco," by T.D. O'Rourke, H.E. Stewart, F.T. Blackburn and T.S. Dickerman, 1/90, (PB90-208596, A05, MF-A01).

NCEER-90-0002 "Nonnormal Secondary Response Due to Yielding in a Primary Structure," by D.C.K. Chen and L.D. Lutes, 2/28/90, (PB90-251976, A07, MF-A01).

NCEER-90-0003 "Earthquake Education Materials for Grades K-12," by K.E.K. Ross, 4/16/90, (PB91-251984, A05, MF-A05). This report has been replaced by NCEER-92-0018.

NCEER-90-0004 "Catalog of Strong Motion Stations in Eastern North America," by R.W. Busby, 4/3/90, (PB90-251984, A05, MF-A01).

NCEER-90-0005 "NCEER Strong-Motion Data Base: A User Manual for the GeoBase Release (Version 1.0 for the Sun3)," by P. Friberg and K. Jacob, 3/31/90 (PB90-258062, A04, MF-A01).

NCEER-90-0006 "Seismic Hazard Along a Crude Oil Pipeline in the Event of an 1811-1812 Type New Madrid Earthquake," by H.H.M. Hwang and C-H.S. Chen, 4/16/90, (PB90-258054, A04, MF-A01).

NCEER-90-0007 "Site-Specific Response Spectra for Memphis Sheahan Pumping Station," by H.H.M. Hwang and C.S. Lee, 5/15/90, (PB91-108811, A05, MF-A01).

NCEER-90-0008 "Pilot Study on Seismic Vulnerability of Crude Oil Transmission Systems," by T. Ariman, R. Dobry, M. Grigoriu, F. Kozin, M. O'Rourke, T. O'Rourke and M. Shinozuka, 5/25/90, (PB91-108837, A06, MF-A01).

NCEER-90-0009 "A Program to Generate Site Dependent Time Histories: EQGEN," by G.W. Ellis, M. Srinivasan and A.S. Cakmak, 1/30/90, (PB91-108829, A04, MF-A01).

NCEER-90-0010 "Active Isolation for Seismic Protection of Operating Rooms," by M.E. Talbott, Supervised by M. Shinozuka, 6/8/9, (PB91-110205, A05, MF-A01).

NCEER-90-0011 "Program LINEARID for Identification of Linear Structural Dynamic Systems," by C-B. Yun and M. Shinozuka, 6/25/90, (PB91-110312, A08, MF-A01).

NCEER-90-0012 "Two-Dimensional Two-Phase Elasto-Plastic Seismic Response of Earth Dams," by A.N. Yiagos, Supervised by J.H. Prevost, 6/20/90, (PB91-110197, A13, MF-A02).

NCEER-90-0013 "Secondary Systems in Base-Isolated Structures: Experimental Investigation, Stochastic Response and Stochastic Sensitivity," by G.D. Manolis, G. Juhn, M.C. Constantinou and A.M. Reinhorn, 7/1/90, (PB91-110320, A08, MF-A01).

NCEER-90-0014 "Seismic Behavior of Lightly-Reinforced Concrete Column and Beam-Column Joint Details," by S.P. Pessiki, C.H. Conley, P. Gergely and R.N. White, 8/22/90, (PB91-108795, A11, MF-A02).

NCEER-90-0015 "Two Hybrid Control Systems for Building Structures Under Strong Earthquakes," by J.N. Yang and A. Danielians, 6/29/90, (PB91-125393, A04, MF-A01).

NCEER-90-0016 "Instantaneous Optimal Control with Acceleration and Velocity Feedback," by J.N. Yang and Z. Li, 6/29/90, (PB91-125401, A03, MF-A01).

NCEER-90-0017 "Reconnaissance Report on the Northern Iran Earthquake of June 21, 1990," by M. Mehrain, 10/4/90, (PB91-125377, A03, MF-A01).

NCEER-90-0018 "Evaluation of Liquefaction Potential in Memphis and Shelby County," by T.S. Chang, P.S. Tang, C.S. Lee and H. Hwang, 8/10/90, (PB91-125427, A09, MF-A01).

NCEER-90-0019 "Experimental and Analytical Study of a Combined Sliding Disc Bearing and Helical Steel Spring Isolation System," by M.C. Constantinou, A.S. Mokha and A.M. Reinhorn, 10/4/90, (PB91-125385, A06, MF-A01). This report is available only through NTIS (see address given above).

NCEER-90-0020 "Experimental Study and Analytical Prediction of Earthquake Response of a Sliding Isolation System with a Spherical Surface," by A.S. Mokha, M.C. Constantinou and A.M. Reinhorn, 10/11/90, (PB91-125419, A05, MF-A01).

NCEER-90-0021 "Dynamic Interaction Factors for Floating Pile Groups," by G. Gazetas, K. Fan, A. Kaynia and E. Kausel, 9/10/90, (PB91-170381, A05, MF-A01).

NCEER-90-0022 "Evaluation of Seismic Damage Indices for Reinforced Concrete Structures," by S. Rodriguez-Gomez and A.S. Cakmak, 9/30/90, PB91-171322, A06, MF-A01).

NCEER-90-0023 "Study of Site Response at a Selected Memphis Site," by H. Desai, S. Ahmad, E.S. Gazetas and M.R. Oh, 10/11/90, (PB91-196857, A03, MF-A01).

NCEER-90-0024 "A User's Guide to Strongmo: Version 1.0 of NCEER's Strong-Motion Data Access Tool for PCs and Terminals," by P.A. Friberg and C.A.T. Susch, 11/15/90, (PB91-171272, A03, MF-A01).

NCEER-90-0025 "A Three-Dimensional Analytical Study of Spatial Variability of Seismic Ground Motions," by L-L. Hong and A.H.-S. Ang, 10/30/90, (PB91-170399, A09, MF-A01).

NCEER-90-0026 "MUMOID User's Guide - A Program for the Identification of Modal Parameters," by S. Rodriguez-Gomez and E. DiPasquale, 9/30/90, (PB91-171298, A04, MF-A01).

NCEER-90-0027 "SARCF-II User's Guide - Seismic Analysis of Reinforced Concrete Frames," by S. Rodriguez-Gomez, Y.S. Chung and C. Meyer, 9/30/90, (PB91-171280, A05, MF-A01).

NCEER-90-0028 "Viscous Dampers: Testing, Modeling and Application in Vibration and Seismic Isolation," by N. Makris and M.C. Constantinou, 12/20/90 (PB91-190561, A06, MF-A01).

NCEER-90-0029 "Soil Effects on Earthquake Ground Motions in the Memphis Area," by H. Hwang, C.S. Lee, K.W. Ng and T.S. Chang, 8/2/90, (PB91-190751, A05, MF-A01).

NCEER-91-0001 "Proceedings from the Third Japan-U.S. Workshop on Earthquake Resistant Design of Lifeline Facilities and Countermeasures for Soil Liquefaction, December 17-19, 1990," edited by T.D. O'Rourke and M. Hamada, 2/1/91, (PB91-179259, A99, MF-A04).

NCEER-91-0002 "Physical Space Solutions of Non-Proportionally Damped Systems," by M. Tong, Z. Liang and G.C. Lee, 1/15/91, (PB91-179242, A04, MF-A01).

NCEER-91-0003 "Seismic Response of Single Piles and Pile Groups," by K. Fan and G. Gazetas, 1/10/91, (PB92-174994, A04, MF-A01).

NCEER-91-0004 "Damping of Structures: Part 1 - Theory of Complex Damping," by Z. Liang and G. Lee, 10/10/91, (PB92-197235, A12, MF-A03).

NCEER-91-0005 "3D-BASIS - Nonlinear Dynamic Analysis of Three Dimensional Base Isolated Structures: Part II," by S. Nagarajaiah, A.M. Reinhorn and M.C. Constantinou, 2/28/91, (PB91-190553, A07, MF-A01). This report has been replaced by NCEER-93-0011.

NCEER-91-0006 "A Multidimensional Hysteretic Model for Plasticity Deforming Metals in Energy Absorbing Devices," by E.J. Graesser and F.A. Cozzarelli, 4/9/91, (PB92-108364, A04, MF-A01).

NCEER-91-0007 "A Framework for Customizable Knowledge-Based Expert Systems with an Application to a KBES for Evaluating the Seismic Resistance of Existing Buildings," by E.G. Ibarra-Anaya and S.J. Fenves, 4/9/91, (PB91-210930, A08, MF-A01).

NCEER-91-0008 "Nonlinear Analysis of Steel Frames with Semi-Rigid Connections Using the Capacity Spectrum Method," by G.G. Deierlein, S-H. Hsieh, Y-J. Shen and J.F. Abel, 7/2/91, (PB92-113828, A05, MF-A01).

NCEER-91-0009 "Earthquake Education Materials for Grades K-12," by K.E.K. Ross, 4/30/91, (PB91-212142, A06, MF-A01). This report has been replaced by NCEER-92-0018.

NCEER-91-0010 "Phase Wave Velocities and Displacement Phase Differences in a Harmonically Oscillating Pile," by N. Makris and G. Gazetas, 7/8/91, (PB92-108356, A04, MF-A01).

NCEER-91-0011 "Dynamic Characteristics of a Full-Size Five-Story Steel Structure and a 2/5 Scale Model," by K.C. Chang, G.C. Yao, G.C. Lee, D.S. Hao and Y.C. Yeh," 7/2/91, (PB93-116648, A06, MF-A02).

NCEER-91-0012 "Seismic Response of a 2/5 Scale Steel Structure with Added Viscoelastic Dampers," by K.C. Chang, T.T. Soong, S-T. Oh and M.L. Lai, 5/17/91, (PB92-110816, A05, MF-A01).

NCEER-91-0013 "Earthquake Response of Retaining Walls; Full-Scale Testing and Computational Modeling," by S. Alampalli and A-W.M. Elgamal, 6/20/91, to be published.

NCEER-91-0014 "3D-BASIS-M: Nonlinear Dynamic Analysis of Multiple Building Base Isolated Structures," by P.C. Tsopelas, S. Nagarajaiah, M.C. Constantinou and A.M. Reinhorn, 5/28/91, (PB92-113885, A09, MF-A02).

NCEER-91-0015 "Evaluation of SEAOC Design Requirements for Sliding Isolated Structures," by D. Theodossiou and M.C. Constantinou, 6/10/91, (PB92-114602, A11, MF-A03).

NCEER-91-0016 "Closed-Loop Modal Testing of a 27-Story Reinforced Concrete Flat Plate-Core Building," by H.R. Somaprasad, T. Toksoy, H. Yoshiyuki and A.E. Aktan, 7/15/91, (PB92-129980, A07, MF-A02).

NCEER-91-0017 "Shake Table Test of a 1/6 Scale Two-Story Lightly Reinforced Concrete Building," by A.G. El-Attar, R.N. White and P. Gergely, 2/28/91, (PB92-222447, A06, MF-A02).

NCEER-91-0018 "Shake Table Test of a 1/8 Scale Three-Story Lightly Reinforced Concrete Building," by A.G. El-Attar, R.N. White and P. Gergely, 2/28/91, (PB93-116630, A08, MF-A02).

NCEER-91-0019 "Transfer Functions for Rigid Rectangular Foundations," by A.S. Veletsos, A.M. Prasad and W.H. Wu, 7/31/91, to be published.

NCEER-91-0020 "Hybrid Control of Seismic-Excited Nonlinear and Inelastic Structural Systems," by J.N. Yang, Z. Li and A. Danielians, 8/1/91, (PB92-143171, A06, MF-A02).

NCEER-91-0021 "The NCEER-91 Earthquake Catalog: Improved Intensity-Based Magnitudes and Recurrence Relations for U.S. Earthquakes East of New Madrid," by L. Seeber and J.G. Armbruster, 8/28/91, (PB92-176742, A06, MF-A02).

NCEER-91-0022 "Proceedings from the Implementation of Earthquake Planning and Education in Schools: The Need for Change - The Roles of the Changemakers," by K.E.K. Ross and F. Winslow, 7/23/91, (PB92-129998, A12, MF-A03).

NCEER-91-0023 "A Study of Reliability-Based Criteria for Seismic Design of Reinforced Concrete Frame Buildings," by H.H.M. Hwang and H-M. Hsu, 8/10/91, (PB92-140235, A09, MF-A02).

NCEER-91-0024 "Experimental Verification of a Number of Structural System Identification Algorithms," by R.G. Ghanem, H. Gavin and M. Shinozuka, 9/18/91, (PB92-176577, A18, MF-A04).

NCEER-91-0025 "Probabilistic Evaluation of Liquefaction Potential," by H.H.M. Hwang and C.S. Lee," 11/25/91, (PB92-143429, A05, MF-A01).

NCEER-91-0026 "Instantaneous Optimal Control for Linear, Nonlinear and Hysteretic Structures - Stable Controllers," by J.N. Yang and Z. Li, 11/15/91, (PB92-163807, A04, MF-A01).

NCEER-91-0027 "Experimental and Theoretical Study of a Sliding Isolation System for Bridges," by M.C. Constantinou, A. Kartoum, A.M. Reinhorn and P. Bradford, 11/15/91, (PB92-176973, A10, MF-A03).

NCEER-92-0001 "Case Studies of Liquefaction and Lifeline Performance During Past Earthquakes, Volume 1: Japanese Case Studies," Edited by M. Hamada and T. O'Rourke, 2/17/92, (PB92-197243, A18, MF-A04).

NCEER-92-0002 "Case Studies of Liquefaction and Lifeline Performance During Past Earthquakes, Volume 2: United States Case Studies," Edited by T. O'Rourke and M. Hamada, 2/17/92, (PB92-197250, A20, MF-A04).

NCEER-92-0003 "Issues in Earthquake Education," Edited by K. Ross, 2/3/92, (PB92-222389, A07, MF-A02).

NCEER-92-0004 "Proceedings from the First U.S. - Japan Workshop on Earthquake Protective Systems for Bridges," Edited by I.G. Buckle, 2/4/92, (PB94-142239, A99, MF-A06).

NCEER-92-0005 "Seismic Ground Motion from a Haskell-Type Source in a Multiple-Layered Half-Space," A.P. Theoharis, G. Deodatis and M. Shinozuka, 1/2/92, to be published.

NCEER-92-0006 "Proceedings from the Site Effects Workshop," Edited by R. Whitman, 2/29/92, (PB92-197201, A04, MF-A01).

NCEER-92-0007 "Engineering Evaluation of Permanent Ground Deformations Due to Seismically-Induced Liquefaction," by M.H. Baziar, R. Dobry and A-W.M. Elgamal, 3/24/92, (PB92-222421, A13, MF-A03).

NCEER-92-0008 "A Procedure for the Seismic Evaluation of Buildings in the Central and Eastern United States," by C.D. Poland and J.O. Malley, 4/2/92, (PB92-222439, A20, MF-A04).

NCEER-92-0009 "Experimental and Analytical Study of a Hybrid Isolation System Using Friction Controllable Sliding Bearings," by M.Q. Feng, S. Fujii and M. Shinozuka, 5/15/92, (PB93-150282, A06, MF-A02).

NCEER-92-0010 "Seismic Resistance of Slab-Column Connections in Existing Non-Ductile Flat-Plate Buildings," by A.J. Durrani and Y. Du, 5/18/92, (PB93-116812, A06, MF-A02).

NCEER-92-0011 "The Hysteretic and Dynamic Behavior of Brick Masonry Walls Upgraded by Ferrocement Coatings Under Cyclic Loading and Strong Simulated Ground Motion," by H. Lee and S.P. Prawel, 5/11/92, to be published.

NCEER-92-0012 "Study of Wire Rope Systems for Seismic Protection of Equipment in Buildings," by G.F. Demetriades, M.C. Constantinou and A.M. Reinhorn, 5/20/92, (PB93-116655, A08, MF-A02).

NCEER-92-0013 "Shape Memory Structural Dampers: Material Properties, Design and Seismic Testing," by P.R. Witting and F.A. Cozzarelli, 5/26/92, (PB93-116663, A05, MF-A01).

NCEER-92-0014 "Longitudinal Permanent Ground Deformation Effects on Buried Continuous Pipelines," by M.J. O'Rourke, and C. Nordberg, 6/15/92, (PB93-116671, A08, MF-A02).

NCEER-92-0015 "A Simulation Method for Stationary Gaussian Random Functions Based on the Sampling Theorem," by M. Grigoriu and S. Balopoulou, 6/11/92, (PB93-127496, A05, MF-A01).

NCEER-92-0016 "Gravity-Load-Designed Reinforced Concrete Buildings: Seismic Evaluation of Existing Construction and Detailing Strategies for Improved Seismic Resistance," by G.W. Hoffmann, S.K. Kunnath, A.M. Reinhorn and J.B. Mander, 7/15/92, (PB94-142007, A08, MF-A02).

NCEER-92-0017 "Observations on Water System and Pipeline Performance in the Limón Area of Costa Rica Due to the April 22, 1991 Earthquake," by M. O'Rourke and D. Ballantyne, 6/30/92, (PB93-126811, A06, MF-A02).

NCEER-92-0018 "Fourth Edition of Earthquake Education Materials for Grades K-12," Edited by K.E.K. Ross, 8/10/92, (PB93-114023, A07, MF-A02).

NCEER-92-0019 "Proceedings from the Fourth Japan-U.S. Workshop on Earthquake Resistant Design of Lifeline Facilities and Countermeasures for Soil Liquefaction," Edited by M. Hamada and T.D. O'Rourke, 8/12/92, (PB93-163939, A99, MF-E11).

NCEER-92-0020 "Active Bracing System: A Full Scale Implementation of Active Control," by A.M. Reinhorn, T.T. Soong, R.C. Lin, M.A. Riley, Y.P. Wang, S. Aizawa and M. Higashino, 8/14/92, (PB93-127512, A06, MF-A02).

NCEER-92-0021 "Empirical Analysis of Horizontal Ground Displacement Generated by Liquefaction-Induced Lateral Spreads," by S.F. Bartlett and T.L. Youd, 8/17/92, (PB93-188241, A06, MF-A02).

NCEER-92-0022 "IDARC Version 3.0: Inelastic Damage Analysis of Reinforced Concrete Structures," by S.K. Kunnath, A.M. Reinhorn and R.F. Lobo, 8/31/92, (PB93-227502, A07, MF-A02).

NCEER-92-0023 "A Semi-Empirical Analysis of Strong-Motion Peaks in Terms of Seismic Source, Propagation Path and Local Site Conditions, by M. Kamiyama, M.J. O'Rourke and R. Flores-Berrones, 9/9/92, (PB93-150266, A08, MF-A02).

NCEER-92-0024 "Seismic Behavior of Reinforced Concrete Frame Structures with Nonductile Details, Part I: Summary of Experimental Findings of Full Scale Beam-Column Joint Tests," by A. Beres, R.N. White and P. Gergely, 9/30/92, (PB93-227783, A05, MF-A01).

NCEER-92-0025 "Experimental Results of Repaired and Retrofitted Beam-Column Joint Tests in Lightly Reinforced Concrete Frame Buildings," by A. Beres, S. El-Borgi, R.N. White and P. Gergely, 10/29/92, (PB93-227791, A05, MF-A01).

NCEER-92-0026 "A Generalization of Optimal Control Theory: Linear and Nonlinear Structures," by J.N. Yang, Z. Li and S. Vongchavalitkul, 11/2/92, (PB93-188621, A05, MF-A01).

NCEER-92-0027 "Seismic Resistance of Reinforced Concrete Frame Structures Designed Only for Gravity Loads: Part I - Design and Properties of a One-Third Scale Model Structure," by J.M. Bracci, A.M. Reinhorn and J.B. Mander, 12/1/92, (PB94-104502, A08, MF-A02).

NCEER-92-0028 "Seismic Resistance of Reinforced Concrete Frame Structures Designed Only for Gravity Loads: Part II - Experimental Performance of Subassemblages," by L.E. Aycardi, J.B. Mander and A.M. Reinhorn, 12/1/92, (PB94-104510, A08, MF-A02).

NCEER-92-0029 "Seismic Resistance of Reinforced Concrete Frame Structures Designed Only for Gravity Loads: Part III - Experimental Performance and Analytical Study of a Structural Model," by J.M. Bracci, A.M. Reinhorn and J.B. Mander, 12/1/92, (PB93-227528, A09, MF-A01).

NCEER-92-0030 "Evaluation of Seismic Retrofit of Reinforced Concrete Frame Structures: Part I - Experimental Performance of Retrofitted Subassemblages," by D. Choudhuri, J.B. Mander and A.M. Reinhorn, 12/8/92, (PB93-198307, A07, MF-A02).

NCEER-92-0031 "Evaluation of Seismic Retrofit of Reinforced Concrete Frame Structures: Part II - Experimental Performance and Analytical Study of a Retrofitted Structural Model," by J.M. Bracci, A.M. Reinhorn and J.B. Mander, 12/8/92, (PB93-198315, A09, MF-A03).

NCEER-92-0032 "Experimental and Analytical Investigation of Seismic Response of Structures with Supplemental Fluid Viscous Dampers," by M.C. Constantinou and M.D. Symans, 12/21/92, (PB93-191435, A10, MF-A03). This report is available only through NTIS (see address given above).

NCEER-92-0033 "Reconnaissance Report on the Cairo, Egypt Earthquake of October 12, 1992," by M. Khater, 12/23/92, (PB93-188621, A03, MF-A01).

NCEER-92-0034 "Low-Level Dynamic Characteristics of Four Tall Flat-Plate Buildings in New York City," by H. Gavin, S. Yuan, J. Grossman, E. Pekelis and K. Jacob, 12/28/92, (PB93-188217, A07, MF-A02).

NCEER-93-0001 "An Experimental Study on the Seismic Performance of Brick-Infilled Steel Frames With and Without Retrofit," by J.B. Mander, B. Nair, K. Wojtkowski and J. Ma, 1/29/93, (PB93-227510, A07, MF-A02).

NCEER-93-0002 "Social Accounting for Disaster Preparedness and Recovery Planning," by S. Cole, E. Pantoja and V. Razak, 2/22/93, (PB94-142114, A12, MF-A03).

NCEER-93-0003 "Assessment of 1991 NEHRP Provisions for Nonstructural Components and Recommended Revisions," by T.T. Soong, G. Chen, Z. Wu, R-H. Zhang and M. Grigoriu, 3/1/93, (PB93-188639, A06, MF-A02).

NCEER-93-0004 "Evaluation of Static and Response Spectrum Analysis Procedures of SEAOC/UBC for Seismic Isolated Structures," by C.W. Winters and M.C. Constantinou, 3/23/93, (PB93-198299, A10, MF-A03).

NCEER-93-0005 "Earthquakes in the Northeast - Are We Ignoring the Hazard? A Workshop on Earthquake Science and Safety for Educators," edited by K.E.K. Ross, 4/2/93, (PB94-103066, A09, MF-A02).

NCEER-93-0006 "Inelastic Response of Reinforced Concrete Structures with Viscoelastic Braces," by R.F. Lobo, J.M. Bracci, K.L. Shen, A.M. Reinhorn and T.T. Soong, 4/5/93, (PB93-227486, A05, MF-A02).

NCEER-93-0007 "Seismic Testing of Installation Methods for Computers and Data Processing Equipment," by K. Kosar, T.T. Soong, K.L. Shen, J.A. HoLung and Y.K. Lin, 4/12/93, (PB93-198299, A07, MF-A02).

NCEER-93-0008 "Retrofit of Reinforced Concrete Frames Using Added Dampers," by A. Reinhorn, M. Constantinou and C. Li, to be published.

NCEER-93-0009 "Seismic Behavior and Design Guidelines for Steel Frame Structures with Added Viscoelastic Dampers," by K.C. Chang, M.L. Lai, T.T. Soong, D.S. Hao and Y.C. Yeh, 5/1/93, (PB94-141959, A07, MF-A02).

NCEER-93-0010 "Seismic Performance of Shear-Critical Reinforced Concrete Bridge Piers," by J.B. Mander, S.M. Waheed, M.T.A. Chaudhary and S.S. Chen, 5/12/93, (PB93-227494, A08, MF-A02).

NCEER-93-0011 "3D-BASIS-TABS: Computer Program for Nonlinear Dynamic Analysis of Three Dimensional Base Isolated Structures," by S. Nagarajaiah, C. Li, A.M. Reinhorn and M.C. Constantinou, 8/2/93, (PB94-141819, A09, MF-A02).

NCEER-93-0012 "Effects of Hydrocarbon Spills from an Oil Pipeline Break on Ground Water," by O.J. Helweg and H.H.M. Hwang, 8/3/93, (PB94-141942, A06, MF-A02).

NCEER-93-0013 "Simplified Procedures for Seismic Design of Nonstructural Components and Assessment of Current Code Provisions," by M.P. Singh, L.E. Suarez, E.E. Matheu and G.O. Maldonado, 8/4/93, (PB94-141827, A09, MF-A02).

NCEER-93-0014 "An Energy Approach to Seismic Analysis and Design of Secondary Systems," by G. Chen and T.T. Soong, 8/6/93, (PB94-142767, A11, MF-A03).

NCEER-93-0015 "Proceedings from School Sites: Becoming Prepared for Earthquakes - Commemorating the Third Anniversary of the Loma Prieta Earthquake," Edited by F.E. Winslow and K.E.K. Ross, 8/16/93, (PB94-154275, A16, MF-A02).

NCEER-93-0016 "Reconnaissance Report of Damage to Historic Monuments in Cairo, Egypt Following the October 12, 1992 Dahshur Earthquake," by D. Sykora, D. Look, G. Croci, E. Karaesmen and E. Karaesmen, 8/19/93, (PB94-142221, A08, MF-A02).

NCEER-93-0017 "The Island of Guam Earthquake of August 8, 1993," by S.W. Swan and S.K. Harris, 9/30/93, (PB94-141843, A04, MF-A01).

NCEER-93-0018 "Engineering Aspects of the October 12, 1992 Egyptian Earthquake," by A.W. Elgamal, M. Amer, K. Adalier and A. Abul-Fadl, 10/7/93, (PB94-141983, A05, MF-A01).

NCEER-93-0019 "Development of an Earthquake Motion Simulator and its Application in Dynamic Centrifuge Testing," by I. Krstelj, Supervised by J.H. Prevost, 10/23/93, (PB94-181773, A-10, MF-A03).

NCEER-93-0020 "NCEER-Taisei Corporation Research Program on Sliding Seismic Isolation Systems for Bridges: Experimental and Analytical Study of a Friction Pendulum System (FPS)," by M.C. Constantinou, P. Tsopelas, Y-S. Kim and S. Okamoto, 11/1/93, (PB94-142775, A08, MF-A02).

NCEER-93-0021 "Finite Element Modeling of Elastomeric Seismic Isolation Bearings," by L.J. Billings, Supervised by R. Shepherd, 11/8/93, to be published.

NCEER-93-0022 "Seismic Vulnerability of Equipment in Critical Facilities: Life-Safety and Operational Consequences," by K. Porter, G.S. Johnson, M.M. Zadeh, C. Scawthorn and S. Eder, 11/24/93, (PB94-181765, A16, MF-A03).

NCEER-93-0023 "Hokkaido Nansei-oki, Japan Earthquake of July 12, 1993, by P.I. Yanev and C.R. Scawthorn, 12/23/93, (PB94-181500, A07, MF-A01).

NCEER-94-0001 "An Evaluation of Seismic Serviceability of Water Supply Networks with Application to the San Francisco Auxiliary Water Supply System," by I. Markov, Supervised by M. Grigoriu and T. O'Rourke, 1/21/94, (PB94-204013, A07, MF-A02).

NCEER-94-0002 "NCEER-Taisei Corporation Research Program on Sliding Seismic Isolation Systems for Bridges: Experimental and Analytical Study of Systems Consisting of Sliding Bearings, Rubber Restoring Force Devices and Fluid Dampers," Volumes I and II, by P. Tsopelas, S. Okamoto, M.C. Constantinou, D. Ozaki and S. Fujii, 2/4/94, (PB94-181740, A09, MF-A02 and PB94-181757, A12, MF-A03).

NCEER-94-0003 "A Markov Model for Local and Global Damage Indices in Seismic Analysis," by S. Rahman and M. Grigoriu, 2/18/94, (PB94-206000, A12, MF-A03).

NCEER-94-0004 "Proceedings from the NCEER Workshop on Seismic Response of Masonry Infills," edited by D.P. Abrams, 3/1/94, (PB94-180783, A07, MF-A02).

NCEER-94-0005 "The Northridge, California Earthquake of January 17, 1994: General Reconnaissance Report," edited by J.D. Goltz, 3/11/94, (PB94-193943, A10, MF-A03).

NCEER-94-0006 "Seismic Energy Based Fatigue Damage Analysis of Bridge Columns: Part I - Evaluation of Seismic Capacity," by G.A. Chang and J.B. Mander, 3/14/94, (PB94-219185, A11, MF-A03).

NCEER-94-0007 "Seismic Isolation of Multi-Story Frame Structures Using Spherical Sliding Isolation Systems," by T.M. Al-Hussaini, V.A. Zayas and M.C. Constantinou, 3/17/94, (PB94-193745, A09, MF-A02).

NCEER-94-0008 "The Northridge, California Earthquake of January 17, 1994: Performance of Highway Bridges," edited by I.G. Buckle, 3/24/94, (PB94-193851, A06, MF-A02).

NCEER-94-0009 "Proceedings of the Third U.S.-Japan Workshop on Earthquake Protective Systems for Bridges," edited by I.G. Buckle and I. Friedland, 3/31/94, (PB94-195815, A99, MF-A06).

NCEER-94-0010 "3D-BASIS-ME: Computer Program for Nonlinear Dynamic Analysis of Seismically Isolated Single and Multiple Structures and Liquid Storage Tanks," by P.C. Tsopelas, M.C. Constantinou and A.M. Reinhorn, 4/12/94, (PB94-204922, A09, MF-A02).

NCEER-94-0011 "The Northridge, California Earthquake of January 17, 1994: Performance of Gas Transmission Pipelines," by T.D. O'Rourke and M.C. Palmer, 5/16/94, (PB94-204989, A05, MF-A01).

NCEER-94-0012 "Feasibility Study of Replacement Procedures and Earthquake Performance Related to Gas Transmission Pipelines," by T.D. O'Rourke and M.C. Palmer, 5/25/94, (PB94-206638, A09, MF-A02).

NCEER-94-0013 "Seismic Energy Based Fatigue Damage Analysis of Bridge Columns: Part II - Evaluation of Seismic Demand," by G.A. Chang and J.B. Mander, 6/1/94, (PB95-18106, A08, MF-A02).

NCEER-94-0014 "NCEER-Taisei Corporation Research Program on Sliding Seismic Isolation Systems for Bridges: Experimental and Analytical Study of a System Consisting of Sliding Bearings and Fluid Restoring Force/Damping Devices," by P. Tsopelas and M.C. Constantinou, 6/13/94, (PB94-219144, A10, MF-A03).

NCEER-94-0015 "Generation of Hazard-Consistent Fragility Curves for Seismic Loss Estimation Studies," by H. Hwang and J-R. Huo, 6/14/94, (PB95-181996, A09, MF-A02).

NCEER-94-0016 "Seismic Study of Building Frames with Added Energy-Absorbing Devices," by W.S. Pong, C.S. Tsai and G.C. Lee, 6/20/94, (PB94-219136, A10, A03).

NCEER-94-0017 "Sliding Mode Control for Seismic-Excited Linear and Nonlinear Civil Engineering Structures," by J. Yang, J. Wu, A. Agrawal and Z. Li, 6/21/94, (PB95-138483, A06, MF-A02).

NCEER-94-0018 "3D-BASIS-TABS Version 2.0: Computer Program for Nonlinear Dynamic Analysis of Three Dimensional Base Isolated Structures," by A.M. Reinhorn, S. Nagarajaiah, M.C. Constantinou, P. Tsopelas and R. Li, 6/22/94, (PB95-182176, A08, MF-A02).

NCEER-94-0019 "Proceedings of the International Workshop on Civil Infrastructure Systems: Application of Intelligent Systems and Advanced Materials on Bridge Systems," Edited by G.C. Lee and K.C. Chang, 7/18/94, (PB95-252474, A20, MF-A04).

NCEER-94-0020 "Study of Seismic Isolation Systems for Computer Floors," by V. Lambrou and M.C. Constantinou, 7/19/94, (PB95-138533, A10, MF-A03).

NCEER-94-0021 "Proceedings of the U.S.-Italian Workshop on Guidelines for Seismic Evaluation and Rehabilitation of Unreinforced Masonry Buildings," Edited by D.P. Abrams and G.M. Calvi, 7/20/94, (PB95-138749, A13, MF-A03).

NCEER-94-0022 "NCEER-Taisei Corporation Research Program on Sliding Seismic Isolation Systems for Bridges: Experimental and Analytical Study of a System Consisting of Lubricated PTFE Sliding Bearings and Mild Steel Dampers," by P. Tsopelas and M.C. Constantinou, 7/22/94, (PB95-182184, A08, MF-A02).

NCEER-94-0023 "Development of Reliability-Based Design Criteria for Buildings Under Seismic Load," by Y.K. Wen, H. Hwang and M. Shinozuka, 8/1/94, (PB95-211934, A08, MF-A02).

NCEER-94-0024 "Experimental Verification of Acceleration Feedback Control Strategies for an Active Tendon System," by S.J. Dyke, B.F. Spencer, Jr., P. Quast, M.K. Sain, D.C. Kaspari, Jr. and T.T. Soong, 8/29/94, (PB95-212320, A05, MF-A01).

NCEER-94-0025 "Seismic Retrofitting Manual for Highway Bridges," Edited by I.G. Buckle and I.F. Friedland, published by the Federal Highway Administration (PB95-212676, A15, MF-A03).

NCEER-94-0026 "Proceedings from the Fifth U.S.-Japan Workshop on Earthquake Resistant Design of Lifeline Facilities and Countermeasures Against Soil Liquefaction," Edited by T.D. O'Rourke and M. Hamada, 11/7/94, (PB95-220802, A99, MF-E08).

NCEER-95-0001 "Experimental and Analytical Investigation of Seismic Retrofit of Structures with Supplemental Damping: Part 1 - Fluid Viscous Damping Devices," by A.M. Reinhorn, C. Li and M.C. Constantinou, 1/3/95, (PB95-266599, A09, MF-A02).

NCEER-95-0002 "Experimental and Analytical Study of Low-Cycle Fatigue Behavior of Semi-Rigid Top-And-Seat Angle Connections," by G. Pekcan, J.B. Mander and S.S. Chen, 1/5/95, (PB95-220042, A07, MF-A02).

NCEER-95-0003 "NCEER-ATC Joint Study on Fragility of Buildings," by T. Anagnos, C. Rojahn and A.S. Kiremidjian, 1/20/95, (PB95-220026, A06, MF-A02).

NCEER-95-0004 "Nonlinear Control Algorithms for Peak Response Reduction," by Z. Wu, T.T. Soong, V. Gattulli and R.C. Lin, 2/16/95, (PB95-220349, A05, MF-A01).

NCEER-95-0005 "Pipeline Replacement Feasibility Study: A Methodology for Minimizing Seismic and Corrosion Risks to Underground Natural Gas Pipelines," by R.T. Eguchi, H.A. Seligson and D.G. Honegger, 3/2/95, (PB95-252326, A06, MF-A02).

NCEER-95-0006 "Evaluation of Seismic Performance of an 11-Story Frame Building During the 1994 Northridge Earthquake," by F. Naeim, R. DiSulio, K. Benuska, A. Reinhorn and C. Li, to be published.

NCEER-95-0007 "Prioritization of Bridges for Seismic Retrofitting," by N. Basöz and A.S. Kiremidjian, 4/24/95, (PB95-252300, A08, MF-A02).

NCEER-95-0008 "Method for Developing Motion Damage Relationships for Reinforced Concrete Frames," by A. Singhal and A.S. Kiremidjian, 5/11/95, (PB95-266607, A06, MF-A02).

NCEER-95-0009 "Experimental and Analytical Investigation of Seismic Retrofit of Structures with Supplemental Damping: Part II - Friction Devices," by C. Li and A.M. Reinhorn, 7/6/95, (PB96-128087, A11, MF-A03).

NCEER-95-0010 "Experimental Performance and Analytical Study of a Non-Ductile Reinforced Concrete Frame Structure Retrofitted with Elastomeric Spring Dampers," by G. Pekcan, J.B. Mander and S.S. Chen, 7/14/95, (PB96-137161, A08, MF-A02).

NCEER-95-0011 "Development and Experimental Study of Semi-Active Fluid Damping Devices for Seismic Protection of Structures," by M.D. Symans and M.C. Constantinou, 8/3/95, (PB96-136940, A23, MF-A04).

NCEER-95-0012 "Real-Time Structural Parameter Modification (RSPM): Development of Innervated Structures," by Z. Liang, M. Tong and G.C. Lee, 4/11/95, (PB96-137153, A06, MF-A01).

NCEER-95-0013 "Experimental and Analytical Investigation of Seismic Retrofit of Structures with Supplemental Damping: Part III - Viscous Damping Walls," by A.M. Reinhorn and C. Li, 10/1/95, (PB96-176409, A11, MF-A03).

NCEER-95-0014 "Seismic Fragility Analysis of Equipment and Structures in a Memphis Electric Substation," by J-R. Huo and H.H.M. Hwang, 8/10/95, (PB96-128087, A09, MF-A02).

NCEER-95-0015 "The Hanshin-Awaji Earthquake of January 17, 1995: Performance of Lifelines," Edited by M. Shinozuka, 11/3/95, (PB96-176383, A15, MF-A03).

NCEER-95-0016 "Highway Culvert Performance During Earthquakes," by T.L. Youd and C.J. Beckman, available as NCEER-96-0015.

NCEER-95-0017 "The Hanshin-Awaji Earthquake of January 17, 1995: Performance of Highway Bridges," Edited by I.G. Buckle, 12/1/95, to be published.

NCEER-95-0018 "Modeling of Masonry Infill Panels for Structural Analysis," by A.M. Reinhorn, A. Madan, R.E. Valles, Y. Reichmann and J.B. Mander, 12/8/95, (PB97-110886, MF-A01, A06).

NCEER-95-0019 "Optimal Polynomial Control for Linear and Nonlinear Structures," by A.K. Agrawal and J.N. Yang, 12/11/95, (PB96-168737, A07, MF-A02).

NCEER-95-0020 "Retrofit of Non-Ductile Reinforced Concrete Frames Using Friction Dampers," by R.S. Rao, P. Gergely and R.N. White, 12/22/95, (PB97-133508, A10, MF-A02).

NCEER-95-0021 "Parametric Results for Seismic Response of Pile-Supported Bridge Bents," by G. Mylonakis, A. Nikolaou and G. Gazetas, 12/22/95, (PB97-100242, A12, MF-A03).

NCEER-95-0022 "Kinematic Bending Moments in Seismically Stressed Piles," by A. Nikolaou, G. Mylonakis and G. Gazetas, 12/23/95, (PB97-113914, MF-A03, A13).

NCEER-96-0001 "Dynamic Response of Unreinforced Masonry Buildings with Flexible Diaphragms," by A.C. Costley and D.P. Abrams," 10/10/96, (PB97-133573, MF-A03, A15).

NCEER-96-0002 "State of the Art Review: Foundations and Retaining Structures," by I. Po Lam, to be published.

NCEER-96-0003 "Ductility of Rectangular Reinforced Concrete Bridge Columns with Moderate Confinement," by N. Wehbe, M. Saiidi, D. Sanders and B. Douglas, 11/7/96, (PB97-133557, A06, MF-A02).

NCEER-96-0004 "Proceedings of the Long-Span Bridge Seismic Research Workshop," edited by I.G. Buckle and I.M. Friedland, to be published.

NCEER-96-0005 "Establish Representative Pier Types for Comprehensive Study: Eastern United States," by J. Kulicki and Z. Prucz, 5/28/96, (PB98-119217, A07, MF-A02).

NCEER-96-0006 "Establish Representative Pier Types for Comprehensive Study: Western United States," by R. Imbsen, R.A. Schamber and T.A. Osterkamp, 5/28/96, (PB98-118607, A07, MF-A02).

NCEER-96-0007 "Nonlinear Control Techniques for Dynamical Systems with Uncertain Parameters," by R.G. Ghanem and M.I. Bujakov, 5/27/96, (PB97-100259, A17, MF-A03).

NCEER-96-0008 "Seismic Evaluation of a 30-Year Old Non-Ductile Highway Bridge Pier and Its Retrofit," by J.B. Mander, B. Mahmoodzadegan, S. Bhadra and S.S. Chen, 5/31/96, (PB97-110902, MF-A03, A10).

NCEER-96-0009 "Seismic Performance of a Model Reinforced Concrete Bridge Pier Before and After Retrofit," by J.B. Mander, J.H. Kim and C.A. Ligozio, 5/31/96, (PB97-110910, MF-A02, A10).

NCEER-96-0010 "IDARC2D Version 4.0: A Computer Program for the Inelastic Damage Analysis of Buildings," by R.E. Valles, A.M. Reinhorn, S.K. Kunnath, C. Li and A. Madan, 6/3/96, (PB97-100234, A17, MF-A03).

NCEER-96-0011 "Estimation of the Economic Impact of Multiple Lifeline Disruption: Memphis Light, Gas and Water Division Case Study," by S.E. Chang, H.A. Seligson and R.T. Eguchi, 8/16/96, (PB97-133490, A11, MF-A03).

NCEER-96-0012 "Proceedings from the Sixth Japan-U.S. Workshop on Earthquake Resistant Design of Lifeline Facilities and Countermeasures Against Soil Liquefaction, Edited by M. Hamada and T. O'Rourke, 9/11/96, (PB97-133581, A99, MF-A06).

NCEER-96-0013 "Chemical Hazards, Mitigation and Preparedness in Areas of High Seismic Risk: A Methodology for Estimating the Risk of Post-Earthquake Hazardous Materials Release," by H.A. Seligson, R.T. Eguchi, K.J. Tierney and K. Richmond, 11/7/96, (PB97-133565, MF-A02, A08).

NCEER-96-0014 "Response of Steel Bridge Bearings to Reversed Cyclic Loading," by J.B. Mander, D-K. Kim, S.S. Chen and G.J. Premus, 11/13/96, (PB97-140735, A12, MF-A03).

NCEER-96-0015 "Highway Culvert Performance During Past Earthquakes," by T.L. Youd and C.J. Beckman, 11/25/96, (PB97-133532, A06, MF-A01).

NCEER-97-0001 "Evaluation, Prevention and Mitigation of Pounding Effects in Building Structures," by R.E. Valles and A.M. Reinhorn, 2/20/97, (PB97-159552, A14, MF-A03).

NCEER-97-0002 "Seismic Design Criteria for Bridges and Other Highway Structures," by C. Rojahn, R. Mayes, D.G. Anderson, J. Clark, J.H. Hom, R.V. Nutt and M.J. O'Rourke, 4/30/97, (PB97-194658, A06, MF-A03).

NCEER-97-0003 "Proceedings of the U.S.-Italian Workshop on Seismic Evaluation and Retrofit," Edited by D.P. Abrams and G.M. Calvi, 3/19/97, (PB97-194666, A13, MF-A03).

NCEER-97-0004 "Investigation of Seismic Response of Buildings with Linear and Nonlinear Fluid Viscous Dampers," by A.A. Seleemah and M.C. Constantinou, 5/21/97, (PB98-109002, A15, MF-A03).

NCEER-97-0005 "Proceedings of the Workshop on Earthquake Engineering Frontiers in Transportation Facilities," edited by G.C. Lee and I.M. Friedland, 8/29/97, (PB98-128911, A25, MR-A04).

NCEER-97-0006 "Cumulative Seismic Damage of Reinforced Concrete Bridge Piers," by S.K. Kunnath, A. El-Bahy, A. Taylor and W. Stone, 9/2/97, (PB98-108814, A11, MF-A03).

NCEER-97-0007 "Structural Details to Accommodate Seismic Movements of Highway Bridges and Retaining Walls," by R.A. Imbsen, R.A. Schamber, E. Thorkildsen, A. Kartoum, B.T. Martin, T.N. Rosser and J.M. Kulicki, 9/3/97, (PB98-108996, A09, MF-A02).

NCEER-97-0008 "A Method for Earthquake Motion-Damage Relationships with Application to Reinforced Concrete Frames," by A. Singhal and A.S. Kiremidjian, 9/10/97, (PB98-108988, A13, MF-A03).

NCEER-97-0009 "Seismic Analysis and Design of Bridge Abutments Considering Sliding and Rotation," by K. Fishman and R. Richards, Jr., 9/15/97, (PB98-108897, A06, MF-A02).

NCEER-97-0010 "Proceedings of the FHWA/NCEER Workshop on the National Representation of Seismic Ground Motion for New and Existing Highway Facilities," edited by I.M. Friedland, M.S. Power and R.L. Mayes, 9/22/97, (PB98-128903, A21, MF-A04).

NCEER-97-0011 "Seismic Analysis for Design or Retrofit of Gravity Bridge Abutments," by K.L. Fishman, R. Richards, Jr. and R.C. Divito, 10/2/97, (PB98-128937, A08, MF-A02).

NCEER-97-0012 "Evaluation of Simplified Methods of Analysis for Yielding Structures," by P. Tsopelas, M.C. Constantinou, C.A. Kircher and A.S. Whittaker, 10/31/97, (PB98-128929, A10, MF-A03).

NCEER-97-0013 "Seismic Design of Bridge Columns Based on Control and Repairability of Damage," by C-T. Cheng and J.B. Mander, 12/8/97, (PB98-144249, A11, MF-A03).

NCEER-97-0014 "Seismic Resistance of Bridge Piers Based on Damage Avoidance Design," by J.B. Mander and C-T. Cheng, 12/10/97, (PB98-144223, A09, MF-A02).

NCEER-97-0015 "Seismic Response of Nominally Symmetric Systems with Strength Uncertainty," by S. Balopoulou and M. Grigoriu, 12/23/97, (PB98-153422, A11, MF-A03).

NCEER-97-0016 "Evaluation of Seismic Retrofit Methods for Reinforced Concrete Bridge Columns," by T.J. Wipf, F.W. Klaiber and F.M. Russo, 12/28/97, (PB98-144215, A12, MF-A03).

NCEER-97-0017 "Seismic Fragility of Existing Conventional Reinforced Concrete Highway Bridges," by C.L. Mullen and A.S. Cakmak, 12/30/97, (PB98-153406, A08, MF-A02).

NCEER-97-0018 "Loss Asssessment of Memphis Buildings," edited by D.P. Abrams and M. Shinozuka, 12/31/97, (PB98-144231, A13, MF-A03).

NCEER-97-0019 "Seismic Evaluation of Frames with Infill Walls Using Quasi-static Experiments," by K.M. Mosalam, R.N. White and P. Gergely, 12/31/97, (PB98-153455, A07, MF-A02).

NCEER-97-0020 "Seismic Evaluation of Frames with Infill Walls Using Pseudo-dynamic Experiments," by K.M. Mosalam, R.N. White and P. Gergely, 12/31/97, (PB98-153430, A07, MF-A02).

NCEER-97-0021 "Computational Strategies for Frames with Infill Walls: Discrete and Smeared Crack Analyses and Seismic Fragility," by K.M. Mosalam, R.N. White and P. Gergely, 12/31/97, (PB98-153414, A10, MF-A02).

NCEER-97-0022 "Proceedings of the NCEER Workshop on Evaluation of Liquefaction Resistance of Soils," edited by T.L. Youd and I.M. Idriss, 12/31/97, (PB98-155617, A15, MF-A03).

MCEER-98-0001 "Extraction of Nonlinear Hysteretic Properties of Seismically Isolated Bridges from Quick-Release Field Tests," by Q. Chen, B.M. Douglas, E.M. Maragakis and I.G. Buckle, 5/26/98, (PB99-118838, A06, MF-A01).

MCEER-98-0002 "Methodologies for Evaluating the Importance of Highway Bridges," by A. Thomas, S. Eshenaur and J. Kulicki, 5/29/98, (PB99-118846, A10, MF-A02).

MCEER-98-0003 "Capacity Design of Bridge Piers and the Analysis of Overstrength," by J.B. Mander, A. Dutta and P. Goel, 6/1/98, (PB99-118853, A09, MF-A02).

MCEER-98-0004 "Evaluation of Bridge Damage Data from the Loma Prieta and Northridge, California Earthquakes," by N. Basoz and A. Kiremidjian, 6/2/98, (PB99-118861, A15, MF-A03).

MCEER-98-0005 "Screening Guide for Rapid Assessment of Liquefaction Hazard at Highway Bridge Sites," by T. L. Youd, 6/16/98, (PB99-118879, A06, not available on microfiche).

MCEER-98-0006 "Structural Steel and Steel/Concrete Interface Details for Bridges," by P. Ritchie, N. Kauhl and J. Kulicki, 7/13/98, (PB99-118945, A06, MF-A01).

MCEER-98-0007 "Capacity Design and Fatigue Analysis of Confined Concrete Columns," by A. Dutta and J.B. Mander, 7/14/98, (PB99-118960, A14, MF-A03).

MCEER-98-0008 "Proceedings of the Workshop on Performance Criteria for Telecommunication Services Under Earthquake Conditions," edited by A.J. Schiff, 7/15/98, (PB99-118952, A08, MF-A02).

MCEER-98-0009 "Fatigue Analysis of Unconfined Concrete Columns," by J.B. Mander, A. Dutta and J.H. Kim, 9/12/98, (PB99-123655, A10, MF-A02).

MCEER-98-0010 "Centrifuge Modeling of Cyclic Lateral Response of Pile-Cap Systems and Seat-Type Abutments in Dry Sands," by A.D. Gadre and R. Dobry, 10/2/98, (PB99-123606, A13, MF-A03).

MCEER-98-0011 "IDARC-BRIDGE: A Computational Platform for Seismic Damage Assessment of Bridge Structures," by A.M. Reinhorn, V. Simeonov, G. Mylonakis and Y. Reichman, 10/2/98, (PB99-162919, A15, MF-A03).

MCEER-98-0012 "Experimental Investigation of the Dynamic Response of Two Bridges Before and After Retrofitting with Elastomeric Bearings," by D.A. Wendichansky, S.S. Chen and J.B. Mander, 10/2/98, (PB99-162927, A15, MF-A03).

MCEER-98-0013 "Design Procedures for Hinge Restrainers and Hinge Sear Width for Multiple-Frame Bridges," by R. Des Roches and G.L. Fenves, 11/3/98, (PB99-140477, A13, MF-A03).

MCEER-98-0014 "Response Modification Factors for Seismically Isolated Bridges," by M.C. Constantinou and J.K. Quarshie, 11/3/98, (PB99-140485, A14, MF-A03).

MCEER-98-0015 "Proceedings of the U.S.-Italy Workshop on Seismic Protective Systems for Bridges," edited by I.M. Friedland and M.C. Constantinou, 11/3/98, (PB2000-101711, A22, MF-A04).

MCEER-98-0016 "Appropriate Seismic Reliability for Critical Equipment Systems: Recommendations Based on Regional Analysis of Financial and Life Loss," by K. Porter, C. Scawthorn, C. Taylor and N. Blais, 11/10/98, (PB99-157265, A08, MF-A02).

MCEER-98-0017 "Proceedings of the U.S. Japan Joint Seminar on Civil Infrastructure Systems Research," edited by M. Shinozuka and A. Rose, 11/12/98, (PB99-156713, A16, MF-A03).

MCEER-98-0018 "Modeling of Pile Footings and Drilled Shafts for Seismic Design," by I. PoLam, M. Kapuskar and D. Chaudhuri, 12/21/98, (PB99-157257, A09, MF-A02).

MCEER-99-0001 "Seismic Evaluation of a Masonry Infilled Reinforced Concrete Frame by Pseudodynamic Testing," by S.G. Buonopane and R.N. White, 2/16/99, (PB99-162851, A09, MF-A02).

MCEER-99-0002 "Response History Analysis of Structures with Seismic Isolation and Energy Dissipation Systems: Verification Examples for Program SAP2000," by J. Scheller and M.C. Constantinou, 2/22/99, (PB99-162869, A08, MF-A02).

MCEER-99-0003 "Experimental Study on the Seismic Design and Retrofit of Bridge Columns Including Axial Load Effects," by A. Dutta, T. Kokorina and J.B. Mander, 2/22/99, (PB99-162877, A09, MF-A02).

MCEER-99-0004 "Experimental Study of Bridge Elastomeric and Other Isolation and Energy Dissipation Systems with Emphasis on Uplift Prevention and High Velocity Near-source Seismic Excitation," by A. Kasalanati and M. C. Constantinou, 2/26/99, (PB99-162885, A12, MF-A03).

MCEER-99-0005 "Truss Modeling of Reinforced Concrete Shear-flexure Behavior," by J.H. Kim and J.B. Mander, 3/8/99, (PB99-163693, A12, MF-A03).

MCEER-99-0006 "Experimental Investigation and Computational Modeling of Seismic Response of a 1:4 Scale Model Steel Structure with a Load Balancing Supplemental Damping System," by G. Pekcan, J.B. Mander and S.S. Chen, 4/2/99, (PB99-162893, A11, MF-A03).

MCEER-99-0007 "Effect of Vertical Ground Motions on the Structural Response of Highway Bridges," by M.R. Button, C.J. Cronin and R.L. Mayes, 4/10/99, (PB2000-101411, A10, MF-A03).

MCEER-99-0008 "Seismic Reliability Assessment of Critical Facilities: A Handbook, Supporting Documentation, and Model Code Provisions," by G.S. Johnson, R.E. Sheppard, M.D. Quilici, S.J. Eder and C.R. Scawthorn, 4/12/99, (PB2000-101701, A18, MF-A04).

MCEER-99-0009 "Impact Assessment of Selected MCEER Highway Project Research on the Seismic Design of Highway Structures," by C. Rojahn, R. Mayes, D.G. Anderson, J.H. Clark, D'Appolonia Engineering, S. Gloyd and R.V. Nutt, 4/14/99, (PB99-162901, A10, MF-A02).

MCEER-99-0010 "Site Factors and Site Categories in Seismic Codes," by R. Dobry, R. Ramos and M.S. Power, 7/19/99, (PB2000-101705, A08, MF-A02).

MCEER-99-0011 "Restrainer Design Procedures for Multi-Span Simply-Supported Bridges," by M.J. Randall, M. Saiidi, E. Maragakis and T. Isakovic, 7/20/99, (PB2000-101702, A10, MF-A02).

MCEER-99-0012 "Property Modification Factors for Seismic Isolation Bearings," by M.C. Constantinou, P. Tsopelas, A. Kasalanati and E. Wolff, 7/20/99, (PB2000-103387, A11, MF-A03).

MCEER-99-0013 "Critical Seismic Issues for Existing Steel Bridges," by P. Ritchie, N. Kauhl and J. Kulicki, 7/20/99, (PB2000-101697, A09, MF-A02).

MCEER-99-0014 "Nonstructural Damage Database," by A. Kao, T.T. Soong and A. Vender, 7/24/99, (PB2000-101407, A06, MF-A01).

MCEER-99-0015 "Guide to Remedial Measures for Liquefaction Mitigation at Existing Highway Bridge Sites," by H.G. Cooke and J. K. Mitchell, 7/26/99, (PB2000-101703, A11, MF-A03).

MCEER-99-0016 "Proceedings of the MCEER Workshop on Ground Motion Methodologies for the Eastern United States," edited by N. Abrahamson and A. Becker, 8/11/99, (PB2000-103385, A07, MF-A02).

MCEER-99-0017 "Quindío, Colombia Earthquake of January 25, 1999: Reconnaissance Report," by A.P. Asfura and P.J. Flores, 10/4/99, (PB2000-106893, A06, MF-A01).

MCEER-99-0018 "Hysteretic Models for Cyclic Behavior of Deteriorating Inelastic Structures," by M.V. Sivaselvan and A.M. Reinhorn, 11/5/99, (PB2000-103386, A08, MF-A02).

MCEER-99-0019 "Proceedings of the 7th U.S.- Japan Workshop on Earthquake Resistant Design of Lifeline Facilities and Countermeasures Against Soil Liquefaction," edited by T.D. O'Rourke, J.P. Bardet and M. Hamada, 11/19/99, (PB2000-103354, A99, MF-A06).

MCEER-99-0020 "Development of Measurement Capability for Micro-Vibration Evaluations with Application to Chip Fabrication Facilities," by G.C. Lee, Z. Liang, J.W. Song, J.D. Shen and W.C. Liu, 12/1/99, (PB2000-105993, A08, MF-A02).

MCEER-99-0021 "Design and Retrofit Methodology for Building Structures with Supplemental Energy Dissipating Systems," by G. Pekcan, J.B. Mander and S.S. Chen, 12/31/99, (PB2000-105994, A11, MF-A03).

MCEER-00-0001 "The Marmara, Turkey Earthquake of August 17, 1999: Reconnaissance Report," edited by C. Scawthorn; with major contributions by M. Bruneau, R. Eguchi, T. Holzer, G. Johnson, J. Mander, J. Mitchell, W. Mitchell, A. Papageorgiou, C. Scaethorn, and G. Webb, 3/23/00, (PB2000-106200, A11, MF-A03).

MCEER-00-0002 "Proceedings of the MCEER Workshop for Seismic Hazard Mitigation of Health Care Facilities," edited by G.C. Lee, M. Ettouney, M. Grigoriu, J. Hauer and J. Nigg, 3/29/00, (PB2000-106892, A08, MF-A02).

MCEER-00-0003 "The Chi-Chi, Taiwan Earthquake of September 21, 1999: Reconnaissance Report," edited by G.C. Lee and C.H. Loh, with major contributions by G.C. Lee, M. Bruneau, I.G. Buckle, S.E. Chang, P.J. Flores, T.D. O'Rourke, M. Shinozuka, T.T. Soong, C-H. Loh, K-C. Chang, Z-J. Chen, J-S. Hwang, M-L. Lin, G-Y. Liu, K-C. Tsai, G.C. Yao and C-L. Yen, 4/30/00, (PB2001-100980, A10, MF-A02).

MCEER-00-0004 "Seismic Retrofit of End-Sway Frames of Steel Deck-Truss Bridges with a Supplemental Tendon System: Experimental and Analytical Investigation," by G. Pekcan, J.B. Mander and S.S. Chen, 7/1/00, (PB2001-100982, A10, MF-A02).

MCEER-00-0005 "Sliding Fragility of Unrestrained Equipment in Critical Facilities," by W.H. Chong and T.T. Soong, 7/5/00, (PB2001-100983, A08, MF-A02).

MCEER-00-0006 "Seismic Response of Reinforced Concrete Bridge Pier Walls in the Weak Direction," by N. Abo-Shadi, M. Saiidi and D. Sanders, 7/17/00, (PB2001-100981, A17, MF-A03).

MCEER-00-0007 "Low-Cycle Fatigue Behavior of Longitudinal Reinforcement in Reinforced Concrete Bridge Columns," by J. Brown and S.K. Kunnath, 7/23/00, (PB2001-104392, A08, MF-A02).

MCEER-00-0008 "Soil Structure Interaction of Bridges for Seismic Analysis," I. PoLam and H. Law, 9/25/00, (PB2001-105397, A08, MF-A02).

MCEER-00-0009 "Proceedings of the First MCEER Workshop on Mitigation of Earthquake Disaster by Advanced Technologies (MEDAT-1), edited by M. Shinozuka, D.J. Inman and T.D. O'Rourke, 11/10/00, (PB2001-105399, A14, MF-A03).

MCEER-00-0010 "Development and Evaluation of Simplified Procedures for Analysis and Design of Buildings with Passive Energy Dissipation Systems," by O.M. Ramirez, M.C. Constantinou, C.A. Kircher, A.S. Whittaker, M.W. Johnson, J.D. Gomez and C. Chrysostomou, 11/16/01, (PB2001-105523, A23, MF-A04).

MCEER-00-0011 "Dynamic Soil-Foundation-Structure Interaction Analyses of Large Caissons," by C-Y. Chang, C-M. Mok, Z-L. Wang, R. Settgast, F. Waggoner, M.A. Ketchum, H.M. Gonnermann and C-C. Chin, 12/30/00, (PB2001-104373, A07, MF-A02).

MCEER-00-0012 "Experimental Evaluation of Seismic Performance of Bridge Restrainers," by A.G. Vlassis, E.M. Maragakis and M. Saiid Saiidi, 12/30/00, (PB2001-104354, A09, MF-A02).

MCEER-00-0013 "Effect of Spatial Variation of Ground Motion on Highway Structures," by M. Shinozuka, V. Saxena and G. Deodatis, 12/31/00, (PB2001-108755, A13, MF-A03).

MCEER-00-0014 "A Risk-Based Methodology for Assessing the Seismic Performance of Highway Systems," by S.D. Werner, C.E. Taylor, J.E. Moore, II, J.S. Walton and S. Cho, 12/31/00, (PB2001-108756, A14, MF-A03).

MCEER-01-0001 "Experimental Investigation of P-Delta Effects to Collapse During Earthquakes," by D. Vian and M. Bruneau, 6/25/01, (PB2002-100534, A17, MF-A03).

MCEER-01-0002 "Proceedings of the Second MCEER Workshop on Mitigation of Earthquake Disaster by Advanced Technologies (MEDAT-2)," edited by M. Bruneau and D.J. Inman, 7/23/01, (PB2002-100434, A16, MF-A03).

MCEER-01-0003 "Sensitivity Analysis of Dynamic Systems Subjected to Seismic Loads," by C. Roth and M. Grigoriu, 9/18/01, (PB2003-100884, A12, MF-A03).

MCEER-01-0004 "Overcoming Obstacles to Implementing Earthquake Hazard Mitigation Policies: Stage 1 Report," by D.J. Alesch and W.J. Petak, 12/17/01, (PB2002-107949, A07, MF-A02).

MCEER-01-0005 "Updating Real-Time Earthquake Loss Estimates: Methods, Problems and Insights," by C.E. Taylor, S.E. Chang and R.T. Eguchi, 12/17/01, (PB2002-107948, A05, MF-A01).

MCEER-01-0006 "Experimental Investigation and Retrofit of Steel Pile Foundations and Pile Bents Under Cyclic Lateral Loadings," by A. Shama, J. Mander, B. Blabac and S. Chen, 12/31/01, (PB2002-107950, A13, MF-A03).

MCEER-02-0001 "Assessment of Performance of Bolu Viaduct in the 1999 Duzce Earthquake in Turkey" by P.C. Roussis, M.C. Constantinou, M. Erdik, E. Durukal and M. Dicleli, 5/8/02, (PB2003-100883, A08, MF-A02).

MCEER-02-0002 "Seismic Behavior of Rail Counterweight Systems of Elevators in Buildings," by M.P. Singh, Rildova and L.E. Suarez, 5/27/02. (PB2003-100882, A11, MF-A03).

MCEER-02-0003 "Development of Analysis and Design Procedures for Spread Footings," by G. Mylonakis, G. Gazetas, S. Nikolaou and A. Chauncey, 10/02/02, (PB2004-101636, A13, MF-A03, CD-A13).

MCEER-02-0004 "Bare-Earth Algorithms for Use with SAR and LIDAR Digital Elevation Models," by C.K. Huyck, R.T. Eguchi and B. Houshmand, 10/16/02, (PB2004-101637, A07, CD-A07).

MCEER-02-0005 "Review of Energy Dissipation of Compression Members in Concentrically Braced Frames," by K.Lee and M. Bruneau, 10/18/02, (PB2004-101638, A10, CD-A10).

MCEER-03-0001 "Experimental Investigation of Light-Gauge Steel Plate Shear Walls for the Seismic Retrofit of Buildings" by J. Berman and M. Bruneau, 5/2/03, (PB2004-101622, A10, MF-A03, CD-A10).

MCEER-03-0002 "Statistical Analysis of Fragility Curves," by M. Shinozuka, M.Q. Feng, H. Kim, T. Uzawa and T. Ueda, 6/16/03, (PB2004-101849, A09, CD-A09).

MCEER-03-0003 "Proceedings of the Eighth U.S.-Japan Workshop on Earthquake Resistant Design f Lifeline Facilities and Countermeasures Against Liquefaction," edited by M. Hamada, J.P. Bardet and T.D. O'Rourke, 6/30/03, (PB2004-104386, A99, CD-A99).

MCEER-03-0004 "Proceedings of the PRC-US Workshop on Seismic Analysis and Design of Special Bridges," edited by L.C. Fan and G.C. Lee, 7/15/03, (PB2004-104387, A14, CD-A14).

MCEER-03-0005 "Urban Disaster Recovery: A Framework and Simulation Model," by S.B. Miles and S.E. Chang, 7/25/03, (PB2004-104388, A07, CD-A07).

MCEER-03-0006 "Behavior of Underground Piping Joints Due to Static and Dynamic Loading," by R.D. Meis, M. Maragakis and R. Siddharthan, 11/17/03, (PB2005-102194, A13, MF-A03, CD-A00).

MCEER-03-0007 "Seismic Vulnerability of Timber Bridges and Timber Substructures," by A.A. Shama, J.B. Mander, I.M. Friedland and D.R. Allicock, 12/15/03.

MCEER-04-0001 "Experimental Study of Seismic Isolation Systems with Emphasis on Secondary System Response and Verification of Accuracy of Dynamic Response History Analysis Methods," by E. Wolff and M. Constantinou, 1/16/04 (PB2005-102195, A99, MF-E08, CD-A00).

MCEER-04-0002 "Tension, Compression and Cyclic Testing of Engineered Cementitious Composite Materials," by K. Kesner and S.L. Billington, 3/1/04, (PB2005-102196, A08, CD-A08).

MCEER-04-0003 "Cyclic Testing of Braces Laterally Restrained by Steel Studs to Enhance Performance During Earthquakes," by O.C. Celik, J.W. Berman and M. Bruneau, 3/16/04, (PB2005-102197, A13, MF-A03, CD-A00).

MCEER-04-0004 "Methodologies for Post Earthquake Building Damage Detection Using SAR and Optical Remote Sensing: Application to the August 17, 1999 Marmara, Turkey Earthquake," by C.K. Huyck, B.J. Adams, S. Cho, R.T. Eguchi, B. Mansouri and B. Houshmand, 6/15/04, (PB2005-104888, A10, CD-A00).

MCEER-04-0005 "Nonlinear Structural Analysis Towards Collapse Simulation: A Dynamical Systems Approach," by M.V. Sivaselvan and A.M. Reinhorn, 6/16/04, (PB2005-104889, A11, MF-A03, CD-A00).

MCEER-04-0006 "Proceedings of the Second PRC-US Workshop on Seismic Analysis and Design of Special Bridges," edited by G.C. Lee and L.C. Fan, 6/25/04, (PB2005-104890, A16, CD-A00).

MCEER-04-0007 "Seismic Vulnerability Evaluation of Axially Loaded Steel Built-up Laced Members," by K. Lee and M. Bruneau, 6/30/04, (PB2005-104891, A16, CD-A00).

MCEER-04-0008 "Evaluation of Accuracy of Simplified Methods of Analysis and Design of Buildings with Damping Systems for Near-Fault and for Soft-Soil Seismic Motions," by E.A. Pavlou and M.C. Constantinou, 8/16/04, (PB2005-104892, A08, MF-A02, CD-A00).

MCEER-04-0009 "Assessment of Geotechnical Issues in Acute Care Facilities in California," by M. Lew, T.D. O'Rourke, R. Dobry and M. Koch, 9/15/04, (PB2005-104893, A08, CD-A00).

MCEER-04-0010 "Scissor-Jack-Damper Energy Dissipation System," by A.N. Sigaher-Boyle and M.C. Constantinou, 12/1/04 (PB2005-108221).

MCEER-04-0011 "Seismic Retrofit of Bridge Steel Truss Piers Using a Controlled Rocking Approach," by M. Pollino and M. Bruneau, 12/20/04 (PB2006-105795).

MCEER-05-0001 "Experimental and Analytical Studies of Structures Seismically Isolated with an Uplift-Restraint Isolation System," by P.C. Roussis and M.C. Constantinou, 1/10/05 (PB2005-108222).

MCEER-05-0002 "A Versatile Experimentation Model for Study of Structures Near Collapse Applied to Seismic Evaluation of Irregular Structures," by D. Kusumastuti, A.M. Reinhorn and A. Rutenberg, 3/31/05 (PB2006-101523).

MCEER-05-0003 "Proceedings of the Third PRC-US Workshop on Seismic Analysis and Design of Special Bridges," edited by L.C. Fan and G.C. Lee, 4/20/05, (PB2006-105796).

MCEER-05-0004 "Approaches for the Seismic Retrofit of Braced Steel Bridge Piers and Proof-of-Concept Testing of an Eccentrically Braced Frame with Tubular Link," by J.W. Berman and M. Bruneau, 4/21/05 (PB2006-101524).

MCEER-05-0005 "Simulation of Strong Ground Motions for Seismic Fragility Evaluation of Nonstructural Components in Hospitals," by A. Wanitkorkul and A. Filiatrault, 5/26/05 (PB2006-500027).

MCEER-05-0006 "Seismic Safety in California Hospitals: Assessing an Attempt to Accelerate the Replacement or Seismic Retrofit of Older Hospital Facilities," by D.J. Alesch, L.A. Arendt and W.J. Petak, 6/6/05 (PB2006-105794).

MCEER-05-0007 "Development of Seismic Strengthening and Retrofit Strategies for Critical Facilities Using Engineered Cementitious Composite Materials," by K. Kesner and S.L. Billington, 8/29/05 (PB2006-111701).

MCEER-05-0008 "Experimental and Analytical Studies of Base Isolation Systems for Seismic Protection of Power Transformers," by N. Murota, M.Q. Feng and G-Y. Liu, 9/30/05 (PB2006-111702).

MCEER-05-0009 "3D-BASIS-ME-MB: Computer Program for Nonlinear Dynamic Analysis of Seismically Isolated Structures," by P.C. Tsopelas, P.C. Roussis, M.C. Constantinou, R. Buchanan and A.M. Reinhorn, 10/3/05 (PB2006-111703).

MCEER-05-0010 "Steel Plate Shear Walls for Seismic Design and Retrofit of Building Structures," by D. Vian and M. Bruneau, 12/15/05 (PB2006-111704).

MCEER-05-0011 "The Performance-Based Design Paradigm," by M.J. Astrella and A. Whittaker, 12/15/05 (PB2006-111705).

MCEER-06-0001 "Seismic Fragility of Suspended Ceiling Systems," H. Badillo-Almaraz, A.S. Whittaker, A.M. Reinhorn and G.P. Cimellaro, 2/4/06 (PB2006-111706).

MCEER-06-0002 "Multi-Dimensional Fragility of Structures," by G.P. Cimellaro, A.M. Reinhorn and M. Bruneau, 3/1/06 (PB2007-106974, A09, MF-A02, CD A00).

MCEER-06-0003 "Built-Up Shear Links as Energy Dissipators for Seismic Protection of Bridges," by P. Dusicka, A.M. Itani and I.G. Buckle, 3/15/06 (PB2006-111708).

MCEER-06-0004 "Analytical Investigation of the Structural Fuse Concept," by R.E. Vargas and M. Bruneau, 3/16/06 (PB2006-111709).

MCEER-06-0005 "Experimental Investigation of the Structural Fuse Concept," by R.E. Vargas and M. Bruneau, 3/17/06 (PB2006-111710).

MCEER-06-0006 "Further Development of Tubular Eccentrically Braced Frame Links for the Seismic Retrofit of Braced Steel Truss Bridge Piers," by J.W. Berman and M. Bruneau, 3/27/06 (PB2007-105147).

MCEER-06-0007 "REDARS Validation Report," by S. Cho, C.K. Huyck, S. Ghosh and R.T. Eguchi, 8/8/06 (PB2007-106983).

MCEER-06-0008 "Review of Current NDE Technologies for Post-Earthquake Assessment of Retrofitted Bridge Columns," by J.W. Song, Z. Liang and G.C. Lee, 8/21/06 06 (PB2007-106984).

MCEER-06-0009 "Liquefaction Remediation in Silty Soils Using Dynamic Compaction and Stone Columns," by S. Thevanayagam, G.R. Martin, R. Nashed, T. Shenthan, T. Kanagalingam and N. Ecemis, 8/28/06 06 (PB2007-106985).

MCEER-06-0010 "Conceptual Design and Experimental Investigation of Polymer Matrix Composite Infill Panels for Seismic Retrofitting," by W. Jung, M. Chiewanichakorn and A.J. Aref, 9/21/06 (PB2007-106986).

MCEER-06-0011 "A Study of the Coupled Horizontal-Vertical Behavior of Elastomeric and Lead-Rubber Seismic Isolation Bearings," by G.P. Warn and A.S. Whittaker, 9/22/06 (PB2007-108679).

MCEER-06-0012 "Proceedings of the Fourth PRC-US Workshop on Seismic Analysis and Design of Special Bridges: Advancing Bridge Technologies in Research, Design, Construction and Preservation," Edited by L.C. Fan, G.C. Lee and L. Ziang, 10/12/06.

MCEER-06-0013 "Cyclic Response and Low Cycle Fatigue Characteristics of Plate Steels," by P. Dusicka, A.M. Itani and I.G. Buckle, 11/1/06 06 (PB2007-106987).

MCEER-06-0014 "Proceedings of the Second US-Taiwan Bridge Engineering Workshop," edited by W.P. Yen, J. Shen, J-Y. Chen and M. Wang, 11/15/06.

MCEER-06-0015 "User Manual and Technical Documentation for the REDARS™ Import Wizard," by S. Cho, S. Ghosh, C.K. Huyck and S.D. Werner, 11/30/06.

MCEER-06-0016 "Hazard Mitigation Strategy and Monitoring Technologies for Urban and Infrastructure Public Buildings: Proceedings of the China-US Workshops," edited by X.Y. Zhou, A.L. Zhang, G.C. Lee and M. Tong, 12/12/06.

MCEER-07-0001 "Static and Kinetic Coefficients of Friction for Rigid Blocks," by C. Kafali, S. Fathali, M. Grigoriu and A.S. Whittaker, 3/20/07.

MCEER-07-0002 "Hazard Mitigation Investment Decision Making: Organizational Response to Legislative Mandate," by L.A. Arendt, D.J. Alesch and W.J. Petak, 4/9/07.

MCEER-07-0003 "Seismic Behavior of Bidirectional-Resistant Ductile End Diaphragms with Unbonded Braces in Straight or Skewed Steel Bridges," by O. Celik and M. Bruneau, 4/11/07.

MCEER-07-0004 "Modeling Pile Behavior in Large Pile Groups Under Lateral Loading," by A.M. Dodds and G.R. Martin, 4/16/07.

MCEER-07-0005 "Experimental Investigation of Blast Performance of Seismically Resistant Concrete-Filled Steel Tube Bridge Piers," by S. Fujikura, M. Bruneau and D. Lopez-Garcia, 4/20/07.

MCEER-07-0006 "Seismic Analysis of Conventional and Isolated Liquefied Natural Gas Tanks Using Mechanical Analogs," by I.P. Christovasilis and A.S. Whittaker, 5/1/07.

MCEER-07-0007 "Experimental Seismic Performance Evaluation of Isolation/Restraint Systems for Mechanical Equipment – Part 1: Heavy Equipment Study," by S. Fathali and A. Filiatrault, 6/6/07.

MCEER
EARTHQUAKE ENGINEERING TO EXTREME EVENTS
University at Buffalo, The State University of New York
Red Jacket Quadrangle ▪ Buffalo, New York 14261
Phone: (716) 645-3391 ▪ Fax: (716) 645-3399
E-mail: *mceer@buffalo.edu* ▪ WWW Site *http://mceer.buffalo.edu*
University at Buffalo *The State University of New York*

ISSN 1520-295X